



Universiteit
Leiden
The Netherlands

Redox interconversion between metal thiolate and disulfide compounds

Jiang, F.

Citation

Jiang, F. (2018, December 7). *Redox interconversion between metal thiolate and disulfide compounds*. Retrieved from <https://hdl.handle.net/1887/68029>

Version: Not Applicable (or Unknown)

License: [Licence agreement concerning inclusion of doctoral thesis in the Institutional Repository of the University of Leiden](#)

Downloaded from: <https://hdl.handle.net/1887/68029>

Note: To cite this publication please use the final published version (if applicable).

Cover Page



Universiteit Leiden



The handle <http://hdl.handle.net/1887/68029> holds various files of this Leiden University dissertation.

Author: Jiang, F.

Title: Redox interconversion between metal thiolate and disulfide compounds

Issue Date: 2018-12-07

Redox Interconversion between Metal Thiolate and Disulfide Compounds

PROEFSCHRIFT

ter verkrijging van
de graad van Doctor aan de Universiteit Leiden,
op gezag van Rector Magnificus Prof. mr. C. J. J. M. Stolker,
volgens besluit van het College voor Promoties
te verdedigen op vrijdag 7 december 2018
klokke 13:45 uur

door

Feng Jiang
geboren te Jiangsu in 1988

Samenstelling Promotiecommissie

Promotores Prof. Dr. E. Bouwman
 Prof. Dr. C. Fonseca Guerra

Overige leden Prof. Dr. H. S. Overkleeft
 Prof. Dr. M. T. M. Koper
 Prof. Dr. B. de Bruin
 (Universiteit van Amsterdam)
 Prof. Dr. Zongwan Mao
 (Sun Yat-sen University, China)

Haste makes waste

欲速则不达

<The Analects of Confucius>

Table of Contents

List of Abbreviations.....	7
Chapter 1 Introduction.....	9
Chapter 2 Redox Interconversion between Cobalt(III) Thiolate and Cobalt(II) Disulfide Compounds.....	23
Chapter 3 Solvent-dependent Redox Interconversion of Cobalt(III) Thiolate and Cobalt(II) Disulfide Compounds.....	45
Chapter 4 The Reactivity of Fe(II) and Co(II) Disulfide Compounds with Dihydrogen Peroxide.....	59
Chapter 5 A Tetranuclear Fluorido-bridged Iron Compound: Fluoride Abstraction from the Tetrafluoridoborate Anion.....	73
Chapter 6 Synthesis and Characterization of a Series of Transition Metal Compounds of Thioether and Disulfide Ligands.....	81
Chapter 7 Summary, Conclusions & Outlook.....	93
Appendix I: Supplementary Information for Chapter 2.....	101
Appendix II: Supplementary Information for Chapter 3.....	121
Appendix III: Supplementary Information for Chapter 4.....	133
Appendix IV: Supplementary Information for Chapter 5.....	141
Appendix V: Supplementary Information for Chapter 6.....	145
Samenvatting	155
List of Publications.....	159
Curriculum Vitae.....	161

List of Abbreviations

a.u.	arbitrary units
Bu	butyl
CcO	cytochrome <i>c</i> oxidase
CDO	cysteine dioxygenase
Cys	cysteine
DCM	dichloromethane
DFT	density functional theory
ESI	electrospray ionization
Eq	equation
ET	electron transfer
Glu	glutamic acid
His	histidine
IR	infrared
<i>J</i>	coupling constant
LMCT	ligand-to-metal charge transfer
m	medium (IR); multiplet (NMR)
min	minutes
Me	methyl
Met	methionine
MLCT	metal-to-ligand charge transfer
NMR	nuclear magnetic resonance
NHases	Nitrile hydratases
MS	mass spectrometry
<i>o</i>	ortho
OTf	trifluoromethanesulfonate
<i>p</i>	para
Ph	phenyl
Py	2-pyridyl
ppm	parts per million
RT	room temperature
s	singlet (NMR); strong (IR)
t	triplet
THF	tetrahydrofuran
TPA	tris(2-pyridylmethyl)amine
Ts	4-toluenesulfonyl
Tyr	tyrosine
UV	ultra-violet
vis	visible
vs	very strong (IR)
w	weak (IR)

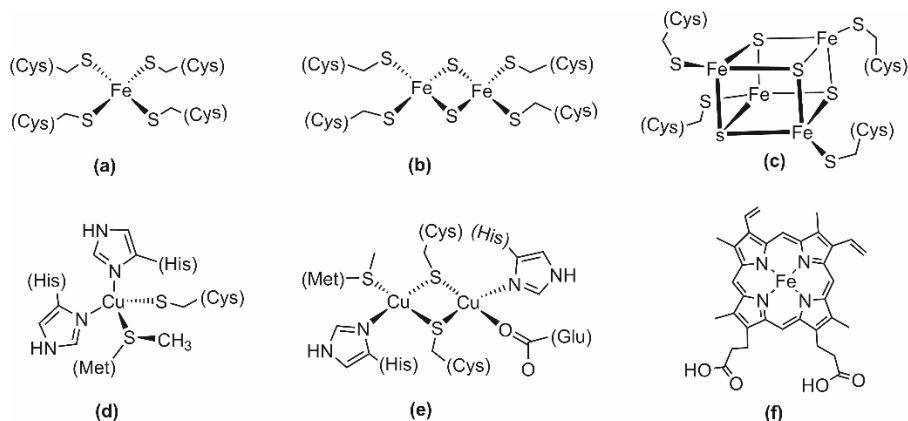
Chapter 1

Introduction

Two types of active sites of copper proteins (Type-1, Cu_A), involved in electron transfer reactions in biological systems, are briefly described. An overview is presented of synthetic models with diamond core [Cu₂S₂] structures that mimic the active sites of Cu_A, including their structure and spectroscopic properties. Furthermore, the redox interconversion reaction of metal thiolate and disulfide compounds is described, which is related to simulation of metal-based thiolate-disulfide interchange occurring in metalloenzymes such as Zn₇MT-3 and ScO.

1.1 General introduction

Electron transfer (ET) reactions promoted by metalloenzymes are of fundamental importance in a large number of biological systems e.g. cellular respiration [1, 2], dioxygen transport [3, 4], and photosynthesis [5]. The dominant redox centers found in ET proteins are iron and copper (Scheme 1.1) [6]. In the last decades, a number copper proteins has been extensively studied using advanced spectroscopic techniques, which provided further insight into the structure and spectroscopic properties of the active sites in these metalloenzymes [7, 8]. Based on the coordination environment, spectroscopic features, and functions of the active sites, copper proteins are classified into six groups, namely, Type-1, Type-2, Type-3, Cu_A, Cu_B and Cu_Z proteins [9]. Among these classes, only Type-1 and Cu_A are involved as ET mediators. Some enzymes containing Type-1 or Cu_A active sites are briefly discussed in the following section [6].



Scheme 1.1. Schematic representation of the active sites of metalloenzymes involved in ET processes (a) mononuclear rubredoxin; (b) binuclear [2Fe-2S] ferredoxin; (c) tetranuclear [4Fe-4S] ferredoxin; (d) Type-1 active site of plastocyanin; (e) Cu_A active site of cytochrome c oxidase; (f) heme b of cytochromes.

1.2 Copper proteins involved in ET processes

1.2.1 Type-1 active site

The Type-1 copper active site not only is present in mononuclear metalloenzymes such as plastocyanin (Scheme 1.1.d), amicyanin, rusticyanin, and azurin, but also is found in some multicopper proteins, such as nitrite reductase, and ascorbate oxidase. The Type-1 copper center in these metalloenzymes is usually coordinated by two nitrogen atoms of histidines and one sulfur atom of cysteine in a trigonal plane, with another distant axial ligand, which is either a sulfur atom of methionine or an oxygen

atom of glutamine/leucine. The copper-to-nitrogen bond distances range from 1.93 to 2.22 Å, whereas the copper to sulfur bond lengths are between 2.07 and 2.30 Å. The metalloenzymes containing a Type-1 copper center are also called “blue copper proteins” as they show an intense blue color in solution. UV-vis spectra of these solutions usually show a strong and characteristic $\text{Cu}^{\text{II}} \leftarrow \text{S}_{\text{cys}}$ charge-transfer transition (LMCT) at 600 nm ($\epsilon = 5 \times 10^3 \text{ M}^{-1} \text{ cm}^{-1}$), causing the typical blue color. EPR spectra of metalloenzymes containing a Type-1 copper center present a narrow hyperfine coupling probably arising from the covalent nature of the Cu-S bond [8, 10]. Normally, Type-1 copper proteins are involved in long-range ET processes in biological systems [11, 12].

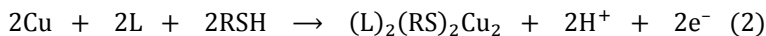
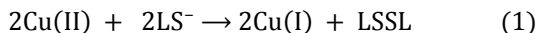
1.2.2 Cu_A active site

The Cu_A active site is found in e.g. cytochrome c oxidase (CcO, Scheme 1.1.e), and nitrous oxide reductase, enzymes that play a vital role in electron-transfer reactions. The Cu_A active site comprises a dinuclear dicopper diamond core [Cu_2S_2], in which both copper centers are in a distorted tetrahedral geometry coordinated by a nitrogen atom of histidine, two bridging thiolate sulfur donors of two cysteines, and a weakly coordinating ligand, which is either a methionine sulfur donor or a backbone carbonyl oxygen atom. The copper-to-nitrogen bond lengths in Cu_A sites range from 1.93 to 2.22 Å, the Cu-S bond distances are around 2.2 Å. Notably, the distance between the two copper centers in the Cu_A site range from 2.43 – 2.60 Å; this rather short distance allows for a direct interaction between the two copper ions. The oxidation state of the two copper centers shuttles between $\text{Cu}^{\text{II}}\text{Cu}^{\text{II}}$ and $\text{Cu}^{\text{I}}\text{Cu}^{\text{II}}$ during ET. Metalloenzymes containing a Cu_A active site commonly give a purple color in solution. Absorption spectra of these purple solutions show two intense absorbance bands at around 480 and 530 nm arising from $\text{Cu} \leftarrow \text{S}$ charge transfer, and another broad band at around 780 nm ascribed to the charge transfer between the copper ions in the mixed-valent state. EPR spectra of proteins containing a Cu_A active site normally present a seven-line hyperfine splitting pattern, which is caused by delocalization of the electron between the two copper ions. Generally, enzymes containing the Cu_A active site are terminal electron acceptors of ET processes [13].

1.3 Synthetic models for Cu_A sites

To obtain further insight into the operation principle of electron transfer within Cu_A active sites, inorganic chemists synthesize small molecule mimics to simulate the structure and spectroscopic properties of Cu_A active sites [14, 15]. The major challenge of the synthesis of mimics resembling the Cu_A active site is that disulfide bonds tend to be formed from two thiolate ligands when reacted with $\text{Cu}(\text{II})$ ions, with

the concomitant reduction of the Cu(II) ions to Cu(I) (equation 1) [16]. Therefore, initial studies focused on the synthesis of dinuclear Cu(I) dithiolate compounds as mimics for the reduced state of Cu_A sites. The first example of a dinuclear Cu(I) compound bridged by two arylthiolate groups was reported over 30 years ago, followed after a few years by a report of a highly similar compound by another group (compounds **C1** and **C2** in scheme 1.2) [17, 18]. Both compounds **C1** and **C2** were synthesized electrochemically starting from copper metal (equation 2). The structures show a [Cu₂S₂] diamond core with Cu···Cu distances of 2.613(3) and 3.0186(12) Å, respectively. The large difference in the Cu···Cu distances is likely induced by the steric effect of the additional methyl groups in compound **C2**. Although compounds **C1** and **C2** replicate a diamond core [Cu₂S₂] with the desired Cu···Cu distances, the cysteine ligands present in the Cu_A site are mimicked with aromatic rather than aliphatic thiolate ligands. Electrochemical oxidation of **C1** and **C2** failed to generate the corresponding mixed-valent or high-valent compounds with a diamond [Cu₂S₂] core.

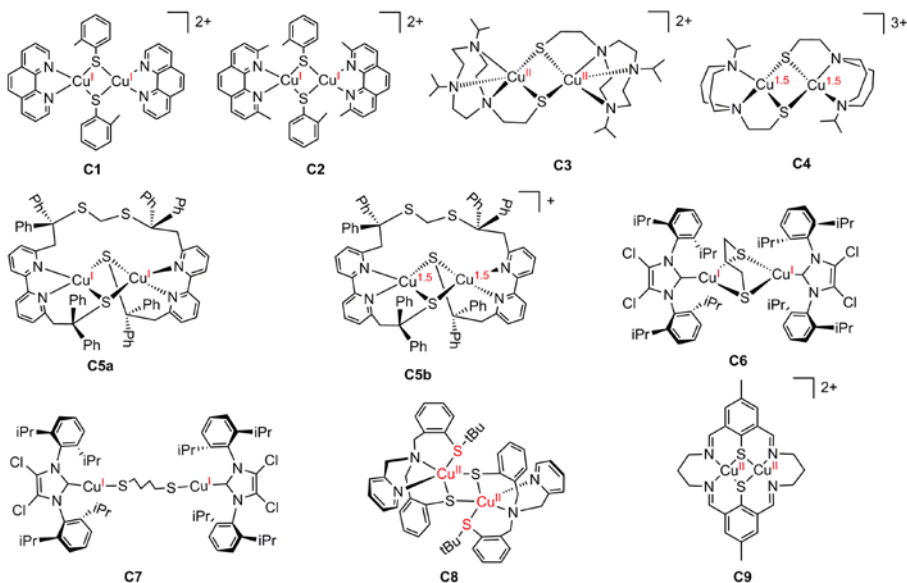


The first dinuclear Cu(II) dithiolate compound (**C3**) was reported by Tolman and coworkers [16]. It was shown that compound **C3** presented the desired [Cu₂S₂] diamond core with two Cu(II) centers bridged by two thiolate groups. The S···S distance in **C3** is 3.093(2) Å, which is much longer than a disulfide bond (~ 2.0 Å), indicating that a Cu(II) thiolate rather than a Cu(I) disulfide compound was obtained. The Cu···Cu distance is 3.340(2) Å, which is much longer than the Cu···Cu distance in Cu_A active sites, accounting for the absence of direct interaction between two copper ions. Interestingly, this compound showed different spectroscopic characteristics in different solvents, which is thought to be related to an equilibrium between mononuclear and dinuclear Cu(II) compounds in these solvents.

Following this work, an unprecedented mixed-valent dicopper(I,II) dithiolate compound **C4** was reported by the same group [19]. The ratio of the ligand and Cu(II) salt (3:2) used in the synthesis is essential for obtaining this mixed-valent compound, as the extra ligand acts as reducing agent for one of the Cu(II) ions. Compound **C4** shows a fully delocalized, mixed-valent dicopper diamond core [Cu^{1.5}S₂] with a Cu···Cu distance of 2.9306(9) Å. This shorter Cu···Cu distance compared to **C3** suggests that the two copper ions may have a direct interaction. This assumption was later confirmed by the observation of a seven-line hyperfine splitting pattern in the EPR spectra of **C4**. Overall, this is the first mimic that closely replicates the geometry

and spectroscopic properties of the resting-state of the Cu_A active site, also including delocalization of the unpaired electron over two copper ions. However, electrochemical reduction of compound **C4** did not yield the desired dicopper(I) compound.

In 2011, Duboc et al. reported the two dinuclear copper dithiolate compounds **C5a** and **C5b**, which were characterized by X-ray crystallography, UV-vis and EPR spectroscopy [20]. Crystal structures show that the two copper ions in both compounds are in trigonal-pyramidal geometries with a [Cu₂S₂] diamond core. Compound **C5a** contains two Cu(I) centers, whereas **C5b** is mixed-valent, containing a Cu(I) and a Cu(II) center. The Cu...Cu distance in **C5a** is 2.6378(14) Å, which is much shorter than in **C5b** (2.9349(11) Å). EPR spectra of **C5b** revealed a seven-line hyperfine splitting pattern, similar to the EPR spectra of Cu_A active sites.



Scheme 1.2. Reported synthetic models as mimics of the Cu_A active site. References are provided in the text.

The mimics reported by Duboc are based on “N₂S₂”-type ligands, resulting in coordination geometries different from that of the copper ions in Cu_A active sites, which are in “NS₂” environments with an additional methionine or a backbone carbonyl group at a longer distance. The additional nitrogen donor in the mimics results in different geometries of the copper centers compared to those in Cu_A. Hence, further study of synthetic models for Cu_A active sites centered on reducing the coordination number of the copper centers. In the last few years, Warren et al.

reported the synthesis of a dicopper(I) dithiolate compound **C6** containing a carbene ligand and 1,3-propanedithiolate as a bridging ligand [21]. The length of the dithiolate ligand is crucial for generating the desired $[\text{Cu}_2\text{S}_2]$ diamond core; the dinuclear **C7** was formed instead with the longer 1,4-butanedithiolate ligand. The $\text{Cu}\cdots\text{Cu}$ distance in **C6** is 2.8387(15) Å. Oxidation of compound **C6** led to the formation of the desired mixed-valent dicopper(I,II) dithiolate compound, which shows EPR spectra similar to that of Cu_A active sites. Unfortunately, a crystal structure of the oxidized compound could not be obtained.

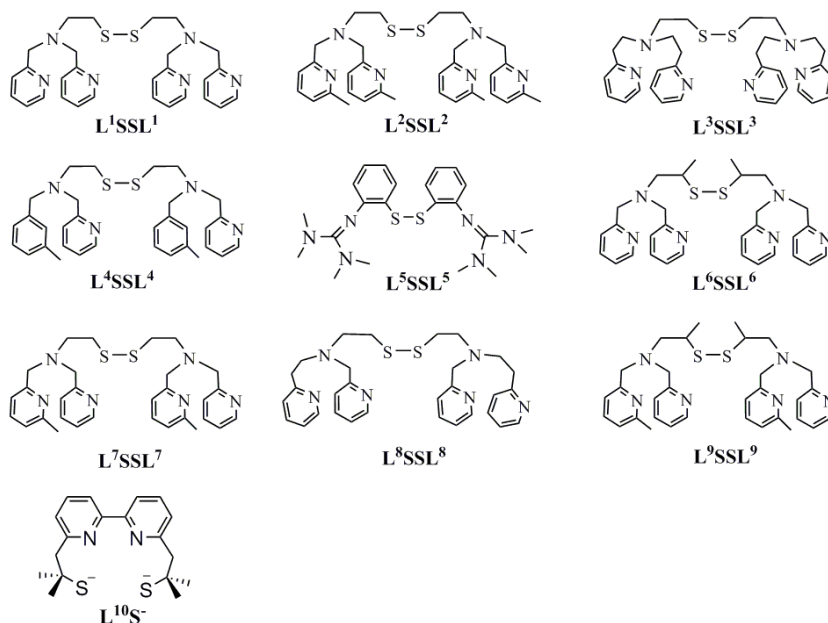
The two other examples **C8** and **C9** with diamond core structures (scheme 1.2) are not further discussed in [22, 23].

1.4 Redox interconversion between metal thiolate/disulfide compounds

1.4.1 General introduction

The study of synthetic models of Cu_A active sites provides useful information on the structure and spectroscopic properties of these copper proteins; however, the operation principle of the electron-transfer reactions occurring in metalloenzymes is still not well understood [24]. In the last decades, several mechanisms have been proposed for the electron-transfer reactions occurring in copper proteins [25-27]. For instance, copper delivery to the Cu_A site of cytochrome c oxidase (CcO) involves Sco proteins; the potential mechanism has been proposed to involve thiolate–disulfide interconversion of two cysteine residues [28, 29]. Metallothionein $\text{Zn}_7\text{MT-3}$ has been reported to exchange its Zn(II) ions with Cu(II) centers of amyloid- β peptide ($\text{CuA}\beta$). During this exchange four Cu(II) ions are reduced to Cu(I) by four cysteine thiolate groups in MT-3 with the formation of two disulfide bonds [28, 30].

The formation of Cu(I) disulfide compounds from the reaction of thiolate ligands with Cu(II) salts provides a potential chemical strategy to investigate the thiolate–disulfide interconversion reaction. In the last decade, a number of dinuclear Cu(II) thiolate compounds have been synthesized, and the redox interconversion of these Cu(II) thiolate compounds to their isomeric Cu(I) disulfide compounds have been investigated (scheme 1.3). Until now, several triggers have been found to influence the thiolate/disulfide interconversion, such as the addition of halide ions or protons, as well as changes in temperature, or the polarity of the solvents used. In addition, also the ligand structure has a distinct influence on the redox interconversion reaction.



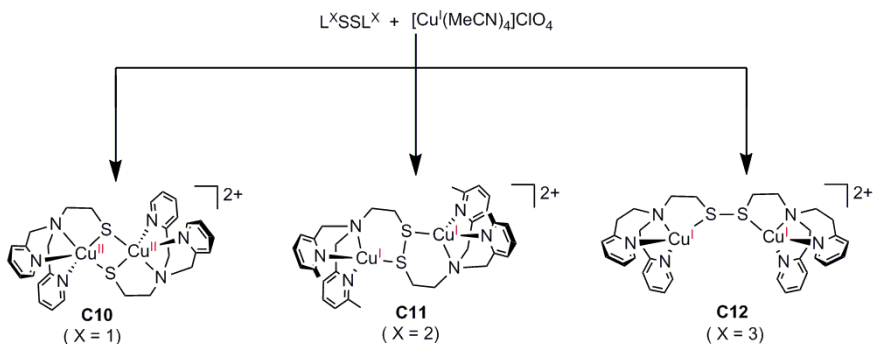
Scheme 1.3. Reported ligands for the synthesis of Cu(II) thiolate or Cu(I) disulfide compounds.

1.4.2 Ligand-induced redox interconversion

Thiolate ligands proved to be efficient reductants for the synthesis of Cu(I) compounds [16, 31]. As discussed above, the ratio of thiolate ligand and Cu(II) salt is crucial to yield the mixed-valent compound **C4** [19]. Another mononuclear Cu(I) compound was synthesized from a Cu(II) salt, with the ligand acting as the reductant [31]. The first paper reporting the synthesis of dinuclear Cu(II) thiolate and Cu(I) disulfide compounds starting from disulfide ligands was published by the group of Itoh in 2001 (Scheme 1.4) [32]. Slight modification of the structure of the disulfide ligand yielded different compounds: use of L¹SSL¹ resulted in the Cu^{II} μ -thiolate compound **C10**, L²SSL² resulted in the Cu^I *transoid*-disulfide compound **C11**, whereas L³SSL³ yielded Cu^I *cisoid*-disulfide compound **C12**.

Compound **C10** reveals a [Cu₂S₂] diamond core with a Cu...Cu distance of 2.96 Å, which is shorter than that in **C3** [16], but similar to that in the mixed-valent dicopper(I,II) compound **C4** [19]. Compound **C10** is EPR silent, indicating a strong antiferromagnetic interaction between the Cu(II) ions. The *transoid*-disulfide dicopper(I) compound **C11** was formed when the ligand L²SSL² was employed. The copper ions in **C11** are in a trigonal pyramidal geometry with a long Cu...Cu distance of 5.16 Å; the two Cu(I) ions are in *transoid* positions relative to the disulfide bond. A

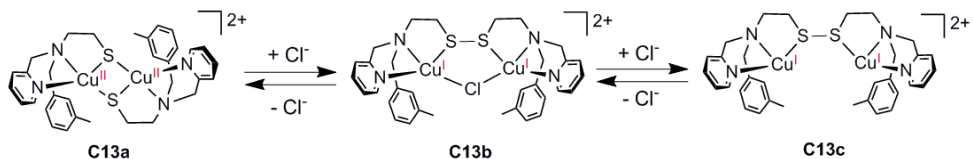
cisoid disulfide Cu(I) compound **C12** was formed when the ligand L³SSL³ was used. The copper ions in **C12** are also in a trigonal pyramidal geometry, with a shorter Cu...Cu distance of 3.91 Å. UV-vis and EPR spectra of both compounds **C11** and **C12** do not present any characteristic bands, in agreement with the presence of Cu(I) rather than Cu(II) centers. Generally, a *transoid* structure as found in **C11** can be regarded as a potential intermediate in the conversion of a *cisoid* structure present in **C12** to the dithiolate structure as present in **C10**, and vice versa.



Scheme 1.4. Schematic representation of the three copper compounds that were obtained from the reaction of three similar disulfide ligands with Cu(I) salt.

1.4.3 Halogen-induced redox interconversion

Treatment of the disulfide ligand L⁴SSL⁴ with two equivalents of [Cu^I(CH₃CN)₄](ClO₄) in acetone under inert atmosphere yields the dark brown-colored bis(μ-thiolato)-dicopper(II) compound **C13a** [33]. The structure of **C13a** shows that both Cu(II) ions are in a square-pyramidal geometry with a S...S distance of 3.13 Å, which is much longer than in a disulfide S–S bond. The Cu...Cu distance is around 2.80 Å, indicating a potential interaction between the two Cu(II) ions.

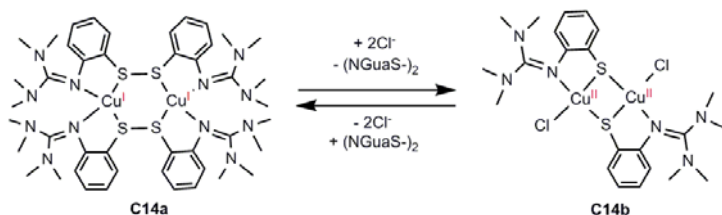


Scheme 1.5. Schematic representation of the redox interconversion between dicopper(II) thiolate **C13a** and disulfide dicopper(I) compound **C13c** mediated by chloride ion.

Upon addition of one equivalent of chloride anion to a dichloromethane solution of **C13a**, the dicopper(I) disulfide compound **C13b** was obtained, which further converted to **C13c** upon addition of another equivalent of chloride (scheme 1.5). The

removal of chloride ions from **C13c** led to the regeneration of compound **C13a** via the intermediate **C13b**.

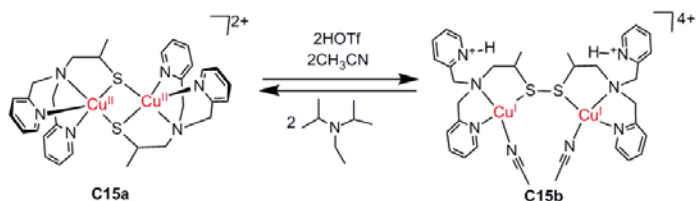
Another example of halogen-induced redox interconversion was reported by the group of Henkel in 2012 (Scheme 1.6) [34]. The Cu(I) disulfide compound **C14a** was synthesized from the disulfide ligand L⁵SSL⁵, in which the Cu(I) ions are in four-coordinate tetrahedral geometries. In contrast to the results reported by Itoh, addition of chloride anions (in the form of Et₄NCl) to the dichloromethane solution of compound **C14a** led to the formation of the dicopper(II) dithiolate compound **C14b** with the loss of one of the ligands. Removal of chloride anions from **C14b** in the presence of additional ligand resulted in the regeneration of **C14a**. Further experiments showed that this interconversion can also be triggered by bromide anions.



Scheme 1.6. Schematic representation of the redox interconversion of compounds **C14a** and **C14b** induced by chloride ions.

1.4.4 Solvent- and proton-induced redox interconversion

Already in 2004, the group of Itoh reported that either a Cu(I) disulfide or the corresponding Cu(II) thiolate compound was formed depending on the coordinating abilities of the used solvent [35]. Recently, the group of Stack reported the Cu(II) thiolate compound **C15a** to be formed from a reaction of the ligand L⁶SSL⁶ with a Cu(I) salt. (Scheme 1.7) [36]. UV-vis combined with X-ray absorption spectroscopy (XAS) showed that in acetonitrile solution the Cu(I) species **C15b** is formed, whereas the Cu(II) compound **C15a** is the dominant species in less-coordinating solvents such as acetone. Addition of two equivalents of trifluoromethanesulfonic acid (HOTf) into a solution of **C15a** in acetonitrile leads to full conversion of the Cu(II) thiolate compound to the corresponding Cu(I) disulfide compound **C15b**, and this reaction can be reversed by addition of a base such as N,N-diisopropylethylamine (DIPEA). This redox reaction also occurs for the disulfide ligand L¹SSL¹ in presence of copper salts.

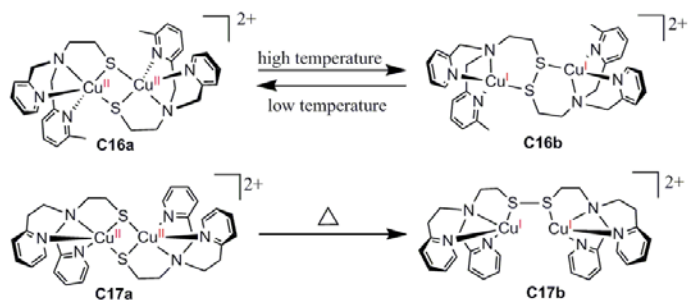


Scheme 1.7. Schematic drawing of the redox interconversion between a Cu^{II} thiolate species to a Cu^I disulfide species upon addition of HOTf/DIPEA.

Recently, a similar study was conducted by our group using the disulfide ligands L⁶SSL⁶, L⁷SSL⁷, L⁸SSL⁸, and L⁹SSL⁹ [37, 38]. It was found that use of polar solvents such as acetonitrile generally results in the formation of Cu(I) disulfide compounds, whereas the use of less polar solvents like acetone stabilize the corresponding Cu(II) thiolate compounds. In contrast to the study reported by the group of Stack, it was found that addition of acid into a solution of the Cu(II) thiolate compound of the ligand L⁶SSL⁶ leads to the protonation and dissociation of the disulfide ligand with the release of Cu(I) ions. This result was corroborated by DFT calculations.

1.4.5 Temperature-induced redox interconversion

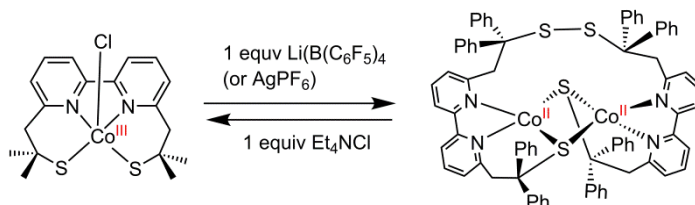
The first temperature-induced redox interconversion between Cu(II) thiolate and Cu(I) disulfide compounds was reported by our group in 2014 [38]. Compound **C16a** obtained from L⁷SSL⁷ was shown to undergo solvent-dependent redox interconversion to **C16b**, but in addition showed a temperature-induced redox interconversion. At low temperatures in methanolic solutions, the Cu(II) compound **C16a** is the dominant species, whereas at higher temperatures, the Cu(I) disulfide **C16b** is predominant. However, this interconversion is only reversible below room temperature; at higher temperatures a Cu(I) species is irreversibly formed, presumably with a transoid conformation. Furthermore, Cu(II) compound **C17a** was obtained from the disulfide ligand L⁸SSL⁸ in methanolic solution [38]. Increasing the temperature of the solution containing compound **C17a** until reflux led to the formation of Cu(I) disulfide compound **C17b**, but reduction of the temperature did not lead to recovery of **C17a**, as confirmed by X-ray structure and UV-vis spectroscopy. Apparently, **C17a** is a kinetic product, which is converted to the thermodynamic Cu(I) disulfide compound **C17b** at higher temperatures.



Scheme 1.8. Schematic drawing of the redox interconversion between a Cu(II) thiolate species to a Cu(I) disulfide species triggered by temperature.

1.4.6 Redox interconversion between cobalt thiolate/disulfide compounds

In the last few years, the study of redox interconversion reactions between metal thiolate and disulfide compounds has gradually switched from copper to other first-row transition metals. The first examples of the interconversion reaction between Co(III) thiolate and Co(II) disulfide compound was reported by the group of Duboc [39, 40]. The unusual triplet-spin ($S = 1$) Co(III) thiolate compound **C18a** was synthesized electrochemically. It was shown that removal of chloride anions from this Co(III) compound by addition of $\text{Li}(\text{B}(\text{C}_6\text{F}_5)_4)$ or AgPF_6 resulted in the formation of the Co(II) disulfide compound **C18b**, whereas addition of chloride anions to compound **C18b** led to the regeneration of **C18a**. Similar reactivity was reported for the Mn(III) thiolate compound based on the same ligand [41].



Scheme 1.9. Schematic representation of the redox interconversion between mononuclear Co(III) compound **C18a** and dinuclear Co(II) compound **C18b** induced by removal or addition of chloride ions.

1.5 Aim and outline of this thesis

The synthesis of Cu(II) thiolate compounds and the investigation of their redox interconversion to the corresponding Cu(I) disulfide compounds has been extensively studied in the last decade, providing improved understanding of the mechanism of electron-transfer reactions occurring in metalloenzymes. However, until now, only limited research focused on metals other than copper, whereas especially cobalt, iron

and manganese redox processes may be similarly important. The goal of the research described in this thesis is to extend the study of redox interconversion reactions from copper to other first-row transition metal ions. In Chapter 1, several types of metalloenzymes are introduced, which are involved in electron-transfer reactions in biological systems. An overview is provided of synthetic models of Cu_A active sites, including their structural and spectroscopic properties. Finally, the state-of-the-art in redox interconversion reactions between metal thiolate and disulfide compounds has been described.

In Chapter 2, our investigation is reported of redox interconversion between Co(II) disulfide and Co(III) thiolate compounds, induced by chloride anions. The formation of mononuclear rather than dinuclear Co(III) compounds is discussed, and supported by DFT calculations. Moreover, the possible formation of iron(II) disulfide and iron(III) thiolate compounds has been explored and the results are compared with that of the cobalt compounds.

In Chapter 3, the redox interconversion reaction between Co(II) disulfide and Co(III) thiolate compounds tuned by solvents is described. In contrast to the redox interconversion between Cu(II) thiolate and Cu(I) disulfide compounds, Co(III) compounds are formed in coordinating solvents such as acetonitrile, whereas Co(II) disulfide compounds are obtained in weakly- or non-coordinating solvents like acetone and dichloromethane.

The study of the oxidation of Co(II) and Fe(II) disulfide compounds is described in Chapter 4. Oxidation of a Co(II) disulfide compound with dihydrogen peroxide yielded a Co(III) sulfinate compound as the final product. It was found that a Co(III) sulfenato derivative is generated as an intermediate, as confirmed by X-ray structure and ESI-MS spectrometry. Oxidation of an iron(II) disulfide compound with dihydrogen peroxide resulted in the formation of an iron(III) sulfonato compound, and studies at low temperature indicated that sulfenato and sulfinato compounds are generated as intermediates.

In Chapter 5, the synthesis and characterization of a novel tetranuclear fluorido-bridged iron(II) compound is described. This compound was obtained from a reaction of a disulfide ligand with iron(II) tetrafluoridoborate, during which the iron(II) center abstracts fluoride ions from the tetrafluoridoborate anion.

The synthesis and characterization of a series of mononuclear transition metal compounds is described in Chapter 6. Their structure and spectroscopic properties are compared with those of related dinuclear compounds.

Finally, in Chapter 7 a summary is presented of the main findings described in this thesis, followed by an outlook, and suggestions for further research in this field is given.

Parts of this thesis have been published (Chapters 2, 4, 5 and 6) [42-45], or is in preparation for submission (Chapter 3).

1.6 References

- [1] M. Wikström, V. Sharma, V.R. Kaila, J.P. Hosler, G. Hummer, *Chem. Rev.*, 115 (2015) 2196-2221.
- [2] J.L. Boer, S.B. Mulrooney, R.P. Hausinger, *Arch. Biochem. Biophys.*, 544 (2014) 142-152.
- [3] W. Nam, *Acc. Chem. Res.*, 40 (2007) 465-465.
- [4] M. Fontecave, J.-L. Pierre, *Coord. Chem. Rev.*, 170 (1998) 125-140.
- [5] R. Cammack, K. Rao, D. Hall, *Biosystems*, 14 (1981) 57-80.
- [6] J. Liu, S. Chakraborty, P. Hosseinzadeh, Y. Yu, S. Tian, I. Petrik, A. Bhagi, Y. Lu, *Chem. Rev.*, 114 (2014) 4366-4469.
- [7] L.M. Mirica, X. Ottenwaelder, T.D.P. Stack, *Chem. Rev.*, 104 (2004) 1013-1046.
- [8] E.I. Solomon, D.W. Randall, T. Glaser, *Coord. Chem. Rev.*, 200 (2000) 595-632.
- [9] R. Malkin, B.G. Malmström, *Adv. Enzymol. Relat. Areas Mol. Biol.*, 33 (1970) 177-244.
- [10] D.W. Randall, S.D. George, B. Hedman, K.O. Hodgson, K. Fujisawa, E.I. Solomon, *J. Am. Chem. Soc.*, 122 (2000) 11620-11631.
- [11] H.B. Gray, *Chem. Soc. Rev.*, 15 (1986) 17-30.
- [12] H.B. Gray, J.R. Winkler, *Proc. Natl. Acad. Sci. U.S.A.*, 102 (2005) 3534-3539.
- [13] J. Farrar, F. Neese, P. Lappalainen, P. Kroneck, M. Saraste, W. Zumft, A. Thomson, *J. Am. Chem. Soc.*, 118 (1996) 11501-11514.
- [14] C. Dennison, *Coord. Chem. Rev.*, 249 (2005) 3025-3054.
- [15] Y. Lu, *Electron transfer: cupredoxins*, Elsevier, Amsterdam, 2003.
- [16] R.P. Houser, J.A. Halfen, V.G. Young, N.J. Blackburn, W.B. Tolman, *J. Am. Chem. Soc.*, 117 (1995) 10745-10746.
- [17] R.K. Chadha, R. Kumar, D.G. Tuck, *Can. J. Chem.*, 65 (1987) 1336-1342.
- [18] A.F. Stange, E. Waldhör, M. Moscherosch, W. Kaim, *Z. Naturforsch. B Chem. Sci.*, 50 (1995) 115-122.
- [19] R.P. Houser, V.G. Young, W.B. Tolman, *J. Am. Chem. Soc.*, 118 (1996) 2101-2102.
- [20] M. Gennari, J. Pécaut, S. DeBeer, F. Neese, M.N. Collomb, C. Duboc, *Angew. Chem. Int. Ed.*, 50 (2011) 5662-5666.
- [21] S. Zhang, T.H. Warren, *Chem. Sci.*, 4 (2013) 1786-1792.
- [22] N.D. Branscombe, A.J. Blake, A. Marin-Becerra, W.S. Li, S. Parsons, L. Ruiz-Ramirez, M. Schröder, *Chem. Commun.*, (1996) 2573-2574.
- [23] W. Rammal, C. Belle, C. Béguin, C. Duboc, C. Philouze, J.-L. Pierre, L. Le Pape, S. Bertaina, E. Saint-Aman, S. Torelli, *Inorg. Chem.*, 45 (2006) 10355-10362.
- [24] C. Jacob, G.I. Giles, N.M. Giles, H. Sies, *Angew. Chem. Int. Ed.*, 42 (2003) 4742-4758.
- [25] R. Singh, G.M. Whitesides, *Thiol-disulfide interchange*, John Wiley & Sons, Inc.: Chichester, UK, 1993.
- [26] W. Maret, *Proc. Natl. Acad. Sci. U.S.A.*, 91 (1994) 237-241.
- [27] R.D. Bach, O. Dmitrenko, C. Thorpe, *J. Org. Chem.*, 73 (2008) 12-21.
- [28] L. Banci, I. Bertini, G. Cavallaro, S. Ciofi-Baffoni, *FEBS J.*, 278 (2011) 2244-2262.
- [29] T.R. Cawthorn, B.E. Poulsen, D.E. Davidson, D. Andrews, B.C. Hill, *Biochem*, 48 (2009) 4448-4454.

- [30] J.T. Pedersen, C. Hureau, L. Hemmingsen, N.H. Heegaard, J. Østergaard, M. Vašák, P. Faller, *Biochem.* 51 (2012) 1697-1706.
- [31] T. Ohta, T. Tachiyama, K. Yoshizawa, T. Yamabe, T. Uchida, T. Kitagawa, *Inorg. Chem.*, 39 (2000) 4358-4369.
- [32] S. Itoh, M. Nagagawa, S. Fukuzumi, *J. Am. Chem. Soc.*, 123 (2001) 4087-4088.
- [33] Y. Ueno, Y. Tachi, S. Itoh, *J. Am. Chem. Soc.*, 124 (2002) 12428-12429.
- [34] A. Neuba, R. Haase, W. Meyer-Klaucke, U. Flörke, G. Henkel, *Angew. Chem. Int. Ed.*, 51 (2012) 1714-1718.
- [35] T. Osako, Y. Ueno, Y. Tachi, S. Itoh, *Inorg. Chem.*, 43 (2004) 6516-6518.
- [36] A.M. Thomas, B.L. Lin, E.C. Wasinger, T.D.P. Stack, *J. Am. Chem. Soc.*, 135 (2013) 18912-18919.
- [37] E.C.M. Ording-Wenker, M. van der Plas, M.A. Siegler, C. Fonseca Guerra, E. Bouwman, *Chem. Eur. J.*, 20 (2014) 16913-16921.
- [38] E.C.M. Ording-Wenker, M. van der Plas, M.A. Siegler, S. Bonnet, F.M. Bickelhaupt, C. Fonseca Guerra, E. Bouwman, *Inorg. Chem.*, 53 (2014) 8494-8504.
- [39] M. Gennari, B. Gerey, N. Hall, J. Pécaut, M.N. Collomb, M. Rouzières, R. Clérac, M. Orio, C. Duboc, *Angew. Chem. Int. Ed.*, 53 (2014) 5318-5321.
- [40] M. Gennari, B. Gerey, N. Hall, J. Pecaut, H. Vezin, M.-N. Collomb, M. Orio, C. Duboc, *Dalton Trans.*, 41 (2012) 12586-12594.
- [41] M. Gennari, D. Brazzolotto, S. Yu, J. Pécaut, C. Philouze, M. Rouzières, R. Clérac, M. Orio, C. Duboc, *Chem. Eur. J.*, 21 (2015) 18770-18778.
- [42] F. Jiang, M.A. Siegler, X. Sun, L. Jiang, C. Fonseca Guerra, E. Bouwman, *Inorg. Chem.*, 57 (2018) 8796-8805.
- [43] F. Jiang, M.A. Siegler, E. Bouwman, *Inorg. Chem. Commun.*, 94 (2018) 53-56.
- [44] F. Jiang, M.A. Siegler, E. Bouwman, *Inorg. Chim. Acta*, 486 (2018) 135-140.
- [45] F. Jiang, M.A. Siegler, E. Bouwman, *Eur. J. Inorg. Chem.*, (2018) in press.

Chapter 2

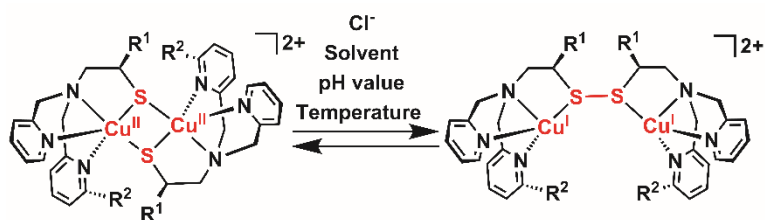
Redox Interconversion between Cobalt(III) Thiolate and Cobalt(II) Disulfide Compounds

The redox interconversion between Co(III) thiolate and Co(II) disulfide compounds has been investigated experimentally and computationally. Reactions of cobalt(II) salts with the disulfide ligand L^1SSL^1 (L^1SSL^1 = di-2-(bis(2-pyridylmethyl)amino)-ethyl disulfide) result in the formation of either the high-spin cobalt(II) disulfide compound $[Co^{II}_2(L^1SSL^1)Cl_4]$, or a low-spin, octahedral cobalt(III) thiolate compound, such as $[Co^{III}(L^1S)(MeCN)_2](BF_4)_2$. Addition of thiocyanate anions to a solution containing the latter compound yielded crystals of $[Co^{III}(L^1S)(NCS)_2]$. The addition of chloride ions to a solution of $[Co^{III}(L^1S)(MeCN)_2](BF_4)_2$ in acetonitrile results in conversion of the cobalt(III) thiolate compound to the cobalt(II) disulfide compound $[Co^{II}_2(L^1SSL^1)Cl_4]$, as monitored with UV-vis spectroscopy; subsequent addition of $AgBF_4$ regenerates the Co(III) compound. Computational studies show that exchange by a chloride anion of the coordinated acetonitrile molecule or thiocyanate anion in compounds $[Co^{III}(L^1S)(MeCN)_2]^{2+}$ and $[Co^{III}(L^1S)(NCS)_2]$ induces a change in the character of the highest occupied molecular orbitals, showing a decrease of the contribution of the p orbital on sulfur and an increase of the d orbital on cobalt. As a comparison, the synthesis of iron compounds was undertaken. X-ray crystallography revealed that structure of the dinuclear iron(II) disulfide compound $[Fe^{II}_2(L^1SSL^1)Cl_4]$ is different from that of the cobalt(II) compound $[Co^{II}_2(L^1SSL^1)Cl_4]$. In contrast to cobalt, reaction of the ligand L^1SSL^1 with $[Fe(MeCN)_6](BF_4)_2$ did not yield the expected Fe(III) thiolate compound. This work is an unprecedented example of redox interconversion between a high-spin Co(II) disulfide compound and a low-spin Co(III) thiolate compound triggered by the nature of the anion.

This chapter has been published as a full paper: Feng Jiang, Maxime A. Siegler, Xiaobo Sun, Lin Jiang, Célia Fonseca Guerra, and Elisabeth Bouwman, *Inorg. Chem.* 2018, 57, 8796-8805

2.1 Introduction

Sulfur-containing metalloenzymes are ubiquitous in biological systems and play fundamental roles in electron-transfer reactions including oxygen transport, nitrite reduction, and the synthesis of neurotransmitters [1-4]. A small number of these metalloenzymes involve thiolate/disulfide interconversion, related to the uptake or release of the metal ions [5-7]. For instance, copper delivery to the Cu_A site of cytochrome c oxidase (CcO) involves Sco proteins, and the potential operation principle has been suggested to involve thiolate/disulfide interconversion of two cysteine residues [8, 9]. Metallothionein Zn₇MT-3 has been reported to exchange its Zn(II) ions with Cu(II) centers of amyloid- β peptide (CuA β). During this exchange four Cu(II) ions are reduced to Cu(I) by four cysteine thiolate groups in MT-3 with the formation of two disulfide bonds [10, 11]. The essence of the thiolate to disulfide oxidation of cysteines is an electron that shuttles from the cysteine thiolate sulfur to the metal ion in a high oxidation state, after which a disulfide is formed and a geometry change takes place of the reduced metal center in the active site. However, to the best of our knowledge, the exact mechanism is not well understood of this interconversion in biological systems [1]. In the last decades, this phenomenon inspired coordination chemists to synthesize metal thiolate compounds and study their redox interconversion. Since the first publication of a mixed-valence (Cu^{II}Cu^I) thiolate compound [12, 13], considerable efforts were put in the synthesis and characterization of Cu(II) thiolate compounds, and the investigation of their redox interconversion to the isomeric Cu(I) disulfide compounds [14-20]. The chloride-dependent redox interconversion between Cu(II) thiolate and Cu(I) disulfide compounds was first reported by Itoh et al. [20], followed later by the group of Henkel [15]. In recent years, our group further investigated the effect of temperature and solvents on the thiolate/disulfide redox interconversion of copper compounds [18]. Up until now, several triggers have been reported to influence the copper thiolate/disulfide redox interconversion like the addition of halide ions [15, 20] or protons [16, 19], as well as changes in temperature [18], and the polarity of solvents [18]. In addition, also ligand structure has a distinct influence on the redox interconversion (Scheme 2.1) [14, 21].



Scheme 2.1. Reported redox interconversion between copper(II) thiolate and copper(I) disulfide compounds triggered by different reaction conditions ($R^1, R^2 = \text{H, CH}_3$).

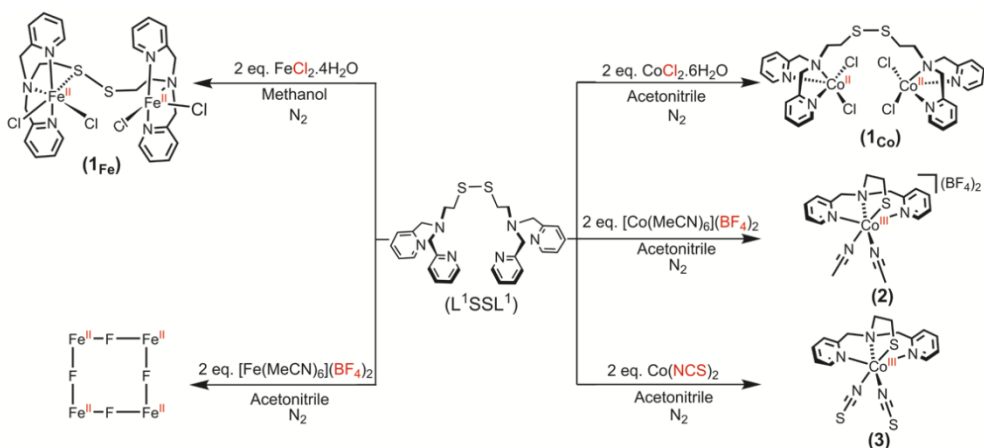
As electron-transfer reactions also take place in metalloenzymes containing metal centers other than copper [22, 23], all of this impressive work inspired us to study whether the thiolate/disulfide redox interconversion could occur for complexes of metal ions like cobalt or iron. Duboc et al. reported the electrochemical synthesis of a triplet-spin state ($S = 1$) Co(III) thiolate compound and its redox interconversion to a Co(II) disulfide compound triggered by the removal of chloride ions [24]. Herein, we report a low-spin ($S = 0$) Co(III) thiolate compound, which was formed directly from a reaction of a cobalt(II) salt with ligand di-2-(bis(2-pyridylmethyl)amino)-ethyl disulfide ($L^1\text{SSL}^1$). The redox interconversion of this Co(III) thiolate compound and the related Co(II) disulfide compound has been investigated. For comparison, the reaction of disulfide ligand $L^1\text{SSL}^1$ with iron(II) salts has been explored. This study not only provides a chemical perspective into the operation principle of electron transfer in metalloenzymes, but also extends the research on thiolate/disulfide interconversion to other metal centers.

2.2 Results

2.2.1 Synthesis and characterization of the cobalt and iron compounds

Ligand di-2-(bis(2-pyridylmethyl)amino)ethyl disulfide ($L^1\text{SSL}^1$) was synthesized using the reported procedure [20]. The coordination compounds were prepared following the procedure shown in Scheme 2.2. All the reactions were carried out under an oxygen-free atmosphere at room temperature, using standard Schlenk-line and glovebox techniques. Addition of 2 equiv of $\text{CoCl}_2 \cdot 6\text{H}_2\text{O}$ to ligand $L^1\text{SSL}^1$ dissolved in acetonitrile led to the formation of a purple solution, from which the compound $[\text{Co}^{\text{II}}_2(L^1\text{SSL}^1)\text{Cl}_4]$ (**1_{Co}**) was isolated in a yield of 64%. Addition of 2 equiv of $\text{FeCl}_2 \cdot 4\text{H}_2\text{O}$ to ligand $L^1\text{SSL}^1$ dissolved in methanol led to the formation of a greenish yellow solution, from which the compound $[\text{Fe}^{\text{II}}_2(L^1\text{SSL}^1)\text{Cl}_4]$ (**1_{Fe}**) was isolated in a yield of 62%. The addition of 2 equiv of $[\text{Co}(\text{MeCN})_6](\text{BF}_4)_2$ to ligand $L^1\text{SSL}^1$ dissolved in acetonitrile resulted in a brown solution from which a compound with the assumed formula $[\text{Co}^{\text{III}}(L^1\text{S})(\text{MeCN})_2](\text{BF}_4)_2$ (**2**) was isolated as a brown oily material (in a yield

of 65%). Reaction of 2 equiv of $\text{Co}(\text{NCS})_2$ with 1 equiv of ligand L^1SSL^1 dissolved in acetonitrile provided a brown precipitate of the Co(III) compound $[\text{Co}^{\text{III}}(\text{L}^1\text{S})(\text{NCS})_2]$ (**3**) in a yield of 70%. In contrast, reaction of 2 equiv of $[\text{Fe}(\text{MeCN})_6](\text{BF}_4)_2$ with 1 equiv of ligand L^1SSL^1 dissolved in acetonitrile did not result in the anticipated Fe(III) thiolate compound but instead yielded a tetranuclear iron(II) fluoride compound [25]. The cobalt and iron compounds were characterized by using ^1H NMR, UV-vis, Raman, and IR spectroscopy, electrospray ionization mass spectrometry (ESI-MS), elemental analysis and single crystal X-ray crystallography.



Scheme 2.2. Reactions of ligand L^1SSL^1 with different cobalt(II) and iron(II) salts.

ESI-MS spectra of purple compound **1_{Co}** dissolved in acetonitrile show a dominant peak (m/z) at 740.8 corresponding to the fragment $[\text{Co}^{\text{II}}_2(\text{L}^1\text{SSL}^1)\text{Cl}_3]^+$ (Figure AI.1). The ^1H NMR spectrum of the compound in dimethyl sulfoxide- d_6 shows broad resonances with shifts down to around 75 ppm (Figure AI.2), indicative of a paramagnetic compound. The effective magnetic moment of compound **1_{Co}** was estimated using Evans' method in dimethyl sulfoxide solution at 20 °C, revealing a μ_{eff} of 6.53 μ_{B} [26, 27]. This value is in agreement with two (weakly interacting) high-spin Co(II) centers (a value of 6.93 μ_{B} is expected for two isolated $S = 3/2$ cobalt(II) ions). ESI-MS spectra of compound **1_{Fe}** dissolved in methanol present a peak (m/z) at 349.1 corresponding to the dicationic species $[\text{Fe}^{\text{II}}_2(\text{L}^1\text{SSL}^1)\text{Cl}_2]^{2+}$ (Figure AI.3). The effective magnetic moment of **1_{Fe}** determined in methanol solution at 20 °C is in agreement with the presence of two high-spin Fe(II) centers in this compound ($\mu_{\text{eff}} = 7.67 \mu_{\text{B}}$; 8.94 μ_{B} is expected for two isolated $S = 2$ iron(II) centers). ESI-MS spectra of **2** dissolved in acetonitrile show a dominant peak (m/z) at 199.8 for the dicationic species $[\text{Co}^{\text{III}}(\text{L}^1\text{S})(\text{MeCN})_2]^{2+}$ (Figure AI.4). The ^1H NMR spectrum of brown compound **2** in acetonitrile- d_3 shows resonances in the diamagnetic region, consistent with the Co(III)

center in this compound being in a low-spin state (Figure AI.5). Similarly, the ^1H NMR spectrum of compound **3** in acetonitrile- d_3 shows resonances in the diamagnetic region (Figure AI.6). ESI-MS spectra of brown compound **3** dissolved in acetonitrile show a dominant peak (m/z) at 375.3 corresponding to the fragment $[\text{Co}^{\text{III}}(\text{L}^1\text{S})(\text{NCS})]^+$ (Figure AI.8).

Confocal Raman spectroscopy using a 476 nm laser was employed to study the disulfide bond in compounds **1_{Co}**, **1_{Fe}**, **2**, and disulfide ligand L^1SSL^1 . The obtained spectra are provided in Figures AI.9 and AI.10. The Raman spectrum of ligand L^1SSL^1 shows clear bands at 522 and 550 cm^{-1} , which are attributed to the S-S bond vibration[28]. These bands are retained in the Raman spectra of **1_{Co}** and **1_{Fe}** and as expected are not present in the spectrum of **2**.

Attempts were undertaken to investigate the electrochemical properties of the cobalt compounds **1_{Co}**, **2** and **3** using cyclic voltammetry in acetonitrile solutions with 0.1 M tetrabutylammonium hexafluoridophosphate as the supporting electrolyte (Figures AI.11–AI.14). Unfortunately, the compounds show multiple, poorly resolved redox waves, making it difficult to assign the various processes occurring in the solutions.

2.2.2 Description of the crystal structures

Single crystals of **1_{Co}** and **3** suitable for X-ray structure determination were obtained by vapor diffusion of diethyl ether and diisopropyl ether into acetonitrile solutions containing the compounds. Single crystals of **1_{Fe}** were grown by vapor diffusion of diethyl ether into a methanolic solution of the compound. Unfortunately, single crystals of **2** could not be obtained, but after 8 weeks from an acetonitrile solution of compound **2** kept in air, crystals were obtained of the cobalt(III) sulfinate compound $[\text{Co}^{\text{III}}(\text{L}^1\text{SO}_2)(\text{MeCN})_2](\text{BF}_4)_2$ (**2_{ox}**). The crystal structure of **2_{ox}** has been determined, and a projection of the structure is provided in Figure AI.15. Crystallographic and refinement data of the structures are provided in Table AI.1. A projection of the dinuclear structure of **1_{Co}** is shown in Figure 2.1a; relevant bond distances and angles are given in Tables 2.1 and 2.2. Compound **1_{Co}** crystallizes in the centrosymmetric space group $P\bar{1}$, with one dinuclear complex and one molecule of diethyl ether cocrystallized in the asymmetric unit. The two Co(II) ions are bound to three nitrogen atoms of the ligand and two chloride ions in distorted trigonal-bipyramidal geometries with the tertiary amine nitrogen and one of the chloride ions in the apical positions. The calculated τ values of the 5-coordinated geometries are 0.60 and 0.72 for Co1 and Co2, respectively. The τ value is determined from the two largest bond angles and is between 0 and 1, where 0 presents a perfect square-planar geometry, and 1 corresponds to an ideal trigonal-bipyramidal geometry [29]. The cobalt-to-

nitrogen bond lengths range from 2.064(2) to 2.311(2) Å. The sulfur atoms of the disulfide bond are noncoordinating; the Co-S distances are 5.9614(8) and 5.9371(7) Å. The distance between the two cobalt ions within the dinuclear structure is 8.1617(6) Å. Hydrogen-bond or stacking interactions are not present in this structure.

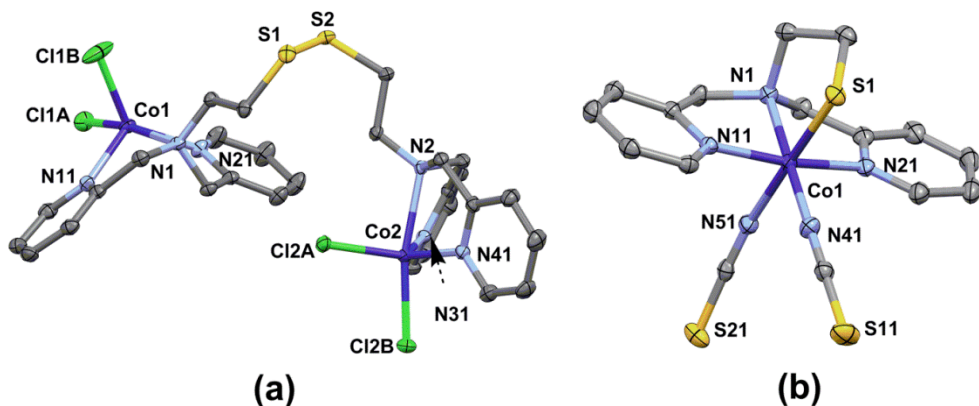


Figure 2.1. Displacement ellipsoid plots (50% probability level) of compounds (a) [Co^{II}₂(L¹SSL¹)Cl₄] (**1_{Co}**) and (b) major component of [Co^{III}(L¹S)(NCS)₂] (**3**) at 110(2) K. The lattice solvent molecule and hydrogen atoms are omitted for clarity. In the structure of **3**, partial oxidation of S1 was found (occupancy of the oxygen atom is 0.178(5)); a projection of the structure of the minor component is shown in Figure AI.16.

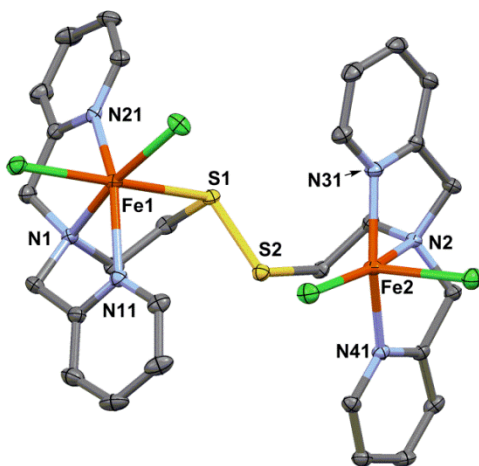


Figure 2.2. Displacement ellipsoid plots (50% probability level) of compound [Fe^{II}₂(L¹SSL¹)Cl₄] (**1_{Fe}**) at 110(2) K. The lattice solvent molecule and hydrogen atoms are omitted for clarity.

A projection of the dinuclear structure of **1_{Fe}** is shown in Figure 2.2; relevant bond distances and angles are presented in Table 2.3. Compound **1_{Fe}** crystallizes in the

monoclinic space group *Cc*, with two lattice methanol solvent molecules in the asymmetric unit. The two Fe(II) centers in this dinuclear compound are in different geometries. Fe1 is in an octahedral geometry coordinated by two chloride ions, one thioether sulfur and three nitrogen donor atoms of the ligand. The three nitrogen donors are bound in a meridional fashion and the two chloride ions are in mutual *cis* positions, one of them *trans* to the thioether sulfur and the other *trans* to the tertiary amine. Fe2 is bound to two chloride ions and three nitrogen donors of the ligand in a pseudo-square-pyramidal geometry with a τ value of 0.25 [29]; also in this case the three nitrogen donors are bound in a meridional fashion in the equatorial plane of the square pyramid. The Fe1–S1 bond length is 2.6925(8) Å, which is much shorter than the Fe2–S2 distance of 3.231(1) Å, but longer than the Fe–S bond distances in some reported thioether-Fe(II) compounds (ranging from 2.200 to 2.285 Å) [30–32]. The Fe–N bond distances range from 2.135(2) to 2.270(3) Å for both Fe^{II} ions, in agreement with a high-spin state ($S = 2$) of both iron(II) centers. One of the two lattice methanol molecules is hydrogen bound to one of the coordinated chloride ions. The crystal packing of this structure shows no stacking interactions.

A projection of the mononuclear structure of **3** is shown in Figure 2.1b; relevant bond distances and angles are presented in Tables 2.1 and 2.2. Compound **3** crystallizes in the orthorhombic space group *Pbca*. The Co(III) ion is coordinated by three nitrogen donor atoms, one thiolate sulfur donor of the tetradentate ligand, and two nitrogen atoms of the thiocyanate anions in an octahedral geometry. The three nitrogen atoms of the tetradentate ligand are bound in a meridional fashion. The Co–S bond length is 2.2355(5) Å, the bond distances between the cobalt center and the five nitrogen donor atoms range from 1.9011(16) to 1.9934(15) Å. The thiocyanate donor atom N51 is at a significantly larger distance than N41, indicative of a larger *trans* influence of the thiolate sulfur donor. When finalizing the refinement, a residual electron density peak of 2.47 e⁻ Å⁻³ was found at *ca.* 1.46 Å from S1. This peak is thought to arise from an oxygen atom, and its presence may result from the partial oxidation of S1 occurring during the crystallization process. Single crystals were obtained only after 3 weeks, during which time dioxygen must have diffused into the flask. Such a mono-oxygenated product likely is an intermediate in the oxidation of Co(III)-thiolate compound **2** to dioxygenated product **2_{ox}**, containing a sulfinate ligand (Figure AI.15). A projection of the compound [Co^{III}(L¹SO)(NCS)₂] (which is present with an occupancy factor of 0.178(5)) is given in Figure AI.16. Hydrogen-bond or stacking interactions are not present in this compound.

Table 2.1. Selected bond distances (Å) in the structures of compounds **1co** and **3**, as well as from the DFT-optimized structures of **1co**, **3**, cationic part of **2**, and the theoretical intermediates [Co^{III}(L¹S)(Cl)(NCS)] (**3a**), and [Co^{III}(L¹S)Cl₂] (**4**).^[a]

Bond	1co		2		3		3a		4	
	XRD	DFT	DFT	XRD	DFT	DFT	DFT	DFT	DFT	
Co1-N1	2.311(2)	2.392	1.942	1.9558(15)	1.947	1.947	1.947	1.950		
Co1-N11	2.064(2)	2.061	1.932	1.9235(14)	1.922	1.916	1.918			
Co1-N21	2.084(2)	2.057	1.932	1.9332(15)	1.924	1.917	1.923			
Co1-S1	5.9614(8)	6.004	2.206	2.2355(5)	2.211	2.208	2.202			
Co1-X1	2.3240(7)	2.330	1.857	1.9011(16)	1.855	1.851	2.261			
Co1-X2	2.2716(8)	2.291	1.951	1.9934(15)	1.934	2.356	2.360			

[a] X1 = Cl1A, X2 = Cl1B for **1co**; X1 = N41, X2 = N51 for **2** and **3**; X1 = N41, X2 = Cl1 for **3a**; X1 = Cl1A, X2 = Cl1B for **4**. All calculations were performed in the solvent.

Table 2.2. Selected bond angles (°) in the structures of **1co** and **3**.

1co		3			
Cl1A-Co1-Cl1B	100.76(3)	S1-Co1-N41	88.93(5)	N51-Co1-N11	88.17(6)
Cl1A-Co1-N1	169.92(6)	S1-Co1-N51	178.43(5)	N51-Co1-N21	91.59(6)
Cl1A-Co1-N11	102.96(6)	S1-Co1-N1	90.38(4)	N1-Co1-N11	84.32(6)
Cl1A-Co-N21	97.12(6)	S1-Co1-N11	92.10(4)	N1-Co1-N21	84.77(6)
Cl1B-Co1-N1	89.29(5)	S1-Co1-N21	88.44(4)	N11-Co1-N21	169.09(6)
Cl1B-Co1-N11	101.81(7)	N41-Co1-N51	89.50(6)		
Cl1B-Co1-N21	133.71(7)	N41-Co1-N1	179.31(7)		
N1-Co1-N11	75.42(8)	N41-Co1-N11	95.65(6)		
N1-Co1-N21	75.05(8)	N41-Co1-N21	95.26(7)		
N11-Co1-N21	115.20(9)	N51-Co1-N1	91.18(6)		

Table 2.3. Selected bond distances (Å) and angles (°) in the crystal structure of [Fe^{II}₂(L¹SSL¹)Cl₄] (**1Fe**), as well as from DFT-optimized structures of the compound with different spin states ($S = 2$ and $S = 0$ for both iron centers).

Distances	XRD	DFT ($S=2,2$)	DFT ($S=0,0$)	Angles	XRD	Angles	XRD
Fe1-N1	2.270(2)	2.355	1.970	Cl1A-Fe1-Cl1B	100.40(3)	Cl2A-Fe2-Cl2B	101.45(3)
Fe1-N11	2.198(2)	2.129	1.942	Cl1A-Fe1-N1	93.12(6)	Cl2A-Fe2-N2	165.76(6)
Fe1-N21	2.187(2)	2.131	1.969	Cl1A-Fe1-N11	93.08(6)	Cl2A-Fe2-N31	103.69(7)
Fe1-S1	2.6925(8)	3.506	2.105	Cl1A-Fe1-N21	93.56(6)	Cl2A-Fe2-N41	102.55(6)
Fe1-Cl1A	2.4228(8)	2.415	2.413	Cl1B-Fe1-N1	166.05(6)	Cl2B-Fe2-N2	92.79(6)
Fe1-Cl1B	2.3419(7)	2.297	2.323	Cl1B-Fe1-N11	108.65(6)	Cl2B-Fe2-N31	94.52(6)
S1-S2	2.0576(9)	2.030	2.979	Cl1B-Fe1-N21	99.94(6)	Cl2B-Fe2-N41	93.26(6)
Fe2-N2	2.255(2)	2.355	1.969	N1-Fe1-N11	73.77(8)	N2-Fe2-N31	75.26(8)
Fe2-N31	2.141(2)	2.129	1.943	N1-Fe1-N21	75.57(8)	N2-Fe2-N41	75.98(8)
Fe2-N41	2.135(2)	2.132	1.968	N11-Fe1-N21	148.92(8)	N31-Fe2-N41	150.51(9)
Fe2-S2	3.231(1)	3.509	2.106	Cl1A-Fe1-S1	170.91(3)	S1-Fe1-N21	79.20(6)
Fe2-Cl2A	2.3035(8)	2.293	2.324	Cl1B-Fe1-S1	86.37(3)		
Fe2-Cl2B	2.4241(8)	2.416	2.414	S1-Fe1-N1	79.83(6)		
Fe1-Fe2	6.0567(6)	7.150	6.433	S1-Fe1-N11	90.45(6)		

2.2.3 UV-vis spectroscopy and reactivity

UV-vis spectra of purple **1co** dissolved in acetonitrile show four absorption bands (Figure 2.3a, black line). The absorption band at 261 nm ($\epsilon = 4.6 \times 10^3 \text{ M}^{-1}\text{cm}^{-1}$) is

assigned to the $\pi \rightarrow \pi^*$ transition of the pyridyl groups, whereas the three low-intensity bands at 524 ($\epsilon = 0.1 \times 10^3 \text{ M}^{-1}\text{cm}^{-1}$), 570 ($\epsilon = 0.1 \times 10^3 \text{ M}^{-1}\text{cm}^{-1}$), and 640 ($\epsilon = 0.1 \times 10^3 \text{ M}^{-1}\text{cm}^{-1}$) nm likely correspond to $d-d$ transitions combined with a $\text{Cl} \rightarrow \text{Co}^{\text{II}}$ charge-transfer transition (LMCT) [33]. Absorption bands for the solid sample appear at 216, 253, 508, 595 and 797 nm (Figure AI.17). UV-vis spectra of brown compound **2** dissolved in acetonitrile reveal three absorption bands (Figure 2.3a, blue line). The band at 262 nm ($\epsilon = 8.1 \times 10^3 \text{ M}^{-1}\text{cm}^{-1}$) is ascribed to $\pi \rightarrow \pi^*$ transition of the pyridyl groups, whereas the two absorption bands at 287 nm ($\epsilon = 6.9 \times 10^3 \text{ M}^{-1}\text{cm}^{-1}$) and 441 nm ($\epsilon = 0.4 \times 10^3 \text{ M}^{-1}\text{cm}^{-1}$) are tentatively ascribed to ligand-to-metal charge-transfer transitions (LMCT). UV-vis spectra of compound **3** dissolved in acetonitrile present four absorption bands (Figure AI.18). The absorption bands at 238 and 279 nm are assigned to the $\pi \rightarrow \pi^*$ transitions of the pyridyl groups, whereas the two absorption bands at 325 and 515 nm likely correspond to LMCT transitions [33, 34]. The UV-vis spectrum of **3** in the solid state presents four absorption bands at 268, 336, 514, and 667 nm (Figure AI.19). UV-vis spectra of **1_{Fe}** dissolved in methanol show one strong absorption band at 256 nm ($\epsilon = 8.6 \times 10^3 \text{ M}^{-1}\text{cm}^{-1}$) corresponding to the $\pi \rightarrow \pi^*$ transition of pyridyl groups. In addition two weaker bands are observed at 313 nm ($\epsilon = 1.0 \times 10^3 \text{ M}^{-1}\text{cm}^{-1}$) and 390 nm ($\epsilon = 1.8 \times 10^3 \text{ M}^{-1}\text{cm}^{-1}$) tentatively ascribed to metal-to-ligand charge transfer (MLCT) transitions (Figure AI.20). The UV-vis spectrum of **1_{Fe}** in the solid state presents two bands: one at 256 nm and another broad band at around 353 nm (Figure AI.21).

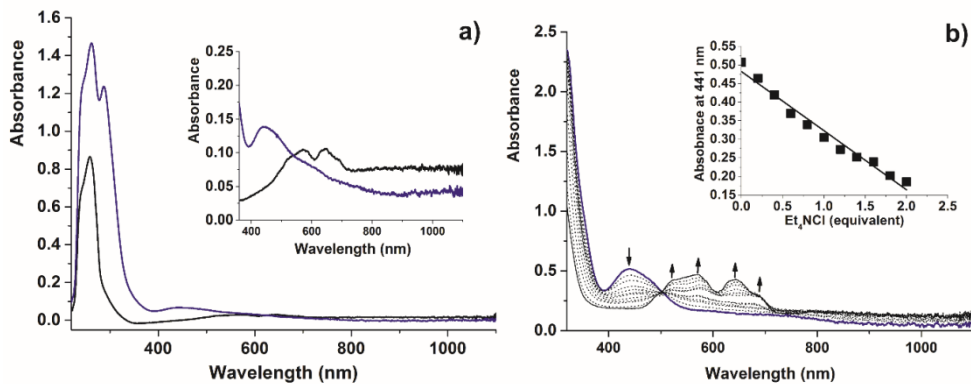
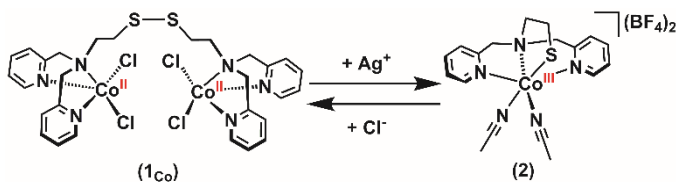


Figure 2.3. (a) UV-vis spectra of **1_{Co}** (black) and **2** (blue). UV-vis spectra were recorded using solutions 1 mM in [Co] with a transmission dip probe path length of 1.8 mm. The inset shows the UV-vis spectra of compounds recorded of solutions 2 mM in [Co]. (b) UV-vis spectra recorded upon addition of Et_4NCl to a solution of the compound $[\text{Co}^{\text{III}}(\text{L}^1\text{S})(\text{MeCN})_2](\text{BF}_4)_2$ (**2**) in acetonitrile. The spectra were recorded in at a concentration of 10 mM [Co] with a transmission dip probe path length of 2.3 mm. The inset shows the change of absorbance at 441 nm with addition of Et_4NCl .

To investigate the potential redox interconversion between the cobalt(II) disulfide compound and the cobalt(III) thiolate compound (Scheme 2.3), tetraethylammonium chloride was titrated into the acetonitrile solution containing Co(III) compound **2** while the reaction was monitored using UV-vis spectroscopy. The UV-vis spectra recorded during the addition of the chloride salt are shown in Figure 2.3b. With the addition of chloride ions into an acetonitrile solution of **2** the intensity of the absorption band at 441 nm gradually decreases until this band completely disappears after the addition of 2 equiv of chloride ion per cobalt center, while three new absorption bands appear at 524, 570, and 640 nm. The final spectrum equals the absorption spectrum of Co(II) compound **1_{Co}**. Conversely, removal of chloride anions from Co(II) disulfide compound **1_{Co}** by titration with AgBF₄ leads to the regeneration of the Co^{III}-thiolate compound, as indicated by UV-vis spectroscopy (Figure AI.22).



Scheme 2.3. Redox interconversion reaction of Co(II) compound **1_{Co}** and Co(III) compound **2** with the addition or removal of chloride anions.

The reaction of **1_{Fe}** with AgBF₄ in methanol solution was investigated as well, monitored by UV-vis spectroscopy under anaerobic conditions; the results are shown in Figure AI.23. With the addition of AgBF₄ the absorption at 313 nm decreases and fully disappears after addition of 4 equiv of AgBF₄, while the absorption band at 390 nm shifts to 368 nm. ESI-MS spectra of the final reaction mixture show the presence of a large number of species including a peak at *m/z* 734.8 for [Fe₂(L¹SSL¹)Cl₃]⁺, indicating that the reaction does not simply yield the anticipated Fe(III) thiolate compound. As described above, the direct reaction of L¹SSL¹ with [Fe(MeCN)₆](BF₄)₂ yielded a tetranuclear Fe(II) compound of the disulfide ligand with bridging fluoride ions [25].

2.2.4 Computational characterization

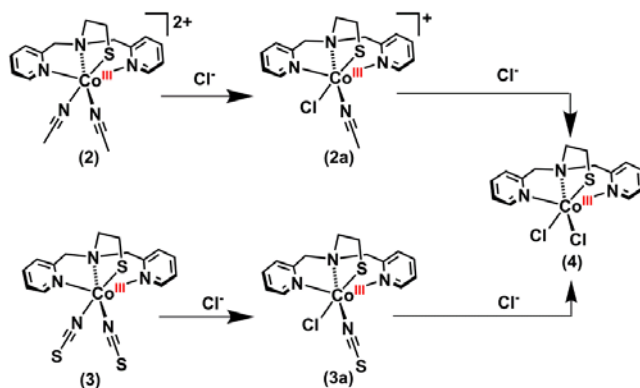
To explore the electronic structures of **1_{Co}**, **1_{Fe}**, **2**, and **3** geometry optimizations were performed for all the compounds starting from the coordinates of the crystal structures. Quartet-spin ($S = 3/2$) and doublet-spin states ($S = 1/2$) of the Co(II) centers were considered for **1_{Co}**. High-spin ($S = 2$) and low-spin ($S = 0$) states of iron(II) centers were taken into account for **1_{Fe}** and for the Co(III) center in the cationic parts of **2** and **3**. The obtained results are presented in Tables 2.1, 2.3, and Tables AI.3–AI.6

and Figures AI.24–AI.27 Comparison of the experimental and computed structures shows that the geometry of the cobalt centers in **1_{Co}** with quartet-spin states (two $S = 3/2$ ions) is more consistent with the crystallographic data. Furthermore, **1_{Co}** with quartet-spin states also has the lowest Gibbs free energy in the solvent, namely, 13 kcal/mol lower than for doublet-spin states (two $S = 1/2$ ions). The optimized (solvation) structure for **1_{Fe}** has the lowest Gibbs free energy with high-spin states (**1_{Fe(2,2,sol)}**, two $S = 2$ Fe^{II} centers), which is 31 and 10 kcal/mol lower than for the compound with two low-spin iron(II) centers (**1_{Fe(0,0,sol)}**, $S = 0$) and the compound with mixed-spin states (**1_{Fe(0,2,sol)}**, $S = 0$ for one iron(II) center and $S = 2$ for the other iron(II) center). The optimized geometry of **1_{Fe}** with two high-spin iron(II) centers is roughly similar to the crystallographic data; however, both Fe(II) ions are in a five-coordinate configuration, with Fe–S bond distances of 3.509 and 3.506 Å. For the optimized compound **1_{Fe(0,0 sol)}** in the low-spin state ($S = 0$ for both Fe^{II} ions), the S–S bond length is 2.979 Å, which is much longer than in the crystal structure of **1_{Fe}**, whereas the Fe–S distances are much shorter than in the crystal structure. Therefore, as the computations did not reproduce the Fe–S distances, the geometry was optimized while keeping the distance between Fe2 and S2 fixed. The structure in the high-spin state (**1_{Fe(2,2,sol,fixation)}**, $S = 2$ for both Fe^{II} centers) still has the lowest Gibbs free energy and the acquired structure is consistent with the crystallographic data. Furthermore, the Gibbs free energy of **1_{Fe(2,2,sol,fixation)}** is nearly the same as that of **1_{Fe(2,2,sol)}**. Apparently, the interaction between Fe2 and S2 is weak, and does not significantly affect the stability of the compound.

Both Co(III) compounds **2** and **3** have the lowest Gibbs free energy in the solvent with a low-spin Co(III) center, namely 25 and 23 kcal/mol lower than those with a high-spin Co(III) center. The selected bond lengths in the optimized structures of compounds **2** and **3** with the lowest energy are provided in Table 2.1. The Co–S bond lengths in the optimized structures of **2** and **3** are 2.206 and 2.211 Å, respectively, comparable to the Co–S bond length (2.2355(5) Å) found in the crystal structure of **3**. The calculations conducted in the gas phase show similar results with those in the solvent.

The addition of chloride anions to a solution containing cobalt(III)–thiolate compound **2** results in formation of cobalt(II)–disulfide compound **1_{Co}**. To investigate this process computationally, the acetonitrile molecules in **2** and the thiocyanate anions in **3** were displaced by chloride ions one by one. The geometries of the theoretical intermediates [Co^{III}(L¹S)(Cl)(MeCN)]⁺ (**2a**), [Co^{III}(L¹S)(Cl)(NCS)] (**3a**), and [Co^{III}(L¹S)Cl₂] (**4**) were optimized and their highest occupied molecular orbitals (HOMOs) were analyzed and compared with those of **2** and **3** (Scheme 2.4). The Gibbs free energies of the two

isomeric intermediates (with the chloride ion placed in the position *trans* to the amine nitrogen donor) are slightly higher than those of intermediates **2a** and **3a** (1 and 2 kcal/mol, respectively). This small difference may be caused by the *trans* influence of the thiolate donor, but this was not investigated in detail. Interestingly, the HOMOs of compounds **3**, **3a** and **4** consist mainly of *p* orbitals on sulfur and *d* orbitals on cobalt with the same total percentage (89% for all of the compounds). It was found that the HOMO gradually consists more of *d* orbital on cobalt and less of the *p* orbital of sulfur, as the number of chloride anions increases and the number of coordinated thiocyanate anions decreases. Similarly, displacement of the acetonitrile molecules in **2** by chloride anions effect the same change on HOMOs (Figure AI.28).



Scheme 2.4. Drawing of compounds **2**, **3**, and theoretical intermediates **2a**, **3a** and **4**.

It has been shown that depending on the experimental conditions dinuclear Cu(II) thiolate compounds $[\text{Cu}^{\text{II}}_2(\text{L}^1\text{S})_2]^{2+}$ with bridging thiolate donor atoms may be generated when L^1SSL^1 or similar disulfide ligands react with Cu(I) salts [14, 18-20, 35]. However, mononuclear rather than dinuclear Co(III) thiolate compounds are formed in our study. In order to understand this difference in reactivity, both the hypothetical dinuclear compounds $[\text{Co}^{\text{III}}_2(\text{L}^1\text{S})_2]^{4+}$ (**5**) and $[\text{Co}^{\text{III}}_2(\text{L}^1\text{S})_2(\text{MeCN})_2]^{4+}$ (**6**) with different spin states ($S = 0, 1$, or 2 for both Co(III) ions) were investigated computationally. As a comparison, the hypothetical mononuclear copper compound $[\text{Cu}^{\text{II}}(\text{L}^1\text{S})(\text{MeCN})]^{+}$ (**7**) and the actual dinuclear copper compound $[\text{Cu}^{\text{II}}_2(\text{L}^1\text{S})_2]^{2+}$ (**8**) were optimized as well. The octahedral mononuclear copper(II) compound $[\text{Cu}^{\text{II}}(\text{L}^1\text{S})(\text{MeCN})_2]^{+}$ and the dinuclear copper(II) compound $[\text{Cu}^{\text{II}}_2(\text{L}^1\text{S})_2(\text{MeCN})_2]^{2+}$ have also been computed but are not discussed here as acetonitrile moved away from the Cu(II) center during the geometry optimization. The obtained results show that **5** has the lowest Gibbs free energy in the solvent with two low-spin cobalt(III) centers (two $S = 0$ ions); two high-spin states (two $S = 2$ ions) or two triplet-spin states (two S

= 1 ions) result in energies that are 40 and 3 kcal/mol higher. The energies of the antiferromagnetically coupled ($S = 0$) species were considered for the dinuclear copper(II) (two $S = 1/2$ ions) and cobalt(III) (two $S = 2$ ions in **5** or **6**, as well as two $S = 1$ ions in **5**) compounds (see Computational Details). Antiferromagnetic coupling ($S = 0$) is not beneficial to stabilize **5**, for $S = 2$ or $S = 1$ states result in Gibbs free energies being 29 and 24 kcal/mol higher than that of the uncoupled systems. The distance between two cobalt(III) ions in optimized geometries of **5** with two high-spin, two triplet-spin, two low-spin states are 3.665, 3.276, and 3.097 Å, respectively (Figure AI.29). Similarly, **6** with two $S = 0$ Co^{III} centers has the lowest Gibbs free energy in solvent. Optimization of **6** with two high-spin Co^{III} centers results in dissociation of the dinuclear structure (see Figure AI.30). Our computational study reveals that dimerization of mononuclear compound **2** to dinuclear compound **5** results in a slight decrease of the Gibbs free energy by 6 kcal/mol; however, formation of **6** leads to an increase of the Gibbs free energy by 19 kcal/mol (Figure 2.4). The formation of dinuclear copper compound **8** from mononuclear compound **7** leads to stabilization, lowering the Gibbs free energy by 33 kcal/mol (Figure 2.4, Tables AI.6 and AI.7).

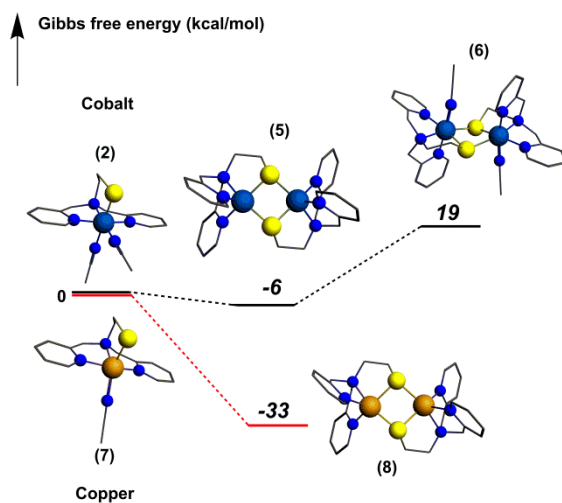


Figure 2.4. Optimized structures (at the the ZORA-OPBE/TZ2P level of theory) of compounds **2**, and **5–8**, and the change in Gibbs free energy (in kcal/mol) upon formation of the dinuclear metal compounds in acetonitrile. The acetonitrile molecules liberated in the reactions were taken into account but are omitted from the drawings for clarity.

2.3 Discussion

The redox interconversion between metal thiolate and disulfide compounds has received considerable attention in the past decade. In this chapter we report the synthesis of four new cobalt and iron compounds $[\text{Co}^{\text{II}}_2(\text{L}^1\text{SSL}^1)\text{Cl}_4]$ (**1_{Co}**),

[Fe^{II}₂(L¹SSL¹)Cl₄] (**1_{Fe}**), [Co^{III}(L¹S)(MeCN)₂](BF₄)₂ (**2**), and [Co^{III}(L¹S)(NCS)₂] (**3**) from reactions of the disulfide ligand L¹SSL¹ with different Co(II) and Fe(II) salts. Whereas the Co(II) compounds are air-stable, the Co(III) thiolate compounds are slightly air-sensitive. The crystal structure of **3** showed the presence (with low occupancy factor) of a complex containing a mono-oxygenated sulfenate ligand, and crystallization of **2** in air after 8 weeks resulted in crystals of oxidized compound **2_{ox}** comprising a dioxygenated sulfinate ligand. ESI-MS spectra of solutions containing **3** taken after 2 h in the air did not show any oxidation products, confirming that this oxidation process is very slow and thus that the effect on the redox studies is negligible. Using UV-vis spectroscopy, we showed that the addition of chloride anions to cobalt(III) compound **2** results in a redox interconversion reaction yielding cobalt(II) disulfide compound **1_{Co}**, whereas removal of the chloride anions from **1_{Co}** regenerates compound **2**. In 2001, the group of Itoh reported the synthesis of a Cu(II) thiolate compound from a similar disulfide ligand [20]. The addition of chloride anions to this Cu(II) thiolate compound led to the redox interconversion reaction to the corresponding Cu(I) disulfide compound, whereas removal of the chloride anions resulted in the regeneration of the Cu(II) thiolate compound. In contrast, the group of Henkel reported a Cu(I) disulfide compound that upon *addition* of chloride ions resulted in the formation of a Cu(II) thiolate compound [15]. Similarly, the group of Duboc recently reported a Co(III) thiolate compound that upon removal of chloride ions resulted in a Co(II) disulfide complex [24]. Clearly, the formation of metal thiolate or disulfide compounds cannot be predicted based on the anions only.

For comparison the synthesis of the related iron(II) compounds has been investigated. Reaction of ligand L¹SSL¹ with FeCl₂·4H₂O results in the formation of the iron(II) disulfide compound [Fe^{II}₂(L¹SSL¹)Cl₄] (**1_{Fe}**), showing a structure that is slightly different from that of [Co^{II}₂(L¹SSL¹)Cl₄] (**1_{Co}**). However, instead of the expected Fe(III)-thiolate compound similar to **2**, reaction of **1_{Fe}** with AgBF₄ did not give conclusive results, and reaction of ligand L¹SSL¹ with [Fe(MeCN)₆](BF₄)₂ resulted in the formation of a fluoride-bridged tetranuclear iron(II) compound [25]. Thus, the redox interconversion in the iron compound appears to be more difficult despite the fact that one of the thioether sulfurs in **1_{Fe}** is coordinating.

In order to understand the reactivity observed for our compounds, DFT calculations were employed to further explore the electronic structure of **1_{Co}**, **1_{Fe}**, **3**, and the cationic part of **2**. The obtained results show that **1_{Co}** has the lowest energy with two high-spin Co(II) centers (two $S = 3/2$ ions), consistent with the crystal structure and the observed effective magnetic moment, whereas low-spin Co(III) centers ($S = 0$) yield the lowest energy structures in compounds **2** and **3**, in agreement with the

crystal data and the diamagnetic NMR spectra. Similarly, **1_{Fe}** has the lowest energy with both iron centers in high-spin states ($S = 2$), in line with the crystal structure and the magnetic susceptibility in solution.

Combination of experimental results and DFT calculations confirm the formation of a low-spin ($S = 0$) mononuclear Co(III)-thiolate compound in contrast to the dinuclear dithiolate-bridged structure reported for Cu(II) and the dinuclear Co(II) compounds with quartet-spin state (two $S = 3/2$ ions) reported by the group of Duboc [18, 24]. The antiferromagnetic interaction between the two Cu(II) ions or the strong antiferromagnetic coupling between two $S = 3/2$ cobalt(II) ions reported by the group of Duboc are likely beneficial for the stabilization of the dinuclear compounds. Our computations show that antiferromagnetic coupling does not stabilize dinuclear cobalt(III) thiolate compounds **5** and **6**. Formation of dinuclear cobalt(III) compound **5** from mononuclear **2** seemingly results in a slightly lower Gibbs free energy, which suggests that in solution **2** and **5** may be in equilibrium. However, the compound that crystallizes from the solution is mononuclear **2**, and the question remains why the cobalt(III) ions in our ligand L^1S^- prefer a low-spin configuration in contrast to the intermediate spin occurring in the Duboc system.

The character of the HOMOs of compounds **2** and **3** and theoretical intermediates **2a**, **3a**, and **4** was investigated to explore the potential dependence of the electron distribution in the HOMO on the presence of different anions, as well as the potential transfer of electron density between cobalt and sulfur. The HOMO of these compounds has mainly character of p orbitals on sulfur and d orbitals on cobalt, and a small shift of the character of the HOMOs from p orbitals on sulfur to d orbitals on cobalt is found upon substitution of the thiocyanate by chloride anions. Our computational investigation on the potential shift of electron density from sulfur to cobalt upon coordination of chloride anions were not conclusive to help understand the experimental finding of the formation of a Co(II) disulfide compound upon addition of chloride ions.

2.4 Summary and conclusions

In this chapter, we report the synthesis of low-spin mononuclear Co(III) thiolate compounds and high-spin dinuclear Co(II) and Fe(II) disulfide compounds from a disulfide ligand L^1SSL^1 in reaction with Co(II) and Fe(II) salts. It is shown that the redox interconversion of this Co(III) thiolate and the corresponding Co(II) disulfide compound is triggered by the addition or removal of chloride anions. DFT calculations show that the HOMO consists gradually more of the d orbital on cobalt and less of the p orbital on sulfur when the thiocyanate molecules in the compound $[Co^{III}(L^1S)(NCS)_2]$

are substituted with chloride ions. This is the first example of a redox interconversion reaction between low-spin Co(III) thiolate and high-spin Co(II) disulfide compounds. Despite the new information that is gained including our computational studies, still more research needs to be done to predict accurately the conditions that trigger the redox interconversion reactions for metal thiolate and disulfide compounds.

2.5 Experimental section

2.5.1 General procedures

All the reagents were purchased from commercial sources and used as received unless noted otherwise. Dry acetonitrile and diethyl ether were obtained from a solvent dispenser (PureSolV 400), and methanol was acquired from commercial vendors and stored on 3 Å molecular sieves. The synthesis of metal compounds was carried out using standard Schlenk-line techniques under a nitrogen atmosphere. ^1H NMR spectra were recorded on a Bruker 300 DPX spectrometer at room temperature. Mass spectra were recorded on a Finnigan Aqua mass spectrometer with electrospray ionization (ESI). IR spectra were acquired on a PerkinElmer UATR spectrum equipped with a single reflection diamond (scan range 400 cm^{-1} to 4000 cm^{-1} , resolution 4 cm^{-1}). UV-vis spectra were collected using a transmission dip probe with variable path lengths and reflection probe on an Avantes Avaspec-2048 spectrometer with Avalight-DH-S-BAL light source. A WITEC alpha300R-Confocal Raman Imaging with the laser wavelength of 476 nm was used to record the Raman spectra, and all of the measurements were carried out under ambient conditions at room temperature. Elemental analyses were performed by the Microanalytical Laboratory Kolbe in Germany. Cyclic voltammetry (CV) was performed with an Autolab PGstat10 potentiostat controlled by GPES4 software. A three-electrode system was used including an Ag/AgCl double junction reference electrode, a glassy carbon working electrode (3 mm diameter), and a Pt wire counter electrode in a solution containing 0.1 M NBu_4PF_6 . In these conditions the Fc/Fc⁺ couple was found to be located at +0.428 V with a peak-to-peak separation of 91 mV in acetonitrile. Potentials are given relative to the Ag/AgCl electrode.

2.5.2 Single crystal X-ray crystallography

All reflection intensities were measured at 110(2) K using a SuperNova diffractometer (equipped with Atlas detector) with Mo K α radiation ($\lambda = 0.71073\text{ \AA}$) under the program CrysAlisPro (version 1.171.36.32 Agilent Technologies, 2013 was used for **1**_{Co}, **2**_{Ox} and **1**_{Fe}; version CrysAlisPro 1.171.39.29c, Rigaku OD, 2017 was used for compound **3**). The same program was used to refine the cell dimensions and for data reduction. The structures were solved with the program SHELXS-2013 or SHELXS-

2014/7 and were refined on F² with SHELXL-2013 or SHELXS-2014/7 [36]. Analytical numeric absorption correction based on a multifaceted crystal model or numerical absorption correction based on Gaussian integration over a multifaceted crystal model were applied using CrysAlisPro. The temperature of the data collection was controlled using the system Cryojet (manufactured by Oxford Instruments). The H atoms were placed at calculated positions using the instructions AFIX 23, AFIX 43 or AFIX 137 with isotropic displacement parameters having values 1.2 or 1.5 U_{eq} of the attached C atoms. The H atoms attached to O1S and O2S (lattice methanol solvent molecules) for **1_{Fe}** were found from difference Fourier maps, and their coordinates were refined freely. The structures of **1_{Co}**, **2_{Ox}**, **1_{Fe}** and **3** are mostly ordered.

For **1_{Fe}**, the absolute configuration was established by anomalous-dispersion effects in diffraction measurements on the crystal, and the Flack and Hooft parameters refine to 0.006(5) and 0.010(6), respectively. While finalizing the refinement of **3**, one residual electron density peak of 2.47 e⁻ Å⁻³ was found at *ca.* 1.46 Å from S1. This peak is thought to be an oxygen atom, and its presence may result from the partial oxidation of S1 occurring during the crystallization process. Its occupancy factor was set to refine freely, and its final value is 0.178(5). Another peak of 0.42 e⁻ Å⁻³ was found at *ca.* 1.12 Å from S1. The nature of this peak is not entirely clear.

2.5.3 Density functional theory (DFT) calculations

All calculations were performed with the Amsterdam Density Functional (ADF) program version r47953 [37, 38], using relativistic DFT at ZORA OPBE/TZ2P for geometry optimization and energies.[39] Solvation in acetonitrile was simulated using the conductor-like screening model (COSMO) [40-43]. All stationary points in the gas phase and in the condensed phase were verified to be minima on the potential energy surface (PES) through vibrational analysis. The energies of the singlet state of the Cu^{II}/Co^{III} μ-thiolate complexes (E^S) have been obtained from the unrestricted broken-symmetry singlet energies (E^{BS}) and the energy of the triplet (E^T) with the approximate projection method of Noodleman: $E^S = 2E^{BS} - E^T$. [44, 45]

The Gibbs free energies ($\Delta G = \Delta H - T\Delta S$) were evaluated with the following procedure. Enthalpies at 298.15 K and 1 atm (ΔH_{298}) were calculated from electronic bond energies (ΔE) in the solvent and vibrational frequencies using standard thermochemistry relations for an ideal gas, according to [46]

$$\Delta H_{298} = \Delta E + \Delta E_{\text{trans},298} + \Delta E_{\text{rot},298} + \Delta E_{\text{vib},0} + \Delta(\Delta E_{\text{vib},0})_{298} + \Delta(pV) \quad (1)$$

Here, $\Delta E_{\text{trans},298}$, $\Delta E_{\text{rot},298}$, and $\Delta E_{\text{vib},0}$ are the differences between the two complexes in translational, rotational and zero-point vibrational energy, respectively; $\Delta(\Delta E_{\text{vib},0})_{298}$ is

the change in the vibrational energy difference as one goes from 0 to 298.15 K. The vibrational energy corrections are based on our frequency calculations in the gas phase. The molar work term $\Delta(pV)$ is $(\Delta n)RT$, with $n=0$. Thermal corrections for the electronic energy are neglected. The entropy ΔS was also obtained from the gas phase calculations. Most systems were optimized in C_1 symmetry. CH_3CN was optimized with C_{3v} symmetry.

2.5.4 Synthesis of the compounds

$[\text{Co}^{\text{II}}_2(\text{L}^1\text{SSL}^1)\text{Cl}_4]$ (**1_{Co}**): Ligand L^1SSL^1 (107.0 mg, 0.207 mmol) was dissolved in 3 mL of dry acetonitrile, and separately $\text{CoCl}_2 \cdot 6\text{H}_2\text{O}$ (98.5 mg, 0.414 mmol) was dissolved in 3 mL of dry acetonitrile. The two solutions were mixed resulting in a purple solution, which was stirred for about 30 min. Then, 8 mL of diethyl ether was added, and a purple precipitate was obtained which was washed with diethyl ether (5×5 mL). Yield: 99.1 mg, 0.13 mmol, 64%. Single crystals suitable for X-ray diffraction were obtained by slow vapor diffusion of diethyl ether into the acetonitrile solution containing the compound; single crystals were obtained after 2 days at room temperature. IR (cm^{-1}): 1606s, 1571w, 1480m, 1442s, 1092w, 1022m, 766vs, 648m, 478w. ESI-MS found (calcd) for $[\text{M}-\text{Cl}]^+$ m/z 740.8 (740.9). Elemental analysis calcd (%) for $\text{C}_{28}\text{H}_{32}\text{Cl}_4\text{Co}_2\text{N}_6\text{S}_2 + 2\text{H}_2\text{O}$: C 41.40, H 4.47, N 10.3; found: C 41.71, H 4.57, N 9.80. UV-vis (acetonitrile at 1 mM $[\text{Co}]$): λ_{max} (ϵ in $\text{M}^{-1} \text{cm}^{-1}$): 261 nm (4.6×10^3), 524 nm (0.1×10^3), 570 nm (0.1×10^3), 640 nm (0.1×10^3).

$[\text{Co}^{\text{III}}(\text{L}^1\text{S})(\text{MeCN})_2](\text{BF}_4)_2$ (**2**): To a yellow solution of ligand L^1SSL^1 (71.2 mg, 0.138 mmol) in 4.6 mL of dry and degassed acetonitrile, solid $[\text{Co}(\text{MeCN})_6](\text{BF}_4)_2$ (131.7 mg, 0.275 mmol) was added, resulting in a brown yellow solution. The acquired solution was stirred for 3 h, and then the volume was reduced to 0.5 mL. Addition of 15 mL of diethyl ether led to the formation of a yellow oil material. The obtained yellow oil material was washed with diethyl ether (3×15 mL). Yield: 103.0 mg, 0.18 mmol, 65%. Single crystals of **2** could not be obtained, but from an acetonitrile solution of compound **2** kept in air, after 8 weeks crystals were obtained of the cobalt(III) sulfinate compound $[\text{Co}^{\text{III}}(\text{L}^1\text{SO}_2)(\text{MeCN})_2](\text{BF}_4)_2$ (**2_{ox}**). IR (cm^{-1}): 1606m, 1481w, 1480w, 1444w, 1292m, 1018s, 764s, 727w, 648w, 523w, 476w. ^1H NMR (300 MHz, acetonitrile- d_3 , RT): δ = 8.39 (2H, Py- H_6), 8.10 (2H, Py- H_4), 7.56 (4H, Py- H_3 , Py- H_5), 5.02 (2H, Py- CH_2), 4.34 (2H, Py- CH_2), 3.12 (N- CH_2 - CH_2 -S), 2.55 (proton probably from the coordinated acetonitrile), 2.09 (H_2O), 1.94 (MeCN). ESI-MS found (calcd) for $\frac{1}{2} [\text{M}-2(\text{BF}_4)]^{2+}$ m/z 199.8 (199.5). UV-vis (acetonitrile at 1 mM $[\text{Co}]$): λ_{max} (ϵ in $\text{M}^{-1} \text{cm}^{-1}$): 262 nm (8.1×10^3), 287 nm (6.9×10^3), 442 nm (0.4×10^3).

[Co^{III}(L¹S)(NCS)₂] (**3**): Ligand L¹SSL¹ (103.9 mg, 0.201 mmol) was dissolved in 5 mL of dry and degassed acetonitrile, to which solid Co(NCS)₂ (70.3 mg, 0.401 mmol) was added, resulting in a dark brown solution. The solution was stirred for 3 h at room temperature, after which the volume was reduced to 2 mL. Addition of 20 mL of diethyl ether resulted in the formation of a dark brown powder. The acquired powder was washed with diethyl ether (3 × 10 mL). Yield: 120.0 mg, 0.28 mmol, 70%. Single crystals suitable for X-ray diffraction were grown by slow vapor diffusion of isopropyl ether into the acetonitrile solution containing the compound; single crystals were obtained after approximately 3 weeks at room temperature. ¹H NMR (300 MHz, acetonitrile-*d*₃, RT): δ = 8.42 (d, 2H, Py-H₆), 8.01 (t, 2H, Py-H₄), 7.59 (t, 2H, Py-H₃), 7.45 (d, 2H, Py-H₅), 4.98 (d, 2H, Py-CH₂), 4.22 (d, 2H, Py-CH₂), 3.65 (d, 2H, S-CH₂-CH₂), 2.95 (t, 2H, S-CH₂-CH₂), 2.14 (H₂O), 1.94 (MeCN). ¹³C NMR (300 MHz, acetonitrile-*d*₃, RT): δ = 30.67 (C-S), 67.95 (Py-C-N), 70.82 (N-CH₂-CH₂-S), 121.88 (Py-C₅), 125.60 (Py-C₃), 139.66 (Py-C₄), 152.37 (Py-C₆), 162.11 (Py-C₂). ESI-MS found (calcd) for [M-NCS]⁺ *m/z* 375.3 (375.1). IR (cm⁻¹): 2106vs, 2090s, 1608m, 1478m, 1445s, 1304m, 1277m, 1229w, 1156w, 1108w, 1054m, 1017w, 993w, 952m, 895m, 821m, 752vs, 786s, 652m, 557w, 532m, 479s. Elemental analysis calcd (%) for C₁₆H₁₆CoN₅S₃: C 44.34, H 3.72, N 16.16; found: C 44.19, H 3.87, N 15.94. UV-vis (acetonitrile at 1 mM [Co]): λ_{max} (ε in M⁻¹cm⁻¹): 238 nm (6.7×10³), 279 nm (8.5×10³), 325 nm (4.8×10³), 515 nm (0.7×10³).

[Fe^{II}₂(L¹SSL¹)Cl₄] (**1**_{Fe}): Ligand L¹SSL¹ (77.7 mg, 0.150 mmol) was dissolved in 6 mL of dry and degassed methanol to which 60.0 mg (0.30 mmol) FeCl₂·4H₂O was added, resulting in a green-yellow solution. The solution was stirred for another 2 h at room temperature, after which 20 mL of dry and degassed diethyl ether was added, yielding a yellow precipitate. The obtained precipitate was filtered and washed with diethyl ether (4 × 15 mL). Yield: 59.3 mg, 0.07 mmol, 62%. Single crystals suitable for X-ray structure determination were grown by slow vapor diffusion of diethyl ether into a methanol solution of this compound; single crystals were obtained after 4 days at room temperature. IR (cm⁻¹): 1604s, 1571w, 1479w, 1442s, 1291w, 1155w, 1088m, 1052m, 1019s, 764vs, 725w, 642w. ESI-MS found (calcd) for 1/2[M-2Cl]²⁺ *m/z* 349.1 (349.0). Elemental analysis calcd (%) for C₂₈H₃₂Cl₄Fe₂N₆S₂+3H₂O: C 40.80, H 4.65, N 10.20; found: C 40.32, H 4.32, N 9.87. UV-vis (methanol at 1 mM [Fe]): λ_{max} (ε in M⁻¹cm⁻¹): 256 nm (8.6×10³), 313 nm (1.0×10³), 390 nm (1.8×10³).

2.6 References

- [1] C. Jacob, G.L. Giles, N.M. Giles, H. Sies, *Angew. Chem., Int. Ed.*, 42 (2003) 4742-4758.
- [2] S. Iwata, C. Ostermeier, B. Ludwig, H. Michel, *Nature*, 376 (1995) 660-669.

- [3] J.A. Kovacs, *Acc. Chem. Res.*, 48 (2015) 2744-2753.
- [4] C.E. Paulsen, K.S. Carroll, *Chem. Rev.*, 113 (2013) 4633-4679.
- [5] A.L. Lamb, A.S. Torres, T.V. O'Halloran, A.C. Rosenzweig, *Nat. Struct. Mol. Biol.*, 8 (2001) 751-755.
- [6] P. Palumaa, L. Kangur, A. Voronova, R. Sillard, *Biochem. J.*, 382 (2004) 307-314.
- [7] E.S. Arnér, A. Holmgren, *FEBS J.*, 267 (2000) 6102-6109.
- [8] L. Banci, I. Bertini, G. Cavallaro, S. Ciofi-Baffoni, *FEBS J.*, 278 (2011) 2244-2262.
- [9] T.R. Cawthorn, B.E. Poulsen, D.E. Davidson, D. Andrews, B.C. Hill, *Biochemistry*, 48 (2009) 4448-4454.
- [10] G. Meloni, V. Sonois, T. Delaine, L. Guilloreau, A. Gillet, J. Teissié, P. Faller, M. Vašák, *Nat. Chem. Biol.*, 4 (2008) 366-372.
- [11] J.T. Pedersen, C. Hureau, L. Hemmingsen, N.H. Heegaard, J. Østergaard, M. Vašák, P. Faller, *Biochemistry*, 51 (2012) 1697-1706.
- [12] R.P. Houser, V.G. Young, W.B. Tolman, *J. Am. Chem. Soc.*, 118 (1996) 2101-2102.
- [13] R.P. Houser, J.A. Halfen, V.G. Young Jr, N.J. Blackburn, W.B. Tolman, *J. Am. Chem. Soc.*, 117 (1995) 10745-10746.
- [14] S. Itoh, M. Nagagawa, S. Fukuzumi, *J. Am. Chem. Soc.*, 123 (2001) 4087-4088.
- [15] A. Neuba, R. Haase, W. Meyer-Klaucke, U. Flörke, G. Henkel, *Angew. Chem. Int. Ed.*, 51 (2012) 1714-1718.
- [16] E. C.M. Ording-Wenker, M. van der Plas, M.A. Siegler, C. Fonseca Guerra, E. Bouwman, *Chem. Eur. J.*, 20 (2014) 16913-16921.
- [17] E.C.M. Ording-Wenker, M.A. Siegler, E. Bouwman, *Inorg. Chim. Acta*, 428 (2015) 193-202.
- [18] E.C.M. Ording-Wenker, M. van der Plas, M.A. Siegler, S. Bonnet, F.M. Bickelhaupt, C. Fonseca Guerra, E. Bouwman, *Inorg. Chem.*, 53 (2014) 8494-8504.
- [19] A.M. Thomas, B.L. Lin, E.C. Wasinger, T.D.P. Stack, *J. Am. Chem. Soc.*, 135 (2013) 18912-18919.
- [20] Y. Ueno, Y. Tachi, S. Itoh, *J. Am. Chem. Soc.*, 124 (2002) 12428-12429.
- [21] T. Ohta, T. Tachiyama, K. Yoshizawa, T. Yamabe, T. Uchida, T. Kitagawa, *Inorg. Chem.*, 39 (2000) 4358-4369.
- [22] S. Okamoto, L.D. Eltis, *Metallomics*, 3 (2011) 963-970.
- [23] J.A. Kovacs, *Chem. Rev.*, 104 (2004) 825-848.
- [24] M. Gennari, B. Gerey, N. Hall, J. Pécaut, M.N. Collomb, M. Rouzières, R. Clérac, M. Orio, C. Duboc, *Angew. Chem. Int. Ed.*, 53 (2014) 5318-5321.
- [25] F. Jiang, M.A. Siegler, E. Bouwman, *Inorg. Chem. Commun.*, 94(2018) 53-56.
- [26] D. Evans, *J. Chem. Soc.*, (1959) 2003-2005.
- [27] G.A. Bain, J.F. Berry, *J. Chem. Educ.*, 85 (2008) 532.
- [28] H.E. Van Wart, A. Lewis, H.A. Scheraga, F.D. Saeva, *Proc. Natl. Acad. Sci. U.S.A.*, 70 (1973) 2619-2623.
- [29] A.W. Addison, T.N. Rao, J. Reedijk, J. van Rijn, G.C. Verschoor, *J. Chem. Soc., Dalton Trans.*, (1984) 1349-1356.
- [30] L.R. Widger, Y. Jiang, A.C. McQuilken, T. Yang, M.A. Siegler, H. Matsumura, P. Moëne-Loccoz, D. Kumar, S.P. De Visser, D.P. Goldberg, *Dalton Trans.*, 43 (2014) 7522-7532.
- [31] D. Sellmann, K.P. Peters, F.W. Heinemann, *Eur. J. Inorg. Chem.*, 2004 (2004) 581-590.
- [32] U.K. Das, S.L. Daifuku, S.I. Gorelsky, I. Korobkov, M.L. Neidig, J.J. Le Roy, M. Murugesu, R.T. Baker, *Inorg. Chem.*, 55 (2016) 987-997.
- [33] A.B.P. Lever, *Inorganic electronic spectroscopy*, 2nd ed., Elsevier, Amsterdam, the Netherlands, 1968.
- [34] B.J. Coe, J.A. Harris, B.S. Brunschwig, I. Asselberghs, K. Clays, J. Garín, J. Orduna, *J. Am. Chem. Soc.*, 127 (2005) 13399-13410.
- [35] A. Neuba, R. Haase, W. Meyer-Klaucke, U. Flörke, G. Henkel, *Angew. Chem., Int. Ed.*, 51 (2012) 1714-1718.

- [36] G.M. Sheldrick, *Acta Crystallogr., Sect. A*, 64 (2008) 112-122.
- [37] G. te Velde, F.M. Bickelhaupt, E.J. Baerends, C. Fonseca Guerra, S.J.A. Van Gisbergen, J.G. Snijders, T. Ziegler, *J. Comput. Chem.*, 22 (2001) 931-967.
- [38] <http://www.scm.com/>.
- [39] M. Swart, A.W. Ehlers, K. Lammertsma, *Mol. Phys.*, 102 (2004) 2467-2474.
- [40] A. Klamt, *J. Phys. Chem.*, 99 (1995) 2224-2235.
- [41] A. Klamt, G. Schuurmann, *J. Chem. Soc. Perk Trans 2*, (1993) 799-805.
- [42] C.C. Pye, T. Ziegler, *Theor. Chem. Acc.*, 101 (1999) 396-408.
- [43] M. Swart, E. Roesler, F.M. Bickelhaupt, *Eur. J. Inorg. Chem.*, (2007) 3646-3654.
- [44] L. Noodleman, *J. Chem. Phys.*, 74 (1981) 5737-5743.
- [45] L. Noodleman, E.J. Baerends, *J. Am. Chem. Soc.*, 106 (1984) 2316-2327.
- [46] F. Jensen, *Introduction to Computational Chemistry*, 2nd ed., Wiley, Chichester, West Sussex, UK, 2006.

Chapter 3

Solvent-dependent Redox Interconversion of Cobalt(III) Thiolate and Cobalt(II) Disulfide Compounds

In this chapter, we describe the synthesis of the cobalt(II) disulfide compounds $[\text{Co}^{\text{II}}_2(\text{L}^{\text{X}}\text{SSL}^{\text{X}})(\text{PO}_2\text{F}_2)_2](\text{PF}_6)_2$ and $[\text{Co}^{\text{II}}_2(\text{L}^{\text{X}}\text{SSL}^{\text{X}})(\text{NO}_3)_4]$ from two different disulfide ligands $\text{L}^{\text{X}}\text{SSL}^{\text{X}}$ in reaction with cobalt(II) salts ($X = 1$, di-2-(bis(2-pyridylmethyl)amino)-ethyl disulfide; $X = 7$, di-2-((6-methyl-2-pyridylmethyl)(2-pyridylmethyl)amino)-ethyl disulfide). The redox interconversion of these cobalt(II) disulfide compounds to their related cobalt(III) thiolate compounds has been investigated. It was found that the compound $[\text{Co}^{\text{II}}_2(\text{L}^1\text{SSL}^1)(\text{PO}_2\text{F}_2)_2](\text{PF}_6)_2$ is stable as such in methanol and dichloromethane solution, but in acetonitrile redox interconversion occurs with the formation of the cobalt(III) thiolate compound $[\text{Co}^{\text{III}}(\text{L}^1\text{S})(\text{MeCN})_2]^{2+}$. The other disulfide compounds do not show this solvent-dependency and remain in the disulfide form in all investigated solvents. This is a rare example of redox interconversion between cobalt(II) disulfide and cobalt(III) thiolate compounds controlled by solvents.

3.1 Introduction

Electron-transfer reactions involving thiolate-disulfide interconversions occur in a number of biological processes and play fundamental roles in e.g. copper transport, regulation of gene expression, and protein folding and stability [1-4]. However, until now, the exact mechanism of these electron-transfer reactions in vivo is not well understood [2]. To gain more insight into the operation principle of the thiolate-disulfide interconversion occurring in metalloenzymes such as metallothionein Zn_7MT_3 [5-7], in the last decades tremendous efforts have been put in the synthesis of copper(II) thiolate compounds and the study of their redox interconversion to the corresponding copper(I) disulfide compounds [8-13]. So far, several triggers have been found to tune this redox interconversion such as protons [10, 12], halide ions [9, 13], as well as the polarity of solvents [11, 12], and changes in temperature [11].

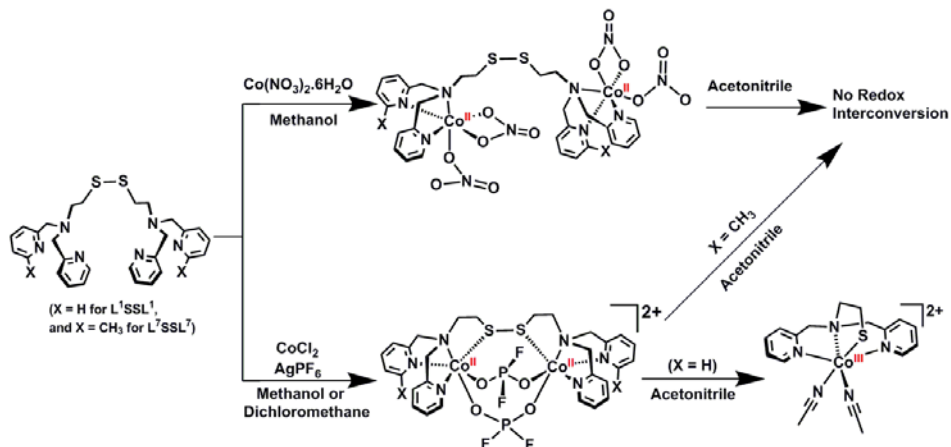
In the last few years, the study of the redox interconversion between metal thiolate and disulfide compounds has progressively moved from copper to other metal ions. The group of Duboc reported the electrochemical synthesis of a cobalt(III) thiolate compound and its redox interconversion to the related cobalt(II) compound induced by the removal of chloride anions [14]. Recently, our group presented the synthesis of a cobalt(III) thiolate compound by the reaction of a disulfide ligand with a cobalt(II) salt containing non-coordinating anions, and the redox interconversion to the isomeric cobalt(II) disulfide compound triggered by the addition of chloride anions [15]. However, to the best of our knowledge, other triggers, such as the polarity of solvents, have not yet been reported to affect the redox interconversion of cobalt(III) thiolate and cobalt(II) disulfide compounds. In this chapter, we report the solvent-dependent formation of cobalt(III) thiolate and the related cobalt(II) disulfide compounds using the rather unique $PF_2O_2^-$ anion.

3.2 Results

3.2.1 Synthesis and characterization of cobalt(II) compounds

The ligands di-2-(bis(2-pyridylmethyl)amino)-ethyl disulfide (L^1SSL^1) and di-2-((6-methyl-2-pyridylmethyl)(2-pyridylmethyl)amino)-ethyl disulfide (L^7SSL^7) were synthesized via reported procedures [8, 13]. Treatment of the ligand L^1SSL^1 with $CoCl_2$ and $AgPF_6$ in methanol resulted in a pink solution from which crystals of $[Co^{II}_2(L^1SSL^1)(PO_2F_2)_2](PF_6)_2$ were isolated (Scheme 3.1). The unexpected presence of the $PO_2F_2^-$ anion is ascribed to the use of an old batch of $AgPF_6$ that apparently was partly hydrolysed. The compound was successfully reproduced in a yield of 30% using a mixture of fresh $AgPF_6$ and commercially available $LiPO_2F_2$ [16]. Similarly, the compound $[Co^{II}_2(L^7SSL^7)(PO_2F_2)_2](PF_6)_2$ was isolated from the old batch of $AgPF_6$, and

then was reproduced in a yield of 52% using a mixture of AgPF_6 and LiPO_2F_2 . The addition of $\text{Co}(\text{NO}_3)_2 \cdot 6\text{H}_2\text{O}$ to a methanolic solution of the ligands L^1SSL^1 or L^7SSL^7 led to the formation of similar pink solutions from which the compounds $[\text{Co}^{\text{II}}_2(\text{L}^1\text{SSL}^1)(\text{NO}_3)_4]$ and $[\text{Co}^{\text{II}}_2(\text{L}^7\text{SSL}^7)(\text{NO}_3)_4]$ were isolated in a yield of 81% and 41%, respectively. All compounds were characterized by single crystal X-ray crystallography, electrospray ionization mass spectrometry (ESI-MS), elemental analysis, IR, UV-vis and nuclear magnetic resonance (NMR) spectroscopy.



Scheme 3.1. Synthetic scheme of the cobalt(II) disulfide compounds $[\text{Co}^{\text{II}}_2(\text{L}^1\text{SSL}^1)(\text{NO}_3)_4]$, $[\text{Co}^{\text{II}}_2(\text{L}^7\text{SSL}^7)(\text{NO}_3)_4]$, $[\text{Co}^{\text{II}}_2(\text{L}^1\text{SSL}^1)(\text{PO}_2\text{F}_2)_2](\text{PF}_6)_2$ and $[\text{Co}^{\text{II}}_2(\text{L}^7\text{SSL}^7)(\text{PO}_2\text{F}_2)_2](\text{PF}_6)_2$.

3.2.2 Single crystal X-ray crystallography

Single crystals of $[\text{Co}^{\text{II}}_2(\text{L}^1\text{SSL}^1)(\text{PO}_2\text{F}_2)_2](\text{PF}_6)_2$, $[\text{Co}^{\text{II}}_2(\text{L}^1\text{SSL}^1)(\text{NO}_3)_4]$ and $[\text{Co}^{\text{II}}_2(\text{L}^7\text{SSL}^7)(\text{PO}_2\text{F}_2)_2](\text{PF}_6)_2$ suitable for X-ray structure determination were obtained by slow vapor diffusion of diethyl ether into the solutions of these compounds. The crystals of $[\text{Co}^{\text{II}}_2(\text{L}^1\text{SSL}^1)(\text{PO}_2\text{F}_2)_2](\text{PF}_6)_2$ obtained from methanol and dichloromethane are isomorphous, as confirmed by single X-ray diffraction. The structure of the crystals obtained from dichloromethane solution is discussed. Projections of the structures of $[\text{Co}^{\text{II}}_2(\text{L}^1\text{SSL}^1)(\text{PO}_2\text{F}_2)_2](\text{PF}_6)_2$ and $[\text{Co}^{\text{II}}_2(\text{L}^1\text{SSL}^1)(\text{NO}_3)_4]$ are given in Figure 3.1; a projection of the structure of $[\text{Co}^{\text{II}}_2(\text{L}^7\text{SSL}^7)(\text{PO}_2\text{F}_2)_2](\text{PF}_6)_2$ is provided in Appendix II, Figure AII.1. Selected bond distances of all three compounds are provided in Table 3.1, selected angles of $[\text{Co}^{\text{II}}_2(\text{L}^1\text{SSL}^1)(\text{PO}_2\text{F}_2)_2](\text{PF}_6)_2$ and $[\text{Co}^{\text{II}}_2(\text{L}^1\text{SSL}^1)(\text{NO}_3)_4]$ are given in Table 3.2, and the refinement data of the structures are summarized in Appendix II, Tables AII.1 and AII.2. The compound $[\text{Co}^{\text{II}}_2(\text{L}^1\text{SSL}^1)(\text{PO}_2\text{F}_2)_2](\text{PF}_6)_2$ crystallizes in the triclinic space group $P\bar{1}$ with 3.3 molecules of dichloromethane co-crystallized in the asymmetric unit. The two Co(II)

ions are bound to three nitrogen donor atoms and one sulfur atom of the ligand and two oxygen atoms of separate difluoridophosphate anions in a distorted octahedral geometry. The three nitrogen donor atoms of the ligand are coordinated in a facial arrangement and the two difluoridophosphate ligands are bridging between the two cobalt(II) centers. The Co–O bond lengths range from 2.0264(13) to 2.0991(13) Å, the Co–S bond lengths are 2.5927(5) and 2.6190(5) Å. The Co–N bond distances are between 2.0797(15) and 2.1405(15) Å, and the S–S bond length is 2.0531(6) Å. The structure of $[\text{Co}^{\text{II}}_2(\text{L}^7\text{SSL}^7)(\text{PO}_2\text{F}_2)_2](\text{PF}_6)_2$ is highly similar (Appendix II, Figure AII.1).

Compound $[\text{Co}^{\text{II}}_2(\text{L}^1\text{SSL}^1)(\text{NO}_3)_4]$ crystallizes in the monoclinic space group $P2_1/n$. Both Co(II) ions are coordinated by three nitrogen donors of the ligand and three oxygen atoms of one monodentate and one bidentate nitrate anion in distorted trigonal-bipyramidal geometries if the two coordinated oxygen atoms from the bidentate nitrate ligand are regarded to occupy one coordination site. The three nitrogen donors are bound in a facial fashion. The Co–O bond distances are between 2.071(3) and 2.354(2) Å; the cobalt-to-nitrogen bond lengths range from 2.060(3) to 2.249(3) Å. The disulfide sulfur atoms are non-coordinating and the S–S bond length is 2.0372(1) Å, which is slightly shorter than in $[\text{Co}^{\text{II}}_2(\text{L}^1\text{SSL}^1)(\text{PO}_2\text{F}_2)_2](\text{PF}_6)_2$. Stacking interactions are not present in the structures, despite the presence of the aromatic pyridine groups.

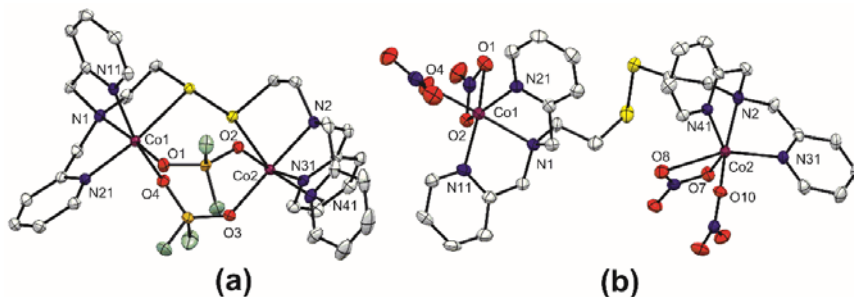


Figure 3.1. Displacement ellipsoid plot (50% probability level) of (a) the cationic part of $[\text{Co}^{\text{II}}_2(\text{L}^1\text{SSL}^1)(\text{PO}_2\text{F}_2)_2](\text{PF}_6)_2$ and (b) $[\text{Co}^{\text{II}}_2(\text{L}^1\text{SSL}^1)(\text{NO}_3)_4]$ at 110(2) K. Lattice solvent molecules, non-coordinating PF_6 anions (for a) and hydrogen atoms are omitted for clarity.

Table 3.1. Selected bond distances (Å) from the structures of the compounds $[\text{Co}^{\text{II}}_2(\text{L}^1\text{SSL}^1)(\text{PO}_2\text{F}_2)_2](\text{PF}_6)_2$, $[\text{Co}^{\text{II}}_2(\text{L}^7\text{SSL}^7)(\text{PO}_2\text{F}_2)_2](\text{PF}_6)_2$ and $[\text{Co}^{\text{II}}_2(\text{L}^1\text{SSL}^1)(\text{NO}_3)_4]$.

Bond lengths	$[\text{Co}^{\text{II}}_2(\text{L}^1\text{SSL}^1)(\text{PO}_2\text{F}_2)_2](\text{PF}_6)_2$	$[\text{Co}^{\text{II}}_2(\text{L}^7\text{SSL}^7)(\text{PO}_2\text{F}_2)_2](\text{PF}_6)_2$	$[\text{Co}^{\text{II}}_2(\text{L}^1\text{SSL}^1)(\text{NO}_3)_4]$
Co1-N1	2.1405(15)	2.139(4)	2.214(3)
Co1-N11	2.1038(15)	2.124(5)	2.085(3)
Co1-N21	2.0797(15)	2.077(5)	2.091(3)
Co1-X1	2.5927(5)	2.7119(16)	2.125(2)
Co1-X2	2.0991(13)	2.057(4)	2.333(3)
Co1-X3	2.0264(13)	2.043(4)	2.071(3)
S1-S2	2.0531(6)	2.052(3)	2.0372(1)

(X1 = S1, X2 = O2, X3 = O3 for $[\text{Co}^{\text{II}}_2(\text{L}^1\text{SSL}^1)(\text{PO}_2\text{F}_2)_2](\text{PF}_6)_2$; X1 = S1, X2 = O2, X3 = O1 for $[\text{Co}^{\text{II}}_2(\text{L}^7\text{SSL}^7)(\text{PO}_2\text{F}_2)_2](\text{PF}_6)_2$; X1 = O1, X2 = O2, X3 = O4 for $[\text{Co}^{\text{II}}_2(\text{L}^1\text{SSL}^1)(\text{NO}_3)_4]$)

Table 3.2. Selected bond angles (°) from the structures of the compounds $[\text{Co}^{\text{II}}_2(\text{L}^1\text{SSL}^1)(\text{PO}_2\text{F}_2)_2](\text{PF}_6)_2$, and $[\text{Co}^{\text{II}}_2(\text{L}^1\text{SSL}^1)(\text{NO}_3)_4]$.

Bond angles	$[\text{Co}^{\text{II}}_2(\text{L}^1\text{SSL}^1)(\text{PO}_2\text{F}_2)_2](\text{PF}_6)_2$	Bond angles	$[\text{Co}^{\text{II}}_2(\text{L}^1\text{SSL}^1)(\text{NO}_3)_4]$
S1-Co1-O2	86.65(4)	N1-Co1-N11	77.8(1)
S1-Co1-O3	99.59(4)	N1-Co1-N21	76.91(11)
S1-Co1-N1	84.93(4)	N1-Co1-O1	88.13(10)
S1-Co1-N11	79.11(4)	N1-Co1-O2	100.55(10)
S1-Co1-N21	163.91(5)	N1-Co1-O4	174.1(1)
O2-Co1-O3	94.19(5)	N11-Co1-N21	115.97(1)
O2-Co1-N1	90.65(6)	N11-Co1-O1	93.75(11)
O2-Co1-N11	163.53(6)	N11-Co1-O2	150.89(11)
O2-Co1-N21	89.57(5)	N11-Co1-O4	102.20(12)
O3-Co1-N1	173.56(6)	N21-Co1-O1	142.3(1)
O3-Co1-N11	96.28(6)	N21-Co1-O2	91.40(10)
O3-Co1-N21	96.28(6)	N21-Co1-O4	108.08(12)
N1-Co1-N11	79.98(6)	O1-Co1-O2	57.18(9)
N1-Co1-N21	79.48(6)	O1-Co1-O4	85.99(11)
N11-Co1-N21	101.84(6)	O2-Co1-O4	76.50(10)

3.2.3 Solution studies of the cobalt(II) compounds

The compound $[\text{Co}^{\text{II}}_2(\text{L}^1\text{SSL}^1)(\text{PO}_2\text{F}_2)_2](\text{PF}_6)_2$ dissolved in acetonitrile gives a yellow coloured solution, whereas solutions in methanol or dichloromethane are pink. ^1H NMR spectra were recorded from solutions of $[\text{Co}^{\text{II}}_2(\text{L}^1\text{SSL}^1)(\text{PO}_2\text{F}_2)_2](\text{PF}_6)_2$ in dichloromethane- d_2 , methanol- d_4 and acetonitrile- d_3 (Appendix II, Figures AII.2, 3, 4). The NMR spectra of the compound in dichloromethane- d_2 and methanol- d_4 show large downfield shifts up to around 70 ppm typical for a paramagnetic compound, whereas the spectra in acetonitrile show resonances in the diamagnetic region, indicating the presence of a low-spin cobalt(III) ion ($S = 0$). The effective magnetic moment of the compound dissolved in methanol was estimated using Evan's method, resulting in a μ_{eff} of 6.56 μ_{B} . This value is consistent with the presence of two high-spin ($S = 3/2$) cobalt(II) centers in methanol solution, possibly with weak antiferromagnetic coupling or partial formation of the low-spin Co^{III} compound (6.93 μ_{B} is expected for two isolated high-spin cobalt(II) centers). The UV-vis spectrum of $[\text{Co}^{\text{II}}_2(\text{L}^1\text{SSL}^1)(\text{PO}_2\text{F}_2)_2](\text{PF}_6)_2$ dissolved in acetonitrile resembles that of the compound

$[\text{Co}^{\text{III}}(\text{L}^1\text{S})(\text{MeCN})_2](\text{BF}_4)_2$ reported in our previous study, showing absorption bands at 240 nm ($\epsilon = 4.5 \times 10^3 \text{ M}^{-1}\text{cm}^{-1}$), 260 nm ($\epsilon = 5.6 \times 10^3 \text{ M}^{-1}\text{cm}^{-1}$), 285 nm ($\epsilon = 3.1 \times 10^3 \text{ M}^{-1}\text{cm}^{-1}$) and 440 nm ($\epsilon = 0.2 \times 10^3 \text{ M}^{-1}\text{cm}^{-1}$) (Figure 3.2) [15]. The peaks at 240 and 260 nm are ascribed to $\pi^* \leftarrow \pi$ transitions of the pyridyl groups, and the peaks at 285 and 440 nm are tentatively ascribed to Co \leftarrow S charge-transfer transitions (LMCT) [17]. In methanolic solution two peaks are observed at 238 ($\epsilon = 6.0 \times 10^3 \text{ M}^{-1}\text{cm}^{-1}$) and 260 nm ($\epsilon = 1.0 \times 10^4 \text{ M}^{-1}\text{cm}^{-1}$), attributed to $\pi^* \leftarrow \pi$ transitions of the pyridyl groups, and another featureless peak at 540 nm ($0.1 \times 10^3 \text{ M}^{-1}\text{cm}^{-1}$) is ascribed to a $d-d$ transition [18]. Titration of small amounts of dichloromethane into a solution of $[\text{Co}^{\text{II}}_2(\text{L}^1\text{SSL}^1)(\text{PO}_2\text{F}_2)_2](\text{PF}_6)_2$ in acetonitrile resulted in changes in the UV-vis spectra, attributed to the gradual formation of a Co(III) thiolate compound or dilution of the solution (Appendix II, Figure AII.5). Further investigation of the different ratio of acetonitrile and dichloromethane solutions of compound $[\text{Co}^{\text{II}}_2(\text{L}^1\text{SSL}^1)(\text{PO}_2\text{F}_2)_2](\text{PF}_6)_2$ showed the significant difference in UV-vis spectra (Appendix II, Figure AII.6). ESI-MS spectra of the compound dissolved in acetonitrile present a dominant peak at m/z 199.5, which fits the fragment $\frac{1}{2}[\text{Co}(\text{L}^1\text{S})(\text{MeCN})_2]^{2+}$, and two peaks at m/z 418.2 and 459.2, corresponding to the fragments $[\text{Co}(\text{L}^1\text{S}) + \text{PO}_2\text{F}_2]^+$ and $[\text{Co}(\text{L}^1\text{S}) + \text{PO}_2\text{F}_2 + \text{MeCN}]^+$, respectively (Appendix II, Figure AII.7). UV-vis spectrum of the solid sample of $[\text{Co}^{\text{II}}_2(\text{L}^1\text{SSL}^1)(\text{PO}_2\text{F}_2)_2](\text{PF}_6)_2$ shows absorption bands at 254, 456, 501, 545 and 1048 nm; the $d-d$ transitions are in agreement with a cobalt(II) center in a trigonal-bipyramidal geometry (Appendix II, Figure AII.8) [18]. The spectroscopic evidence in combination with the knowledge obtained in our previous study indicates that the cobalt(II) disulfide compound $[\text{Co}^{\text{II}}_2(\text{L}^1\text{SSL}^1)(\text{PO}_2\text{F}_2)_2](\text{PF}_6)_2$ is stable as such in methanol or dichloromethane solutions, but undergoes redox interconversion to the cobalt(III) thiolate compound $[\text{Co}^{\text{III}}(\text{L}^1\text{S})(\text{MeCN})_2]^{2+}$ when dissolved in acetonitrile.

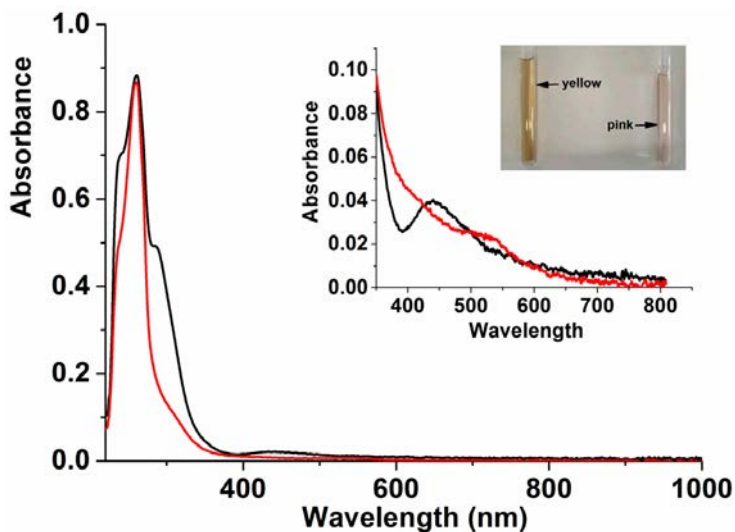


Figure 3.2. UV-vis spectra of the compound $[\text{Co}^{\text{II}}_2(\text{L}^1\text{SSL}^1)(\text{PO}_2\text{F}_2)_2](\text{PF}_6)_2$ dissolved in methanol (red line) and in acetonitrile (black line); UV-vis spectra were recorded using solutions 1 mM [Co] (0.5 mM of the dinuclear compound) with a transmission dip probe path length of 1.8 mm. The inset shows the UV-vis spectra of 2.2 mM [Co] in acetonitrile (black) and 4.4 mM [Co] in methanol (red).

Solutions of $[\text{Co}^{\text{II}}_2(\text{L}^7\text{SSL}^7)(\text{PO}_2\text{F}_2)_2](\text{PF}_6)_2$ are colored pink both in acetonitrile and methanol. ^1H NMR spectra of the compound dissolved in acetonitrile- d_3 show downfield shifts up to around 70 ppm, indicating the presence of paramagnetic cobalt ions (Appendix II, Figure AII.9). The solubility of the compound in methanol- d_4 is poor, resulting in a featureless NMR spectrum. The effective magnetic moment of the compound dissolved in acetonitrile was estimated by Evan's method to be $6.59 \mu_{\text{B}}$, in agreement with the presence of two high-spin ($S = 3/2$) cobalt(II) centers with weak antiferromagnetic coupling, or partial conversion to the Co^{III} thiolate compound. The UV-vis spectra in acetonitrile show absorption bands at 236 nm ($\epsilon = 5.0 \times 10^3 \text{ M}^{-1}\text{cm}^{-1}$) and 262 nm ($\epsilon = 1.0 \times 10^4 \text{ M}^{-1}\text{cm}^{-1}$) corresponding to $\pi^* \leftarrow \pi$ transition of the pyridyl groups. The featureless band at 510 nm ($\epsilon = 0.2 \times 10^3 \text{ M}^{-1}\text{cm}^{-1}$) is ascribed to a $d-d$ transition of the cobalt(II) ions (Appendix II, Figure AII.10) [18]. The UV-vis spectra in methanol show similar features. The ESI-MS spectrum of a solution of the compound in acetonitrile shows a peak at m/z 432.3 ascribed to the dicationic species $[\text{Co}^{\text{II}}_2(\text{L}^7\text{SSL}^7)(\text{PO}_2\text{F}_2)_2]^{2+}$ (Appendix II, Figure AII.11). The UV-vis spectrum of a solid sample of $[\text{Co}^{\text{II}}_2(\text{L}^7\text{SSL}^7)(\text{PO}_2\text{F}_2)_2](\text{PF}_6)_2$ shows absorption bands at 260 and 456 nm, as well as three bands at 504, 523, and 546 nm (Appendix II, Figure AII.12), which is similar to the UV-vis spectrum of the solid sample of $[\text{Co}^{\text{II}}_2(\text{L}^1\text{SSL}^1)(\text{PO}_2\text{F}_2)_2](\text{PF}_6)_2$. The obtained results suggest that the compound $[\text{Co}^{\text{II}}_2(\text{L}^7\text{SSL}^7)(\text{PO}_2\text{F}_2)_2](\text{PF}_6)_2$ is stable as

such in different solvents, in contrast to the non-methylated compound comprising ligand L¹SSL¹.

Solutions of [Co^{II}₂(L¹SSL¹)(NO₃)₄] are colored pink, both in acetonitrile and methanol. The compound does not dissolve in dichloromethane. The ¹H NMR spectra of the compound dissolved in acetonitrile-*d*₃ and methanol-*d*₄ show downfield shifts up to around 75 ppm (Appendix II, Figure AII.13, 14). The effective magnetic moment of the compound dissolved in dimethylformamide was estimated by Evan's method to be 6.25 μ_B, in agreement with two high-spin (*S* = 3/2) cobalt(II) centers. The UV-vis spectra in acetonitrile show absorption bands at 235 nm (ε = 7×10³ M⁻¹cm⁻¹) and 261 nm (ε = 1×10⁴ M⁻¹cm⁻¹), corresponding to π*←π transition of the pyridyl groups, and a featureless band at 510 nm (ε = 0.2×10³ M⁻¹cm⁻¹) arising from a *d-d* transition of the cobalt(II) ions (Appendix II, Figure AII.15)[18]. The UV-vis spectra in methanol show similar features. The lack of a sulfur-to-cobalt LMCT transition in both solvents and the pink color of the solutions indicated the presence of a Co(II) disulfide compound in both solvents. The ESI-MS spectra of the compound in acetonitrile show a peak at *m/z* 379.4 ascribed to the dicationic species [Co^{II}₂(L¹SSL¹)(NO₃)₂]²⁺ (Appendix II, Figure AII.16). The UV-vis spectrum of a solid sample of [Co^{II}₂(L¹SSL¹)(NO₃)₄] shows absorption bands at 260, 385, and 680 nm, as well as a broad band between 460 and 540 nm (Appendix II, Figure AII.17). The obtained results suggest that in contrast to [Co^{II}₂(L¹SSL¹)(PO₂F₂)₂](PF₆)₂ the compound [Co^{II}₂(L¹SSL¹)(NO₃)₄] does not undergo redox interconversion in acetonitrile.

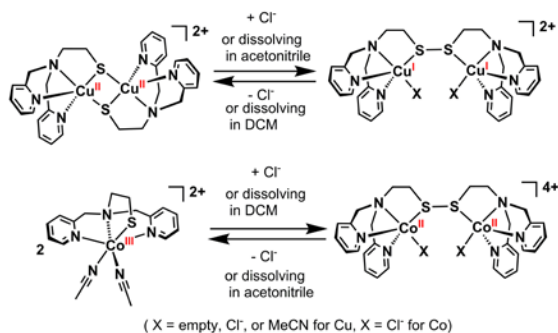
The compound [Co^{II}₂(L⁷SSL⁷)(NO₃)₄] does not dissolve in acetonitrile, but a methanolic solution of the compound is pink colored. The effective magnetic moment of the compound dissolved in methanol is 6.47 μ_B, in agreement with the presence of two high-spin cobalt(II) centers. UV-vis spectra of the compound show strong absorption bands at 233 and 263 nm, as well as a featureless band at 510 nm, similar to the spectra of [Co^{II}₂(L¹SSL¹)(NO₃)₄]. ESI-MS spectra of the compound in methanol show a peak at *m/z* 393.2 ascribed to the dicationic species [Co^{II}₂(L⁷SSL⁷)(NO₃)₂]²⁺.

3.3 Discussion

In the last decade, the redox interconversion reaction between copper(II) thiolate and copper(I) disulfide compounds has been extensively studied for ligands based on the scaffold L¹SSL¹. In recent years the group of Duboc, using another ligand set, expanded the study of redox isomerization to other transition metals, notably cobalt, manganese and iron [14, 19, 20]. The topic appears to be rather complex, as different results are obtained upon subtle changes in the ligand systems, choice of anions or solvents.

Studies of the copper compounds of the ligand L¹SSL¹ and two related ligands (methylated on the four pyridine rings, or with ethylene bridges instead of methylene) were first reported in 2001 [8]. Starting from the disulfide ligand and [Cu(MeCN)₄](ClO₄) in acetonitrile, a dinuclear copper(II) thiolate compound was formed with L¹SSL¹, whereas the two other ligands resulted in the formation of the copper(I) disulfide compounds. In other studies, it was shown that coordination of chloride anions or acetonitrile molecules to such copper(II) thiolate compounds results in the (partial and reversible) formation of their copper(I) disulfide analogs (Scheme 3.2); the extent to which this redox isomerization reaction proceeds appeared to be strongly depended on the ligand structure [11-13].

Different results are obtained when the same ligand L¹SSL¹ is used in combination with cobalt(II) instead of copper(I) salts. The presence of (coordinating) chloride ions induces the formation of the cobalt(II) disulfide compound, which is similar to the result with copper. However, in contrast to copper, the cobalt(III) thiolate species seem to be favored in acetonitrile solutions, but only in combination with specific anions, and depending on the ligand structure. Thus, for the ligand L¹SSL¹ the use of tetrafluoridoborate or difluoridophosphate in acetonitrile leads to the formation of the cobalt(III) thiolate species, with two coordinating acetonitrile molecules. However, the matter is more complicated for cobalt: unexpectedly, the use of the coordinating thiocyanate anion also leads to the formation of the corresponding Co^{III} thiolate compound, which is formed even in methanol or dichloromethane (unpublished results; see (Appendix II, Figure AII.18)).



Scheme 3.2. Reported redox interconversion between metal thiolate and disulfide compounds, tuned by anions or different solvents. For simplicity only the basic ligand structure for L¹SSL¹ is shown, however, the reactions are strongly dependent on the exact ligand structure.

It seems that for the ligand system based on the L¹SSL¹ scaffold, the formation of the copper(II) thiolate redox isomer is mainly dictated by the coordination strength of the

anion or the solvent: coordinating anions (Cl⁻) or solvents (acetonitrile) lead to the formation of the copper(I) disulfide. In contrast, the formation of the cobalt(III) thiolate compound seems to be related to the ligand-field strength of the anion or solvent, rather than the coordinating strength. Ligands (solvent or anion) inducing a large ligand-field splitting result in the formation of a low-spin cobalt(II) disulfide compound with one single electron in a high-energy orbital and a 19-electron count. It is understandable that this low-spin state results in redox isomerization to form the low-spin cobalt(III) thiolate compound, as then a stable compound is formed with an 18-electron count. For the Duboc system again another driving force is operative, as in that case the addition of coordinating ligands seem to favor the formation of the cobalt(III) thiolate redox isomer.

3.4 Conclusion

We have described the synthesis and characterization of four new cobalt(II) disulfide compounds, based on the ligands L¹SSL¹ and L⁷SSL⁷, and using the anions PO₂F₂ and NO₃. It is shown that a coordinating solvent such as acetonitrile induces redox interconversion of the compound [Co^{II}₂(L¹SSL¹)(PO₂F₂)₂](PF₆)₂ to the corresponding cobalt(III) thiolate compound. Remarkably, the cobalt(II) disulfide compound of the related ligand L⁷SSL⁷, in which two methyl groups are present at two of the pyridine rings, does not show this redox interconversion in any of the investigated solvents. This result seems to be in disagreement with our hypothesis that formation of the cobalt(III) thiolate is triggered by ligands that induce larger ligand-field splitting, as generally the methylation of a pyridine is expected to increase the ligand-field strength. Future studies will be directed to generate further understanding of the factors influencing the redox isomerization of cobalt, iron and manganese compounds of disulfide ligands.

3.5 Experimental section

3.5.1 General procedures

All reagents were obtained from commercial sources and used as received unless noted otherwise. LiPO₂F₂ was purchased from ChemFish co. Ltd, China. Acetonitrile and diethyl ether were obtained from a solvent dispenser (PureSolv 400). Dichloromethane and methanol were purchased from commercial vendors and stored on 3 Å molecular sieves. The synthesis of cobalt compounds was carried out using standard Schlenk-line techniques under a nitrogen atmosphere. ¹H NMR and ¹³C NMR spectra were recorded on a Bruker 300 DPX spectrometer at room temperature. Mass spectra were recorded on a Finnigan Aqua mass spectrometer with electrospray ionization (ESI). IR spectra were acquired on a PerkinElmer UATR spectrum equipped

with a single reflection diamond (scan range 400 cm⁻¹ to 4000 cm⁻¹, resolution 4 cm⁻¹). UV-vis spectra were collected using a transmission dip probe with variable path length on an Avantes Avaspec-2048 spectrometer with Avalight-DH-S-BAL light source. Elemental analyses were performed by the Microanalytical Laboratory Kolbe in Germany.

3.5.2 Single crystal X-ray crystallography

For compounds [Co^{II}₂(L¹SSL¹)(NO₃)₄] and [Co^{II}₂(L¹SSL¹)(PO₂F₂)₂](PF₆)₂, all reflection intensities were measured at 110(2) K using a SuperNova diffractometer (equipped with Atlas detector) with Mo K α radiation ($\lambda = 0.71073 \text{ \AA}$) under the program CrysAlisPro (Version CrysAlisPro 1.171.39.29c, Rigaku OD, 2017). The same program was used to refine the cell dimensions and for data reduction. The structure was solved with the program SHELXS-2014/7 and was refined on F^2 with SHELXL-2014/7 [21]. Numerical absorption correction based on gaussian integration over a multifaceted crystal model was applied using CrysAlisPro. The temperature of the data collection was controlled using the system Cryojet (manufactured by Oxford Instruments). The H atoms were placed at calculated positions using the instructions AFIX 23 or AFIX 43 with isotropic displacement parameters having values 1.2 U_{eq} of the attached C atoms. The structures of compounds [Co^{II}₂(L¹SSL¹)(NO₃)₄] and [Co^{II}₂(L¹SSL¹)(PO₂F₂)₂](PF₆)₂ are partly disordered. For the compound [Co^{II}₂(L⁷SSL⁷)(PO₂F₂)₂](PF₆)₂, The data was collected in a Bruker APEX II CCD diffractometer at the Advanced Light Source beamline 11.3.1 at Lawrence Berkeley National Laboratory from a silicon (111) monochromator (T = 100, K, $\lambda = 0.7749 \text{ \AA}$). The crystal was taken directly from its solution, with a drop of Paratone-N oil and immediately put into the cold stream or dry N₂ on the goniometer. The structure was solved by direct methods and the refinement on F^2 and all further calculations were carried out with the SHELX-TL suite.

For the compound [Co^{II}₂(L¹SSL¹)(NO₃)₄], one of the coordinating nitrate anions is disordered over two orientations; the occupancy factor of the major component refines to 0.905(4). The crystal that was mounted on the diffractometer was twinned with two components. The twin relationship corresponds to a twofold axis along c^* . The BASF scale factor refines to 0.3725(8).

For the compound [Co^{II}₂(L¹SSL¹)(PO₂F₂)₂](PF₆)₂, the two PF₆⁻ counter ions are found to be disordered over either two or three orientations. All occupancy factors can be retrieved from the cif file. The asymmetric unit also contains four lattice dichloromethane solvent molecules. One solvent molecule is found to be partially occupied with an occupancy factor refined to 0.923(2). Another solvent molecule is found at a site of inversion symmetry, and is also partially occupied. The occupancy

factor refines to 0.4146(17). The two species that bridge the two Co metal centers (Co1 and Co2) were identified as two difluoridophosphate counter ions. The occupancy factors of P1, O1, O2, F1, F2 and P2, O3, O4, F3, F4 were set to refine freely, and their refined values (with esd) are 0.980(3), 1.043(6), 1.040(6), 1.001(5), 1.002(5) and 0.980(3), 1.058(6), 1.046(6), 1.004(5), 1.011(5), respectively. A quick search on the CSD confirm that the P–O and P–F bond distances are consistent with those found in this crystal structure.

3.5.3 Synthesis of the cobalt compounds

[Co^{II}₂(L¹SSL¹)(PO₂F₂)₂](PF₆)₂: The compound [Co^{II}₂(L¹SSL¹)(PO₂F₂)₂](PF₆)₂ was unexpectedly obtained from an old batch of AgPF₆, and was successfully reproduced using fresh AgPF₆ in combination with LiPO₂F₂. The ligand L¹SSL¹ (0.20 mmol; 103.2 mg) was dissolved in 5 mL dry and degassed methanol, and then CoCl₂ (0.20 mmol; 47.9 mg) was added, giving a dark purple solution. After stirring for 30 min a purple suspension was obtained. Then, AgPF₆ (0.80 mmol; 202.3 mg) and LiPO₂F₂ (0.40 mmol, 43.1 mg) were added to the reaction mixture, resulting in a pink solution with a white precipitate. The obtained mixture was stirred for another two hours, and filtered through celite, yielding a clear red solution. The obtained red solution was evaporated to 1 mL, to which 15 mL diethyl ether was added, yielding an oily material. This oily material was dissolved in dichloromethane; vapor diffusion of diethyl ether into this solution resulted in the formation of pink crystals. Yield: 64.0 mg, 0.06 mmol, 30%. ESI-MS in acetonitrile: found (calcd) for ½[Co(L¹S) + 2MeCN]²⁺ *m/z* 199.5 (199.5); [Co(L¹S) + PO₂F₂]⁺ *m/z* 418.2 (418.0); [Co(L¹S) + PO₂F₂ + MeCN]⁺ *m/z* 459.2 (459.0). Elemental analysis calcd for C₂₈H₃₂Co₂F₁₆N₆O₄P₄S₂: C 29.86, H 2.86, N 7.46; Found: C 30.07, H 3.24, N 7.71. UV-vis in CH₃CN at 1 mM [Co] concentration: 238 nm ($\epsilon = 4.5 \times 10^3 \text{ M}^{-1} \text{ cm}^{-1}$), 260 nm ($\epsilon = 5.6 \times 10^3 \text{ M}^{-1} \text{ cm}^{-1}$), and 286 nm ($\epsilon = 3.1 \times 10^3 \text{ M}^{-1} \text{ cm}^{-1}$), 441 nm ($\epsilon = 2 \times 10^2 \text{ M}^{-1} \text{ cm}^{-1}$); UV-vis in MeOH at 1 mM [Co] concentration: 238 ($\epsilon = 6.0 \times 10^3 \text{ M}^{-1} \text{ cm}^{-1}$), 260 nm ($\epsilon = 1.0 \times 10^4 \text{ M}^{-1} \text{ cm}^{-1}$), 540 nm ($1.0 \times 10^2 \text{ M}^{-1} \text{ cm}^{-1}$). IR spectrum (cm⁻¹): 1609w, 1443w, 1283m, 1154m, 1027w, 922w, 828s, 764m, 652w, 554s.

[Co^{II}₂(L¹SSL¹)(NO₃)₄]: The ligand L¹SSL¹ (0.10 mmol; 51.67 mg) was dissolved in 5 mL dry and degassed acetonitrile, and then Co(NO₃)₂·6H₂O (0.20 mmol; 58.21 mg) was added, giving a dark red solution. After stirring for 1 h, 30 mL diethyl ether was added, resulting in a pink precipitate. The obtained precipitate was collected by filtration and washed with diethyl ether (2×20 mL). Yield: 71 mg, 0.08 mmol, 81%. Single crystals suitable for X-ray diffraction were grown by vapor diffusion of diethyl ether into a methanolic solution of the compound. ESI-MS in acetonitrile: found (calcd) for ½[M – 2NO₃]²⁺ *m/z* 379.4 (379.3). Elemental analysis calcd for C₂₈H₃₂Co₂N₁₀O₁₂S₂: C 38.10, H

3.65, N 15.87; Found: C 38.17, H 3.74, N 15.81. UV-vis in CH₃CN at 1 mM [Co] concentration: 235 nm ($\epsilon = 7 \times 10^4 \text{ M}^{-1} \text{ cm}^{-1}$), 261 nm ($\epsilon = 1 \times 10^4 \text{ M}^{-1} \text{ cm}^{-1}$), 512 nm ($\epsilon = 2 \times 10^2 \text{ M}^{-1} \text{ cm}^{-1}$); UV-vis in MeOH at 1 mM [Co] concentration: 235 nm ($\epsilon = 7 \times 10^4 \text{ M}^{-1} \text{ cm}^{-1}$), 261 nm ($\epsilon = 1 \times 10^4 \text{ M}^{-1} \text{ cm}^{-1}$), 511 nm ($\epsilon = 2 \times 10^2 \text{ M}^{-1} \text{ cm}^{-1}$). IR spectrum (cm^{-1}): 2971w, 1609m, 1484m, 1460s, 1304s, 1280s, 1159w, 1102w, 1056w, 1023s, 952w, 885w, 862w, 884w, 810w, 767m, 736 w, 651w, 473w.

[Co^{II}₂(L⁷SSL⁷)(PO₂F₂)₂](PF₆)₂: The ligand L⁷SSL⁷ (0.20 mmol; 108.1 mg) was dissolved in 5 mL dry and degassed acetonitrile, and then CoCl₂ (0.40 mmol; 51.5 mg) was added, giving a dark purple solution. After stirring for 1 h, a purple suspension was obtained, to which AgPF₆ (0.80 mmol; 200.9 mg) and LiPO₂F₂ (0.40 mmol, 42.3 mg) were added, resulting in a pink solution with a white precipitate. The obtained mixture was stirred for 24 hours and then filtered through celite, yielding a clear red solution. The obtained red solution was evaporated to 2 mL, to which 20 mL diethyl ether was added, which yielded a pink precipitate. The obtained precipitate was collected by filtration and washed with diethyl ether (3×15 mL). Single crystals suitable for synchrotron X-ray diffraction were grown by vapor diffusion of diethyl ether into an acetonitrile solution containing the compound. Yield: 119 mg, 0.10 mmol, 52%. ESI-MS in which solvent found (calcd) for $\frac{1}{2}[\text{M} - 2 \text{ PO}_2\text{F}_2]^{2+}$ m/z 432.3 (432.1). UV-vis in acetonitrile at 2 mM [Co] concentration: 236 nm ($\epsilon = 5.0 \times 10^3 \text{ M}^{-1}\text{cm}^{-1}$), 262 nm ($\epsilon = 1.0 \times 10^4 \text{ M}^{-1}\text{cm}^{-1}$) and 510 nm ($\epsilon = 0.15 \times 10^3 \text{ M}^{-1}\text{cm}^{-1}$). Elemental analysis calcd for C₃₀H₃₆Co₂F₁₆N₆O₄P₄S₂ + 2H₂O: C 30.27, H 3.39, N 7.06; Found: C 29.81, H 2.88, N 7.40. IR spectrum (cm^{-1}): 1610w, 1446w, 1307m, 1160m, 1023w, 923w, 830w, 766m, 654w, 556s.

[Co^{II}₂(L⁷SSL⁷)(NO₃)₄]: The ligand L⁷SSL⁷ (0.10 mmol; 54.7 mg) was dissolved in 5 mL dry methanol, and then Co(NO₃)₂·6H₂O (0.20 mmol; 58.7 mg) was added, giving a dark red solution. After stirring for 1h, 15 mL diethyl ether was added, resulting in a pink precipitate. The obtained precipitate was collected by filtration and washed with diethyl ether (2×10 mL). Yield: 32 mg, 0.04 mmol, 41%. ESI-MS in which solvent found (calcd) for $\frac{1}{2}[\text{M} - 2 \text{ NO}_3]^{2+}$ m/z 393.4 (393.3). UV-vis in MeOH at 1 mM [Co]: 233 nm ($\epsilon = 7.0 \times 10^4 \text{ M}^{-1} \text{ cm}^{-1}$), 263 nm ($\epsilon = 1.0 \times 10^4 \text{ M}^{-1} \text{ cm}^{-1}$), 510 nm ($\epsilon = 0.2 \times 10^3 \text{ M}^{-1} \text{ cm}^{-1}$). Elemental analysis calcd for for C₃₀H₃₆Co₂N₁₀O₁₂S₂ + CH₃OH + 0.5H₂O: C 39.12, H 4.34, N 14.72; Found: C 39.08, H 4.84, N 15.21. IR spectrum (cm^{-1}): 1608m,1464s, 1287s, 1162w, 1093w, 1020m, 768m, 647w.

3.6. References

- [1] H.F. Gilbert, *Methods Enzymol.*, 251 (1995) 8-28.
- [2] C. Jacob, G.I. Giles, N.M. Giles, H. Sies, *Angew. Chem., Int. Edit.*, 42 (2003) 4742-4758.
- [3] R. Singh, G.M. Whitesides, *Sulphur-containing functional groups*, John Wiley & Sons, Inc., 1993.
- [4] E.I. Solomon, U.M. Sundaram, T.E. Machonkin, *Chem. Rev.*, 96 (1996) 2563-2606.
- [5] G. Meloni, P. Faller, M. Vasak, *J. Biol. Chem.*, 282 (2007) 16068-16078.
- [6] G. Meloni, V. Sonois, T. Delaine, L. Guilloreau, A. Gillet, J. Teissié, P. Faller, M. Vašák, *Nat. Chem. Biol.*, 4 (2008) 366.
- [7] J.T. Pedersen, C. Hureau, L. Hemmingsen, N.H. Heegaard, J. Østergaard, M. Vašák, P. Faller, *Biochemistry*, 51 (2012) 1697-1706.
- [8] S. Itoh, M. Nagagawa, S. Fukuzumi, *J. Am. Chem. Soc.*, 123 (2001) 4087-4088.
- [9] A. Neuba, R. Haase, W. Meyer-Klaucke, U. Flörke, G. Henkel, *Angew. Chem. Int. Ed.*, 51 (2012) 1714-1718.
- [10] E.C.M. Ording-Wenker, M. van der Plas, M.A. Siegler, C. Fonseca Guerra, E. Bouwman, *Chem. Eur. J.*, 20 (2014) 16913-16921.
- [11] E.C. Ording-Wenker, M. van der Plas, M.A. Siegler, S. Bonnet, F.M. Bickelhaupt, C. Fonseca Guerra, E. Bouwman, *Inorg. Chem.*, 53 (2014) 8494-8504.
- [12] A.M. Thomas, B.-L. Lin, E.C. Wasinger, T.D.P. Stack, *J. Am. Chem. Soc.*, 135 (2013) 18912-18919.
- [13] Y. Ueno, Y. Tachi, S. Itoh, *J. Am. Chem. Soc.*, 124 (2002) 12428-12429.
- [14] M. Gennari, B. Gerey, N. Hall, J. Pécaut, M.N. Collomb, M. Rouzières, R. Clérac, M. Orio, C. Duboc, *Angew. Chem., Int. Edit.*, 53 (2014) 5318-5321.
- [15] F. Jiang, M.A. Siegler, X. Sun, L. Jiang, C. Fonseca. Guerra, E. Bouwman, *Inorg. Chem.*, 57 (2018) 8796-8805.
- [16] The chemical LiPO_2F_2 was purchased from <http://www.chemfish.com/>.
- [17] I.K. Adzamlı, K. Libson, J. Lydon, R. Elder, E. Deutsch, *Inorg. Chem.*, 18 (1979) 303-311.
- [18] A.B.P. Lever, *Inorganic electronic spectroscopy*, 2nd ed., Elsevier, 1968.
- [19] L. Wang, F.G. Cantú Reinhard, C. Philouze, S. Demeshko, S.P. de visser, F. Meyer, M. Gennari, C. Duboc, *Chem. Eur. J.*, 24(2018) 11973-11982.
- [20] M. Gennari, D. Brazzolotto, S. Yu, J. Pécaut, C. Philouze, M. Rouzières, R. Clérac, M. Orio, C. Duboc, *Chem. Eur. J.*, 21 (2015) 18770-18778.
- [21] G.M. Sheldrick, *Acta Crystallogr. C*, 71 (2015) 3-8.

Chapter 4

The Reactivity of Fe(II) and Co(II) Disulfide Compounds with Dihydrogen Peroxide

The reactivity of two metal disulfide compounds $[M^{II}_2(L^1SSL^1)Cl_4]$ ($M = Co$ and Fe , $L^1SSL^1 = di-2-(bis(2-pyridylmethyl)amino)ethyl$ disulfide) with dihydrogen peroxide has been investigated. Reaction of the iron(II) disulfide compound $[Fe^{II}_2(L^1SSL^1)Cl_4]$ with H_2O_2 results in the formation of the mononuclear Fe(III) sulfonate compound $[Fe^{III}(L^1SO_3)Cl_2]$. The crystal structure combined with EPR spectroscopy confirms that a high-spin ($S = 5/2$) Fe(III) center was generated, which is coordinated by three nitrogen donors and one oxygen atom of the sulfonate group of the tetradentate ligand, and two chloride ions in an octahedral geometry. In contrast, reaction of the compound $[Co^{II}_2(L^1SSL^1)Cl_4]$ with H_2O_2 yielded the mononuclear Co(III) sulfinato compound $[Co^{III}(L^1SO_2)Cl_2]$. The crystal structure and NMR spectroscopy show that in this case a low-spin ($S = 0$) cobalt(III) center was obtained, which is coordinated by three nitrogen donors and one sulfur atom of the sulfinato group of the tetradentate ligand and two chloride ions in an octahedral geometry.

This chapter has been published as a full paper: Feng Jiang, Maxime A. Siegler, and Elisabeth Bouwman, Eur. J. Inorg. Chem. 2018, in press

4.1 Introduction

Reactions involving dioxygen assisted by metalloenzymes occur in numerous biological systems and play fundamental roles important for health like DNA replication and repair [1, 2], as well as the biosynthesis of physiologically vital hormones and neurotransmitters [3, 4]. A typical example is provided by the non-heme iron enzyme cysteine dioxygenase (CDO), which catalyzes the oxidation of the thiolate of cysteine to a sulfinic acid group. It is believed that some neurological diseases such as Parkinson and Alzheimer are related to the absence of the enzyme CDO [5, 6]. Another example concerns the cobalt or iron-containing enzyme nitrile hydratase (NHase), where the metal centers are coordinated by two nitrogen atoms from the peptide backbone, one sulfur donor of a cysteine group in the apical position, and two other sulfur donor atoms originating from a sulfenate and a sulfinate group (Figure 4.1). In this case, dioxygen is most likely the oxidant to modify the cysteine sulfur atoms of the enzyme in vivo, which modifies the activity of the enzymes [7, 8]. As understanding of the degradation pathways of metalloenzymes is of considerable importance, bioinorganic chemists have undertaken the synthesis of Ni^{II}, Cu^{II}, Zn^{II} analogues of N₄S, N₃S, or N₂S₂ ligands, and investigated their reactivity with oxidizing agents [9-15]. The study of the oxidation sensitivity of Fe^{II} thiolate compounds has been described as helpful for the understanding of the role of the metalloenzyme CDO [16-19].

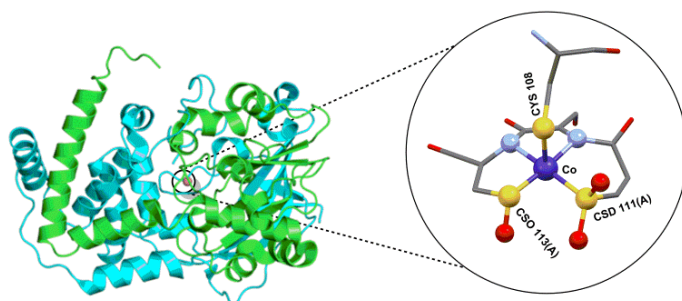
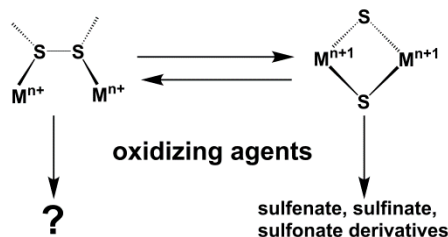


Figure 4.1. Schematic impression of the Co-factor of Nitrile Hydratase obtained from *Pseudonocardia thermophila* (yellow, sulfur; purple, cobalt; pale-blue, nitrogen; red, oxygen). The sixth coordination site is normally occupied by water creating an octahedral geometry [20].

Despite the considerable progress made in the last decades, study of the oxidation of sulfur ligands in metal compounds is still important in terms of the following two aspects. First of all, so far most research focused on the study of the oxidation of thiolate compounds of nickel [10, 12, 13, 21, 22], or iron [17, 18, 22-29], related to the oxidation sensitivity of hydrogenases, whereas only few studies have been reported concerning the oxidation sensitivity of cobalt compounds as mimics of the

metalloenzyme Co-NHase [30]. Secondly, the redox interconversion between high-valent metal thiolate and low-valent metal disulfide compounds has been studied in the last decade, especially for copper but more recently also for cobalt compounds (Scheme 4.1) [19, 31-36]. However, up till now, only a limited number of studies has been reported on the oxidation of metal disulfide compounds [37]. To the best of our knowledge, only the group of Karlin reported the reactivity of a Cu(I) disulfide compound with dioxygen, which was shown to result in the formation of a copper(II) sulfonate compound [37]. In the last few years, Torelli et al.[38] investigated the mechanism of S-S bond cleavage of a Cu(II) disulfide compound, and spectroscopic evidence showed that, in aqueous conditions, water acts as the nucleophile to attack the S-S bond, yielding the sulfinato and sulfonate derivatives. Herein we report the reactivity of two metal disulfide compounds $[M^{II}_2(L^1SSL^1)Cl_4]$ ($M = Fe, Co$; $L^1SSL^1 =$ (di-2-(bis(2-pyridylmethyl)amino)ethyl disulfide)) with dihydrogen peroxide.

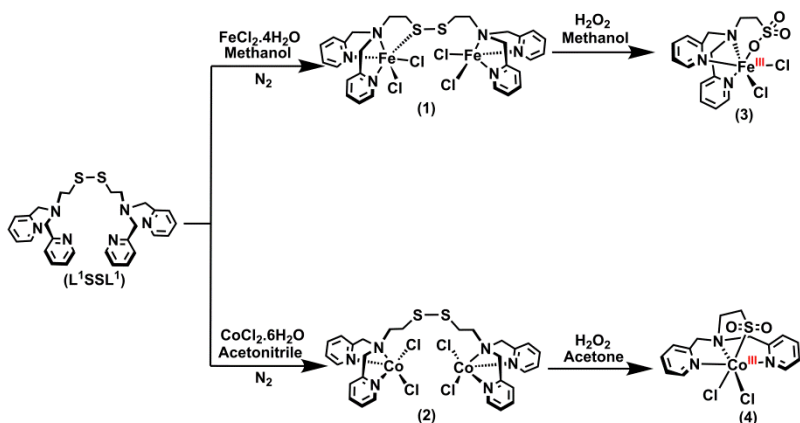


Scheme 4.1. Overview of the redox interconversion between metal thiolate and disulfide compounds, and the potential oxidative processes.

4.2 Results

4.2.1 Synthesis and characterization of the oxidized iron and cobalt compounds

The ligand L^1SSL^1 and the coordination compounds $[Fe^{II}_2(L^1SSL^1)Cl_4]$ (**1**) and $[Co^{II}_2(L^1SSL^1)Cl_4]$ (**3**) were synthesized via reported procedures [34, 36, 39]. The addition of 80 equivalents of H_2O_2 to one equivalent of **1** in methanol resulted in a color change from yellow to dark brown, then back to yellow with in a few seconds. From this reaction mixture the compound $[Fe^{III}(L^1SO_3)Cl_2]$ (**2**) was isolated in a yield of 58% (Scheme 4.2). Similarly, the addition of ~80 equivalents of H_2O_2 to one equivalent of **3** in acetone led to the formation of the compound $[Co^{III}(L^1SO_2)Cl_2]$ (**4**) in a yield of 83%. The compounds were characterized with 1H NMR, UV-Vis, and IR spectroscopy, electrospray ionization mass spectrometry (ESI-MS), elemental analysis and single crystal X-ray crystallography.



Scheme 4.2. Synthesis scheme of the metal(II) disulfide compounds **1** and **3**, and the oxidation products **2** and **4**.

Full characterization of **1** and **3** has been reported in our previous study [39]. The ESI-MS spectrum of **2** dissolved in methanol presents a dominant peak (m/z) at 189.2 assigned to the fragment $\frac{1}{2}[Fe(L^1SO_3)(H_2O)]^{2+}$ (Figure AIII.1). The IR spectrum of **2** shows two intense absorption bands at around 1022 and 1146 cm^{-1} likely corresponding to the symmetric and asymmetric S=O bond stretching frequencies [40]. The EPR spectrum of **2** dissolved in dimethyl sulfoxide shows a rather broad, isotropic spectrum with a g value of around 4.25, typical for an Fe(III) center in a high-spin state ($S = 5/2$; Figure AIII.2) [41]. The ESI-MS spectrum of **4** dissolved in acetonitrile shows a dominant peak (m/z) at 425.5 fitting the fragment $[Co^{III}(L^1SO_2)Cl(MeCN)]^+$, and a peak at 384.4 corresponding to the fragment $[Co^{III}(L^1SO_2)Cl]^+$ (Figure AIII.3). The IR spectrum of **4** shows two strong absorption bands at 1074 and 1173 cm^{-1} ascribed to vibrations of the sulfinyl group [42]. The signals in the 1H NMR spectrum of **4** dissolved in acetonitrile- d_3 are observed in the diamagnetic region, consistent with the Co(III) center in this compound being in a low-spin state ($S = 0$; Figure AIII.4).

4.2.2 Description of the crystal structures

The crystal structures of **1** and **3** have been reported in our previous study [39]. Single crystals of **2** and **4** suitable for X-ray structure determination were acquired by slow vapor diffusion of diethyl ether into solutions of the compounds in dimethylformamide and acetone, respectively. Crystallographic and refinement data of the structures are summarized in the Supporting Information Table AIII.1. Projections of the structures are provided in Figure 4.2, selected bond distances and angles are given in Table 4.1. Compound **2** crystallizes in the monoclinic space group

$P2_1/c$ with two crystallographically independent molecules of the compound and one lattice dimethylformamide solvent molecule in the asymmetric unit. The two independent molecules have very similar conformations. The Fe^{III} ion is coordinated by the three nitrogen donors from the tetradentate ligand bound in a facial arrangement, one oxygen donor atom of the sulfonate group and two chloride ions in a slightly distorted octahedral geometry with one of the chloride ions bound *trans* to the tertiary amine and the other *trans* to one of the pyridine nitrogen atoms. The Fe-O bond lengths are 1.9666(13)/1.9870(13) Å, and the Fe-N bond distances range from 2.1421(16) to 2.2516(15) Å. There are no hydrogen-bonding or stacking interactions present in the structure of **2**.

Compound **4** crystallizes in the monoclinic space group $P2_1/n$ with one molecule of the compound and three lattice water solvent molecules in the asymmetric unit. The hydrogen atoms in two of the three water molecules are disordered over two different orientations. The cobalt(III) ion is coordinated by three nitrogen donors of the ligand bound in a meridional fashion, the sulfur donor of the sulfinate group and two chloride ions in an octahedral configuration. The Co-S bond length is 2.1820(5) Å; the Co-N bond distances range from 1.9311(16) to 1.9724(15) Å, which are much shorter than the Co-N distances in **3**, and in agreement with a low-spin ($S = 0$) state of cobalt(III) ion. The Co-Cl1 distance is significantly shorter than the Co-Cl2 distance (2.2504(5) and 2.3274(5) Å, respectively), indicative of the larger *trans* influence of the sulfinate sulfur donor atom. The lattice water molecules are hydrogen bonded to one of the oxygen atoms of the sulfinate group. The crystal packing of **4** does not contain stacking interactions.

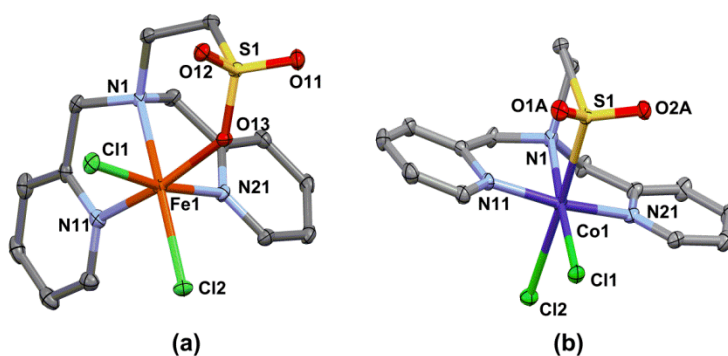


Figure 4.2. Displacement ellipsoid plots (50% probability level) of (a) compound **2** and (b) compound **4** at 110(2) K. The lattice solvent molecules and hydrogen atoms are omitted for clarity.

Table 4.1. Selected bond distances (Å) and angles (°) from the crystal structure of compounds **2** and **4**.^{[a][b]}

Distances/Angles	2	4	Distances/Angles	2	4
M-N1	2.2516(15)	1.9724(15)	M-X	1.9666(13)	2.1820(5)
M-N11	2.1998(15)	1.9311(16)	M-Cl1	2.2850(5)	2.2504(5)
M-N21	2.1530(17)	1.9499(16)	M-Cl2	2.2758(5)	2.3274(5)
Cl1-M-Cl2	97.793(19)	91.783(18)	Cl2-M-X	97.13(4)	176.81(2)
Cl1-M-N1	168.37(4)	176.17(5)	N1-M-N11	77.26(6)	85.09(7)
Cl1-M-N11	92.01(4)	96.57(5)	N1-M-N21	77.28(6)	83.17(7)
Cl1-M-N21	96.79(4)	95.23(5)	N1-M-X	87.92(6)	88.90(5)
Cl1-M-X	96.60(4)	87.706(18)	N11-M-X	80.92(6)	168.17(7)
Cl2-M-N1	92.25(4)	91.70(5)	N11-M-X	89.60(5)	88.44(5)
Cl2-M-N11	167.37(4)	88.49(5)	N21-M-X	163.83(6)	92.79(5)
Cl2-M-N21	89.99(4)	90.40(5)			

[a] M = Fe1, X = O13 for **2**, M = Co1, X=S1 for **4**. [b] For compound **2**, the bond distances and angles are given only for one of the two crystallographically independent Fe complexes (complex A).

4.2.3 Monitoring the reactivity of **1** and **3** with H₂O₂

UV-Vis spectra of **1** dissolved in methanol show absorption bands at 256, 313 and 390 nm [39]. UV-Vis spectra of compound **2** dissolved in methanol show an intense absorption band at 258 nm ($\epsilon = 4 \times 10^3 \text{ M}^{-1} \text{ cm}^{-1}$) assigned to the $\pi \rightarrow \pi^*$ transitions of the pyridyl groups, as well as two weak bands at 377 nm ($\epsilon = 0.5 \times 10^3 \text{ M}^{-1} \text{ cm}^{-1}$) and 485 nm ($\epsilon = 0.1 \times 10^3 \text{ M}^{-1} \text{ cm}^{-1}$) tentatively ascribed to ligand-to-metal charge transfer transitions (LMCT) (Figure AIII.5).

The formation of the mononuclear sulfonato-iron(III) compound **2** by the reaction of **1** with H₂O₂ in methanol was monitored using UV-Vis spectroscopy at room temperature. The addition of an excess of 35% H₂O₂ (0.2 mmol, 40 equivalents to **1**) to the solution containing **1** resulted in a color change from yellow to dark brown, and then back to yellow immediately. The reaction occurred very fast, UV-Vis spectra showed a new band at 375 nm appearing instantly after addition of H₂O₂ and increasing in intensity during the whole process. In contrast, the band at 394 nm decreases rapidly until it disappears (Figure AIII.6). Isosbestic points are not observed, suggesting that more than one compound is formed during this process. Attempts have been performed to trap the intermediates, first by lowering the temperature to -41 °C, but the spectra were nearly identical with those obtained at room temperature (Figure AIII.7). Upon further reducing the temperature to -78 °C, the reaction slows down and the spectra show the formation of a new band at 375 nm with a gradual decrease of the band at 394 nm. At this reaction temperature an isosbestic point is observed, indicating the transformation to one new compound (Figure 4.3). An ESI-MS spectrum recorded of this reaction mixture shows peaks at *m/z* 381.1, 397.1 and 429.2, corresponding to the fragments [Fe^{III}(L¹SO₂)Cl]⁺, [Fe^{III}(L¹SO₃)Cl]⁺, and

$[\text{Fe}^{\text{III}}(\text{L}^1\text{SO}_3)\text{Cl} + \text{CH}_3\text{OH}]^+$, respectively (Figure AIII.8). This clearly shows that the sulfinato-iron(III) compound is an intermediate; the observation of the sulfonate-compound must be due to the high rate of the reaction at room temperature while transferring the solution to the mass spectrometer. An absorption band that could potentially be ascribed to interactions of the iron center with dihydrogen peroxide (e.g. a hydroperoxido-to-iron(III) LMCT) was not found [43]. Further attempts were undertaken to slow down the oxidation process by titration of small amounts of H_2O_2 into the methanolic solution of **1**, but unfortunately did not result in additional information (Figure AIII.9). An attempt was made to trap a potential alkylperoxido-Fe(III) intermediate by the reaction of **1** with $t\text{BuOOH}$ at $-41\text{ }^\circ\text{C}$, but unfortunately this attempt was also not successful (Figure AIII.10).

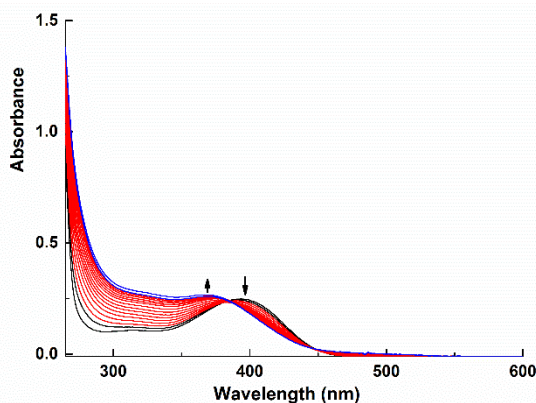


Figure 4.3. The change in UV-Vis spectra upon addition of H_2O_2 (0.8 mmol, 80 equivalents to **1**) to compound **1** in methanolic solution at $-78\text{ }^\circ\text{C}$. UV-Vis spectra were recorded using a solution 2 mM in $[\text{Fe}]$ (10 mL) with a transmission dip probe path length of 1.2 mm. Spectra were recorded every 30 seconds over a period of 10 minutes.

Compound **3** is stable in air. UV-Vis spectra of **3** dissolved in acetonitrile show absorption bands at 261, 524, 570, and 640 nm [39]. UV-Vis spectra of **4** dissolved in acetonitrile present several absorption bands, the one at 236 nm is attributed to $\pi \rightarrow \pi^*$ transitions of the pyridyl groups ($\epsilon = 1.1 \times 10^4\text{ M}^{-1}\text{ cm}^{-1}$), whereas two bands at 327 ($\epsilon = 9.5 \times 10^3\text{ M}^{-1}\text{ cm}^{-1}$) and 525 nm ($\epsilon = 0.5 \times 10^3\text{ M}^{-1}\text{ cm}^{-1}$) likely correspond to LMCT transitions (Figure AIII.11) [19, 39].

The reaction of **3** with H_2O_2 in acetonitrile was monitored using UV-Vis spectroscopy at room temperature. The addition of 35% H_2O_2 (0.8 mmol, 80 equivalent to **3**) to a solution of **3** in acetonitrile resulted in a gradual color change from purple to brown-yellow over a period of 1.5 hours. UV-Vis spectra showed the appearance of two new absorption bands at 311 and 421 nm. At the same time the peaks at 524, 570, and 640

nm assigned to Co(II) *d-d* transitions combined with Co^{II}←Cl charge transfer transitions (LMCT) decreased in intensity (Figure 4.4). The spectra are slightly different from the UV-Vis spectrum of the isolated product, indicating the possibility of multiple products formed in this oxidative process. Again, attempts to trap potential intermediates in the oxidation process by titration of small aliquots of H₂O₂ into the solution of **3** unfortunately were unsuccessful (Figure AIII.12). However, an ESI-MS spectrum of the reaction mixture of **3** and H₂O₂ recorded after around one hour presents a dominant peak (*m/z*) at 368.1, which can be assigned to the mono-oxygenated fragment [Co^{III}(L¹SO)Cl]⁺ (Figure AIII.13).

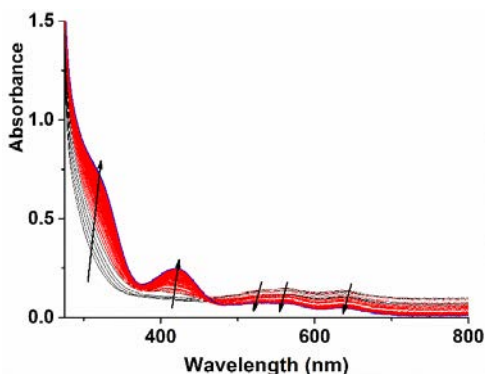


Figure 4.4. The change in UV-Vis spectra of **3** in acetonitrile solution upon addition of H₂O₂. UV-Vis spectra were recorded using a solution 2 mM in [Co] with a transmission dip probe path length of 2 mm; spectra were recorded every 30 seconds.

4.3 Discussion

Synthesis of transition metal compounds and investigation of their reactivity with oxidizing agents has attracted considerable attention in the last decades. Different S-oxygenated metal derivatives can be formed, depending on the nature of the ligand, coordination environment, oxidizing agents, and the frontier orbitals of the metal centers [44, 45]. In this manuscript, we describe the reactivity of two metal disulfide compounds with dihydrogen peroxide. Reaction of the iron(II) compound [Fe^{II}₂(L¹SSL¹)Cl₄] (**1**) with H₂O₂ yielded the mononuclear high-spin (*S* = 5/2) sulfonato-Fe(III) compound [Fe^{III}(L¹SO₃)Cl₂] (**2**) as the final product, which was confirmed by single crystal X-ray crystallography and EPR spectroscopy. The oxidation reaction occurs very fast; UV-Vis spectroscopy showed the reaction to be complete within several minutes. Analysis of a reaction carried out at -78 °C, showed that a sulfinato-iron(III) compound is formed as the first intermediate. Unfortunately, even at low reaction temperatures and with controlled addition of H₂O₂ the formation of potential hydroperoxido-iron(III) adducts was not observed. An alkylperoxido-

iron(III) intermediate was captured by the reaction of a mononuclear iron(II) compound of a N₄S thioether ligand in a reaction with ^tBuOOH [43], but such a reaction was unsuccessful for compound **1**. Similarly, a potential μ-peroxido-diron(III) intermediate reported in the previous study was not observed in our reactions [46].

The reactivity of iron(II) or iron(III) thiolate compounds with dioxygen has been extensively studied [44], but to the best of our knowledge, the oxidation of iron(II) disulfide compounds has not been investigated. Oxidation of iron(II) or iron(III) thiolate compounds generally results in the formation of sulfinato derivatives [47], but the formation of a sulfenato-iron(III) compound was reported by Kovacs and coworkers [48]. Rare examples have been reported of high-spin (*S* = 2) iron(II) and low-spin (*S* = ½) iron(III) sulfonate compounds, which were obtained by controlled oxidation of the iron(II) center or thiolate sulfur atom [26, 40]. In our case, both the iron(II) centers and the disulfide sulfur atoms are oxidized, yielding a high-spin (*S* = 5/2) sulfonato-Fe(III) compound.

The reactivity of the cobalt(II) disulfide compound [Co^{II}₂(L¹SSL¹)Cl₄] (**3**) with H₂O₂ has also been studied. The crystal structure combined with NMR spectra showed that this reaction yielded the low-spin sulfinato-Co(III) compound [Co^{III}(L¹SO₂)Cl₂] (**4**). Attempts have been undertaken to crystallize the sulfenato intermediate that was observed in ESI-MS by the fragment [Co^{III}(L¹SO)Cl]⁺, but unfortunately were not successful. However, we have shown in our previous study that such a monooxygenated intermediate indeed exists, as the compound [Co^{III}(L¹SO)(NCS)₂] was captured upon partial oxidation during the crystallization of the cobalt(III) thiolate compound [Co^{III}(L¹S)(NCS)₂] [39]. In the last decades, quite some research has been performed on the synthesis of S-oxygenated cobalt(III) compounds by reactions of cobalt(III) salts with S-oxygenated ligands, or via oxidation of cobalt(III) thiolate compounds in order to obtain mimics for the active site of the metalloenzyme Co-NHase [47, 49, 50]. Dutta et al. reported the reactivity of a cobalt(II) thiolate compound of a tetradentate N₂S₂ ligand with dioxygen [30]. The results indicated that oxidation of the cobalt(II) thiolate compound involved two steps. First, one of the thiolate donors is oxidized to a sulfinato group, which is a fast step, upon which the cobalt(II) ion is slowly oxidized to cobalt(III). Still, our case is the first example of the oxidation of a cobalt(II) disulfide compound, where both the cobalt(II) center and the disulfide sulfur atoms are oxidized, yielding a low-spin cobalt(III) sulfinato compound.

4.4 Summary and conclusions

In this chapter, we report the reactivity of the two metal disulfide compounds **1** and **3** with H₂O₂. Reaction of the iron(II) compound **1** with H₂O₂ resulted in the mononuclear

high-spin ($S = 5/2$) sulfonato-Fe(III) compound **2**, whereas reaction of the cobalt(II) compound **3** with H_2O_2 yielded the low-spin ($S = 0$) sulfinato-Co(III) derivative **4**. Monitoring the reactions of metal disulfide compounds **1** and **3** with H_2O_2 , at different reaction conditions by UV-Vis spectroscopy has not revealed any potential hydroperoxido-metal or μ -peroxide-di-metal intermediates in these reactions. However, results from ESI-MS and a previous study indicate that the oxidation of the cobalt compound proceeds via a relatively stable sulfenato-cobalt(III) compound. This study provides a rare example of the oxidation of metal disulfide compounds. Despite the fact that new insight has been gained concerning the formation of different S-oxygenated metal derivatives by the reactions of iron(II) or cobalt(II) disulfide compounds with H_2O_2 , still additional studies need to be carried out to further investigate the mechanism of oxidation of metal disulfide compounds.

4.5 Experimental section

4.5.1 General procedures

All chemicals were acquired from commercial vendors and used as received unless noted otherwise. Acetonitrile and diethyl ether were obtained from a solvent purification system (PureSolv 400), and methanol, dimethylformamide (DMF) were purchased from commercial sources and stored on 3 Å molecular sieves. The syntheses of transition metal disulfide compounds were carried out by standard Schlenk-line techniques under an atmosphere of dinitrogen. ^1H NMR and ^{13}C NMR spectra were carried out on a Bruker 300 DPX spectrometer at room temperature and chemical shifts were referenced against the solvent peak. Mass spectra were recorded on a Finnigan Aqua mass spectrometer with electrospray ionization (ESI). IR spectra were recorded on a PerkinElmer UATR spectrum equipped with single reflection diamond (resolution 4 cm^{-1} , scan range 400 cm^{-1} to 4000 cm^{-1}). Ultraviolet-visible (UV-Vis) spectra were collected using a transmission dip probe with variable path length on an Avantes Avaspec-2048 spectrometer with Avalight-DH-S-BAL light source. Elemental analyses were performed by the Microanalytical Laboratory Kolbe in Germany.

4.5.2 Single crystal X-ray crystallography

All reflection intensities were measured at 110(2) K using a SuperNova diffractometer (equipped with Atlas detector) with Mo $K\alpha$ radiation ($\lambda = 0.71073\text{ \AA}$) under the program CrysAlisPro (Version 1.171.36.32 Agilent Technologies, 2013). The same program was used to refine the cell dimensions and for data reduction. The structure was solved with the program SHELXS-2014/7 and was refined on F^2 with SHELXL-2014/7 [51]. Numerical absorption correction based on Gaussian integration over a

multifaceted crystal model was applied using CrysAlisPro. The temperature of the data collection was controlled using the system Cryojet (manufactured by Oxford Instruments). The H atoms were placed at calculated positions (unless otherwise specified) using the instructions AFIX 23, AFIX 43 or AFIX 137 with isotropic displacement parameters having values 1.2 or 1.5 U_{eq} of the attached C atoms. The structure of **2** is ordered. The structure of **4** is mostly ordered except for some H atoms from the lattice water solvent molecules.

4.5.3 Synthesis of the compounds

[Fe^{III}(LSO₃)Cl₂] (**2**): The compound [Fe^{II}₂(L¹SSL¹)Cl₄] (38.5 mg, 0.05 mmol) was dissolved in 10 mL dry and degassed methanol and cooled in an ice bath. To this solution 345 μ L 35% (4.0 mmol) H₂O₂ was added, leading to a color change from yellow to dark brown, and then back to yellow. The obtained yellow solution was stirred for another 4 hours, after which time the solvent was evaporated to yield a yellow precipitate. The yellow precipitate was recrystallized from a mixture of methanol and diethyl ether, yielding a light-yellow powder. Yield: 25.0 mg, 0.058 mmol, 58%. Crystals suitable for X-ray structure determination were acquired by slow vapor diffusion of diethyl ether into a dimethylformamide (DMF) solution containing this compound, yielding single crystals after approximately 12 days. IR (cm⁻¹): 476m, 504m, 551m, 541m, 591s, 652.84m, 645m, 721w, 746s, 771s, 782s, 814w, 841w, 897w, 919w, 932s, 969s, 984s, 1003s, 1020s, 1046w, 1057w, 1076w, 1096m, 1146vs, 1189w, 1235m, 1263s, 1288m, 1359w, 1430m, 1448m, 1462m, 1476w, 1571w, 1606s. ESI-MS found (calcd) for 1/2[M - 2Cl + H₂O]⁺ m/z 189.2 (190.0). Elemental analysis calcd (%) for C₁₄H₁₆Cl₂FeN₃O₃S: C, 38.83; H, 3.72; N, 9.70; found: C, 38.85; H, 3.84; N, 9.25.

[Co^{III}(LSO₂)Cl₂] (**4**): The compound [Co^{II}₂(L¹SSL¹)Cl₄] (40.6 mg, 0.052 mmol) was suspended in 5 mL dry acetone. To this suspension 402 μ L 35% H₂O₂ (4.60 mmol) was added, upon which the color of the suspension changed from purple to brown and the suspended solid gradually dissolved. The final solution was stirred for another 3 days, yielding a purple precipitate. The obtained precipitate was washed with diethyl ether (4 \times 15 mL). Yield: 15 mg, 0.036 mmol, 34%. Crystals suitable for X-ray structure determination were obtained by slow vapor diffusion of diethyl ether into an acetone solution containing this compound, yielding crystals after about 1 week. ¹H NMR (300 MHz, dmsd-d₆, RT): δ = 8.66 (d, 2H, Py-H₆), 8.12 (t, 2H, Py-H₄), 7.63 (t, 2H, Py-H₃), 7.54 (d, 2H, Py-H₅), 5.11 (d, 2H, Py-CH₂), 4.57 (d, 2H, Py-CH₂), 3.05 (d, 2H, S-CH₂-CH₂), 2.90 (t, 2H, S-CH₂-CH₂), 3.33 (H₂O), 2.50 (DMSO). IR (cm⁻¹): 531s, 572m, 654w, 686m, 719m, 771s, 797w, 820w, 912s, 947s, 996w, 1059s, 1074vs, 1164m, 1177m, 1180s, 1210s, 1228s, 1238s, 1286m, 1433w, 1444m, 1462m, 1483m, 1609m. ESI-MS found

(calcd) for $[M - Cl]^+ m/z$ 384.4 (384.7), $[M - Cl + MeCN]^+ m/z$ 425.5 (425.8). Elemental analysis calcd (%) for $C_{14}H_{16}Cl_2CoN_3O_2S + 1/2H_2O$: C 39.18, H 3.99, N 9.79; found C 39.16, H 3.91, N 9.73.

4.6 References

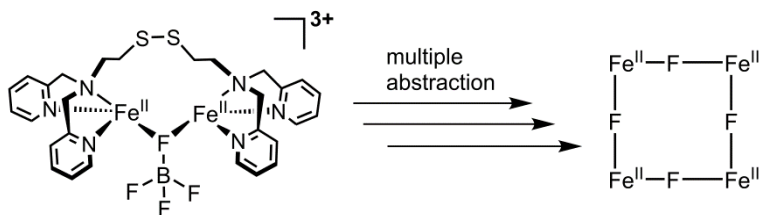
- [1] L. Que Jr, *Science*, 253 (1991) 273-275.
- [2] P. Nordlund, P. Reichard, *Annu. Rev. Biochem.*, 75 (2006) 681-706.
- [3] L.C. Stewart, J.P. Klinman, *Annu. Rev. Biochem.*, 57 (1988) 551-590.
- [4] E.I. Solomon, D.E. Heppner, E.M. Johnston, J.W. Ginsbach, J. Cirera, M. Qayyum, M.T. Kieber-Emmons, C.H. Kjaergaard, R.G. Hadt, L. Tian, *Chem. Rev.*, 114 (2014) 3659-3853.
- [5] J.E. Dominy, J. Hwang, M.H. Stipanuk, *Am. J. Physiol. Endocrinol. Metab.*, 293 (2007) E62-E69.
- [6] I. Galván, G. Ghanem, A.P. Møller, *BioEssays*, 34 (2012) 565-568.
- [7] A. Miyanaga, S. Fushinobu, K. Ito, T. Wakagi, *Biochem. Biophys. Res. Commun.*, 288 (2001) 1169-1174.
- [8] T. Murakami, M. Nojiri, H. Nakayama, M. Odaka, M. Yohda, N. Dohmae, K. Takio, T. Nagamune, I. Endo, *Protein Sci.*, 9 (2000) 1024-1030.
- [9] E. Bouwman, J. Reedijk, *Coord. Chem. Rev.*, 249 (2005) 1555-1581.
- [10] C.S. Mullins, C.A. Grapperhaus, B.C. Frye, L.H. Wood, A.J. Hay, R.M. Buchanan, M.S. Mashuta, *Inorg. Chem.*, 48 (2009) 9974-9976.
- [11] R.M. Buonomo, I. Font, M.J. Maguire, J.H. Reibenspies, T. Tuntulani, M.Y. Darensbourg, *J. Am. Chem. Soc.*, 117 (1995) 963-973.
- [12] R.K. Henderson, E. Bouwman, A.L. Spek, J. Reedijk, *Inorg. Chem.*, 36 (1997) 4616-4617.
- [13] L.R. Widger, Y. Jiang, M.A. Siegler, D. Kumar, R. Latifi, S.P. de Visser, G.N. Jameson, D.P. Goldberg, *Inorg. Chem.*, 52 (2013) 10467-10480.
- [14] E.C.M. Ordning-Wenker, M.A. Siegler, M. Lutz, E. Bouwman, *Inorg. Chem.*, 52 (2013) 13113-13122.
- [15] R.A. de Sousa, E. Galardon, M. Rat, M. Giorgi, I. Artaud, *J. Inorg. Biochem.*, 99 (2005) 690-697.
- [16] I.M. Wasser, S. De Vries, P. Moënné-Loccoz, I. Schröder, K.D. Karlin, *Chem. Rev.*, 102 (2002) 1201-1234.
- [17] A.C. McQuilken, Y. Jiang, M.A. Siegler, D.P. Goldberg, *J. Am. Chem. Soc.*, 134 (2012) 8758-8761.
- [18] M.J. Rose, N.M. Betterley, P.K. Mascharak, *J. Am. Chem. Soc.*, 131 (2009) 8340-8341.
- [19] M. Gennari, B. Gerey, N. Hall, J. Pécaut, M.N. Collomb, M. Rouzières, R. Clérac, M. Orio, C. Duboc, *Angew. Chem. Int. Ed.*, 53 (2014) 5318-5321.
- [20] <http://www.ebi.ac.uk>.
- [21] N. Goswami, D.M. Eichhorn, *Inorg. Chem.*, 38 (1999) 4329-4333.
- [22] O. Fazio, M. Gnida, W. Meyer-Klaucke, W. Frank, W. Kläui, *Eur. J. Inorg. Chem.*, 2002 (2002) 2891-2896.
- [23] T.G. Traylor, F. Xu, *J. Am. Chem. Soc.*, 112 (1990) 178-186.
- [24] C.-M. Lee, C.-H. Hsieh, A. Dutta, G.-H. Lee, W.-F. Liaw, *J. Am. Chem. Soc.*, 125 (2003) 11492-11493.
- [25] J.A. Kovacs, L.M. Brines, *Acc. Chem. Res.*, 40 (2007) 501-509.
- [26] Y. Jiang, L.R. Widger, G.D. Kasper, M.A. Siegler, D.P. Goldberg, *J. Am. Chem. Soc.*, 132 (2010) 12214-12215.
- [27] A.R. McDonald, M.R. Bukowski, E.R. Farquhar, T.A. Jackson, K.D. Koehntop, M.S. Seo, R.F. De Hont, A. Stubna, J.A. Halfen, E. Münck, *J. Am. Chem. Soc.*, 132 (2010) 17118-17129.

- [28] E. Nam, P.E. Alokolaro, R.D. Swartz, M.C. Gleaves, J. Pikul, J.A. Kovacs, *Inorg. Chem.*, 50 (2011) 1592-1602.
- [29] M. Sallmann, I. Siewert, L. Fohlmeister, C. Limberg, C. Knispel, *Angew. Chem. Int. Ed.*, 51 (2012) 2234-2237.
- [30] A. Dutta, M. Flores, S. Roy, J.C. Schmitt, G.A. Hamilton, H.E. Hartnett, J.M. Shearer, A.K. Jones, *Inorg. Chem.*, 52 (2013) 5236-5245.
- [31] S. Itoh, M. Nagagawa, S. Fukuzumi, *J. Am. Chem. Soc.*, 123 (2001) 4087-4088.
- [32] A. Neuba, R. Haase, W. Meyer-Klaucke, U. Flörke, G. Henkel, *Angew. Chem. Int. Ed.*, 51 (2012) 1714-1718.
- [33] E. C. M. Ording-Wenker, M. van der Plas, M.A. Siegler, C. Fonseca Guerra, E. Bouwman, *Chem. Eur. J.*, 20 (2014) 16913-16921.
- [34] E. C. M. Ording-Wenker, M. van der Plas, M.A. Siegler, S. Bonnet, F.M. Bickelhaupt, C. Fonseca Guerra, E. Bouwman, *Inorg. Chem.*, 53 (2014) 8494-8504.
- [35] A.M. Thomas, B.L. Lin, E.C. Wasinger, T.D.P. Stack, *J. Am. Chem. Soc.*, 135 (2013) 18912-18919.
- [36] Y. Ueno, Y. Tachi, S. Itoh, *J. Am. Chem. Soc.*, 124 (2002) 12428-12429.
- [37] Y. Lee, D.-H. Lee, A.A.N. Sarjeant, K.D. Karlin, *J. Inorg. Biochem.*, 101 (2007) 1845-1858.
- [38] C. Esmieu, M. Orio, L. Le Pape, C. Lebrun, J. Pécaut, S. Ménage, S. Torelli, *Inorg. Chem.*, 55 (2016) 6208-6217.
- [39] F. Jiang, M.A. Siegler, X. Sun, L. Jiang, C.F. Guerra, E. Bouwman, *Inorg. Chem.*, 57(2018) 8796-8805.
- [40] M.G. O'Toole, M. Kreso, P.M. Kozlowski, M.S. Mashuta, C.A. Grapperhaus, *J. Biol. Inorg. Chem.*, 13 (2008) 1219.
- [41] P.J. Cappillino, J.R. Miecznikowski, L.A. Tyler, P.C. Tarves, J.S. McNally, W. Lo, B.S.T. Kasibhatla, M.D. Krzyaniak, J. McCracken, F. Wang, *Dalton Trans.*, 41 (2012) 5662-5677.
- [42] I.K. Adzamlı, K. Libson, J. Lydon, R. Elder, E. Deutsch, *Inorg. Chem.*, 18 (1979) 303-311.
- [43] L.R. Widger, Y. Jiang, A.C. McQuilken, T. Yang, M.A. Siegler, H. Matsumura, P. Moënne-Loccoz, D. Kumar, S.P. De Visser, D.P. Goldberg, *Dalton Trans.*, 43 (2014) 7522-7532.
- [44] A.C. McQuilken, D.P. Goldberg, *Dalton Trans.*, 41 (2012) 10883-10899.
- [45] T.M. Cocker, E. Bachman, *Inorg. Chem.*, 40 (2001) 1550-1556.
- [46] F. Avenier, C. Herrero, W. Leibl, A. Desbois, R. Guillot, J.P. Mahy, A. Aukauloo, *Angew. Chem. Int. Ed.*, 52 (2013) 3634-3637.
- [47] T.C. Harrop, P.K. Mascharak, *Acc. Chem. Res.*, 37 (2004) 253-260.
- [48] P. Lugo-Mas, A. Dey, L. Xu, S.D. Davin, J. Benedict, W. Kaminsky, K.O. Hodgson, B. Hedman, E.I. Solomon, J.A. Kovacs, *J. Am. Chem. Soc.*, 128 (2006) 11211-11221.
- [49] R. Elder, M.J. Heeg, M.D. Payne, M. Trkula, E. Deutsch, *Inorg. Chem.*, 17 (1978) 431-440.
- [50] M. Lundeen, R.L. Firor, K. Seff, *Inorg. Chem.*, 17 (1978) 701-706.
- [51] G.M. Sheldrick, *Acta Crystallogr. C*, 71 (2015) 3-8.

Chapter 5

A Tetranuclear Fluorido-bridged Iron Compound: Fluoride Abstraction from the Tetrafluoridoborate Anion

The novel iron(II) fluoride cluster $[Fe^{II}_4(L^1SSL^1)_2F_6(MeCN)_2](BF_4)_2$ ($L^1SSL^1 = di-2-(bis(2-pyridylmethyl)amino)ethyl\ disulfide$) has been synthesized by reaction of the ligand L^1SSL^1 with $[Fe(MeCN)_6](BF_4)_2$. The crystal structure shows that a tetranuclear iron(II) compound is formed through the bridging of two dinuclear iron(II) units by four fluoride anions. The ^{19}F NMR spectrum distinguishes both the terminal and bridging fluoride ions in this compound. The new compound is a rare Fe^{II} fluoride cluster with four Fe^{II} and four F^- ions arranged in a nearly perfect square plane, which obtained its fluoride ions from the tetrafluoridoborate anion.



This chapter has been published as a short communication paper: Feng Jiang, Maxime A. Siegler, and Elisabeth Bouwman, *Inorg. Chem. Comm.* 94 (2018) 53–56

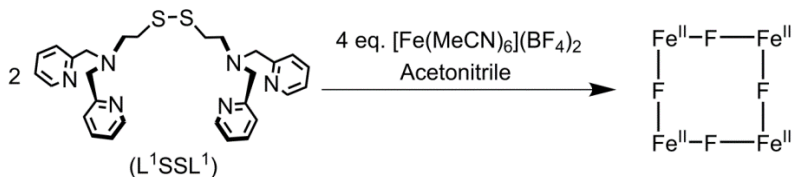
5.1 Introduction

The synthesis of transition metal fluoride compounds has received considerable attention in the last decades because of their special structural characteristics and potential application in the field of magnetic materials [1-3]. Two main strategies have been employed to synthesize metal fluoride compounds: the first one is based on the addition of fluoride salts like NaF or AsF₃ as fluorinating agents; the other one is based on the use of metal tetrafluoridoborate as starting salts, which generate fluoride ions upon decomposition. In the last decades, tremendous efforts have been put in the synthesis of copper(II) fluoride compounds from copper tetrafluoridoborate [4-7]. Recently, Reger et al. reported the synthesis of a series of linear dinuclear Fe^{II}, Co^{II}, Ni^{II}, Cu^{II}, Zn^{II}, Cd^{II} compounds starting from the respective metal tetrafluoridoborate salts, where two metal ions are bridged by one fluoride ion forming a M–F–M configuration [8, 9]. Besides that, two dinuclear fluoro-bridged zinc and cadmium compounds were synthesized based on a porphyrin ligand by the group of Sessler [10]. Most of these metal fluoride compounds are stabilized by hydrogen-bond interactions or they are the linear compounds (M–F–M). In this communication we report a novel tetranuclear Fe^{II} fluoride cluster obtained by reaction of a disulfide ligand with iron(II) tetrafluoridoborate. This compound was formed in an attempt to create an Fe(III) thiolate compound in a study concerning potential redox interconversion reactions of disulfide ligands with Co(II) and Fe(II) salts (see Chapter 2) [11].

5.2 Results and Discussion

5.2.1 Synthesis and characterization of the iron(II) compound

The ligand di-2-(bis(2-pyridylmethyl)amino)ethyl disulfide (L¹SSL¹) was synthesized via the reported procedure [12, 13]. Under an inert atmosphere, treatment of the disulfide ligand L¹SSL¹ with [Fe(MeCN)₆](BF₄)₂ in acetonitrile at room temperature resulted in a brownish purple solution from which the compound [Fe^{II}₄(L¹SSL¹)₂F₆(MeCN)₂](BF₄)₂ was isolated in a yield of 42% (Scheme 1). The compound was characterized by single crystal X-ray crystallography, electrospray ionization mass spectrometry (ESI-MS), elemental analysis, magnetic susceptibility measurement, UV–Vis and nuclear magnetic resonance (NMR) spectroscopy.



Scheme 5.1. Schematic overview of the reaction of ligand L^1SSL^1 with $[Fe(MeCN)_6](BF_4)_2$ in acetonitrile. The structure drawing is simplified for clarity.

UV-Vis spectra of the compound $[Fe^{II}_4(L^1SSL^1)_2F_6(MeCN)_2](BF_4)_2$ dissolved in acetonitrile present two absorption bands, one at 258 nm ($11 \times 10^3 \text{ M}^{-1} \text{ cm}^{-1}$) arising from $\pi^* \leftarrow \pi$ transitions of the pyridyl groups, and one at 349 nm ($1.2 \times 10^3 \text{ M}^{-1} \text{ cm}^{-1}$) likely corresponding to an $N \leftarrow Fe$ charge transfer transition (MLCT) (Appendix, Figure AIV.1). ESI-MS spectra of the compound dissolved in acetonitrile show peaks (m/z) at 333.3 and 685.2 corresponding to the dicationic and monocationic species $[Fe^{II}_2(L^1SSL^1)F_2]^{2+}$ and $[Fe^{II}_2(L^1SSL^1)F_3]^+$, respectively (Appendix, Figure AIV.2). 1H NMR spectroscopy of the compound $[Fe^{II}_4(L^1SSL^1)_2F_6(MeCN)_2](BF_4)_2$ dissolved in acetonitrile- d_3 resulted in a spectrum with broad resonances down to around 90 ppm (Appendix, Figure AIV.3). The ^{19}F NMR spectrum of the compound $[Fe^{II}_4(L^1SSL^1)_2F_6(MeCN)_2](BF_4)_2$ presents a strong sharp peak at 136 ppm that is assigned to the fluorine atoms of the BF_4^- anions, as well as two broad peaks with lower intensity at 160 and 190 ppm, which likely correspond to the terminal fluoride ions F3 and the bridging fluoride ions F1 and F2, respectively (Appendix, Figure AIV.4). [14, 15] A SQUID measurement was conducted for the compound in the range 2 – 300 K, showing the $\chi_M T$ value at 300 K to be $11.60 \text{ cm}^3 \text{ mol}^{-1} \text{ K}$, showing only a small antiferromagnetic interaction (Figure 1). The value at 300 K is only slightly smaller than the theoretical value estimated from four isolated high-spin state ($S = 2$) iron(II) centers in octahedral geometries, ($\chi_M T = 12.0 \text{ cm}^3 \text{ mol}^{-1} \text{ K}$ for $g = 2$) [16].

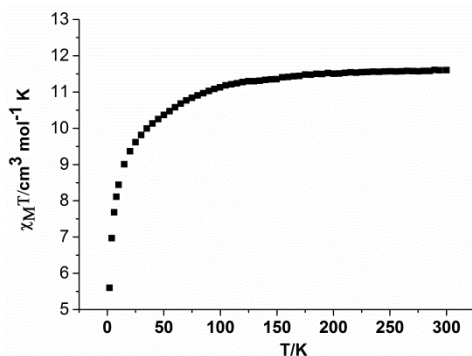


Figure 5.1. Plot of $\chi_M T$ vs. T for the compound $[Fe^{II}_4(L^1SSL^1)_2F_6(MeCN)_2](BF_4)_2$.

5.2.2 Description of the crystal structure

Single crystals of the compound $[\text{Fe}^{\text{II}}_4(\text{L}^1\text{SSL}^1)_2\text{F}_6(\text{MeCN})_2](\text{BF}_4)_2$ suitable for X-ray structure determination were obtained by slow vapor diffusion of diethyl ether into an acetonitrile solution containing the compound. A projection of the compound is given in Figure 2; additional information about the refinement is provided in the Appendix table AIV.1 and selected bond distances and angles are given in Table 1. The compound $[\text{Fe}^{\text{II}}_4(\text{L}^1\text{SSL}^1)_2\text{F}_6(\text{MeCN})_2](\text{BF}_4)_2$ crystallizes in the monoclinic space group $C2/c$, and only one half of the tetranuclear molecule is crystallographically independent in the asymmetric unit. The independent unit does not simply contain a dinuclear compound built from one disulfide ligand and two iron(II) centers, but rather two times half of such a dinuclear compound, linearly bridged by one fluoride ion ($\text{Fe1-F1-Fe2} = 163.62(10)^\circ$, $\text{Fe1-F1-Fe2}^* = 166.88(10)^\circ$). The tetranuclear compound with two-fold rotation symmetry is formed via bridging fluoride ions, with the two-fold rotation axis passing perpendicular through the Fe_4F_4 plane. Each iron(II) center is coordinated by three facially-bound nitrogen donor atoms of the ligand and two fluoride ions bridging to two other iron centers. A nitrogen atom of acetonitrile occupies the sixth coordination site for the Fe1 centers, whereas the octahedral geometry of the Fe2 ion is completed with an additional terminal fluoride ion. The bond distances between Fe and N range from 2.122(2) to 2.236(2) Å, indicating a high-spin state ($S = 2$) of the Fe^{II} centers [17, 18]. The bond distance between Fe2 and the terminal fluoride ion F3 is 1.8234(16) Å, and the bond distances between Fe2 and the bridging fluoride ions F1 and F2 are 1.9032(14) and 1.8970(14) Å, respectively. Remarkably, all bond lengths of the iron(II) center Fe1 are slightly longer than the bond lengths of Fe2. Specifically, the bond distances between Fe1 and the bridging F1 and F2 ions are 2.0110(14) and 2.0618(14) Å, respectively. The four iron(II) centers and the four bridging fluoride ions together form a nearly planar arrangement, with the octahedral iron centers at the corners of the square. The terminally coordinated apical fluoride ions bound to Fe2 both reside on one side of the plane, whereas the apically bound acetonitrile molecules on Fe1 are located on the other side of the plane. The diethyl-disulfide bridging the two amine nitrogens within one ligand L^1SSL^1 connect two opposite corners of the square plane.

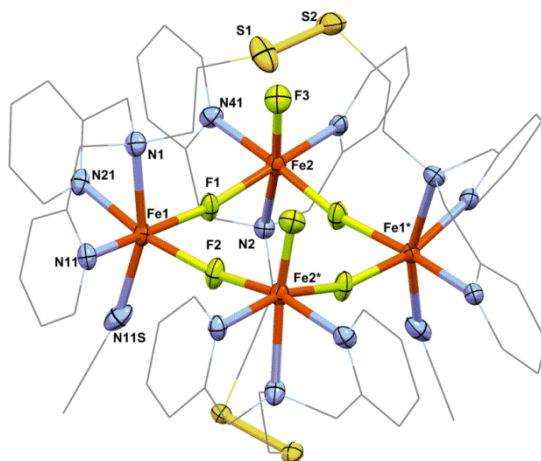


Figure 5.2. Displacement ellipsoid plots (50% probability level) of the cationic part of the compound $[\text{Fe}^{\text{II}}_4(\text{L}^1\text{SSL}^1)_2\text{F}_6(\text{MeCN})_2](\text{BF}_4)_2$ at 110(2) K. Hydrogen atoms, BF_4^- counter ions, and disorder are omitted for clarity. Carbon atoms are shown using the wireframe style.

In a previous study, we reported a tetranuclear Cu^{II} fluoride compound formed from a similar dinucleating disulfide ligand and copper(II) tetrafluoroborate [5]. The crystal structure showed that the two dinuclear copper(II) units in this compound are symmetrically bridged by water, fluoride, and tetrafluoroborate anions. This copper(II) fluoride cluster features additional hydrogen-bond interactions between the fluoride ions and coordinated water molecules [5].

In many cases it appears that hydrogen-bond interactions are vital to stabilize such macrocyclic metal fluoride compounds. For example, the group of Sessler reported fluoro-bridged zinc and cadmium compounds, for which the authors suggest the hydrogen-bond interactions between the protons of the non-coordinating pyrrole rings in the ligand and the fluoride ions to play an important role in the stabilization of the compounds [10]. Apparently, our compound $[\text{Fe}^{\text{II}}_4(\text{L}^1\text{SSL}^1)_2\text{F}_6(\text{MeCN})_2](\text{BF}_4)_2$ does not need such stabilization, as it does not contain any potential hydrogen-bond donors.

Several mechanisms were put forward for the formation of metal fluoride compounds from tetrafluoroborate salts, like strong-base assisted decomposition, hydrolysis, or Lewis-acid assisted fluoride abstraction [9, 19]. As strong base or water was not present in our reaction, this excludes the first two mechanisms. The BF_4^- decomposition pathway leading to our compound therefore is likely Lewis-acid assisted fluoride abstraction, which is similar to the mechanism suggested by the group of Sessler [10].

Table 5.1. Selected bond distances (Å) and angles (°) of the compound [Fe^{II}₄(L¹SSL¹)₂F₆-(MeCN)₂](BF₄)₂.

Selected bond distances (Å)			
Fe1-F1	2.0110(14)	Fe2-F1	1.9032(14)
Fe1-F2	2.0618(14)	Fe2-F2	1.8970(14)
Fe1-N1	2.236(2)	Fe2-N2	2.228(6)
Fe1-N11	2.122(2)	Fe2-N31	2.109(6)
Fe1-N21	2.163(2)	Fe2-N41	2.143(6)
Fe1-N1S	2.127(3)	Fe2-F3	1.8234(16)
Fe1-Fe2	3.8744(5)	Fe2*-Fe1	3.9329(5)
Selected bond angles (°)			
F1-Fe1-F2	82.68(6)	F2-Fe2-N31	92.1(3)
F1-Fe1-N1S	98.33(8)	F2-Fe2-N41	167.5(6)
F1-Fe1-N11	166.54(7)	F2-Fe2-N2	91.1(3)
F1-Fe1-N21	86.65(7)	F2-Fe2-F1	95.05(6)
F1-Fe1-N1	94.64(7)	F2-Fe2-F3	101.61(7)
F2-Fe1-N1S	93.41(8)	N31-Fe2-N41	81.8(6)
F2-Fe1-N11	87.49(7)	N31-Fe2-N2	79.9(5)
F2-Fe1-N21	168.72(7)	N31-Fe2-F1	164.4(4)
F2-Fe1-N1	100.86(7)	N31-Fe2-F3	94.2(4)
N1S-Fe1-N11	91.39(9)	N41-Fe2-N2	77.2(8)
N1S-Fe1-N21	91.75(9)	N41-Fe2-F1	88.5(5)
N1S-Fe1-N1	161.81(8)	N41-Fe2-F3	89.7(6)
N11-Fe1-N21	102.42(8)	N2-Fe2-F1	86.1(3)
N11-Fe1-N1	78.16(8)	N2-Fe2-F3	166.2(3)
N21-Fe1-N1	76.29(8)	F1-Fe2-F3	97.93(7)
Fe1-F1-Fe2	163.62(10)	Fe1-F2-Fe2	166.88(10)

5.3 Conclusion

In conclusion, we have described the structure of a novel tetranuclear Fe^{II} fluoride cluster with an unusual planar arrangement of the Fe₄F₄ core, which is formed by the abstraction of fluoride ions from the tetrafluoridoborate anion.

5.4 Experimental section

5.4.1 General procedures

All the reagents were obtained from commercial sources and used as received unless noted otherwise. Acetonitrile and diethyl ether were obtained from a solvent dispenser (PureSolV 400). The synthesis of the compound was carried out using standard Schlenk-line techniques under a nitrogen atmosphere. ¹H NMR and ¹⁹F NMR spectra were recorded on a Bruker 500 DPX spectrometer at room temperature. Mass spectra were recorded on a Finnigan Aqua mass spectrometer with electrospray ionization (ESI). IR spectra were acquired on a PerkinElmer UATR spectrum equipped with a single reflection diamond (scan range 400 cm⁻¹ to 4000 cm⁻¹, resolution 4 cm⁻¹). UV-vis spectra were collected using a transmission dip probe with the path length of 0.31 cm on an Avantes Avaspec-2048 spectrometer with Avalight-DH-S-BAL light source. Elemental analyses were performed by the Microanalytical Laboratory Kolbe

in Germany. The magnetic measurements were carried out on a sample of 6.50 mg powder of the compound $[\text{Fe}^{\text{II}}_4(\text{L}^1\text{SSL}^1)_2\text{F}_6(\text{MeCN})_2](\text{BF}_4)_2$. The sample was mounted on a plastic straw before introduction in a MPMS-XL Quantum Design SQUID magnetometer. The magnetization measurements were performed in a field of 0.5 T at temperatures from 300 to 2 K. Corrections for the diamagnetism of the sample were calculated using Pascal's constants [20].

5.4.2 Single crystal X-ray crystallography

All reflection intensities were measured at 110(2) K using a SuperNova diffractometer (equipped with Atlas detector) with Mo $K\alpha$ radiation ($\lambda = 0.71073 \text{ \AA}$) under the program CrysAlisPro (Version 1.171.36.32 Agilent Technologies, 2013). The same program was used to refine the cell dimensions and for data reduction. The structure was solved with the program SHELXS-2013 (Sheldrick, 2008) and was refined on F^2 with SHELXL-2013.[21] Analytical numeric absorption correction based on a multifaceted crystal model was applied using CrysAlisPro. The temperature of the data collection was controlled using the system Cryojet (manufactured by Oxford Instruments). The H atoms were placed at calculated positions using the instructions AFIX 23, AFIX 43 or AFIX 137 with isotropic displacement parameters having values 1.2 or 1.5 U_{eq} of the attached C atoms. The structure is partly disordered.

The Fe cluster is found at sites of twofold axial symmetry, and only one half of the molecule is crystallographically independent. The organic ligand coordinated to Fe2 (including the N-CH₂-CH₂-S-S-CH₂-CH₂-N bridge) and one of the two BF₄⁻ counter ions are found to be disordered over three orientations. All occupancy factors for each component of the disorder can be found in the CIF file.

5.4.3 Synthesis of the compound $[\text{Fe}^{\text{II}}_4(\text{L}^1\text{SSL}^1)_2\text{F}_6(\text{MeCN})_2](\text{BF}_4)_2$

To a pale-yellow solution of ligand L¹SSL¹ (51.95 mg, 0.1 mmol) in 5 mL acetonitrile, 95.10 mg (0.2 mmol) $[\text{Fe}(\text{MeCN})_6](\text{BF}_4)_2$ was added, immediately resulting in a brownish purple solution. The acquired solution was stirred for about 3 h, and then evaporated to 2 mL. After that, 20 mL diethyl ether was added, and some brownish purple precipitate was formed. The precipitate was washed with diethyl ether (4 × 20 mL). Yield: 35 mg, 42%. IR (cm⁻¹): 645w, 725w, 763s, 788m, 1020vs, 1260w, 1446w, 1608s. ESI-MS found (calcd.) for $[\text{Fe}^{\text{II}}_2(\text{L}^1\text{SSL}^1)\text{F}_2]^{2+}$ m/z 333.3 (333.1); for $[\text{Fe}^{\text{II}}_2(\text{L}^1\text{SSL}^1)\text{F}_3]^+$ m/z 685.2 (685.1). Elemental analysis calcd (%) for C₅₆H₆₄B₂F₁₄Fe₄N₁₂S₄+8H₂O: C 39.83, H 4.78, N 9.95; found: C 39.92, H 4.37, N 9.47.

5.5. References

- [1] B.L. Pagenkopf, E.M. Carreira, *Chem. Eur. J.*, 5 (1999) 3437-3442.
- [2] K.S. Pedersen, M.A. Sørensen, J. Bendix, *Coord. Chem. Rev.*, 299 (2015) 1-21.
- [3] T. Birk, *ChemistryOpen*, 2 (2013) 13-16.
- [4] S.C. Lee, R. Holm, *Inorg. Chem.*, 32 (1993) 4745-4753.
- [5] E.C. Ording-Wenker, M.A. Siegler, E. Bouwman, *Inorg. Chim. Acta*, 428 (2015) 193-202.
- [6] J. Ackermann, F. Meyer, H. Pritzkow, *Inorg. Chim. Acta*, 357 (2004) 3703-3711.
- [7] J. Manzur, A. Vega, A.M. García, C. Acuña, M. Sieger, B. Sarkar, M. Niemeyer, F. Lissner, T. Schleid, W. Kaim, *Eur. J. Inorg. Chem.*, 2007 (2007) 5500-5510.
- [8] D.L. Reger, A.E. Pascui, M.D. Smith, J. Jezierska, A. Ozarowski, *Inorg. Chem.*, 51 (2012) 11820-11836.
- [9] D.L. Reger, R.P. Watson, J.R. Gardinier, M.D. Smith, P.J. Pellechia, *Inorg. Chem.*, 45 (2006) 10088-10097.
- [10] E. Tomat, L. Cuesta, V.M. Lynch, J.L. Sessler, *Inorg. Chem.*, 46 (2007) 6224-6226.
- [11] F. Jiang, M.A. Siegler, X. Sun, L. Jiang, C.I. Fonseca Guerra, E. Bouwman, *Inorg. Chem.*, 57 (2018) 8796-8805.
- [12] M. Taki, S. Teramae, S. Nagatomo, Y. Tachi, T. Kitagawa, S. Itoh, S. Fukuzumi, *J. Am. Chem. Soc.*, 124 (2002) 6367-6377.
- [13] E.C.M. Ording-Wenker, M.A. Siegler, M. Lutz, E. Bouwman, *Dalton Trans.*, 44 (2015) 12196-12209.
- [14] T. Kiczanski, J.F. Stebbins, *J. Non-Cryst. Solids*, 306 (2002) 160-168.
- [15] A. Zheng, S.-B. Liu, F. Deng, *J. Phys. Chem. C*, 113 (2009) 15018-15023.
- [16] S. Bonnet, M.A. Siegler, J.S. Costa, G. Molnár, A. Bousseksou, A.L. Spek, P. Gamez, J. Reedijk, *Chem. Commun.*, (2008) 5619-5621.
- [17] J. Oliver, D. Mullica, B. Hutchinson, W. Milligan, *Inorg. Chem.*, 19 (1980) 165-169.
- [18] L.R. Widger, Y. Jiang, M.A. Siegler, D. Kumar, R. Latifi, S.P. de Visser, G.N. Jameson, D.P. Goldberg, *Inorg. Chem.*, 52 (2013) 10467-10480.
- [19] M. Guichelaar, J. Van Hest, J. Reedijk, *Inorg. Nucl. Chem. Lett.*, 10 (1974) 999-1004.
- [20] G.A. Bain, J.F. Berry, *J. Chem. Educ.*, 85 (2008) 532.
- [21] G.M. Sheldrick, *Acta Crystallogr A*, 64 (2008) 112-122.

Chapter 6

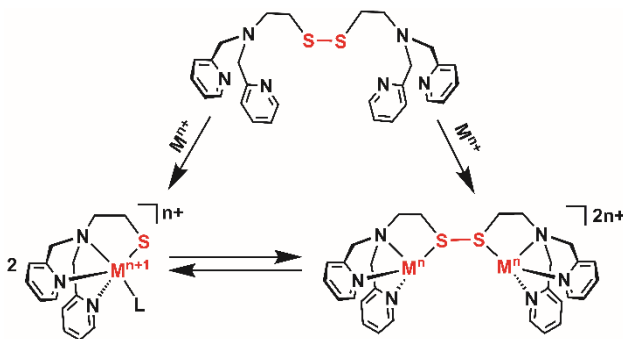
Synthesis and Characterization of a Series of Transition Metal Compounds of Thioether and Disulfide Ligands

A series of mononuclear metal compounds $[M^{\text{II}}(L^1SCH_3)Cl_2]$ ($M = Co, Cu, Fe, Mn, L^1SCH_3 = 2\text{-}(\text{methylthio})\text{-}N,N\text{-bis}(\text{pyridin-2-ylmethyl})\text{aminoethane}$) has been synthesized and characterized. The structures and spectroscopic properties of these compounds are compared to the related dinuclear compounds $[M^{\text{II}}_2(L^1SSL^1)Cl_4]$ ($M = Co, Cu, Fe$), which were obtained from the reactions of disulfide ligand L^1SSL^1 with the corresponding metal chloride salts ($L^1SSL^1 = \text{di-2-}(\text{bis}(2\text{-pyridylmethyl})\text{amino})\text{-ethyl disulfide}$). The crystal structures show that the metal centers in the mononuclear compounds $[Co^{\text{II}}(L^1SCH_3)Cl_2]$, $[Cu^{\text{II}}(L^1SCH_3)Cl_2]$ and $[Mn^{\text{II}}(L^1SCH_3)Cl_2]$ are in trigonal-bipyramidal geometries coordinated by three nitrogen donors of the tetradentate ligand and two chloride ions, with configurations similar to that of metal centers in $[Co^{\text{II}}_2(L^1SSL^1)Cl_4]$ and $[Cu^{\text{II}}_2(L^1SSL^1)Cl_4]$. In contrast, the iron(II) center in $[Fe^{\text{II}}(L^1SCH_3)Cl_2]$ is coordinated by three nitrogen donors and one sulfur atom of the tetradentate ligand and two chloride ions in an octahedral geometry, which is similar to the geometry of one of the Fe(II) centers in the dinuclear compound $[Fe^{\text{II}}_2(L^1SSL^1)Cl_4]$, where two iron(II) centers are in different geometries. UV-vis spectra of the mononuclear compounds are comparable to those of the related dinuclear compounds.

This chapter has been published as a full paper: Feng Jiang, Maxime A. Siegler, and Elisabeth Bouwman, *Inorganica Chim. Acta* 2018, in press

6.1 Introduction

The synthesis of transition metal compounds to mimic active sites in sulfur-rich metalloenzymes has received considerable attention in the last decades, as it provides a uniquely chemical perspective into the functions of metalloenzymes in e.g. oxidation, electron transfer, and nitrogen fixation [1-5]. Metal compounds with sulfur donors can be synthesized from disulfide, thioether or thiolate-containing ligands. Generally, the sulfur atoms in disulfide and thioether groups are rather weak donor atoms, quite often not coordinating to the metal center. On the other hand, thiolate ligands are highly oxidation sensitive, resulting in the formation of disulfides or oxygenated sulfur donors. In the past few years, however, the use of disulfide ligands has been shown to result in the formation of either low-valent metal disulfide compounds or high-valent metal thiolate compounds. This intriguing redox interconversion has been investigated mainly for copper, but more recently also for cobalt (Scheme 6.1) [6-11]. Such studies assist in gaining understanding of the disulfide-thiolate conversion and electron transfer in metalloenzymes, such as the Cu_A site of cytochrome c oxidase. Thiolate ligands are frequently used to synthesize especially iron and nickel compounds [12-14]. Their reactivity with oxidizing agents is further explored to elaborate on the mechanism of degradation of metalloenzymes such as cysteine dioxygenase (CDO) by dioxygen [15-19]. Metal compounds containing thioether ligands are studied as mimics for the active site in enzymes such as galactose oxidase [20, 21].



Scheme 6.1. Synthesis of low-valent metal disulfide compounds and high-valent metal thiolate compounds from disulfide ligands.

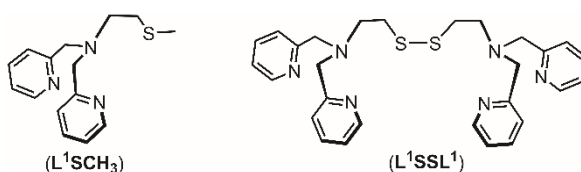
In the last few years, our group synthesized the metal disulfide compounds $[M^{II}_2(L^1SSL^1)Cl_4]$ ($M = Co, Fe$) from the disulfide ligand L^1SSL^1 ($L^1SSL^1 =$ di-2-(bis(2-pyridylmethyl)amino)-ethyl disulfide, see Scheme 1) from reactions with the metal(II) chloride salts [22]. The two iron(II) centers in $[Fe^{II}_2(L^1SSL^1)Cl_4]$ are in different

geometries: one is coordinated by three nitrogen donors and one sulfur atom of the ligand, and two chloride ions in an octahedral geometry, whereas the other is coordinated by three nitrogen donors of the ligand and two chloride ions in a trigonal-bipyramidal geometry [22]. Herein we report the synthesis of a series of metal compounds (Fe, Co, Cu, Mn) of the thioether-containing ligand L^1SCH_3 ($L^1SCH_3 = 2$ - (methylthio)- N,N -bis(pyridin-2-ylmethyl)aminoethane)). The spectroscopic and structural properties of these compounds have been investigated and are compared with those of the related dinuclear metal disulfide compounds.

6.2 Results

6.2.1 Synthesis of metal compounds

The ligands L^1SSL^1 and L^1SCH_3 (Scheme 6.2) were synthesized via reported procedures [21, 23]. The reactions with cobalt(II), manganese(II) and copper(II) chloride salts ($CoCl_2 \cdot 6H_2O$, $CuCl_2$, $MnCl_2 \cdot 4H_2O$) were carried out in air, whereas reactions with $FeCl_2 \cdot 4H_2O$ were performed under oxygen-free conditions. The addition of one equivalent of the metal(II) chlorides to one equivalent of thioether ligand L^1SCH_3 dissolved in acetonitrile or methanol led to the formation of compounds $[Co^{II}(L^1SCH_3)Cl_2]$ (yield 56%), $[Mn^{II}(L^1SCH_3)Cl_2]$ (yield 58%), $[Cu^{II}(L^1SCH_3)Cl_2]$ (yield 72%), and $[Fe^{II}(L^1SCH_3)Cl_2]$ (yield 45%). Reaction of two equivalents of $CuCl_2$ with one equivalent of the disulfide ligand L^1SSL^1 dissolved in acetonitrile led to the formation of the dinuclear compound $[Cu^{II}_2(L^1SSL^1)Cl_4]$ in a yield of 45%. All compounds were further characterized with ESI-MS spectrometry, 1H NMR, IR and UV-vis spectroscopy, single crystal X-ray crystallography, and elemental analysis.



Scheme 6.2. The ligands L^1SCH_3 and L^1SSL^1 used in the reactions.

6.2.2 Description of the crystal structures

Single crystals of $[Co^{II}(L^1SCH_3)Cl_2]$, $[Fe^{II}(L^1SCH_3)Cl_2]$, $[Cu^{II}(L^1SCH_3)Cl_2]$, and $[Mn^{II}(L^1SCH_3)Cl_2]$ suitable for X-ray structure determination were obtained by slow vapor diffusion of diethyl ether into solutions of the compounds. Single crystals of $[Cu^{II}_2(L^1SSL^1)Cl_4]$ were obtained by slow evaporation of a DMF solution of the compound. Crystallographic and refinement data for each structure are collected in the supporting information, Tables S1 and S2. Projections of the structures are shown

in Figures 6.1 and 6.2; selected bond distances and angles are given in Tables 6.1 and 6.2. Stacking interactions are not present in any of the structures, despite the presence of the pyridine rings.

The compound $[\text{Co}^{\text{II}}(\text{L}^1\text{SCH}_3)\text{Cl}_2]$ crystallizes in the monoclinic space group Cc with one mononuclear compound in the asymmetric unit. The $\text{Co}(\text{II})$ ion is coordinated by three nitrogen donors of the tetradentate ligand and two chloride ions in a distorted trigonal-bipyramidal geometry with a τ value of 0.77 [24]. The Co-N bond lengths range from 2.074(2) to 2.2990(19) Å, whereas the two Co-Cl bond lengths are very similar (2.3046(6) and 2.3049(6) Å).

The compounds $[\text{Fe}^{\text{II}}(\text{L}^1\text{SCH}_3)\text{Cl}_2]$, $[\text{Mn}^{\text{II}}(\text{L}^1\text{SCH}_3)\text{Cl}_2]$, and $[\text{Cu}^{\text{II}}(\text{L}^1\text{SCH}_3)\text{Cl}_2]$ all crystallize in the monoclinic space group $P2_1/c$ with one complex molecule in the asymmetric unit. In all three compounds the three nitrogen donor atoms of the ligand are bound to the metal center in a meridional arrangement, and both chloride anions are coordinated. The compounds differ in their interactions with the sulfur donor atom of the tetradentate ligand. The $\text{Fe}(\text{II})$ center is in a slightly distorted octahedral geometry completed by coordination of the sulfur atom of the tetradentate ligand. The Fe1-S1 bond distance is 2.6972(6) Å, and the Fe-N bond lengths range between 2.1689(16) and 2.2773(15) Å. The Fe-Cl2 bond length of 2.4481(5) Å is slightly longer than Fe1-Cl1 bond length (2.3275(5) Å), indicative of the larger *trans* influence of the thioether donor.

The coordination sphere of the $\text{Mn}(\text{II})$ ion is in between square pyramidal and trigonal bipyramidal with a τ value of 0.42. The Mn-S bond distance is 2.8325(4) Å, indicating a weak electrostatic interaction most likely causing the change in geometry to square pyramidal, as compared to the cobalt compound. However, this Mn-S distance is significantly longer than that found in $[\text{Fe}^{\text{II}}(\text{L}^1\text{SCH}_3)\text{Cl}_2]$. The Mn-N bond lengths range between 2.2366(10) and 2.3503(10) Å, and thus are slightly longer than the Co-N bond lengths in $[\text{Co}^{\text{II}}(\text{L}^1\text{SCH}_3)\text{Cl}_2]$.

The $\text{Cu}(\text{II})$ ion is in a distorted square-pyramidal geometry with a τ value of 0.22. The Cu-S distance is 2.9961(4) Å, which is again longer than the Mn-S distance in $[\text{Mn}^{\text{II}}(\text{L}^1\text{SCH}_3)\text{Cl}_2]$. The Cu-N bond lengths are in the range of 2.0061(11) to 2.0789(11) Å, much shorter than those in the other compounds. Cl2 is located in the axial position with a bond distance of 2.6570(4) Å, whereas the Cu-Cl1 bond length in the basal plane is 2.2673(3) Å.

The compound $[\text{Cu}^{\text{II}}_2(\text{L}^1\text{SSL}^1)\text{Cl}_4]$ crystallizes in the monoclinic space group $P2_1$, with two crystallographically independent molecules in the asymmetric unit. As the two independent molecules have similar conformations, the description is based on one

molecule only (molecule A with Cu1/Cu2). Both Cu(II) centers in $[\text{Cu}^{\text{II}}_2(\text{L}^1\text{SSL}^1)\text{Cl}_4]$ are coordinated by two chloride ions, and three nitrogen atoms of the ligand. However, the τ value for Cu1 (0.03, square pyramidal geometry) significantly differs from that for Cu2 (0.33, distorted square pyramidal geometry). The Cu-N bond lengths range between 2.005(5) and 2.101(8) Å, similar as in $[\text{Cu}^{\text{II}}(\text{L}^1\text{SCH}_3)\text{Cl}_2]$, but shorter than in $[\text{Co}^{\text{II}}_2(\text{L}^1\text{SSL}^1)\text{Cl}_4]$ [22]. The sulfur atoms of the disulfide bond are non-coordinating. The distances between Cu1-S1 and Cu2-S2 are 3.113(4) and 4.824(2) Å, respectively, which are much longer than that in $[\text{Cu}^{\text{II}}(\text{L}^1\text{SCH}_3)\text{Cl}_2]$. However, the shorter Cu1-S1 distance may be the cause of the difference in coordination geometry of the two copper ions.

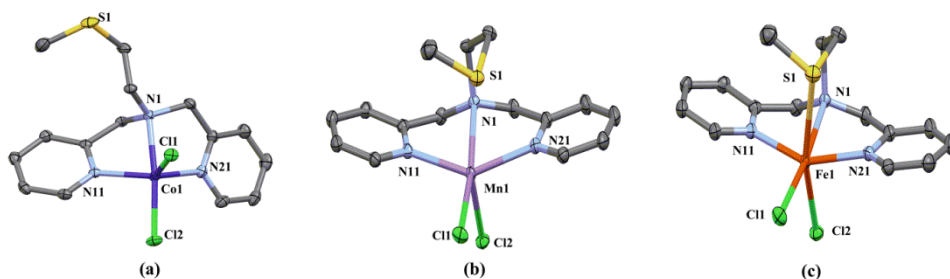


Figure 6.1. Displacement ellipsoid plots (50% probability level) of compounds (a) $[\text{Co}^{\text{II}}(\text{L}^1\text{SCH}_3)\text{Cl}_2]$, (b) $[\text{Mn}^{\text{II}}(\text{L}^1\text{SCH}_3)\text{Cl}_2]$; (c) $[\text{Fe}^{\text{II}}(\text{L}^1\text{SCH}_3)\text{Cl}_2]$ at 110(2) K. All hydrogen atoms are omitted for clarity.

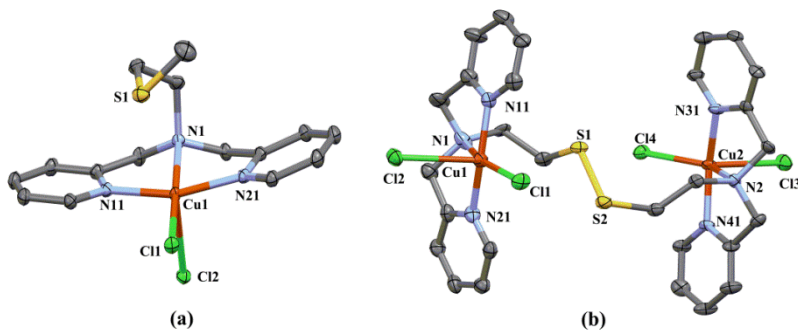


Figure 6.2. Displacement ellipsoid plots (50% probability level) of compounds (a) $[\text{Cu}^{\text{II}}(\text{L}^1\text{SCH}_3)\text{Cl}_2]$, (b) $[\text{Cu}^{\text{II}}_2(\text{L}^1\text{SSL}^1)\text{Cl}_4]$ at 110(2) K. All hydrogen atoms are omitted for clarity.

Table 6.1. Selected bond distances and angles of compounds [Co^{II}(L¹SCH₃)Cl₂], [Cu^{II}(L¹SCH₃)Cl₂], [Mn^{II}(L¹SCH₃)Cl₂] and [Fe^{II}(L¹SCH₃)Cl₂].

Distances/Angles	[Co ^{II} (L ¹ SCH ₃)Cl ₂]	[Cu ^{II} (L ¹ SCH ₃)Cl ₂]	[Mn ^{II} (L ¹ SCH ₃)Cl ₂]	[Fe ^{II} (L ¹ SCH ₃)Cl ₂]
M1-N1	2.2990(19)	2.0789(11)	2.3503(10)	2.2773(15)
M1-N11	2.074(2)	2.0069(11)	2.2366(10)	2.1689(16)
M1-N21	2.083(2)	2.0061(11)	2.2550(10)	2.1781(16)
M1-S1	5.8887(8)	2.9961(4)	2.8325(4)	2.6972(6)
M1-Cl1	2.3049(6)	2.2673(3)	2.3858(4)	2.3275(5)
M1-Cl2	2.3046(6)	2.6570(4)	2.4513(4)	2.4481(5)
N11-M1-N21	119.35(7)	161.05(5)	144.54(4)	148.85(6)
N11-M1-N1	75.89(7)	81.20(4)	72.85(4)	74.70(6)
N21-M1-N1	75.92(7)	81.05(4)	73.12(4)	75.03(6)
N11-M1-Cl2	95.29(6)	89.80(3)	89.27(3)	96.38(4)
N21-M1-Cl2	99.59(6)	96.62(3)	91.22(3)	90.33(4)
N1-M1-Cl2	165.81(5)	89.45(3)	89.68(3)	89.08(4)
N11-M1-Cl1	119.06(6)	99.30(3)	101.36(3)	100.72(4)
N21-M1-Cl1	114.38(6)	97.67(3)	110.69(3)	108.66(4)
N1-M1-Cl1	91.79(5)	174.05(3)	169.90(3)	172.98(4)
Cl2-M1-Cl1	102.27(2)	96.473(12)	99.468(13)	96.795(19)
N11-M1-S1	-	74.45(3)	90.00(3)	92.10(4)
N21-M1-S1	-	96.10(3)	72.84(3)	75.45(4)
N1-M1-S1	-	80.59(3)	76.92(3)	79.82(4)
Cl1-M1-S1	-	93.807(12)	95.049(12)	95.184(18)
Cl2-M1-S1	-	162.414(12)	161.494(12)	163.767(19)

Table 6.2. Selected bond distances and angles of compound [Cu^{II}₂(L¹SSL¹)Cl₄] (only values for molecule A with the Cu1 and Cu2 metal centers are provided).

Distances (Å)		Angles (°)			
Cu1-N1	2.101(8)	N11-Cu1-N21	161.4(3)	N41-Cu2-N31	162.7(2)
Cu1-N11	2.008(7)	N11-Cu1-N1	80.8(3)	N41-Cu2-N2	81.5(2)
Cu1-N21	2.010(7)	N21-Cu1-N1	81.1(3)	N31-Cu2-N2	81.3(3)
Cu1-Cl1	2.266(2)	N11-Cu1-Cl1	98.48(18)	N41-Cu2-Cl4	96.24(18)
Cu1-Cl2	2.561(2)	N21-Cu1-Cl1	97.5(2)	N31-Cu2-Cl4	96.30(18)
Cu2-N2	2.071(6)	N1-Cu1-Cl1	163.0(2)	N2-Cu2-Cl4	142.87(18)
Cu2-N31	2.012(6)	N11-Cu1-Cl2	91.78(18)	N41-Cu2-Cl3	90.49(17)
Cu2-N41	2.005(5)	N21-Cu1-Cl2	94.00(19)	N31-Cu2-Cl3	94.17(18)
Cu2-Cl3	2.447(2)	N1-Cu1-Cl2	94.3(2)	N2-Cu2-Cl3	99.53(18)
Cu2-Cl4	2.2628(1)	Cl1-Cu1-Cl2	102.69(8)	Cl4-Cu2-Cl3	117.58(7)
S1-S2	2.032(3)				
Cu1-Cu2	7.762(1)				

6.2.3 Solution and solid studies of compounds

UV-vis spectra of compound [Co^{II}(L¹SCH₃)Cl₂] dissolved in acetonitrile present three absorption bands. The absorption band at 256 nm ($\epsilon = 4.1 \times 10^3 \text{ M}^{-1} \text{ cm}^{-1}$) is assigned to the $\pi^* \leftarrow \pi$ transition of the pyridyl groups, whereas the two bands at 548 ($\epsilon = 2.0 \times 10^2 \text{ M}^{-1} \text{ cm}^{-1}$) and 629 ($\epsilon = 1.5 \times 10^2 \text{ M}^{-1} \text{ cm}^{-1}$) nm arise from *d-d* transitions of the cobalt(II) ion, likely combined with a Co^{II}←Cl charge transfer transition (LMCT) (Figure S1) [25]. ESI-MS spectra of this compound dissolved in acetonitrile show a dominant peak (*m/z*) at 367.2 corresponding to the fragment [Co^{II}(L¹SCH₃)Cl]⁺

(Figure S2). The effective magnetic moment of $[\text{Co}^{\text{II}}(\text{L}^1\text{SCH}_3)_2\text{Cl}_2]$ was estimated using Evans' method in dimethyl sulfoxide solution at 20 °C, showing a μ_{eff} of 4.52 μ_{B} . This value is consistent with a high-spin ($S = 3/2$) Co(II) center (3.87 is expected for $S = 3/2$) [26, 27]. The absorption spectrum of the compound in the solid state apart from the intense charge transfer band at 257 nm, shows three d-d transitions at 549, 653, and 876 nm typical for a 5-coordinate cobalt(II) ion (Figure S3) [28].

UV-vis spectra of $[\text{Fe}^{\text{II}}(\text{L}^1\text{SCH}_3)_2\text{Cl}_2]$ dissolved in methanol reveal two absorption bands and a shoulder (Figure S4). The absorption band at 254 nm ($\epsilon = 4.0 \times 10^3 \text{ M}^{-1} \text{ cm}^{-1}$) is ascribed to the $\pi^* \leftarrow \pi$ transition of pyridyl groups, whereas the band at 396 ($\epsilon = 1.0 \times 10^3 \text{ M}^{-1} \text{ cm}^{-1}$) nm is tentatively assigned to a metal-to-ligand charge transfer transition (MLCT). The UV-vis spectrum is similar to that of the related dinuclear compound $[\text{Fe}^{\text{II}}_2(\text{L}^1\text{SSL}^1)_2\text{Cl}_4]$ [22]. The ESI-MS spectrum of the compound dissolved in methanol presents a dominant peak (m/z) at 364.5 for the cationic species $[\text{Fe}^{\text{II}}(\text{L}^1\text{SCH}_3)_2\text{Cl}]^+$ in addition to a peak of the solvated species $[\text{Fe}^{\text{II}}(\text{L}^1\text{SCH}_3)_2\text{Cl}(\text{MeOH})]^+$ ($m/z = 395.5$; Figure S5). The effective magnetic moment of $[\text{Fe}^{\text{II}}(\text{L}^1\text{SCH}_3)_2\text{Cl}_2]$ dissolved in methanol was estimated using the Evans' method, giving a μ_{eff} of 4.61 μ_{B} . This value is in agreement with a high-spin Fe(II) center (4.90 is expected for $S = 2$). The absorption spectrum of the compound in the solid state shows a broad absorption from 250 to 500 nm for the charge transfer transitions, in addition to a weak $d-d$ transition at around 1000 nm (Figure S6).

The UV-vis spectrum of compound $[\text{Mn}^{\text{II}}(\text{L}^1\text{SCH}_3)_2\text{Cl}_2]$ dissolved in acetonitrile presents essentially a single absorption band at 260 nm ($\epsilon = 1.1 \times 10^3 \text{ M}^{-1} \text{ cm}^{-1}$) ascribed to the $\pi^* \leftarrow \pi$ transition of the pyridyl groups. A weak band at 317 nm ($\epsilon = 4 \times 10^2 \text{ M}^{-1} \text{ cm}^{-1}$) is tentatively assigned to an Mn \leftarrow Cl charge-transfer transition (LMCT) (Figure S7). The ESI-MS spectrum of the compound dissolved in methanol shows a peak (m/z) at 363.0 corresponding to the fragment $[\text{Mn}^{\text{II}}(\text{L}^1\text{SCH}_3)_2\text{Cl}]^+$ (Figure S8). The effective magnetic moment of the compound was found to be 6.56 μ_{B} , in agreement with a high-spin Mn(II) center (5.92 is expected for $S = 5/2$). The absorption spectrum of the solid compound only shows the charge-transfer bands (Figure S9).

The UV-vis spectrum of $[\text{Cu}^{\text{II}}(\text{L}^1\text{SCH}_3)_2\text{Cl}_2]$ dissolved in methanol presents three absorption bands. The absorption band at 256 nm ($\epsilon = 7.4 \times 10^3 \text{ M}^{-1} \text{ cm}^{-1}$) is assigned to the $\pi^* \leftarrow \pi$ transition of the pyridyl groups, whereas the band at 290 nm ($\epsilon = 1.8 \times 10^3 \text{ M}^{-1} \text{ cm}^{-1}$) probably arises from a Cu \leftarrow Cl charge transfer transition (LMCT) (Figure S10). A weak band at 814 nm ($2 \times 10^2 \text{ M}^{-1} \text{ cm}^{-1}$) corresponds to the $d-d$ transition of the Cu(II) center. The ESI-MS spectrum of the compound dissolved in acetonitrile shows a dominant peak (m/z) at 371.0 fitting the fragment $[\text{Cu}^{\text{II}}(\text{L}^1\text{SCH}_3)_2\text{Cl}]^+$ (Figure S11). Apart from the intense charge-transfer transitions, the absorption spectrum of

the compound $[\text{Cu}^{\text{II}}(\text{L}^1\text{SCH}_3)_2\text{Cl}_2]$ in the solid state shows the *d-d* transition of the copper(II) center as a broad band with a maximum at 713 nm (Figure S12).

The UV-vis spectrum of $[\text{Cu}^{\text{II}}_2(\text{L}^1\text{SSL}^1)_4\text{Cl}_4]$ dissolved in methanol shows an obvious *d-d* transition of Cu(II) at 690 nm ($\epsilon = 1.5 \times 10^2 \text{ M}^{-1} \text{ cm}^{-1}$), in addition to an absorption band at 291 nm ($\epsilon = 3.6 \times 10^3 \text{ M}^{-1} \text{ cm}^{-1}$) likely corresponding to the Cu←Cl charge transfer transition (LMCT), and a band at 258 nm ($\epsilon = 1.0 \times 10^4 \text{ M}^{-1} \text{ cm}^{-1}$) assigned to the $\pi^* \leftarrow \pi$ transition of the pyridyl groups (Figure S13). The ESI-MS spectrum of the dinuclear compound dissolved in methanol shows a dominant peak (*m/z*) at 356.1 corresponding to the fragment $\frac{1}{2}[\text{Cu}^{\text{II}}_2(\text{L}^1\text{SSL}^1)_4\text{Cl}_4]^{2+}$, as well as a peak at 747.0 fitting the fragment $[\text{Cu}^{\text{II}}_2(\text{L}^1\text{SSL}^1)_4\text{Cl}_4]^+$ (Figure S14). The absorption spectrum of the compound in the solid state shows the *d-d* transition as a broad band with maximum absorbance at 732 nm (Figure S15).

6.3 Discussion and conclusion

In this manuscript, we report the synthesis of a series of mononuclear metal compounds $[\text{M}^{\text{II}}(\text{L}^1\text{SCH}_3)_2\text{Cl}_2]$ (M = Co, Cu, Mn, Fe) containing a thioether ligand as well as the dinuclear compound $[\text{Cu}^{\text{II}}_2(\text{L}^1\text{SSL}^1)_4\text{Cl}_4]$ containing a disulfide ligand. The crystal structures combined with the magnetic susceptibility data confirm that the metal centers in these compounds all are in high-spin states. The coordination geometries of the metal centers in the compounds $[\text{Co}^{\text{II}}(\text{L}^1\text{SCH}_3)_2\text{Cl}_2]$, $[\text{Cu}^{\text{II}}(\text{L}^1\text{SCH}_3)_2\text{Cl}_2]$, and $[\text{Mn}^{\text{II}}(\text{L}^1\text{SCH}_3)_2\text{Cl}_2]$ are similar to those found in the related dinuclear compounds $[\text{Co}^{\text{II}}_2(\text{L}^1\text{SSL}^1)_4\text{Cl}_4]$ and $[\text{Cu}^{\text{II}}_2(\text{L}^1\text{SSL}^1)_4\text{Cl}_4]$. The structures of the series $[\text{M}^{\text{II}}(\text{L}^1\text{SCH}_3)_2\text{Cl}_2]$ show an interesting continuous trend: whereas the iron(II) center in $[\text{M}^{\text{II}}(\text{L}^1\text{SCH}_3)_2\text{Cl}_2]$ is in an octahedral geometry with coordination of the thioether sulfur (at 2.6972(6) Å), going via the manganese(II) (2.8325(4) Å) and copper(II) (2.9961(4) Å) to cobalt(II) (5.8887(8) Å) the thioether sulfur progressively is at a larger distance from the metal center. This results in distorted square-pyramidal geometries for the Cu(II) and Mn(II) centers and a trigonal-bipyramidal geometry for the Co(II) center.

This trend is also partly visible in the structures of the dinuclear compounds $[\text{M}^{\text{II}}_2(\text{L}^1\text{SSL}^1)_4\text{Cl}_4]$. The structure of $[\text{Co}^{\text{II}}_2(\text{L}^1\text{SSL}^1)_4\text{Cl}_4]$ is relatively symmetrical: both cobalt(II) ions are in trigonal-bipyramidal geometries with the disulfide sulfur donor atoms at non-coordinating distances. The structures of $[\text{Cu}^{\text{II}}_2(\text{L}^1\text{SSL}^1)_4\text{Cl}_4]$ and $[\text{Fe}^{\text{II}}_2(\text{L}^1\text{SSL}^1)_4\text{Cl}_4]$ are asymmetric with the two metal ions in different geometries; the M-S distances are shorter, resulting in square-pyramidal or octahedral configurations for the metal ions. These shorter M-S distances result in progressively shorter metal-metal distances: in $[\text{M}^{\text{II}}_2(\text{L}^1\text{SSL}^1)_4\text{Cl}_4]$ the M...M distances are 8.1617(6), 7.762(1) Å, and 6.0567(6) Å for cobalt(II), copper(II) and iron(II), respectively. The dinuclear compounds generally show longer M-S distances than the related mononuclear

compounds, indicating that the disulfide sulfur atom is slightly weaker ligand than the thioether sulfur donor.

6.4 Experimental section

6.4.1 General procedures

All chemicals were purchased from commercial vendors and used as received unless noted otherwise. Acetonitrile and diethyl ether were obtained from a solvent purification system (PureSolV 400). Methanol, acetone and hexane were acquired from commercial sources and stored on 3 Å molecular sieves. The synthesis of Co(II), Cu(II) and Mn(II) compounds was carried out in air, whereas the synthesis of Fe(II) compounds was carried out under an inert atmosphere using standard Schlenk-line techniques. ^1H NMR and ^{13}C NMR spectra of the ligands L^1SSL^1 and L^1SCH_3 were recorded on a Bruker 300 DPX spectrometer. Mass spectra were recorded on a Finnigan Aqua mass spectrometer with electrospray ionization (ESI). IR spectra were acquired on a PerkinElmer UATR spectrum equipped with single reflection diamond (scan range 400 cm^{-1} to 4000 cm^{-1} , resolution 4 cm^{-1}). UV-vis spectra were collected using a transmission dip probe with variable path length and reflection probe on an Avantes Avaspec-2048 spectrometer with Avalight-DH-S-BAL light source. Elemental analyses were performed by the Microanalytical Laboratory Kolbe in Germany.

6.4.2 Single crystal X-ray crystallography

All reflection intensities were measured at 110(2) K using a SuperNova diffractometer (equipped with Atlas detector) with Mo $\text{K}\alpha$ radiation ($\lambda = 0.71073\text{ \AA}$) for compounds $[\text{Co}^{\text{II}}(\text{L}^1\text{SCH}_3)\text{Cl}_2]$, $[\text{Cu}^{\text{II}}(\text{L}^1\text{SCH}_3)\text{Cl}_2]$, $[\text{Mn}^{\text{II}}(\text{L}^1\text{SCH}_3)\text{Cl}_2]$, and $[\text{Fe}^{\text{II}}(\text{L}^1\text{SCH}_3)\text{Cl}_2]$, and with Cu $\text{K}\alpha$ radiation ($\lambda = 1.54178\text{ \AA}$) for the compound $[\text{Cu}^{\text{II}}_2(\text{L}^1\text{SSL}^1)\text{Cl}_4]$ under the program CrysAlisPro (Version CrysAlisPro 1.171.39.29c, Rigaku OD, 2017 or Version 1.171.36.32 Agilent Technologies, 2013). The same program was used to refine the cell dimensions and for data reduction. The structure was solved with the program SHELXS-2014/7 [29], and was refined on F^2 with SHELXL-2014/7. Numerical absorption correction based on Gaussian integration over a multifaceted crystal model was applied using CrysAlisPro for $[\text{Co}^{\text{II}}(\text{L}^1\text{SCH}_3)\text{Cl}_2]$, $[\text{Cu}^{\text{II}}(\text{L}^1\text{SCH}_3)\text{Cl}_2]$, $[\text{Mn}^{\text{II}}(\text{L}^1\text{SCH}_3)\text{Cl}_2]$, and $[\text{Fe}^{\text{II}}(\text{L}^1\text{SCH}_3)\text{Cl}_2]$. Analytical numeric absorption correction using a multifaceted crystal model was applied using CrysAlisPro for $[\text{Cu}^{\text{II}}_2(\text{L}^1\text{SSL}^1)\text{Cl}_4]$. The temperature of the data collection was controlled using the system Cryojet (manufactured by Oxford Instruments). The H atoms were placed at calculated positions using the instructions AFIX 23, AFIX 43 or AFIX 137 with isotropic displacement parameters having values 1.2 or 1.5 Ueq of the attached C atoms.

The structure of $[\text{Co}^{\text{II}}(\text{L}^1\text{SCH}_3)\text{Cl}_2]$ is ordered. The absolute structure configuration was established by anomalous-dispersion effects in diffraction measurements on the crystal, and the Flack and Hooft parameters refine to 0.011(5) and 0.013(3), respectively. The structures of $[\text{Cu}^{\text{II}}(\text{L}^1\text{SCH}_3)\text{Cl}_2]$, $[\text{Fe}^{\text{II}}(\text{L}^1\text{SCH}_3)\text{Cl}_2]$, $[\text{Mn}^{\text{II}}(\text{L}^1\text{SCH}_3)\text{Cl}_2]$ are ordered. The structure of $[\text{Cu}^{\text{II}}_2(\text{L}^1\text{SSL}^1)\text{Cl}_4]$ is partly disordered. The asymmetric unit contains two crystallographically independent molecules. The C1X–C2X–S1X fragments (X = A, B) are disordered over two orientations, and the occupancy factors of the major components of the disorder refine to 0.798(13) and 0.673(11). The crystal is pseudomerohedrally twinned, and the twin relationship is given by $M = (-1\ 0\ 0 / 0\ -1\ 0 / 0\ 0\ 1)$. The general and racemic twinning were refined simultaneously using the instruction TWIN $-1\ 0\ 0\ 0\ -1\ 0\ 0\ 0\ 1\ -4$, and the three BASF twin component factors refine to 0.230(13), 0.226(15) and 0.215(13).

6.4.3 Synthesis of metal compounds

$[\text{Co}^{\text{II}}(\text{L}^1\text{SCH}_3)\text{Cl}_2]$: The ligand L^1SCH_3 (54.7 mg, 0.2 mmol) was dissolved in 2 mL acetonitrile, and separately $\text{CoCl}_2 \cdot 6\text{H}_2\text{O}$ (47.8 mg, 0.2 mmol) was dissolved in 2 mL acetonitrile. The two solutions were mixed resulting in a purple suspension, which was stirred for another 30 min. Then, 20 mL diethyl ether was added and a purple precipitate was formed immediately. The obtained precipitate was washed with diethyl ether (3×20 mL). Yield: 45.1 mg, 0.1 mmol, 56%; Single crystals suitable for X-ray structure determination were obtained by slow vapor diffusion of diethyl ether into an acetonitrile solution of the compound; single crystals were obtained after about 2 days at room temperature. IR (cm^{-1}): 487m, 507m, 646m, 763s, 787s, 1022s, 1053m, 1097m, 1154m, 1308m, 1440s, 1479m, 1605s. ESI-MS found (calcd) for $[\text{M} - \text{Cl}]^+$ m/z : 367.2 (367.1). Elemental analysis calcd (%) for $\text{C}_{15}\text{H}_{19}\text{Cl}_2\text{CoN}_3\text{S}$: C 44.68, H 4.75, N 10.42; Found: C 44.02, H 4.89, N 10.27.

$[\text{Fe}^{\text{II}}(\text{L}^1\text{SCH}_3)\text{Cl}_2]$: To a yellow solution of L^1SCH_3 (48.6 mg, 0.2 mmol) dissolved in 5 mL methanol, solid $\text{FeCl}_2 \cdot 4\text{H}_2\text{O}$ (35.4 mg, 0.2 mmol) was added, immediately resulting in a yellow solution. The obtained solution was stirred for 2 h at room temperature under inert atmosphere. After that, 50 mL diethyl ether was added, yielding a yellow precipitate. The obtained precipitate was washed with diethyl ether (3×20 mL). Yield: 32 mg, 0.1 mmol, 45%. Single crystals suitable for X-ray structure determination were obtained by slow vapor diffusion of diethyl ether into a methanolic solution of the compound; single crystals were obtained after about 1 week at room temperature. IR (cm^{-1}): 481w, 640w, 729w, 776m, 794s, 983w, 1017m, 1050m, 1294m, 1442m, 1475m, 1601m. ESI-MS found (calcd) for $[\text{M} - \text{Cl}]^+$ m/z : 364.5 (364.7). Elemental analysis calcd (%) for $\text{C}_{15}\text{H}_{19}\text{Cl}_2\text{FeN}_3\text{S} + \text{H}_2\text{O}$: C 43.08, H 5.06, N 10.05; Found: C 42.64, H 4.65, N 10.34.

[Cu^{II}(L¹SCH₃)Cl₂]: Ligand L¹SCH₃ (160.3 mg, 0.6 mmol) was dissolved in 10 mL acetonitrile. To this solution solid CuCl₂ (78.9 mg, 0.6 mmol) was added, yielding a blue solution. The obtained solution was stirred overnight at room temperature, after which 80 mL diethyl ether was added, resulting in a blue precipitate. The solid was collected by filtration and was washed with diethyl ether (4 × 5 mL). Yield: 172.1 mg, 0.4 mmol, 72%. Single crystals suitable for X-ray structure determination were obtained by vapor diffusion of diethyl ether into an acetonitrile solution of the compound; Single crystals were obtained after approximately 1 week at room temperature. IR (cm⁻¹): 1606s, 1573w, 1479s, 1442s, 1379w, 1351w, 1310w, 1286w, 1153m, 1111m, 1094s, 1052s, 1027s, 992m, 962w, 852m, 787s, 771s, 727m, 652m, 536m. ESI-MS found (calcd) for [M - Cl]⁺ *m/z* 371.0 (371.0). Elemental analysis calcd (%) for C₁₅H₁₉Cl₂CuN₃S + 0.3 C₄H₁₀O: C 45.24, H 5.16, N 9.77; Found: C 44.64, H 5.25, N 9.61.

[Mn^{II}(L¹SCH₃)Cl₂]: Ligand L¹SCH₃ (206.4 mg, 0.8 mmol) was dissolved in 10 mL methanol; to this solution solid MnCl₂·4H₂O (149.5 mg, 0.8 mmol) was added, yielding a pale yellow solution. The obtained solution was stirred for overnight at room temperature. Then, 80 mL diethyl ether was added, leading to a pale-yellow, oily material. The solution was decanted and the obtained oily material was re-dissolved in 10 mL acetonitrile. To the resulting solution 80 mL diethyl ether was added, yielding a pale yellow precipitate, which was collected by filtration and washed with diethyl ether (4 × 5 mL). Yield: 177 mg, 0.4 mmol, 58%. Single crystals suitable for X-ray structure determination were obtained by slow vapor diffusion of diethyl ether into an acetonitrile solution of the compound; Single crystals were obtained after around 1 week at room temperature. IR (cm⁻¹): 1602s, 1569m, 1477m, 1443s, 1295s, 1161m, 1094m, 1050m, 1016s, 794s, 775s, 730m, 641m. ESI-MS found (calcd) for [M - Cl]⁺ *m/z* 363.0 (363.0). Elemental analysis calcd (%) for C₁₅H₁₉Cl₂MnN₃S + 0.5 H₂O: C 44.13, H 4.94, N 10.29; Found: C 43.84, H 4.90, N 10.19.

[Cu^{II}₂(L¹SSL¹)Cl₄]: To a solution of L¹SSL¹ (103.3 mg, 0.2 mmol) in 4 mL acetonitrile, solid CuCl₂ (53.8 mg, 0.4 mmol) was added, resulting in a blue solution. The obtained solution was stirred for about 30 min, during which time a blue precipitate formed. The blue precipitate was collected by filtration and washed with diethyl ether (3 × 10 mL). Yield: 70.7 mg, 0.1 mmol, 45%. Single crystals suitable for X-ray structure determination were obtained by slow evaporation of a solution of the compound in dimethylformamide in the back of a fume hood. Single crystals were obtained after approximately 1 month at room temperature. IR (cm⁻¹): 1607s, 1572w, 1479m, 1441s, 1350w, 1305w, 1286m, 1249w, 1103w, 1053s, 1029s, 963w, 978w, 877m, 819w, 784vs, 762vs, 723w, 652w. ESI-MS found (calcd) for ½[M - 2Cl]²⁺ *m/z* 357.1 (357.3);

[M - Cl]⁺ *m/z* 749.0 (749.0). Elemental analysis calcd (%) for C₂₈H₃₂Cl₄Cu₂N₆S₂ + 0.5 H₂O: C 42.32, H 4.19, N 10.58; Found: C 42.43, H 4.21, N 10.59.

6.5 References

- [1] M. Zhao, H.-B. Wang, L.-N. Ji, Z.-W. Mao, *Chem. Soc. Rev.*, 42 (2013) 8360-8375.
- [2] I.M. Wasser, S. De Vries, P. Moënne-Loccoz, I. Schröder, K.D. Karlin, *Chem. Rev.*, 102 (2002) 1201-1234.
- [3] W. Nam, *Acc. Chem. Res.*, 40 (2007), 465-465.
- [4] C. Belle, W. Rammal, J.-L. Pierre, *J. Inorg. Biochem.*, 99 (2005) 1929-1936.
- [5] B.A. MacKay, M.D. Fryzuk, *Chem. Rev.*, 104 (2004) 385-402.
- [6] E.C.M. Ordning-Wenker, M. van der Plas, M.A. Siegler, S. Bonnet, F.M. Bickelhaupt, C. Fonseca Guerra, E. Bouwman, *Inorg. Chem.*, 53 (2014) 8494-8504.
- [7] M. Gennari, B. Gerey, N. Hall, J. Pécaut, M.N. Collomb, M. Rouzières, R. Clérac, M. Orio, C. Duboc, *Angew. Chem. Int. Ed.*, 53 (2014) 5318-5321.
- [8] A.M. Thomas, B.L. Lin, E.C. Wasinger, T.D.P. Stack, *J. Am. Chem. Soc.*, 135 (2013) 18912-18919.
- [9] E.C. Ordning - Wenker, M. van der Plas, M.A. Siegler, C. Fonseca Guerra, E. Bouwman, *Chem. Eur. J.*, 20 (2014) 16913-16921.
- [10] Y. Ueno, Y. Tachi, S. Itoh, *J. Am. Chem. Soc.*, 124 (2002) 12428-12429.
- [11] S. Itoh, M. Nagagawa, S. Fukuzumi, *J. Am. Chem. Soc.*, 123 (2001) 4087-4088.
- [12] S. Luo, D.F. Bruggeman, M.A. Siegler, E. Bouwman, *Inorg. Chim. Acta*, 477 (2018) 24-30.
- [13] S. Luo, M.A. Siegler, E. Bouwman, *Organometallics*, 37 (2017) 740-747.
- [14] G. Gezer, D.D. Jiménez, M.A. Siegler, E. Bouwman, *Dalton Trans.*, 46 (2017) 7506-7514.
- [15] J.D. Franolic, W.Y. Wang, M. Millar, *J. Am. Chem. Soc.*, 114 (1992) 6587-6588.
- [16] B. Horn, C. Limberg, C. Herwig, B. Braun, *Inorg. Chem.*, 53 (2014) 6867-6874.
- [17] X. Liu, S.K. Ibrahim, C. Tard, C.J. Pickett, *Coord. Chem. Rev.*, 249 (2005) 1641-1652.
- [18] A.R. McDonald, M.R. Bukowski, E.R. Farquhar, T.A. Jackson, K.D. Koehntop, M.S. Seo, R.F. De Hont, A. Stubna, J.A. Halfen, E. Münck, *J. Am. Chem. Soc.*, 132 (2010) 17118-17129.
- [19] S.A. Mirza, R.O. Day, M.J. Maroney, *Inorg. Chem.*, 35 (1996) 1992-1995.
- [20] T. Ohta, T. Tachiyama, K. Yoshizawa, T. Yamabe, T. Uchida, T. Kitagawa, *Inorg. Chem.*, 39 (2000) 4358-4369.
- [21] E.C. Ordning-Wenker, M.A. Siegler, M. Lutz, E. Bouwman, *Dalton Trans.*, 44 (2015) 12196-12209.
- [22] F. Jiang, M.A. Siegler, X. Sun, C.F. Guerra, E. Bouwman, *Inorg. Chem.*, 2018 (2018) 8796-8805.
- [23] Y. Ueno, Y. Tachi, S. Itoh, *J. Am. Chem. Soc.*, 124 (2002) 12428-12429.
- [24] A.W. Addison, T.N. Rao, J. Reedijk, J. van Rijn, G.C. Verschoor, *Journal of the Chemical Society, Dalton Transactions*, (1984) 1349-1356.
- [25] A. Dutta, M. Flores, S. Roy, J.C. Schmitt, G.A. Hamilton, H.E. Hartnett, J.M. Shearer, A.K. Jones, *Inorg. Chem.*, 52 (2013) 5236-5245.
- [26] G.A. Bain, J.F. Berry, *J. Chem. Educ.*, 85 (2008) 532.
- [27] D. Evans, *Journal of the Chemical Society (Resumed)*, (1959) 2003-2005.
- [28] B.P. A., *Inorganic electronic spectroscopy* 2nd edition, Elsevier, 1984.
- [29] G.M. Sheldrick, *Acta Crystallogr., Sect. A*, 64 (2008) 112-122.

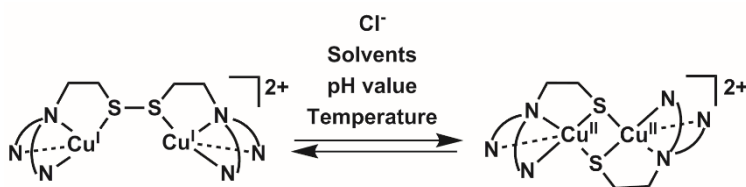
Chapter 7

Summary, Conclusion and Outlook

7.1 Summary

7.1.1 Introduction

Electron-transfer reactions assisted by metalloenzymes are ubiquitous and play fundamental roles in biological systems such as dioxygen transport, nitrite reduction, as well as the synthesis of neurotransmitters [1-4]. However, understanding the exact mechanism of electron-transfer reactions occurring in metalloenzymes is still a long-term challenge [2]. In the last decades, synthetic models of enzyme active sites by well-designed ligands provided a chemical perspective into how these reactions take place [5-8]. Among them, tremendous efforts have been put in the synthesis of copper(II) thiolate compounds with a diamond core $[\text{Cu}_2\text{S}_2]$ structure, and in the investigation of the redox interconversion of these copper(II) thiolate compounds to their isomeric copper(I) disulfide compounds (Scheme 7.1) [9-14]. These studies aimed to simulate the structure, spectroscopic properties, and electron-transfer processes of Cu_A active sites.

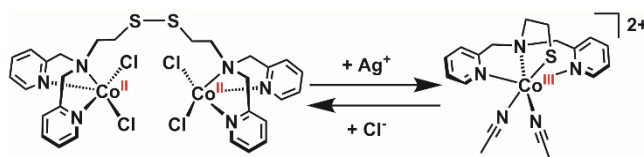


Scheme 7.1. Schematic representation of the redox interconversion between copper(II) thiolate and copper(I) disulfide compounds.

7.1.2 Redox interconversion between cobalt thiolate/cobalt(II) compounds

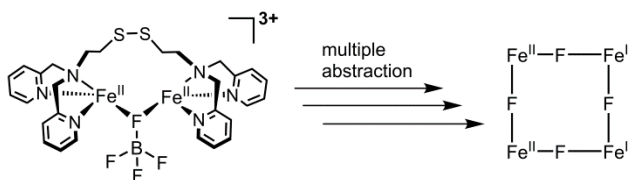
As described in Chapter 1, redox interconversion between copper(II) thiolate and copper(I) disulfide compounds has been extensively studied. However, only few studies have been reported concerning other transition metal compounds with disulfide/thiolate ligands. In Chapter 2, the synthesis is described of one cobalt(II) disulfide and two cobalt(III) thiolate compounds starting from the disulfide ligand L^1SSL^1 in reaction with different cobalt(II) salts. Cobalt(III) thiolate compounds were formed when cobalt(II) salts with BF_4^- , PF_6^- , or NCS^- anions were employed, whereas use of CoCl_2 resulted in a cobalt(II) disulfide compound. Further investigation revealed that the addition of chloride ions to a solution of the cobalt(III) thiolate compound in acetonitrile results in conversion to the cobalt(II) disulfide compound, as monitored with UV-vis spectroscopy (Scheme 7.2); subsequent addition of AgBF_4 regenerates

the Co(III) thiolate compound. Computational studies revealed that substitution of the coordinated acetonitrile molecule or thiocyanate anion in cobalt(III) thiolate compounds by a chloride anion induces a change in the character of the highest occupied molecular orbital, showing a decrease of the contribution of the *p* orbital on sulfur and an increase of the contribution of the *d* orbital on cobalt.



Scheme 7.2. Redox interconversion between cobalt(III) thiolate and cobalt(II) disulfide compounds induced by addition/removal of chloride anions in acetonitrile solution.

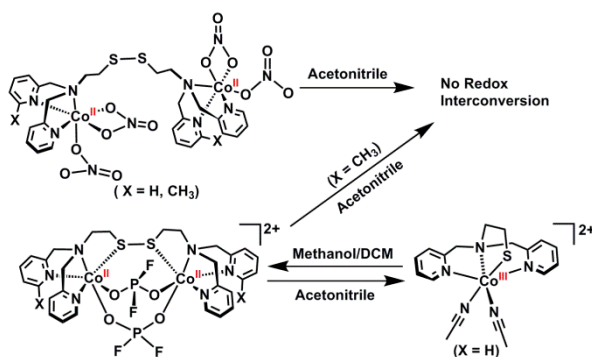
A dinuclear iron(II) disulfide compound was formed from the ligand L¹SSL¹ in reaction with FeCl₂·4H₂O. The two iron(II) centers in this compound are found in two different geometries, which are different from the related cobalt(II) disulfide compound. Reaction of the ligand L¹SSL¹ with [Fe(MeCN)₆](BF₄)₂ yielded an iron(II) fluoride cluster rather than the expected Fe(III) thiolate compound (Scheme 7.3). The novel tetranuclear cluster comprising both terminal and bridging fluoride ions reveals a unique and nearly planar [Fe₄F₄] core, as is described in Chapter 5.



Scheme 7.3. Schematic representation of the formation of an iron(II) fluoride cluster comprising a unique, nearly planar [Fe₄F₄] core.

Four cobalt(II) disulfide compounds with different disulfide ligands (L¹SSL¹, L²SSL²) and different anions (PO₂F₂⁻, NO₃⁻) were isolated and characterized using various methods, as reported in Chapter 3 (Scheme 7.4); the ligand L²SSL² has a methyl group at two of the pyridine rings. The cobalt(II) compounds with PO₂F₂⁻ anions were unexpectedly formed from an old batch of AgPF₆, but were successfully reproduced using the solid salt LiPO₂F₂. Single crystal X-ray crystallography showed that in all cobalt(II) compounds the cobalt(II) ions are

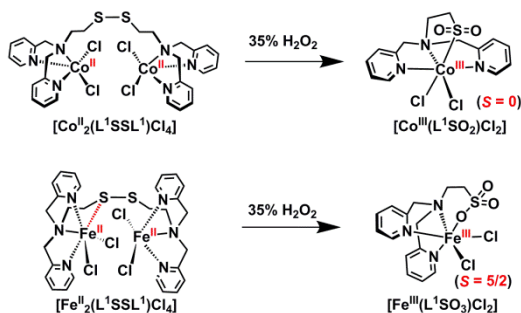
in octahedral geometries. Solution studies revealed that the cobalt(II) disulfide compound with the ligand L^1SSL^1 and $PO_2F_2^-$ anions is stable as such in the solvents dichloromethane and methanol, but in acetonitrile redox interconversion occurs with the formation of the cobalt(III) thiolate compound $[Co^{III}(L^1S)(MeCN)_2]^{2+}$. This interconversion does not occur for the compound with NO_3^- anions. Further investigation revealed that both cobalt(II) disulfide compounds of the disulfide ligand L^2SSL^2 also do not show this redox interconversion in any of the investigated solvents.



Scheme 7.4. Schematic representation of the redox interconversion between cobalt(III) thiolate and cobalt(II) disulfide compounds.

7.1.3 Reactivity of Fe^{II} and Co^{II} disulfide compounds with dihydrogen peroxide

Investigation of the reactivity of metal thiolate compounds with dioxygen has attracted considerable attention in the last decades, aimed at the understanding of oxidation sensitivity of metalloenzymes in biological system [15-22]. However, the study of the oxidation of metal disulfide compounds is still rare [19]. It was found that oxidation of the iron(II) disulfide compound described in Chapter 2 resulted in the formation of a mononuclear high-spin ($S = 5/2$) sulfonato-Fe(III) compound as the final product, whereas oxidation of the related cobalt(II) disulfide compound yielded the low-spin ($S = 0$) sulfinato-cobalt(III) derivative (Scheme 7.5). ESI-MS spectra of the reaction mixture in combination with the results of a previous study indicated that oxidation of the cobalt compound proceeds via a relatively stable sulfenato-cobalt(III) compound [23].



Scheme 7.5. Schematic representation of oxidation of metal disulfide compounds.

7.1.4 Synthesis and characterization of a series of transition metal compounds of thioether and disulfide ligands

In Chapter 6, the synthesis and characterization has been described of a series of transition metal compounds $[\text{M}^{\text{II}}(\text{L}^1\text{SCH}_3)\text{Cl}_2]$ ($\text{M} = \text{Co}, \text{Cu}, \text{Mn}, \text{Fe}$) of a tetradentate ligand containing a thioether donor. The structural and spectroscopic properties of these compounds are compared to those of the related dinuclear disulfide compounds $[\text{M}^{\text{II}}_2(\text{L}^1\text{SSL}^1)\text{Cl}_4]$. The crystal structures combined with the magnetic susceptibility data confirmed that the metal centers in these compounds all are in high-spin states. The geometries of the central ion in the series $[\text{M}^{\text{II}}(\text{L}^1\text{SCH}_3)\text{Cl}_2]$ show an interesting continuous trend: whereas the iron(II) center in $[\text{M}^{\text{II}}(\text{L}^1\text{SCH}_3)\text{Cl}_2]$ is in an octahedral geometry with coordination of the thioether sulfur (at 2.6972(6) Å), going via the manganese(II) (2.8325(4) Å) and copper(II) (2.9961(4) Å) to cobalt(II) (5.8887(8) Å) the thioether sulfur progressively is at a larger distance from the metal center. This results in distorted square-pyramidal geometries for the copper(II) and manganese(II) centers and a trigonal-bipyramidal geometry for the cobalt(II) center. This trend is also partly visible in the structures of the dinuclear compounds $[\text{M}^{\text{II}}_2(\text{L}^1\text{SSL}^1)\text{Cl}_4]$. Generally, the dinuclear compounds generally show longer M-S distances than the related mononuclear compounds, indicating that the disulfide sulfur atom is a slightly weaker ligand than the thioether sulfur donor.

7.2 Conclusions and outlook

In the last decade, the redox interconversion between metal thiolate and disulfide compounds has been extensively investigated for copper, but not for other transition metal ions. In this thesis, our investigations are described of the possibility to extend the metal thiolate/disulfide redox interconversion

reactions to cobalt or iron compounds. A number of cobalt(II) disulfide and cobalt(III) thiolate compounds of different ligands and different anions are reported in this thesis. It was revealed that the anion of cobalt(II) salts, the structure of disulfide ligands, and the type of solvent influence the formation of either cobalt(II) disulfide or cobalt(III) thiolate compounds. However, a consistent trend cannot be provided to predict which of the species is generated.

- The interconversion is not related to the binding strength of the anion: whereas the coordinating chloride ion leads to the formation of cobalt(II) disulfide compounds, use of the coordinating thiocyanate ion leads to the formation of cobalt(III) thiolate compounds.
- The interconversion is not related to the polarity of the solvent, nor on the potential binding strength of the solvent: the solvents chloroform (non-polar and non-coordinating) and methanol (highly polar and coordinating) lead to formation of cobalt(II) disulfide compounds, whereas acetonitrile (medium polarity and coordinating) leads to the corresponding cobalt(III) thiolate compound (for L^1SSL^1 as the ligand in combination with the $PF_2O_2^-$ anion).

One general observation is that the cobalt(II) ions in the disulfide compounds are in the high-spin state in all cases reported in this thesis, whereas the cobalt(III) ions in the thiolate compounds are in a low-spin state. An important conclusion of this work therefore is that the cobalt(II) disulfide to cobalt(III) thiolate interconversion reaction might be related to the ligand field strength of the ligand, and the binding strength and ligand field strength of the anions and solvent used. A larger ligand field splitting of the ligand in combination with a large ligand-field splitting caused by the anion or coordinating solvent will ultimately lead to the formation of low-spin cobalt(II) ions. In an octahedral geometry this results in the presence of a single electron in a high-energy antibonding d orbital; transfer of this high-energy electron to a p orbital of a nearby disulfide sulfur atom then effectively results in the oxidation of the cobalt center with the reduction of the disulfide to thiolate groups.

Indeed, computational studies revealed that exchange of the coordinated acetonitrile molecule or thiocyanate anion in cobalt(III) thiolate compounds by a chloride anion induces a change in the character of the highest occupied molecular orbital, showing a decrease of the contribution of the p orbital on sulfur and an increase of the contribution of the d orbital on cobalt; however,

this effect appeared to be rather small. Ultimately this should result in the formation of the cobalt(II) disulfide compound, although this was not found to occur in the minimization process. Thus, in the future, more computational studies should be conducted to clarify the mechanism of these redox interconversion reactions in detail.

Further systematic studies should be undertaken to investigate the subtle balance of the redox interconversion and its dependence on the combinations of ligand field strengths of the ligand and anions or coordinating solvents. Thus, the effect may be studied of different halogen anions (F⁻, Br⁻, I⁻) or other coordinating co-ligands on the position of the redox interconversion reactions.

Although the cobalt thiolate/disulfide redox interconversion reactions have been largely extended in this thesis, the effect of the addition/removal of protons, and changes in temperature to these redox reactions is still worthy of investigation.

Apart from the cobalt compounds, two iron(II) disulfide compounds were reported in this thesis (Chapter 2 and 5). However, so far we were not able to trigger the conversion of these compounds to their respective iron(III) thiolate compounds. Further studies are necessary to reveal what would trigger such a redox interconversion. Not only would this be interesting for the iron(II)/iron(III) redox couple, but similar studies can also be done for the manganese(II)/manganese(III) couple.

7.3 References

- [1] S. Iwata, C. Ostermeier, B. Ludwig, H. Michel, *Nature*, 376 (1995) 660-669.
- [2] C. Jacob, G.L. Giles, N.M. Giles, H. Sies, *Angew. Chem. Int. Edit.*, 42 (2003) 4742-4758.
- [3] J.A. Kovacs, *Acc. Chem. Res.*, 48 (2015) 2744-2753.
- [4] J.T. Pedersen, C. Hureau, L. Hemmingsen, N.H. Heegaard, J. Østergaard, M. Vašák, P. Faller, *Biochem.*, 51 (2012) 1697-1706.
- [5] K.D. Karlin, *Science*, 261 (1993) 701-708.
- [6] E. Kim, E.E. Chufán, K. Kamaraj, K.D. Karlin, *Chem. Rev.*, 104 (2004) 1077-1134.
- [7] E.Y. Tshuva, S.J. Lippard, *Chem. Rev.*, 104 (2004) 987-1012.
- [8] S. Friedle, E. Reisner, S.J. Lippard, *Chem. Soc. Rev.*, 39 (2010) 2768-2779.
- [9] E.C.M. Ording-Wenker, M. van der Plas, M.A. Siegler, S. Bonnet, F.M. Bickelhaupt, C. Fonseca Guerra, E. Bouwman, *Inorg Chem*, 53 (2014) 8494-8504.
- [10] E.C.M. Ording-Wenker, M. van der Plas, M.A. Siegler, C. Fonseca Guerra, E. Bouwman, *Chem. Eur. J.*, 20 (2014) 16913-16921.
- [11] A.M. Thomas, B.L. Lin, E.C. Wasinger, T.D.P. Stack, *J. Am. Chem. Soc.*, 135 (2013) 18912-18919.

- [12] A. Neuba, R. Haase, W. Meyer-Klaucke, U. Flörke, G. Henkel, *Angew. Chem. Int. Edit.*, 51 (2012) 1714-1718.
- [13] Y. Ueno, Y. Tachi, S. Itoh, *J. Am. Chem. Soc.*, 124 (2002) 12428-12429.
- [14] S. Itoh, M. Nagagawa, S. Fukuzumi, *J. Am. Chem. Soc.*, 123 (2001) 4087-4088.
- [15] E.C.M. Ordning-Wenker, M.A. Siegler, M. Lutz, E. Bouwman, *Inorg. Chem.*, 52 (2013) 13113-13122.
- [16] A. Dutta, M. Flores, S. Roy, J.C. Schmitt, G.A. Hamilton, H.E. Hartnett, J.M. Shearer, A.K. Jones, *Inorg. Chem.*, 52 (2013) 5236-5245.
- [17] A.C. McQuilken, Y. Jiang, M.A. Siegler, D.P. Goldberg, *J. Am. Chem. Soc.*, 134 (2012) 8758-8761.
- [18] C.S. Mullins, C.A. Grapperhaus, B.C. Frye, L.H. Wood, A.J. Hay, R.M. Buchanan, M.S. Mashuta, *Inorg. Chem.*, 48 (2009) 9974-9976.
- [19] Y. Lee, D.-H. Lee, A.A.N. Sarjeant, K.D. Karlin, *J. Inorg. Biochem.*, 101 (2007) 1845-1858.
- [20] P. Lugo-Mas, A. Dey, L. Xu, S.D. Davin, J. Benedict, W. Kaminsky, K.O. Hodgson, B. Hedman, E.I. Solomon, J.A. Kovacs, *J. Am. Chem. Soc.*, 128 (2006) 11211-11221.
- [21] R.A. de Sousa, E. Galardon, M. Rat, M. Giorgi, I. Artaud, *J. Inorg. Biochem.*, 99 (2005) 690-697.
- [22] J.A. Kovacs, *Science*, 299 (2003) 1024-1025.
- [23] F. Jiang, M.A. Siegler, X. Sun, L. Jiang, C. Fonseca Guerra, E. Bouwman, *Inorg. Chem.*, 57 (2018) 8796-8805.

Appendix I

Supplementary information on Chapter 2

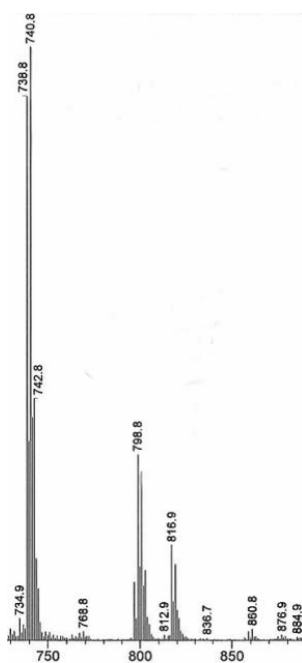


Figure AI.1. ESI-MS spectrum of compound **1c₀** dissolved in acetonitrile. ESI-MS found (calcd) for $[M-Cl]^+$ m/z 740.8 (740.9); for $[M-Cl+MeCN+H_2O]^+$ m/z 798.1 (798.8).

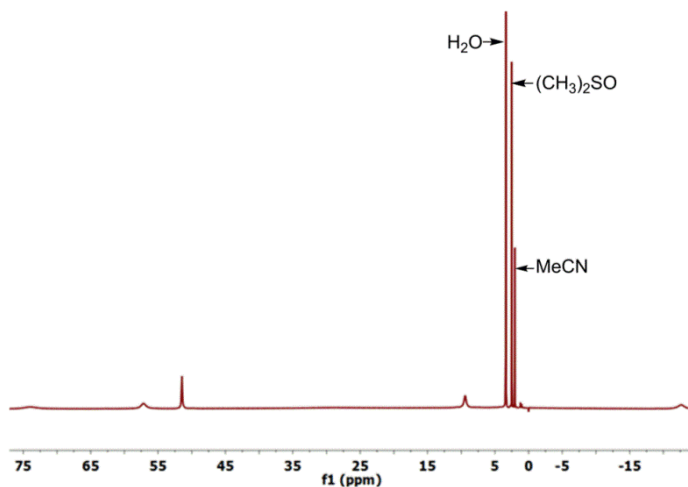


Figure A1.2. ^1H NMR spectrum of compound 1_{c0} dissolved in dimethyl sulfoxide- d_6 .

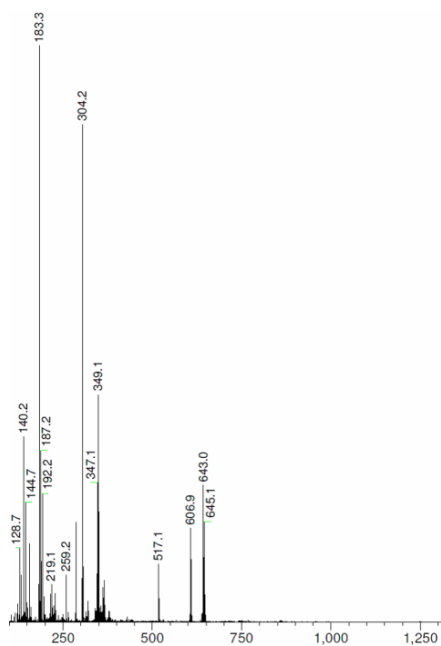


Figure A1.3. ESI-MS spectrum of Fe^{II} disulfide compound 1_{Fe} dissolved in methanol. ESI-MS found (calcd) for $\frac{1}{4}[\text{Fe}^{\text{II}}_2(\text{L}^1\text{SSO}_2\text{L}^1)\cdot 4\text{H}_2\text{O}]^{4+}$, m/z 183.3 (183.1), $\frac{1}{2}[\text{Fe}^{\text{II}}(\text{L}^1\text{SSL}^1)\cdot 2\text{H}_2\text{O}]^{2+}$, m/z 304.2 (304.1) $\frac{1}{2}[\text{Fe}^{\text{II}}_2(\text{L}^1\text{SSL}^1)\text{Cl}_2]^{2+}$ m/z 349.1 (349.0), $[\text{L}^1\text{SSL}^1+\text{H}]^+$ m/z 517.1 (517.2), $[\text{Fe}^{\text{II}}(\text{L}^1\text{SSL}^1)\text{Cl}_2 + \text{H}]^+$ m/z 643.0 (643.1).

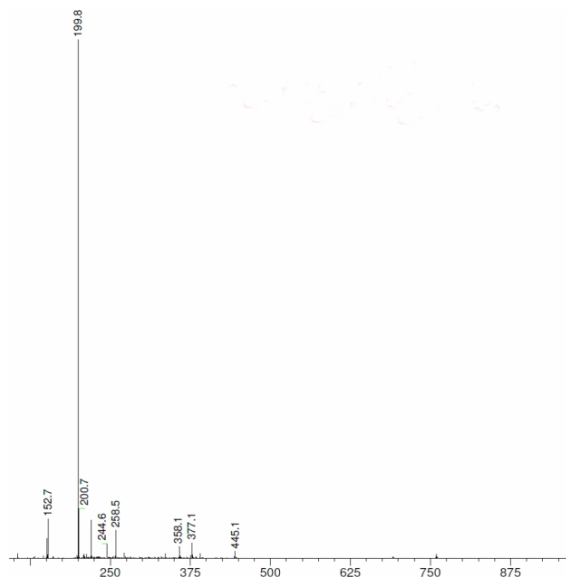


Figure A1.4. ESI-MS spectrum of compound **2** dissolved in acetonitrile. ESI-MS found (calcd) for $\frac{1}{2}[\text{M}-2(\text{BF}_4)+2\text{MeCN}]^{2+}$ m/z 199.8 (199.5).

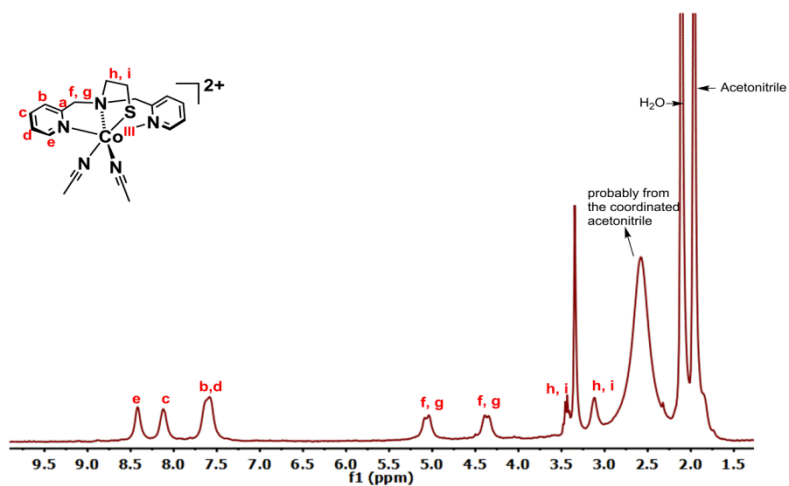


Figure A1.5. ^1H NMR spectrum of compound **2** dissolved in acetonitrile- d_3 .

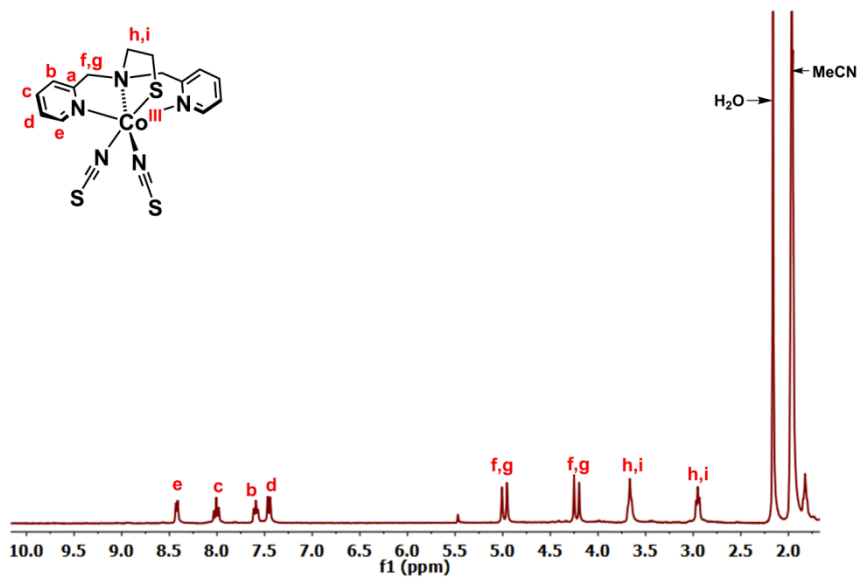


Figure A1.6. ^1H NMR spectrum of compound **3** dissolved in acetonitrile- d_3 .

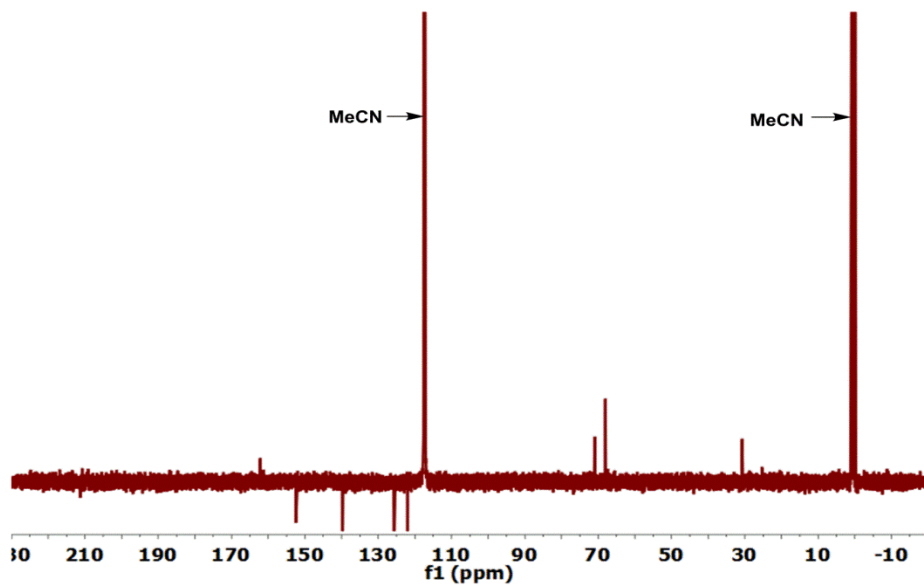


Figure A1.7. ^{13}C NMR spectrum of compound **3** dissolved in acetonitrile- d_3 .

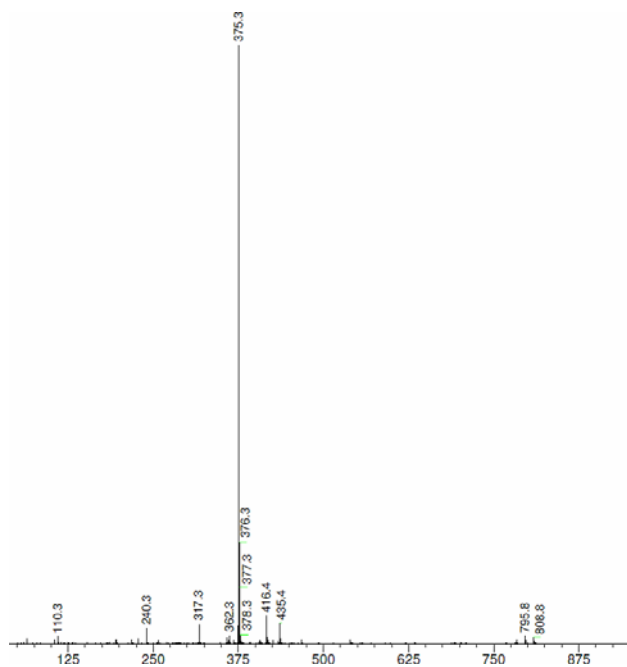


Figure A1.8. ESI-MS spectrum of compound **3** dissolved in acetonitrile. ESI-MS found (calcd) for $[M-NCS]^+$ m/z 375.3 (375.4).

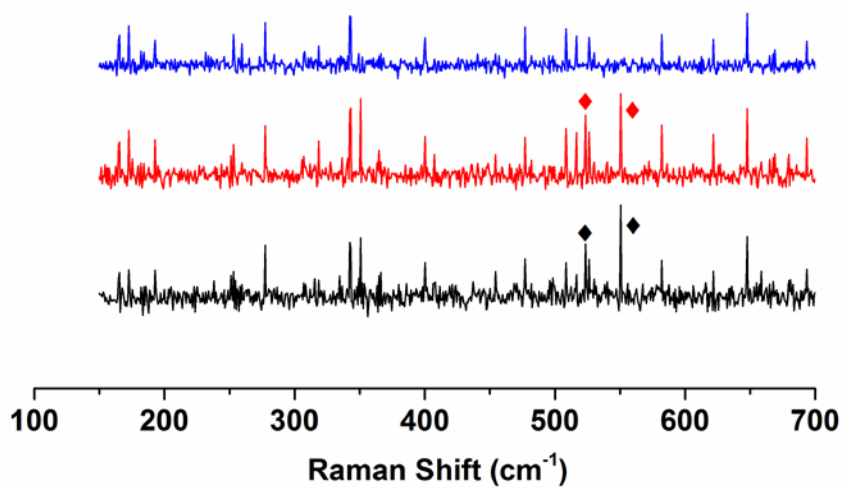


Figure A1.9. Raman spectra of ligand L^1SSL^1 (black line), compounds **1c_o** (red line), and **2** (blue line). The diamonds represent the peaks arising from the S-S bond vibration.

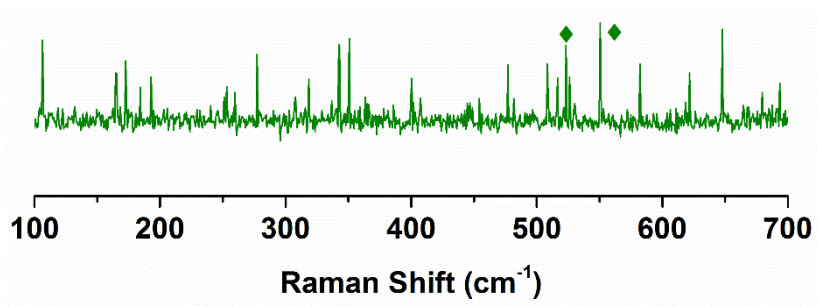


Figure AI.10. Raman spectra of compound **1Fe**. The diamonds represent the peaks arising from the S-S bond vibration.

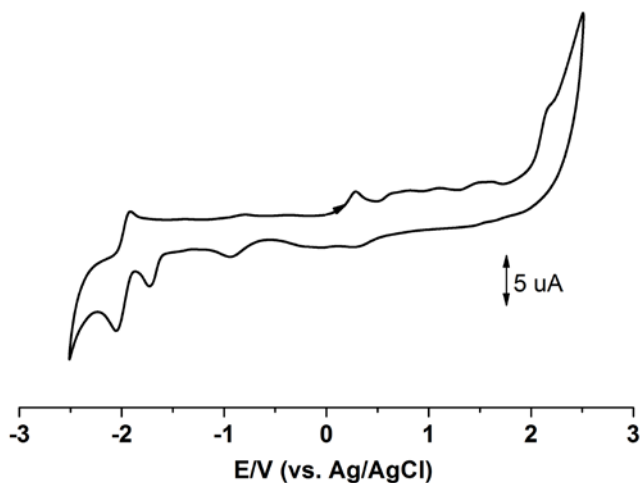


Figure AI.11. The cyclic voltammograms of compound **1Co** (1 mM) in an acetonitrile solution containing 0.1 M NBu₄PF₆ as the supporting electrolyte and using a glassy carbon electrode at a scan rate of 100 mV s⁻¹. The potential is given vs. Ag/AgCl.

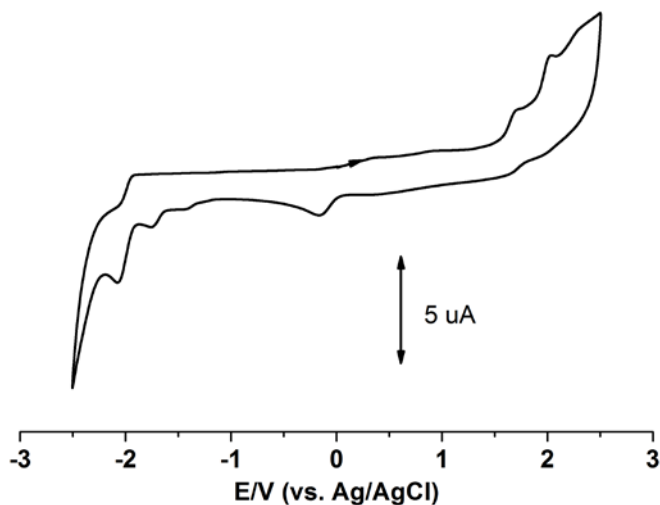


Figure AI.12. The cyclic voltammograms of compound **2** (2 mM) in an acetonitrile solution containing 0.1 M TBAPF₆ as the supporting electrolyte and using a glassy carbon electrode at a scan rate of 100 mV s⁻¹. The potential is given vs. Ag/AgCl.

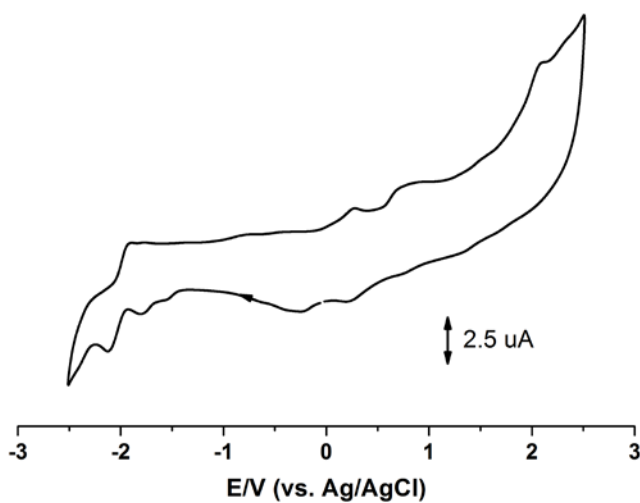


Figure AI.13. The cyclic voltammograms of compound **3** (2 mM) in an acetonitrile solution containing 0.1 M NBu₄PF₆ as the supporting electrolyte and using a glassy carbon electrode at a scan rate of 100 mV s⁻¹. The potential is given vs. Ag/AgCl.

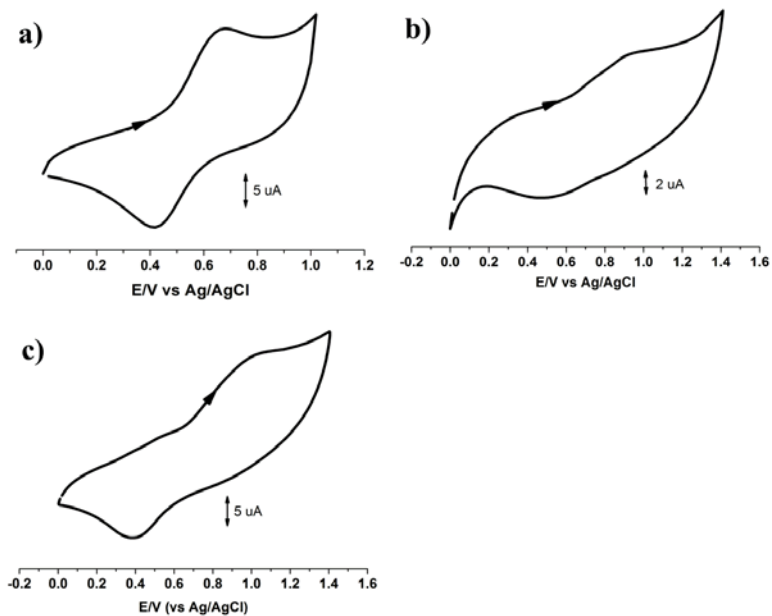


Figure Al.14. The cyclic voltammograms of (a) compound **1_c** (1 mM), (b) compound **2** (2 mM), and (c) compound **3** (2 mM) in an acetonitrile solution containing 0.1 M NBu_4PF_6 as the supporting electrolyte and using a glassy carbon electrode at a scan rate of 100 mV s^{-1} . Potentials are given vs. Ag/AgCl .

Table AI.1. Crystallographic and structure refinement data of compounds **1_{Co}**, **2_{Ox}**, **3** and **1_{Fe}**.

	1_{Co}	2_{Ox}	3	1_{Fe}
Chemical formula	C ₂₈ H ₃₂ Cl ₄ Co ₂ N ₆ S ₂ ·C ₄ H ₁₀ O	C ₁₈ H ₂₂ CoN ₅ O ₂ S ·2(BF ₄)·2(C ₂ H ₃ N)	C ₁₆ H ₁₆ CoN ₅ O _{0.18} S ₃	C ₂₈ H ₃₂ Cl ₄ Co ₂ N ₆ S ₂ ·2(CH ₄ O)
Formula Weight	850.49	687.12	436.33	834.30
Crystal system, space group	Triclinic, <i>P</i> -1	Triclinic, <i>P</i> -1	Orthorhombic, <i>Pbca</i>	Monoclinic, <i>Cc</i>
Temperature (K)	110	110	110	110
<i>a</i> , <i>b</i> , <i>c</i> (Å)	8.2673(2), 13.6866(4), 17.1779(7)	11.7231 (3), 13.1844 (3), 20.0200 (6)	11.0351(2), 16.5646(3), 19.6200(4)	28.6815(7), 9.11583(17), 15.3360(4)
α , β , γ (°)	90.875(3), 102.152(3), 92.315(2)	70.877 (2), 86.502 (2), 81.384 (2)	90, 90, 90	90, 116.791(3), 90
<i>V</i> (Å ³)	1898.03(11)	2890.35 (14)	3586.38(12)	3579.27(17)
<i>Z</i>	2	4	8	4
Radiation type	Mo <i>K</i> α	Mo <i>K</i> α	Mo <i>K</i> α	Mo <i>K</i> α
μ (mm ⁻¹)	1.30	0.753	1.32	1.264
Crystal size (mm)	0.35 × 0.24 × 0.07	0.37 × 0.13 × 0.06	0.28 × 0.21 × 0.13	0.31 × 0.24 × 0.17
Diffractometer	SuperNova, Dual, Cu at zero, Atlas	SuperNova, Dual, Cu at zero, Atlas	SuperNova, Dual, Cu at zero, Atlas	SuperNova, Dual, Cu at zero, Atlas
<i>T</i> _{min} , <i>T</i> _{max}	0.755, 0.925	0.561, 1.000	0.436, 1.000	0.556, 0.729
No. of measured, independent and observed [<i>I</i> > 2 σ (<i>I</i>)] reflections	29644, 8726, 6714	41812, 13267, 10130	52080, 4121, 3755	26618, 7654, 7433
<i>R</i> _{int}	0.047	0.040	0.036	0.0291
(<i>sin</i> θ / λ) _{max} (Å ⁻¹)	0.650	0.650	0.650	0.650
<i>R</i> [<i>F</i> ² > 2 σ (<i>F</i> ²)], <i>wR</i> (<i>F</i> ²), <i>S</i>	0.040, 0.089, 1.03	0.043, 0.105, 1.04	0.028, 0.070, 1.09	0.022, 0.049, 1.03
No. of reflections	8726	13267	4121	7654
No. of parameters	426	817	236	423
H-atom treatment	H-atom parameters constrained	H-atom parameters constrained	H-atom parameters constrained	H-atom parameters constrained
$\Delta\rho$ _{max} , $\Delta\rho$ _{min} (e Å ⁻³)	0.83, -1.00	0.71, -0.46	0.85, -0.59	0.31, -0.20

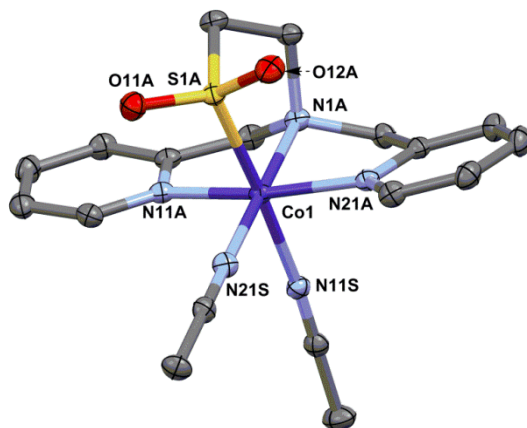


Figure AI.15. Displacement ellipsoid plot (50% probability level) of the cationic part of cobalt(III) sulfinate compound **2_{ox}**.

Table AI.2. Selected bond distances (Å) and angles (°) for the crystal structure of compound [Co^{III}{L¹SO₂}(MeCN)₂](BF₄)₂ (**2_{ox}**).

Distance (Å)			
Co1–N1A	1.9494(19)	Co1–S1A	2.1837(6)
Co1–N11A	1.944(2)	Co1–N11S	2.010(2)
Co1–N21A	1.9384(19)	Co1–N21S	1.916(2)
Angles (°)			
N21S–Co1–N21A	95.38(8)	N11A–Co1–N11S	88.97(8)
N21S–Co1–N11A	96.49(8)	N1A–Co1–N11S	92.38(8)
N21A–Co1–N11A	168.11(8)	N21S–Co1–S1A	89.34(6)
N21S–Co1–N1A	179.06(8)	N21A–Co1–S1A	87.55(6)
N21A–Co1–N1A	85.13(8)	N11A–Co1–S1A	93.23(6)
N11A–Co1–N1A	83.01(8)	N1A–Co1–S1A	89.89(6)
N21S–Co1–N11S	88.40(8)	N11S–Co1–S1A	177.01(6)
N21A–Co1–N11S	90.72(8)		

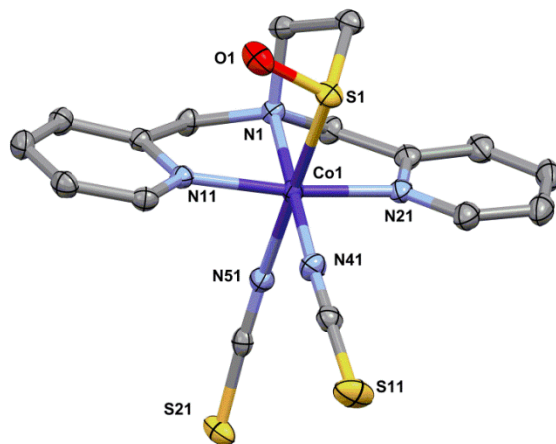


Figure AI.16. Displacement ellipsoid plot (50% probability level) of the oxidized part of the compound **3** present with an occupancy factor of 0.178(5) at 110(2) K. All hydrogen atoms are omitted for clarity.

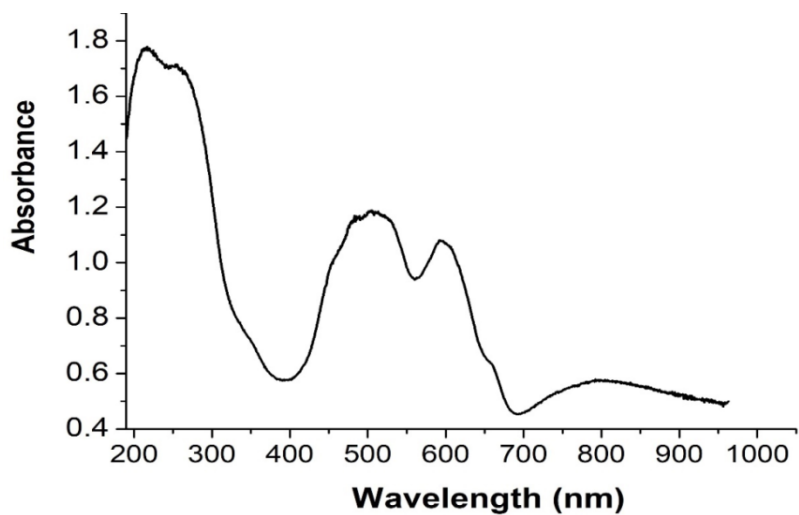


Figure AI.17. UV-vis spectrum of compound **1c** in the solid state.

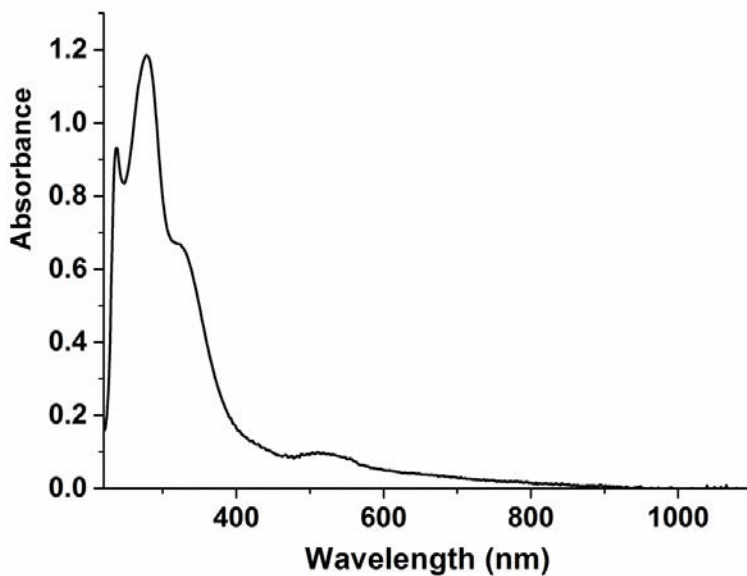


Figure A1.18. UV-vis spectrum of compound **3** dissolved in acetonitrile. UV-vis spectra were recorded using solutions 1 mM in [Co] with a transmission dip probe path length of 1.4 mm.

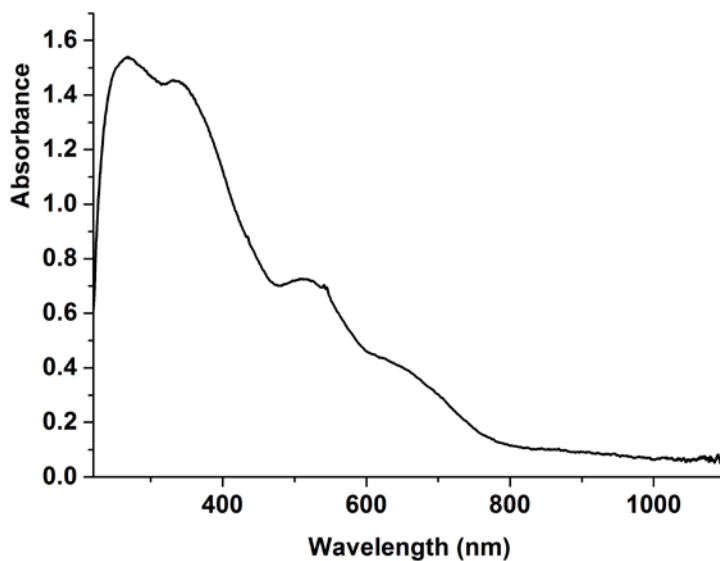


Figure A1.19. UV-vis spectrum of compound **3** in solid state.

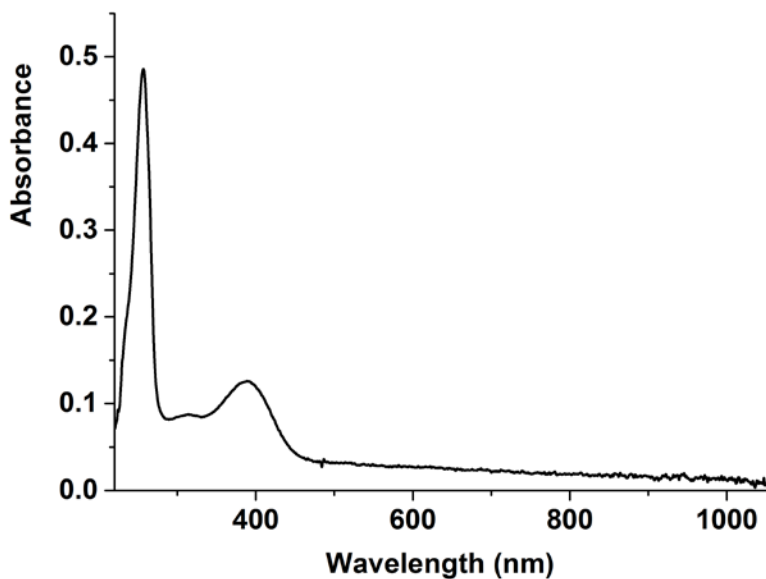


Figure Al.20. UV-vis spectrum of compound 1_{Fe} dissolved in methanol. UV-vis spectra were recorded using solutions 1 mM in [Fe] with a transmission dip probe path length of 1.2 mm.

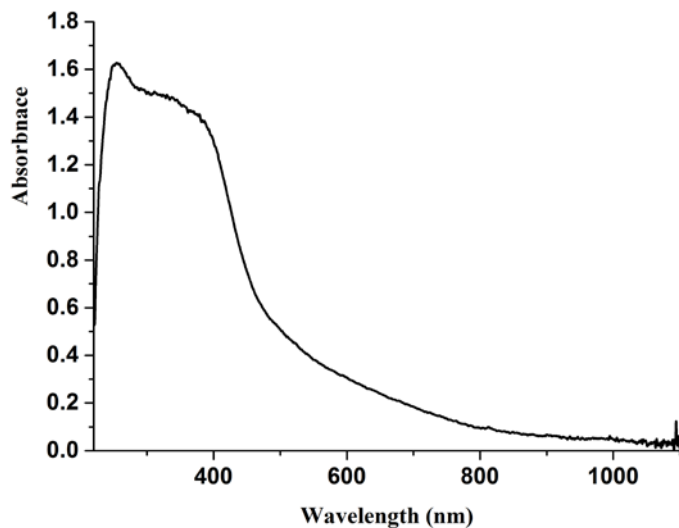


Figure Al.21. UV-vis spectrum of the compound 1_{Fe} in solid state.

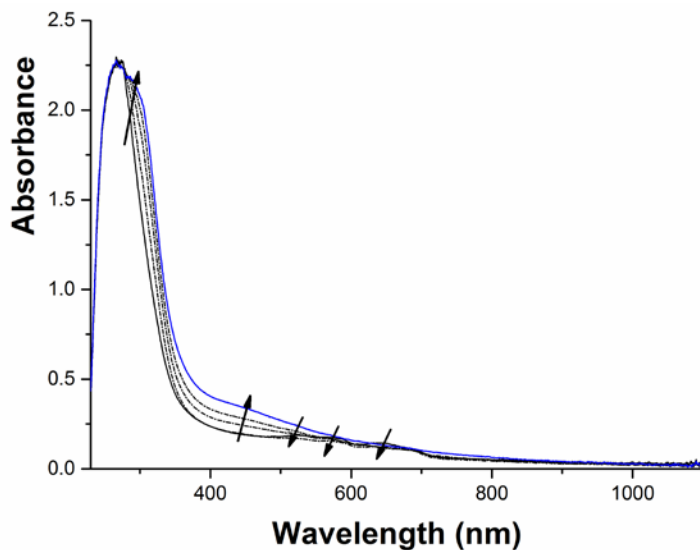


Figure AI.22. UV-vis spectra recorded upon addition of AgBF_4 to a solution of the compound $\mathbf{1}_{\text{Co}}$. The spectra were recorded in at a concentration of 5 mM $[\text{Co}]$ with a transmission dip probe path length of 1.8 mm.

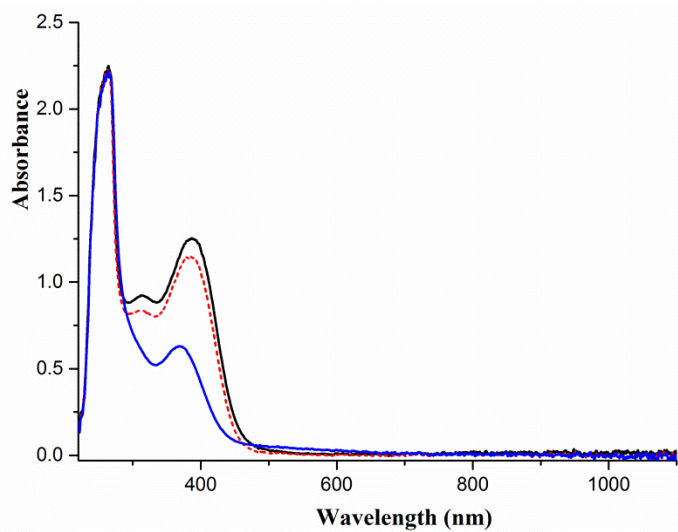


Figure AI.23. UV-vis spectra recorded upon addition of 2 equiv. (red dotted line), and 4 equiv. (blue line) AgBF_4 to a solution of the compound $\mathbf{1}_{\text{Fe}}$. The spectra were recorded in at a concentration of 2 mM $[\text{Fe}]$ with a transmission dip probe path length of 2.2 mm.

Table AI.3. The total energies (kcal/mol) of the compound **1_{Co}** in the gas phase and in acetonitrile with different spin states ($S = 1/2, 3/2$).

1_{Co}	$S = 3/2$	$S = 1/2$
Energy(gas)	-10456	-10440
Gibbs energy(gas)	-10153	-10133
Energy(solvated)	-10496	-10488
Gibbs energy(solvated)	-10194	-10181

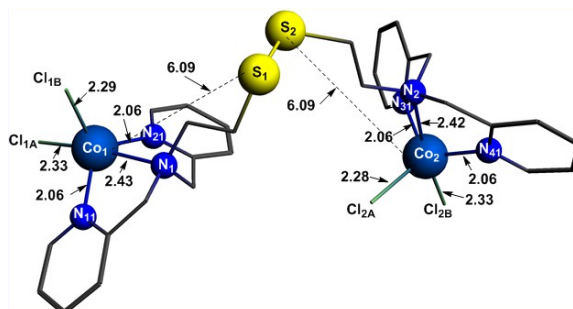


Figure AI.24. The optimized structure of the compound **1_{Co}** with the two cobalt(II) centers in a high-spin state ($S = 3/2$) with COSMO model (acetonitrile).

Table AI.4. The total energies (kcal/mol) of the cationic part of the compound **2** and compound **3** under gas phase and in acetonitrile with different spin states ($S = 0$ and 2).

2	$S = 2$	$S = 0$
Energy(gas)	-6476	-6500
Gibbs Energy(gas)	-6280	-6299
Energy(solvated)	-6608	-6638
Gibbs Energy(solvated)	-6412	-6437
3	$S = 2$	$S = 0$
Energy(gas)	-6052	-6069
Gibbs Energy(gas)	-5898	-5911
Energy(solvated)	-6070	-6097
Gibbs Energy(solvated)	-5916	-5939

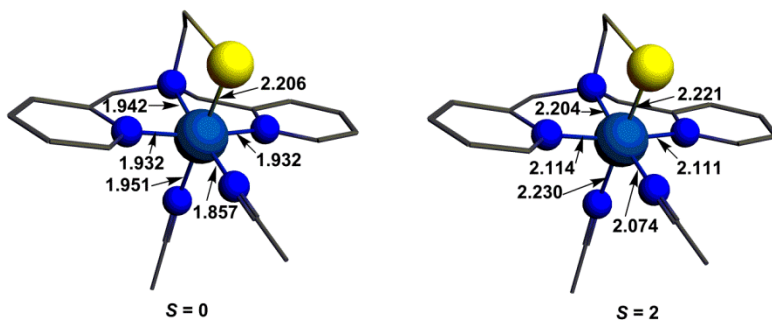


Figure AI.25. The optimized structures of the cationic part of compound **2** in different spin states with COSMO model (acetonitrile).

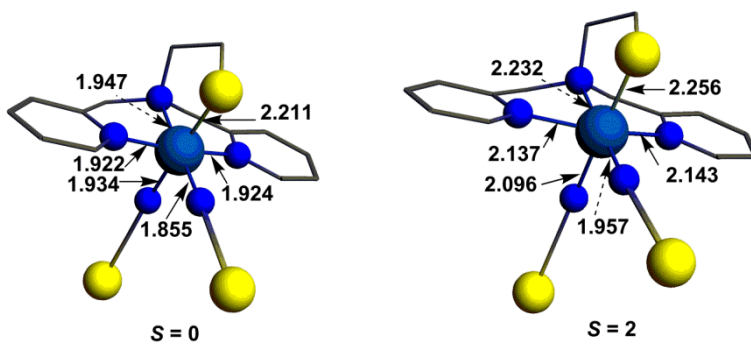


Figure AI.26. The optimized structure of compound **3** in different spin states with COSMO model (acetonitrile).

Table AI.5. The total energies (kcal/mol) of compound **1Fe** under gas phase and solvent with different spin states.

(1Fe)	<i>S</i> = 2, 2	<i>S</i> = 0, 0	<i>S</i> = 0, 2
Energy(gas)	-10515.7	-10488.9	-10502.8
Gibbs Energy(gas)	-10214.5	-10178.9	-10197.5
Energy(solvated)	-10564.6	-10542.9	-10559.3
Gibbs Energy(solvated)	-10263.5	-10232.9	-10253.9

Table AI.6. The total energies (kcal/mol) of the compound **1_{Fe}** under gas phase and solvent with different spin states and keeping the Fe1-S1 bond frozen.

(1_{Fe})	$S = 2, 2$	$S = 0, 0$	$S = 0, 2$
Energy(gas)	-10513.6	-10476.9	-10497.2
Gibbs Energy(gas)	-10211.3	-10168.2	-10192.3
Energy(solvated)	-10564.8	-10528.0	-10544.7
Gibbs Energy(solvated)	-10262.6	-10219.3	-10239.8

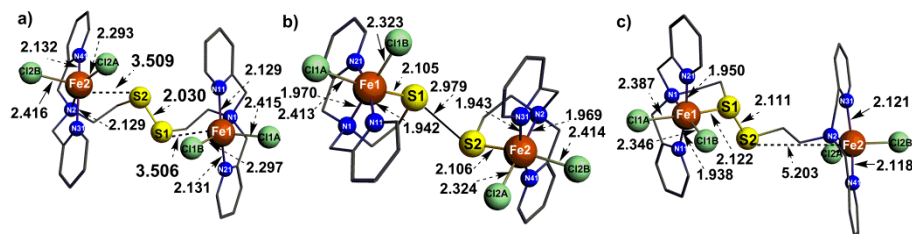


Figure AI.27. The optimized structures of the compound **1_{Fe}** with a) high-spin states ($S = 2$ for both iron center), b) low-spin states ($S = 0$ for both iron centers), c) mixed-spin states ($S = 0$ for one iron center, and $S = 2$ for another iron center) with COSMO model (methanol).

Table AI.7. The total energies (kcal/mol) of acetonitrile, and the cobalt compounds **5** and **6** with different spin states and their related antiferromagnetically coupled species (AF(1,1) is the antiferromagnetically coupled species obtained from the compound **5** with two triplet-spin cobalt(III) centers, AF(2,2) is the antiferromagnetically coupled species obtained from the compound **5** with two high-spin cobalt(III) centers).

5	$S = 0, 0$	$S = 1, 1$	AF(1,1)	$S = 2, 2$	AF(2,2)
Energy (gas)	-9345	-9346	-9318	-9316	-9286
Gibbs energy (gas)	-9033	-9035	-9007	-9008	-8979
Energy (solvated)	-9816	-9812	-9788	-9772	-9742
Gibbs energy (solvated)	-9504	-9501	-9477	-9464	-9435
6	$S = 0, 0$		$S = 2, 2$		
Energy (gas)	-11089		The		
Gibbs energy (gas)	-10721		structure		
Energy (solvated)	-11535		has been		
Gibbs energy (solvated)	-11167		broken		

Table AI.8. The total energies (kcal/mol) of acetonitrile, and the copper compounds **7** and **8** (AF(1/2,1/2) is the antiferromagnetically coupled species obtained from the compound **8** with two doublet-spin copper(II) centers).

	Acetonitrile	7	8	AF(1/2,1/2)
Gibbs energy (gas)	-837	-5525	-9368	-9363
Energy (gas)	-850	-5696	-9676	-9671
Gibbs energy (solvated)	-844	-5569	-9487	-9483
Energy (solvated)	-857	-5740	-9795	-9791

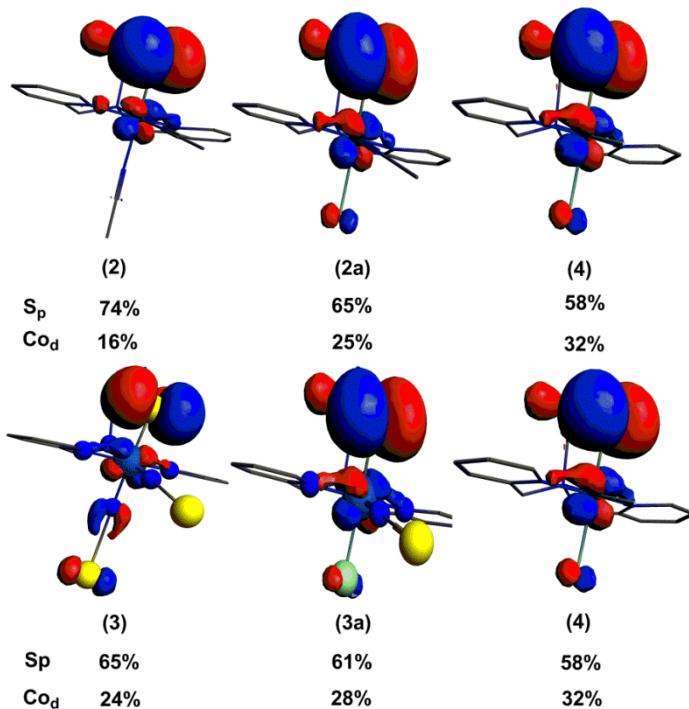


Figure AI.28. Plots showing the character of the HOMOs of compounds **2**, **3**, and the hypothetical compounds **2a**, **3a** and **4**.

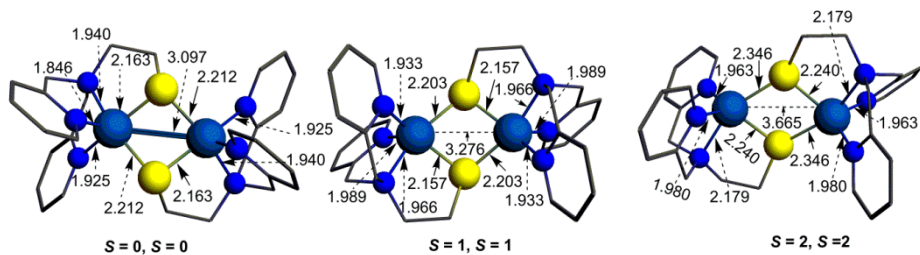


Figure A1.29. The optimized structures of compound 5 in different spin states with COSMO model (acetonitrile).

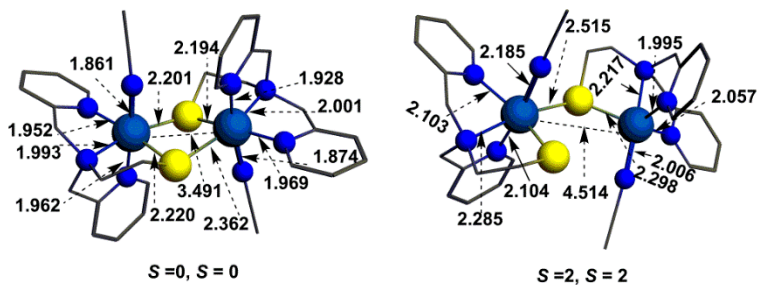


Figure A1.30. The optimized structures of compound 6 in different spin states with COSMO model (acetonitrile).

Appendix II

Supplementary information on Chapter 3

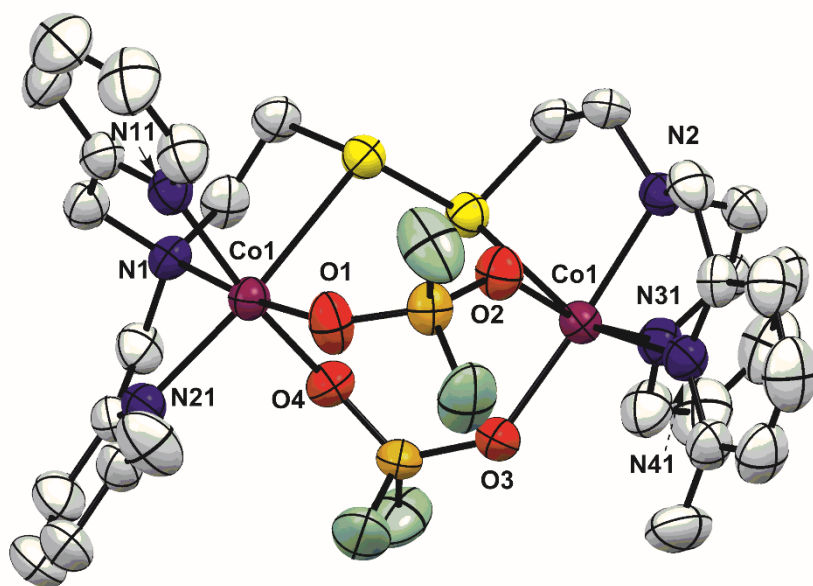


Figure AII.1. Displacement ellipsoid plot (50% probability level) of the compound $[\text{Co}^{\text{II}}_2(\text{L}^7\text{SSL}^7)(\text{PO}_2\text{F}_2)_2](\text{PF}_6)_2$ at 110(2) K. The lattice solvent molecule and hydrogen atoms are omitted for clarity.

Table AII.1. Experimental details for compounds $[\text{Co}^{\text{II}}_2(\text{L}^1\text{SSL}^1)(\text{NO}_3)_4]$ and $[\text{Co}^{\text{II}}_2(\text{L}^1\text{SSL}^1)(\text{PO}_2\text{F}_2)_2](\text{PF}_6)_2$.

Compounds	$[\text{Co}^{\text{II}}_2(\text{L}^1\text{SSL}^1)(\text{NO}_3)_4]$	$[\text{Co}^{\text{II}}_2(\text{L}^1\text{SSL}^1)(\text{PO}_2\text{F}_2)_2](\text{PF}_6)_2$
Chemical formula	$\text{C}_{28}\text{H}_{32}\text{Co}_2\text{N}_{10}\text{O}_{12}\text{S}_2$	$\text{C}_{28}\text{H}_{32}\text{Co}_2\text{F}_4\text{N}_6\text{O}_4\text{P}_2\text{S}_2 \cdot 2(\text{F}_6\text{P}) \cdot 3.338(\text{CH}_2\text{Cl}_2)$
M_r	882.61	1409.92
Crystal system, space group	Monoclinic, $P2_1/n$	Triclinic, $P-1$
Temperature (K)	110	110
a, b, c (Å)	8.1948 (2), 13.6066 (8), 33.1859 (13)	12.9871 (2), 13.7863 (3), 15.2272 (3)
β (°)	105.678 (3)	83.4006 (16)
V (Å ³)	3562.7 (3)	2616.93 (9)
Z	4	2
Radiation type	Mo $K\alpha$	Mo $K\alpha$
μ (mm ⁻¹)	1.12	1.28
Crystal size (mm)	0.18 × 0.12 × 0.06	0.37 × 0.26 × 0.16
Diffractometer	SuperNova, Dual, Cu at zero, Atlas	SuperNova, Dual, Cu at zero, Atlas
$T_{\text{min}}, T_{\text{max}}$	0.806, 1.000	0.473, 1.000
No. of measured, independent and observed reflections [$I > 2\sigma(I)$]	22306, 8369, 6063	40131, 11994, 10992
R_{int}	0.032	0.021
$(\sin \theta/\lambda)_{\text{max}}$ (Å ⁻¹)	0.623	0.650
$R[F^2 > 2\sigma(F^2)], wR(F^2), S$	0.040, 0.081, 0.90	0.030, 0.071, 1.04
No. of reflections	8369	11994
No. of parameters	501	844
No. of restraints	145	922
$\Delta\rho_{\text{max}}, \Delta\rho_{\text{min}}$ (e Å ⁻³)	1.14, -0.77	1.22, -0.55

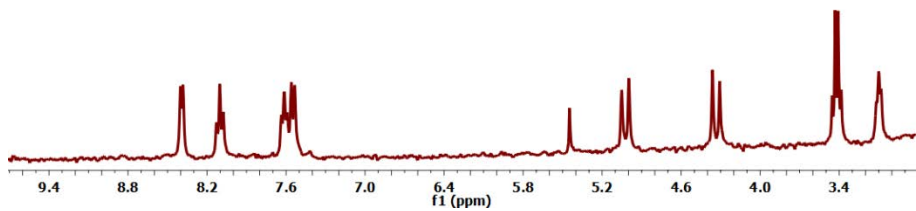


Figure AII.2. ^1H NMR spectrum of $[\text{Co}^{\text{III}}(\text{L}^1\text{S})(\text{MeCN})_2]^{2+}$, obtained upon dissolution of the compound $[\text{Co}^{\text{II}}_2(\text{L}^1\text{SSL}^1)(\text{PO}_2\text{F}_2)_2](\text{PF}_6)_2$ in acetonitrile- d_3 .

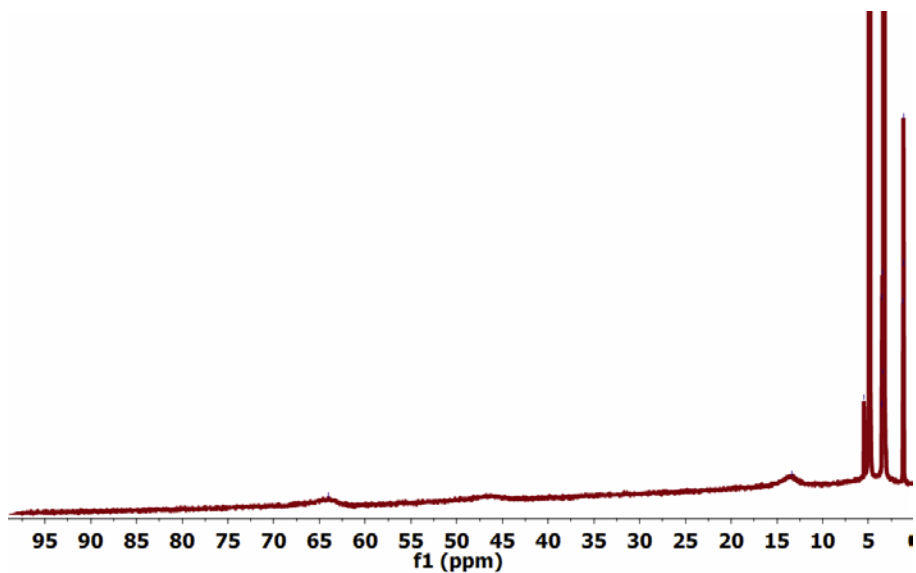


Figure AII.3. ^1H NMR spectrum of $[\text{Co}^{\text{II}}_2(\text{L}^1\text{SSL}^1)(\text{PO}_2\text{F}_2)_2](\text{PF}_6)_2$ in methanol- d_4 .

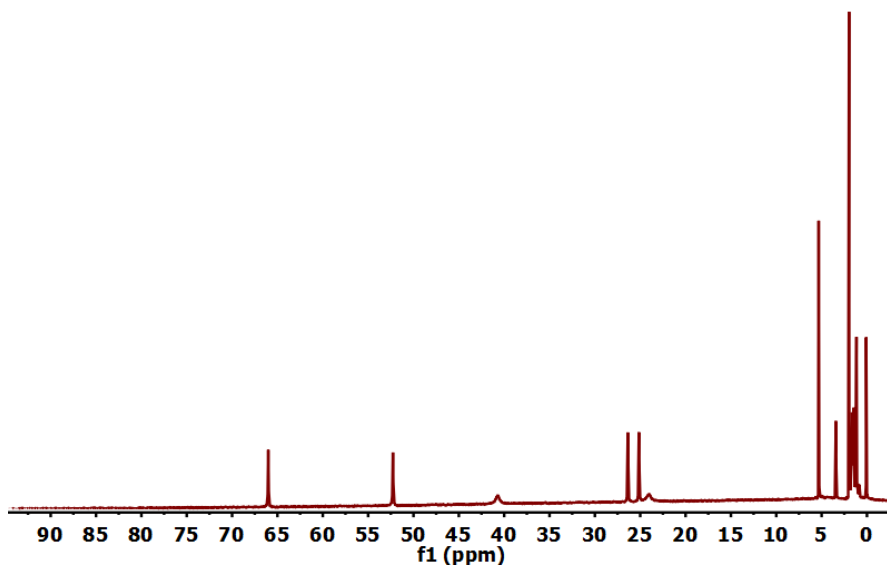


Figure AII.4. ^1H NMR spectrum of $[\text{Co}^{\text{II}}_2(\text{L}^1\text{SSL}^1)(\text{PO}_2\text{F}_2)_2](\text{PF}_6)_2$ in dichloromethane- d_2 .

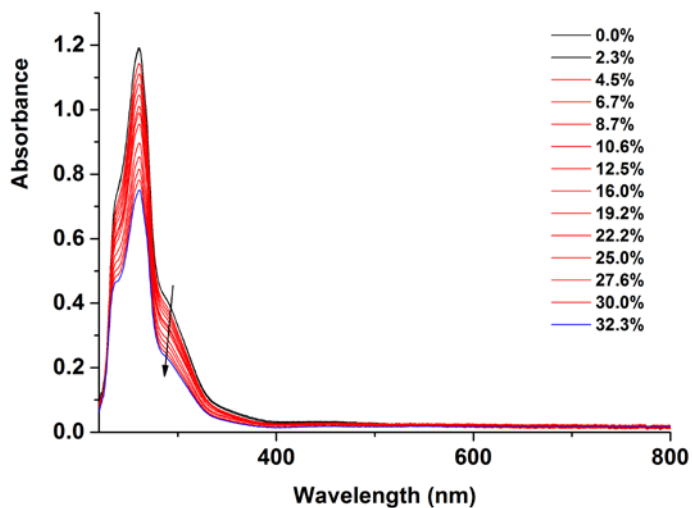


Figure AII 5. UV-vis spectra of $[\text{Co}^{\text{II}}_2(\text{L}^1\text{SSL}^1)(\text{PO}_2\text{F}_2)_2](\text{PF}_6)_2$ dissolved in 4.2 mL acetonitrile with variable amounts of dichloromethane added at 1.1 mM $[\text{Co}]$ concentration recorded with a transmission dip probe at a path length of 1.8 mm.

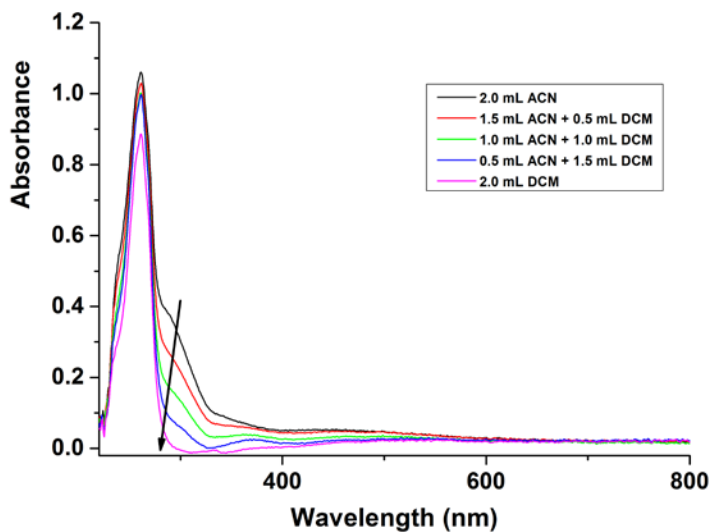


Figure AII.6. UV-vis spectra of the different ratios of acetonitrile and dichloromethane solution of $[\text{Co}^{\text{II}}_2(\text{L}^1\text{SSL}^1)(\text{PO}_2\text{F}_2)_2](\text{PF}_6)_2$ in 10 mL at 1.1 mM $[\text{Co}]$ concentration recorded with a transmission dip probe at a path length of 1.8 mm.

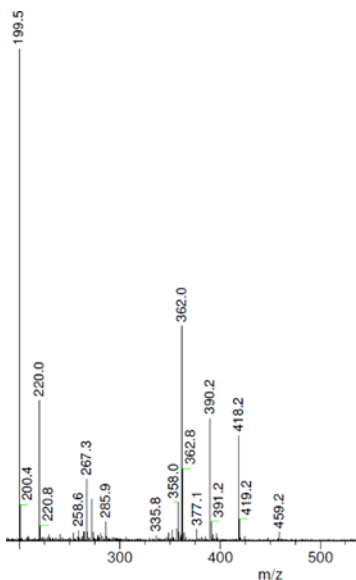


Figure AII.7. ESI-MS spectrum of $[\text{Co}^{\text{II}}_2(\text{L}^1\text{SSL}^1)(\text{PO}_2\text{F}_2)_2](\text{PF}_6)_2$ dissolved in acetonitrile. ESI-MS combined with simulated spectrum found (calcd) for $\frac{1}{2}[\text{Co}(\text{L}^1\text{S}) + 2\text{MeCN}]^{2+}$ m/z 199.5 (195.5); $[\text{Co}(\text{L}^1\text{S}) + \text{PO}_2\text{F}_2]^+$ m/z 418.2 (418.1); $[\text{Co}(\text{L}^1\text{S}) + \text{PO}_2\text{F}_2 + \text{MeCN}]^+$ 459.2 (459.1).

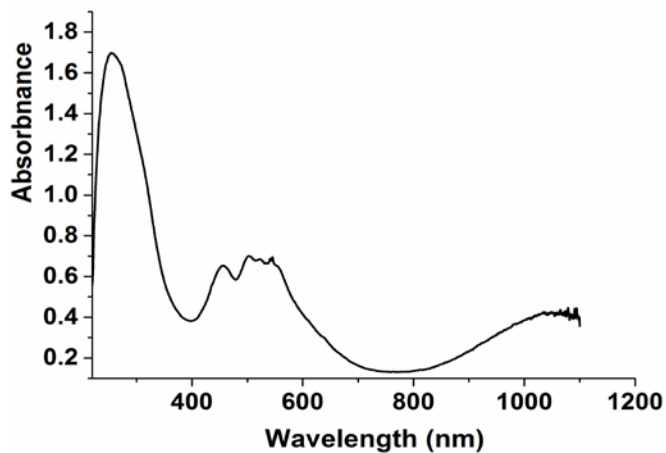


Figure AII.8. UV-vis spectrum for the solid sample of $[\text{Co}^{\text{II}}_2(\text{L}^1\text{SSL}^1)(\text{PO}_2\text{F}_2)_2](\text{PF}_6)_2$ obtained from a dichloromethane solution.

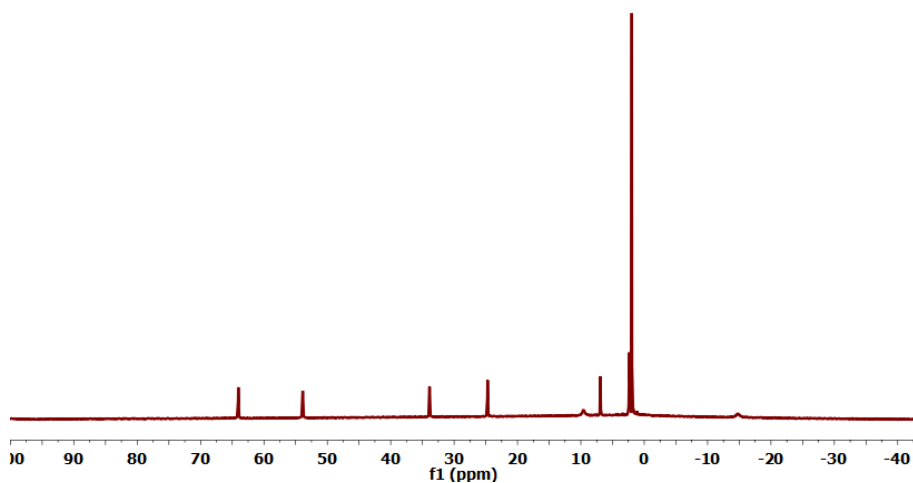


Figure AII.9. ^1H NMR spectrum of the compound $[\text{Co}^{\text{II}}_2(\text{L}^7\text{SSL}^7)(\text{PO}_2\text{F}_2)_2](\text{PF}_6)_2$ in acetonitrile- d_3 .

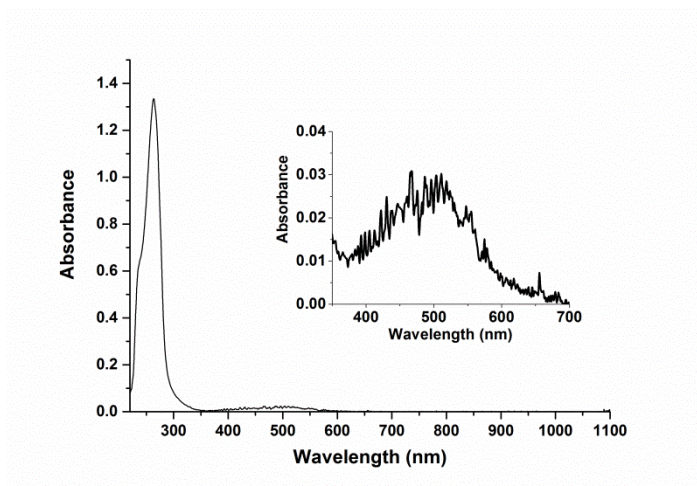


Figure AII.10. UV-vis spectrum of the compound $[\text{Co}^{\text{II}}_2(\text{L}^7\text{SSL}^7)(\text{PO}_2\text{F}_2)_2](\text{PF}_6)_2$ in acetonitrile. UV-vis spectra in solution were recorded using a solution 2 mM in $[\text{Co}]$ with a transmission dip probe path length of 1.2 mm. The inset shows the solution 4 mM in $[\text{Co}]$.

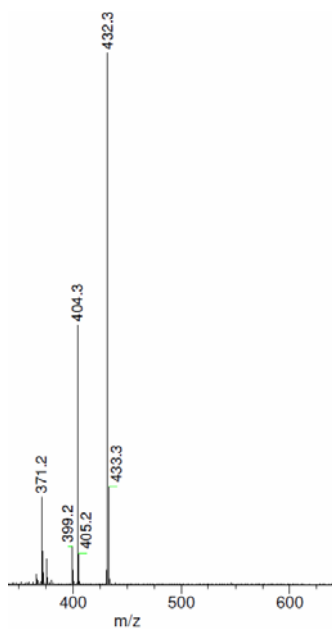


Figure AII.11. ESI-MS spectrum of $[\text{Co}^{\text{II}}_2(\text{L}^7\text{SSL}^7)(\text{PO}_2\text{F}_2)_2](\text{PF}_6)_2$ dissolved in acetonitrile. ESI-MS found (calcd) for $[\text{Co}^{\text{II}}_2(\text{L}^7\text{SSL}^7)(\text{PO}_2\text{F}_2)_2]^{2+}$ m/z 432.3 (432.1).

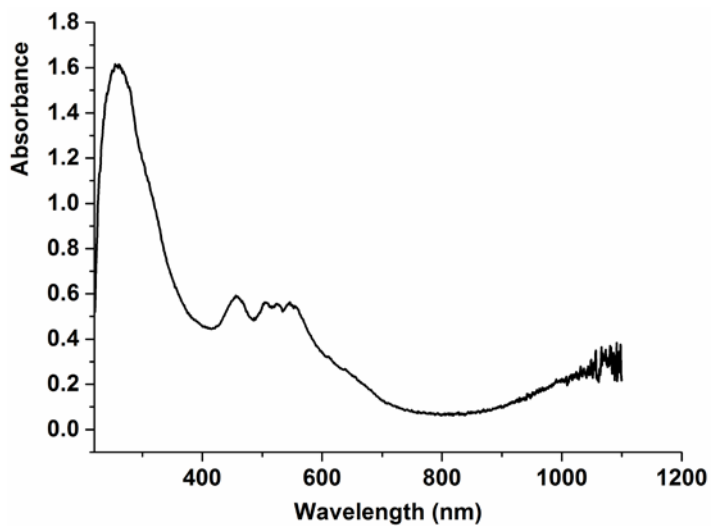


Figure AII.12. UV-vis spectrum for the solid sample of $[\text{Co}^{\text{II}}_2(\text{L}^7\text{SSL}^7)(\text{PO}_2\text{F}_2)_2](\text{PF}_6)_2$.

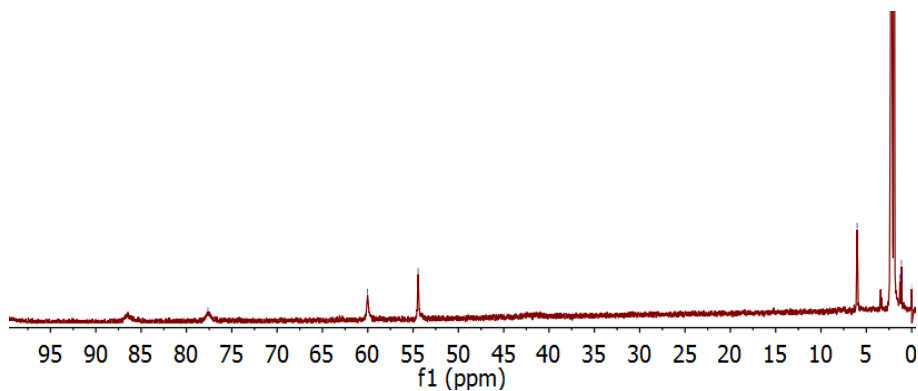


Figure AII.13. ^1H NMR spectrum of compound $[\text{Co}^{\text{II}}_2(\text{L}^1\text{SSL}^1)(\text{NO}_3)_4]$ dissolved in acetonitrile- d_3 .

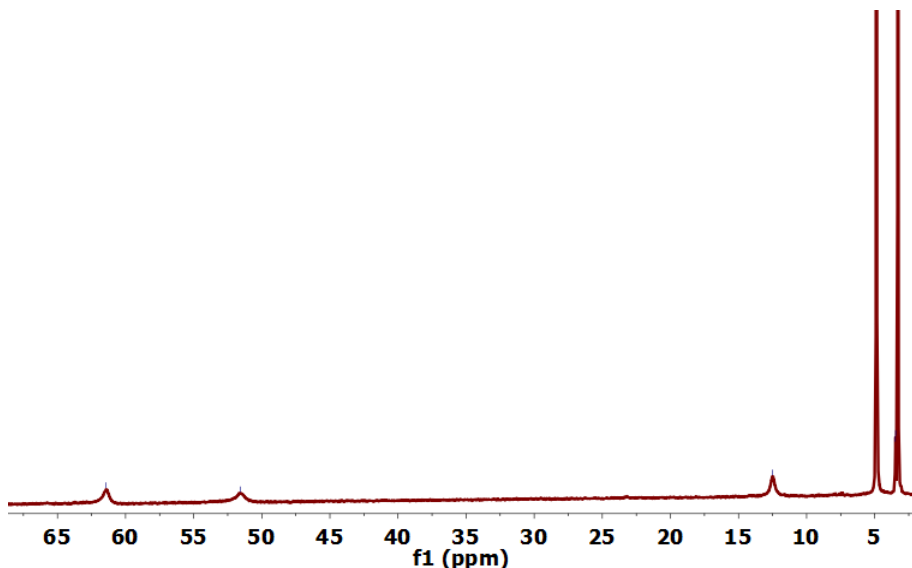


Figure AII.14. ^1H NMR spectrum of compound $[\text{Co}^{\text{II}}_2(\text{L}^1\text{SSL}^1)(\text{NO}_3)_4]$ dissolved in methanol- d_4 .

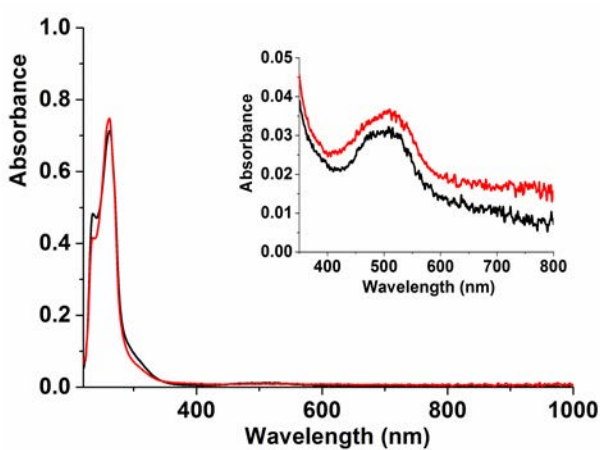


Figure AII.15. UV-vis spectra of the compound $[\text{Co}^{\text{II}}_2(\text{L}^1\text{SSL}^1)(\text{NO}_3)_4]$ in methanol (red line) and in acetonitrile (black line). UV-vis spectra were recorded using solutions 1 mM in $[\text{Co}]$ with a transmission dip probe path length of 1.4 mm. The inset shows the UV-vis spectra of 2 mM $[\text{Co}]$ in acetonitrile (black) with a path length of 1.4 mm and 2 mM $[\text{Co}]$ in methanol (red) with a path length of 1.8 mm.

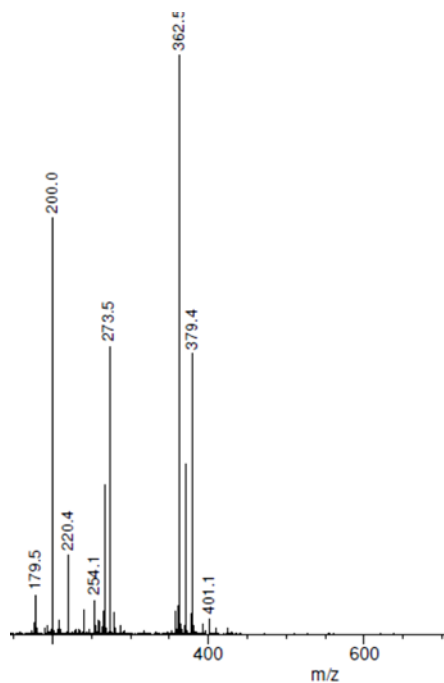


Figure AII.16. ESI-MS spectrum of the compound $[\text{Co}^{\text{II}}_2(\text{L}^1\text{SSL}^1)(\text{NO}_3)_4]$ in acetonitrile, ESI-MS found (calcd) for $\frac{1}{2} [\text{M} - 2 \text{NO}_3]^{2+}$ m/z 379.4 (379.3); $\frac{1}{2} [\text{M} - 4 \text{NO}_3 + 2\text{HCO}_2]^{2+}$ m/z 362.5 (362.1).

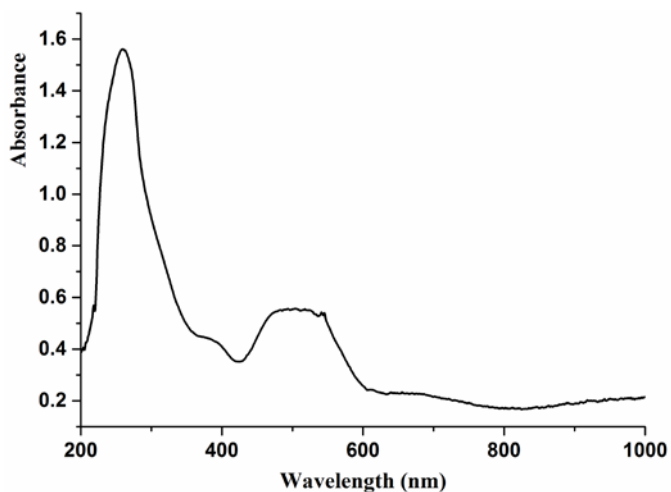


Figure AII.17. UV-vis spectrum of the compound $[\text{Co}^{\text{II}}_2(\text{L}^1\text{SSL}^1)(\text{NO}_3)_4]$ in the solid state.

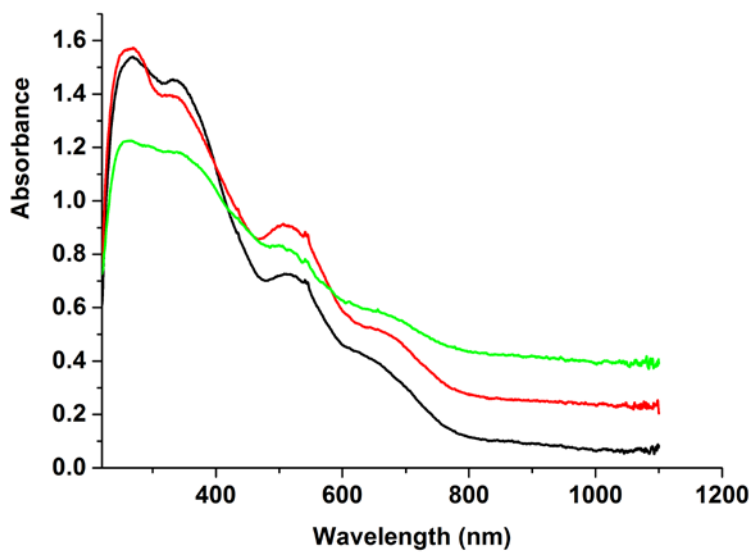


Figure AII.18. UV-vis spectra of the compound $[\text{Co}^{\text{III}}(\text{L}^1\text{S})(\text{NCS})_2]$ in the solid state obtained from acetonitrile (black line), methanol (red line), and acetone (green line).

Appendix III

Supplementary information on Chapter 4

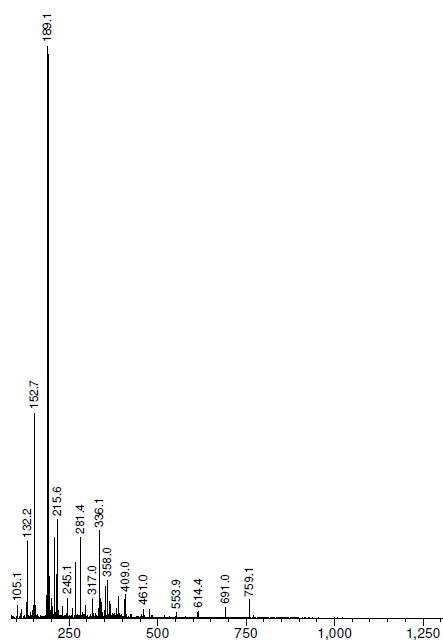


Figure AIII.1. ESI-MS spectrum of the Fe(III) compound **2** dissolved in methanol. ESI-MS found (calcd) for $\frac{1}{2}[\text{Fe}(\text{L}^1\text{SO}_3)(\text{H}_2\text{O})]^{2+}$ m/z 189.2 (190.0).

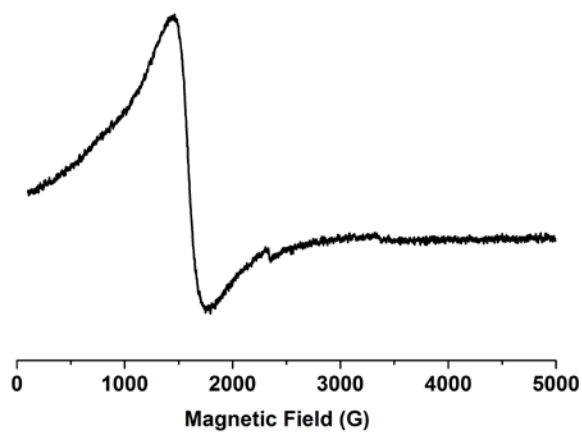


Figure AIII.2. EPR spectrum of the compound **2** dissolved in DMSO. The experiment was performed at 20 K.

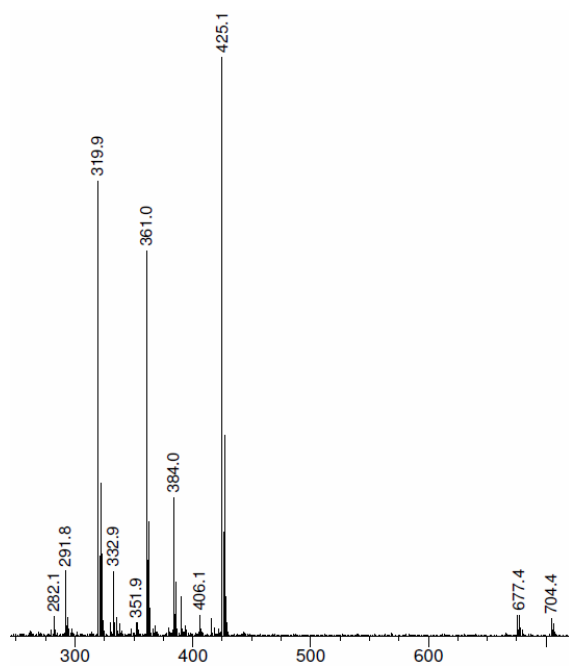


Figure AIII.3. ESI-MS spectrum of the Co(III) compound **4** dissolved in acetonitrile. ESI-MS found (calcd) for $[\text{Co}^{\text{III}}(\text{L}^1\text{SO}_2)\text{Cl}]^+$ m/z 384.4 (384.0); $[\text{Co}^{\text{III}}(\text{L}^1\text{SO}_2)\text{Cl} + \text{MeCN}]^+$ m/z 425.5 (425.1).

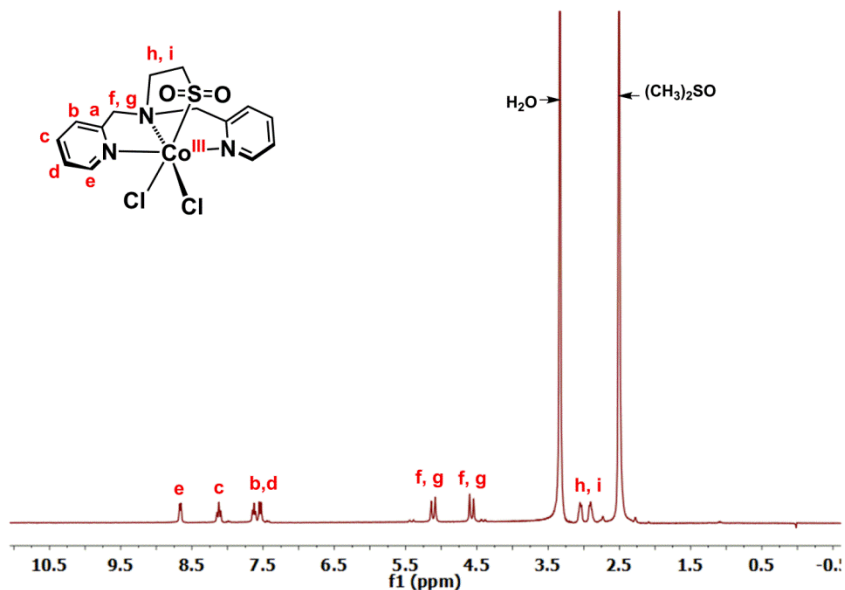


Figure AIII.4. NMR spectrum of compound **4** dissolved in DMSO- d_6 .

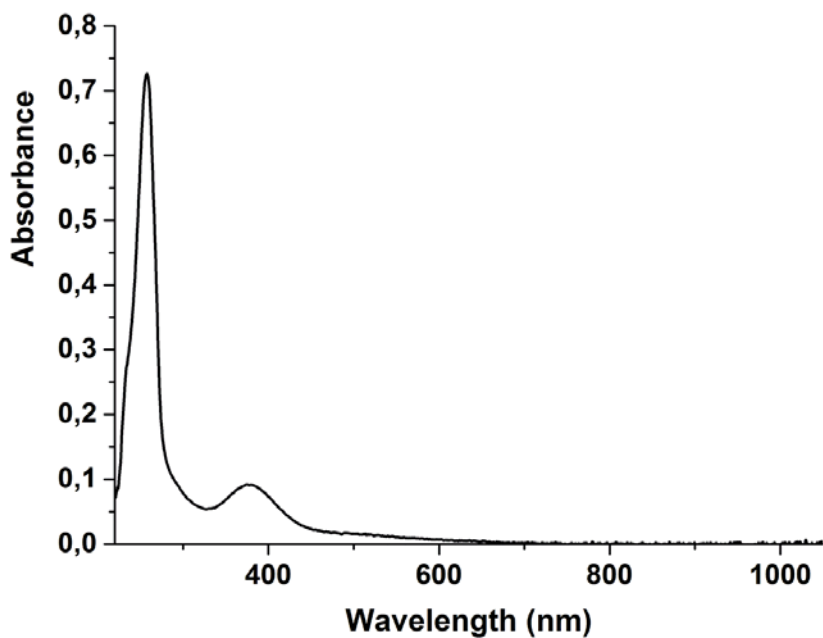


Figure AIII.5. UV-vis spectrum of compound **2** dissolved in methanol. UV-Vis spectra in solution were recorded using a solution 1 mM in [Fe] with a transmission dip probe path length of 1.8 mm.

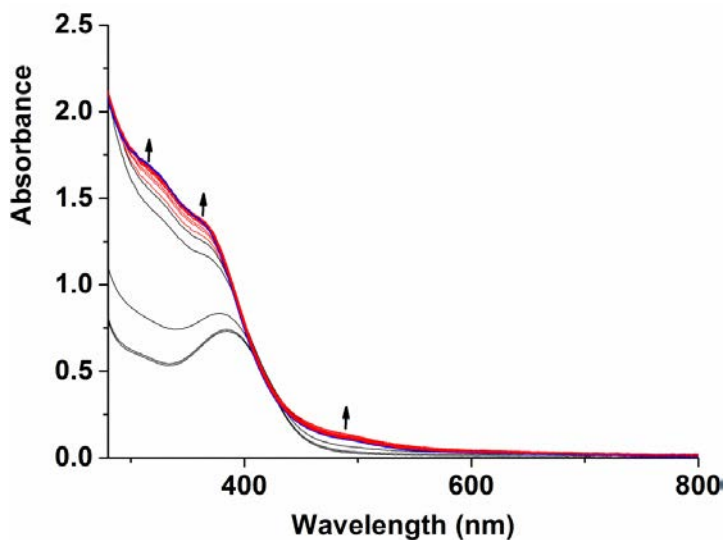


Figure AIII.6. The change of UV-vis spectra upon addition of H_2O_2 (0.2 mmol, 40 equivalents to the compound **1**) to compound **1** in methanolic solution in the first two minutes under room temperature. UV-vis spectra were recorded using a solution 2 mM in $[\text{Fe}]$ (5 mL) with a transmission dip probe path length of 2.8 mm. Spectra recorded every 1 second over a period of 5 minutes.

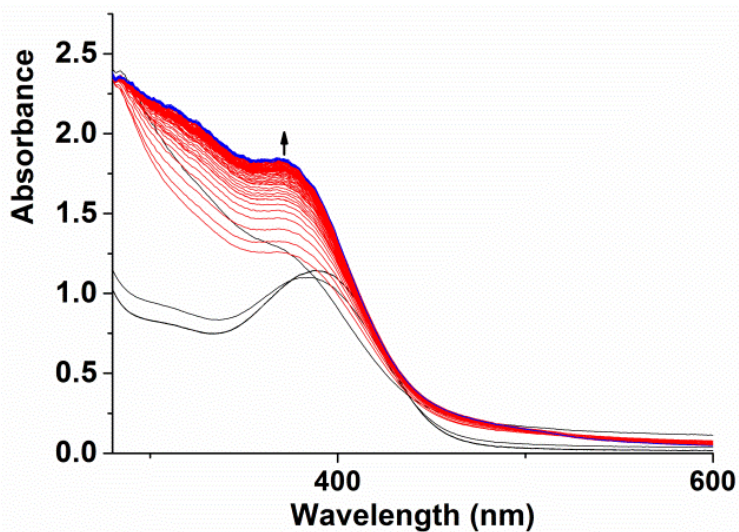


Figure AIII.7. The change of UV-vis spectra upon addition of H_2O_2 (0.8 mmol, 80 equivalents to the compound **1**) to compound **1** in methanolic solution in the first two minutes under room temperature. UV-vis spectra were recorded using a solution 4 mM in $[\text{Fe}]$ (5 mL) with a transmission dip probe path length of 2.8 mm. Spectra recorded every 1 second over a period of 3 minutes.

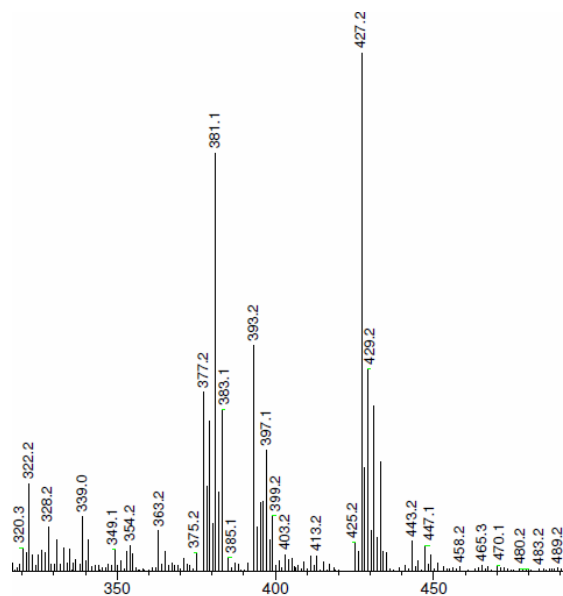


Figure AIII.8. ESI-MS spectrum of reaction mixture of the compound **1** with excess 35% H_2O_2 (80 equivalents to the compound **1**) in methanol at -78°C . ESI-MS found (calcd) for $[\text{Fe}^{\text{III}}(\text{L}^1\text{SO}_2)\text{Cl}]^+$ m/z 381.1 (381.0); $[\text{Fe}^{\text{III}}(\text{L}^1\text{SO}_3)\text{Cl}]^+$ m/z 397.1 (397.0), $[\text{Fe}^{\text{III}}(\text{L}^1\text{SO}_3)\text{Cl} + \text{CH}_3\text{OH}]^+$ m/z 429.2 (429.1).

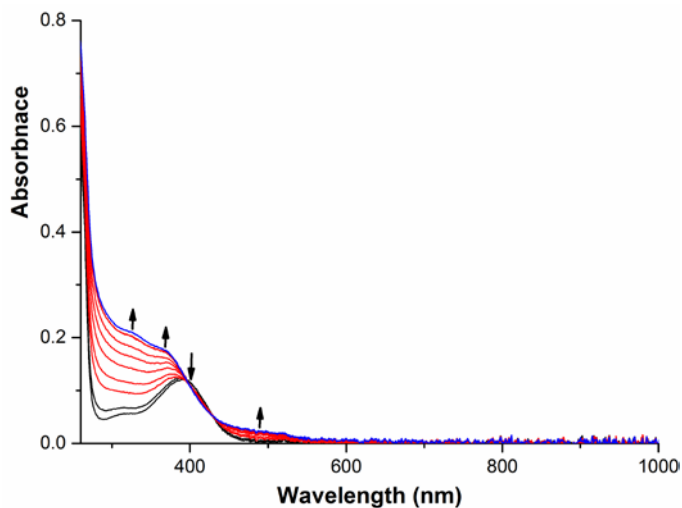


Figure AIII.9. The change in UV-vis when H_2O_2 (5 μL /each time) was titrated into a solution of compound **1** in methanol at room temperature. UV-vis spectra were recorded using a solution 2 mM in $[\text{Fe}]$ (10 mL) with a transmission dip probe path length of 0.9 mm.

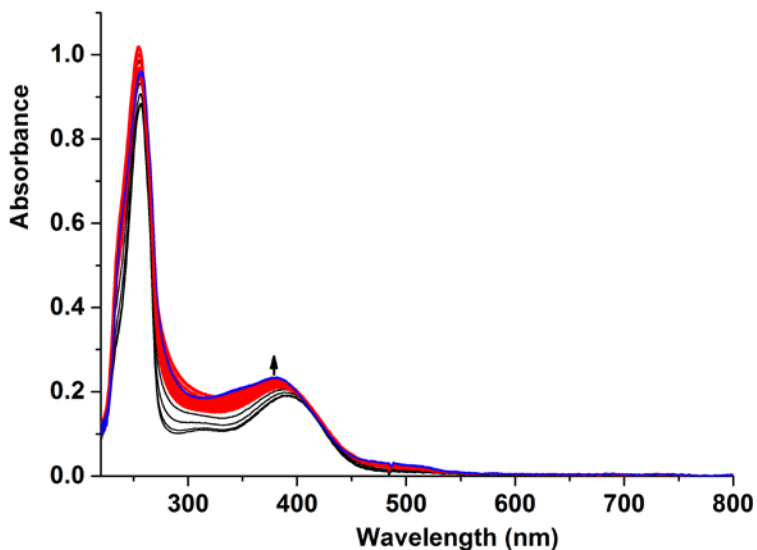


Figure AIII.10. The change of UV-vis spectral when $t\text{-BuOOH}$ (0.2 mmol, 40 equivalents to the compound **1**) was added to compound **1** dissolved in methanol. UV-vis spectra were recorded using a solution 2 mM in $[\text{Fe}]$ (5 mL) with a transmission dip probe path length of 0.9 mm at $-41\text{ }^{\circ}\text{C}$. Spectra recorded every 30 seconds over a period of 3 minutes, and then recorded every 3 seconds over a period of 20 minutes.

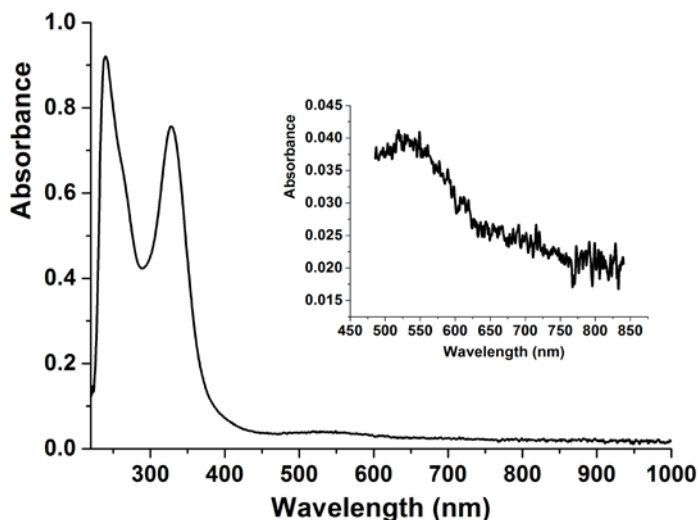


Figure AIII.11. UV-vis spectrum of compound **4** dissolved in acetonitrile. The UV-vis spectrum was recorded using the solution 1 mM in $[\text{Co}]$ with a transmission dip probe path length of 1.6 mm at room temperature. The inset shows the amplified part of UV-vis spectra from 450 nm to 850 nm.

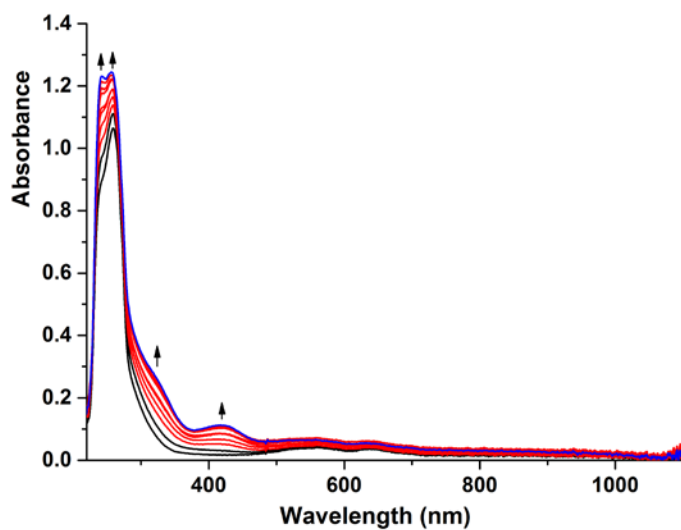


Figure AIII.12. The change in UV-vis spectra when H_2O_2 ($5 \mu\text{L}$ /each time) was titrated into a solution of compound **3** in acetonitrile at room temperature. UV-vis spectra were recorded using a solution 2 mM in $[\text{Co}]$ (10 mL) with a transmission dip probe path length of 1.3 mm .

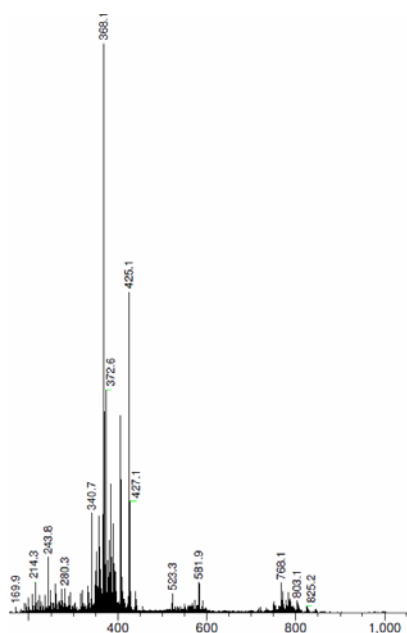


Figure AIII.13. ESI-MS spectrum of the reaction mixture of **3** with H_2O_2 after the first one hour. ESI-MS found (calcd) for $[\text{Co}^{\text{III}}(\text{L}^1\text{SO})\text{Cl}]^+$ m/z 368.0; $[\text{Co}^{\text{III}}(\text{L}^1\text{SO}_2)\text{Cl} + \text{MeCN}]^+$ m/z 425.0).

Table AIII.1. Crystallographic and structures refinement data for compounds **2** and **4**.

	2	4
Chemical formula	2(C ₁₄ H ₁₆ Cl ₂ FeN ₃ O ₃ S)·C ₃ H ₇ NO	C ₁₄ H ₁₆ Cl ₂ CoN ₃ O ₂ S·3(H ₂ O)
Formula Weight	939.31	474.23
Crystal System	monoclinic	monoclinic
Space Group	<i>P2₁/c</i>	<i>P2₁/n</i>
<i>a</i> (Å)	14.059(4)	8.3845(3)
<i>b</i> (Å)	22.0371(6)	14.5303(4)
<i>c</i> (Å)	12.5600 (3)	15.1848(5)
α (°)	90	90
β (°)	100.192(2)	91.740(3)
γ (°)	90	90
<i>V</i> (Å ³)	3829.96(18)	1849.10(10)
<i>Z</i>	4	4
<i>D</i> _{calc} (g.cm ³)	1.629	1.703
<i>T</i> _{min} – <i>T</i> _{max}	0.449, 1.000	0.642, 1.000
Crystal Size(mm)	0.60 x 0.28 x 0.10	0.36 x 0.21 0.12
μ (mm ⁻¹)	1.201	1.362
No. of Reflections	35704	14470
No. of unique reflections	8788	4242
No. of reflections observed [<i>I</i> > 2 σ (<i>I</i>)]	7513	3698
No. of parameters	480	260
R1/WR2 [<i>I</i> > 2 σ (<i>I</i>)]	0.0301, 0.0650	0.0288, 0.0699
R1/WR2 [all reflections]	0.0390, 0.0696	0.0346, 0.0736
Goodness of fit (GOF)	1.063	1.045
Residual electron density (e Å ⁻³)	0.49/-0.40	0.49/-0.37

Appendix IV

Supplementary information on Chapter 5

Table AIV.1. Crystallographic and structure refinement data for complex $[\text{Fe}^{\text{II}}_4(\text{L}^1\text{SSL}^1)_2\text{F}_6(\text{MeCN})_2](\text{BF}_4)_2$.

$[\text{Fe}^{\text{II}}_4(\text{L}^1\text{SSL}^1)_2\text{F}_6(\text{MeCN})_2](\text{BF}_4)_2$	
chemical formula	$\text{C}_{60}\text{H}_{70}\text{F}_6\text{Fe}_4\text{N}_{14}\text{S}_4 \cdot 4(\text{BF}_4)$
M_r	1800.18
crystal system, space group	Monoclinic, $C2/c$
Temperature (K)	110
a, b, c (Å)	15.0882(6), 19.6485(8), 25.1426(9)
β (°)	101.306(4)
V (Å ³)	7309.1(5)
Z	4
Radiation type	Mo $K\alpha$
μ (mm ⁻¹)	1.00
Crystal size (mm)	$0.21 \times 0.20 \times 0.08$
Diffractometer	SuperNova, Dual, Cu at zero, Atlas diffractometer
T_{\min}, T_{\max}	0.852, 0.944
No. of measured, independent and observed [$I > 2\sigma(I)$] reflections	28835, 8397, 6664
R_{int}	0.034
$(\sin \theta/\lambda)_{\text{max}}$ (Å ⁻¹)	0.650
$R[F^2 > 2\sigma(F^2)], wR(F^2), S$	0.042, 0.107, 1.04
No. of reflections	8397
No. of parameters	909
No. of restraints	1943
	$w = 1/[\sigma^2(F_o^2) + (0.0439P)^2 + 14.6984P]$
	where $P = (F_o^2 + 2F_c^2)/3$
$\Delta\rho_{\text{max}}, \Delta\rho_{\text{min}}$ (e Å ⁻³)	0.77, -0.53

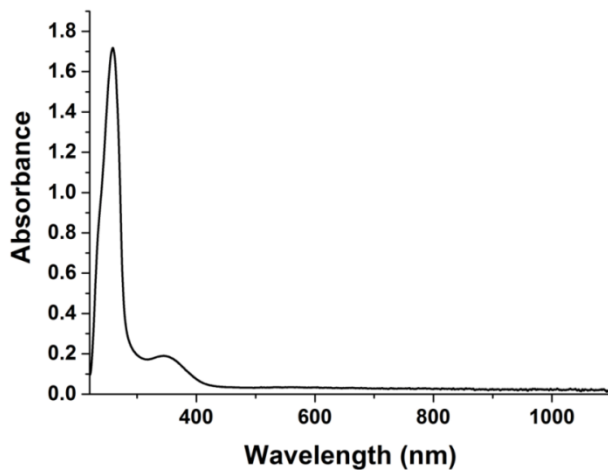


Figure AIV.1. UV-vis spectrum of the complex $[\text{Fe}^{\text{II}}_4(\text{L}^1\text{SSL}^1)_2\text{F}_6(\text{MeCN})_2](\text{BF}_4)_2$ in acetonitrile at room temperature. 1 mM [Fe] with a transmission dip probe path length of 0.31 cm.

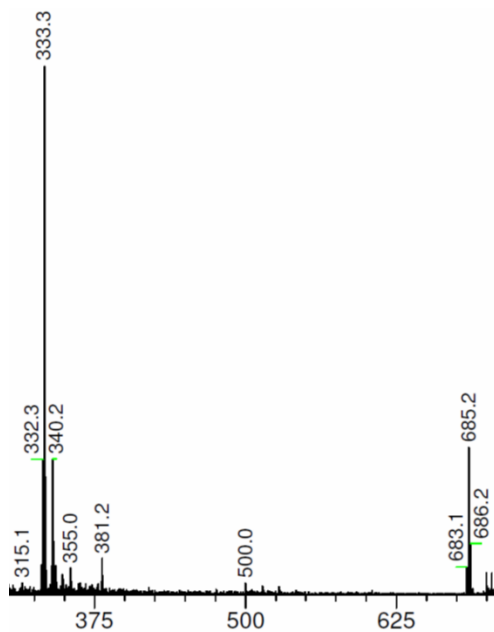


Figure AIV.2. ESI-MS spectrum of compound $[\text{Fe}^{\text{II}}_4(\text{L}^1\text{SSL}^1)_2\text{F}_6(\text{MeCN})_2](\text{BF}_4)_2$ in acetonitrile.

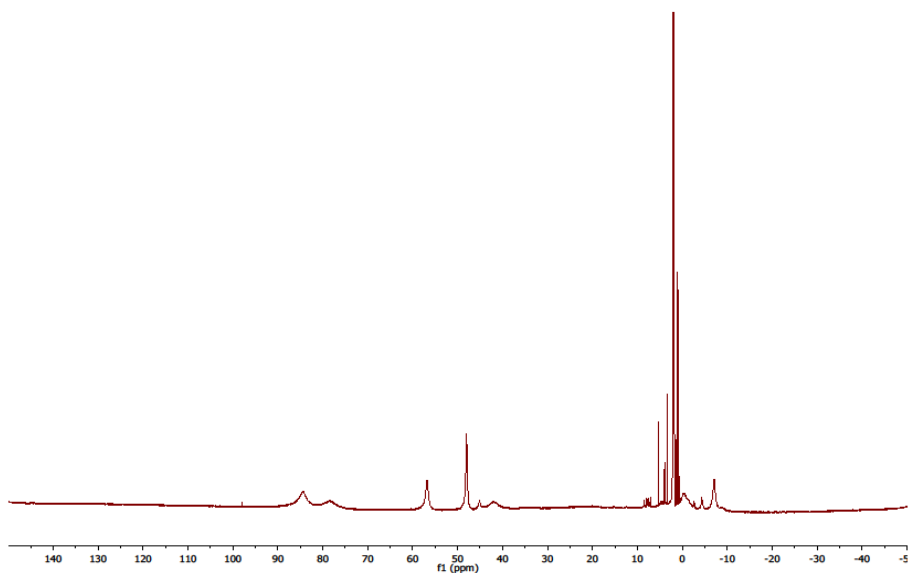


Figure AIV.3. ^1H NMR spectrum of the complex $[\text{Fe}^{\text{II}}_4(\text{L}^1\text{SSL}^1)_2\text{F}_6(\text{MeCN})_2](\text{BF}_4)_2$ in acetonitrile- d_3 at room temperature.

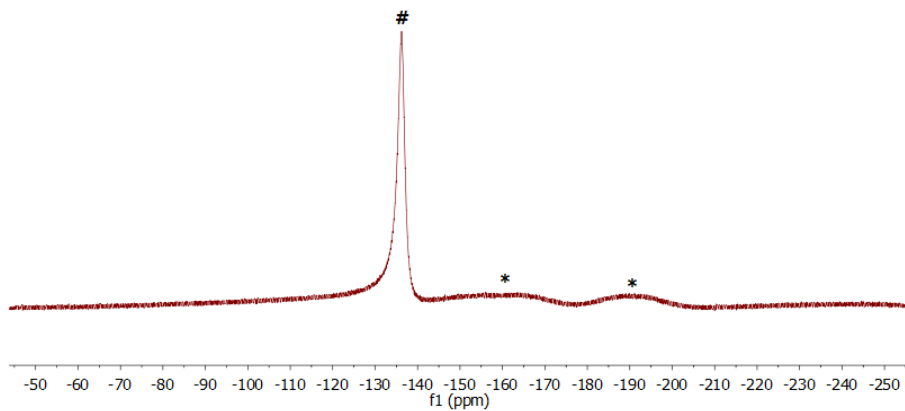


Figure AIV.4. ^{19}F NMR spectrum of complex $[\text{Fe}^{\text{II}}_4(\text{L}^1\text{SSL}^1)_2\text{F}_6(\text{MeCN})_2](\text{BF}_4)_2$ in acetonitrile- d_3 at room temperature.

Appendix V

Supplementary information on Chapter 6

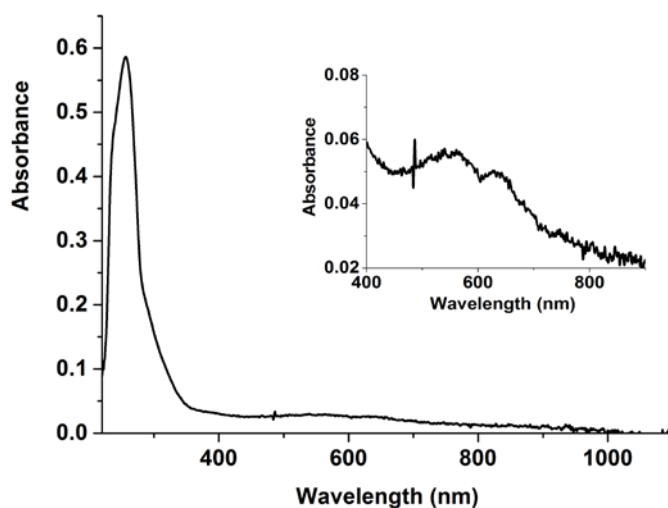


Figure AV.1. UV-vis spectrum of the compound [Co^{II}(L¹SCH₃)Cl₂] dissolved in acetonitrile, recorded using solution 1 mM in [Co] with a transmission dip probe path length of 1.3 mm. The inset shows the UV-vis spectrum recorded of a solution 2 mM in [Co].

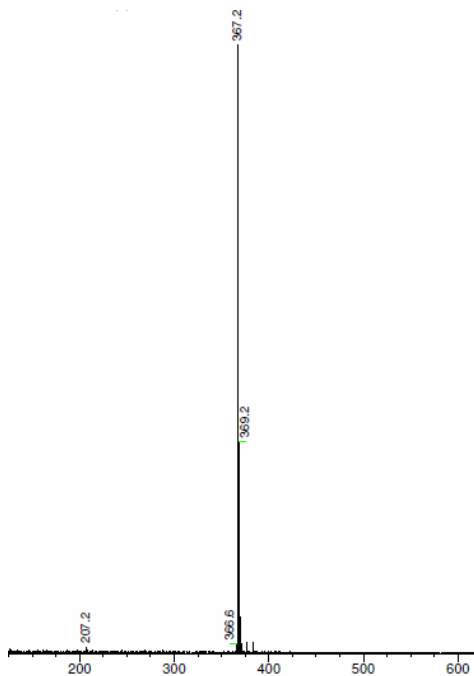


Figure AV.2. ESI-MS spectrum of the compound $[\text{Co}^{\text{II}}(\text{L}^1\text{SCH}_3)\text{Cl}_2]$ dissolved in acetonitrile. ESI-MS found (calcd) for $[\text{M}-\text{Cl}]^+$ m/z 367.2 (367.1).

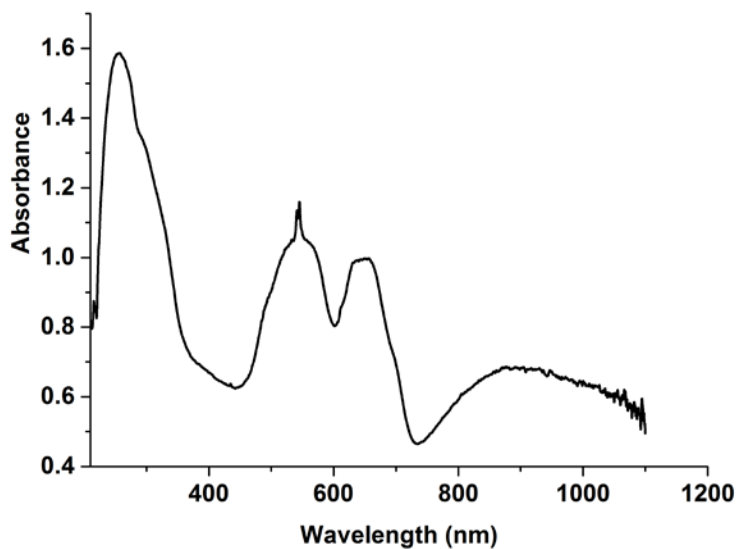


Figure AV.3. UV-vis spectrum of the compound $[\text{Co}^{\text{II}}(\text{L}^1\text{SCH}_3)\text{Cl}_2]$ in the solid state.

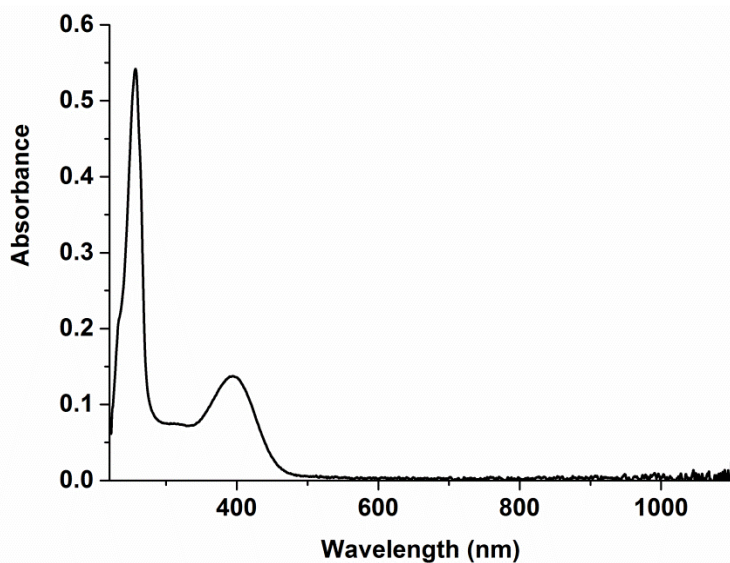


Figure AV.4. UV-vis spectrum of the compound $[\text{Fe}^{\text{II}}(\text{L}^1\text{SCH}_3)\text{Cl}_2]$ dissolved in methanol, recorded using a solution 1 mM in $[\text{Fe}]$ with a transmission dip probe path length of 1.3 mm.

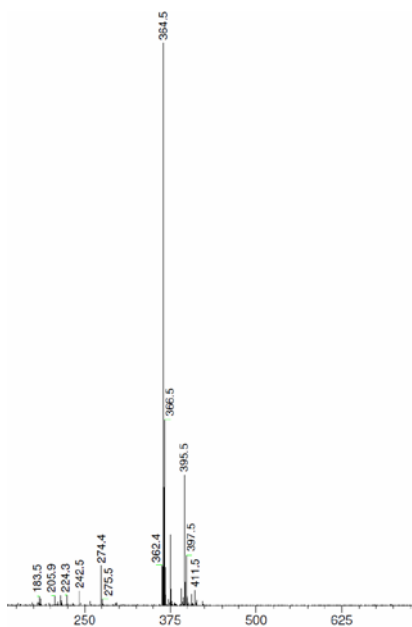


Figure AV.5. ESI-MS spectrum of the compound $[\text{Fe}^{\text{II}}(\text{L}^1\text{SCH}_3)\text{Cl}_2]$ dissolved in methanol. ESI-MS found (calcd) for $[\text{M}-\text{Cl}]^+$ m/z 364.5 (364.1).

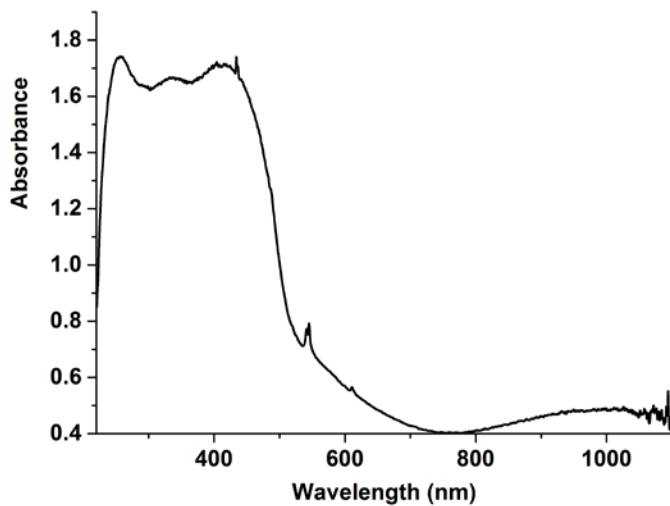


Figure AV.6. UV-vis spectrum of the compound $[\text{Fe}^{\text{II}}(\text{L}^1\text{SCH}_3)\text{Cl}_2]$ in the solid state.

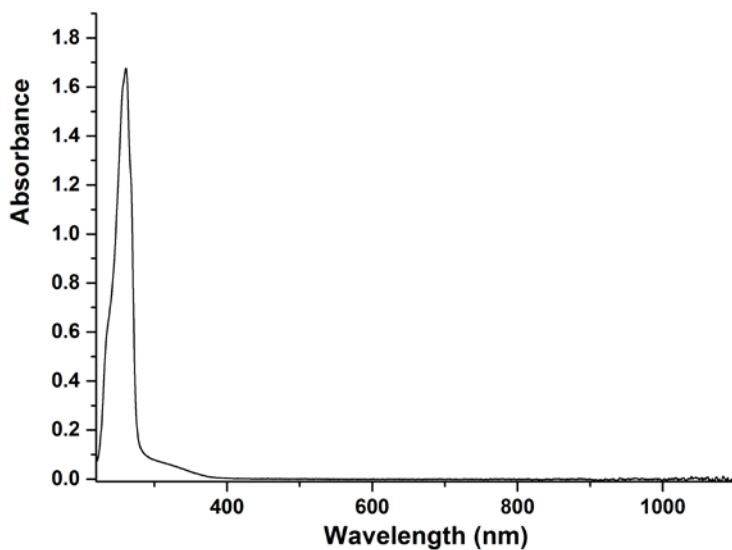


Figure AV.7. UV-vis spectrum of the compound $[\text{Mn}^{\text{II}}(\text{L}^1\text{SCH}_3)\text{Cl}_2]$ dissolved in acetonitrile, recorded using a solution 1 mM in $[\text{Mn}]$ with a transmission dip probe path length of 1.2 mm.

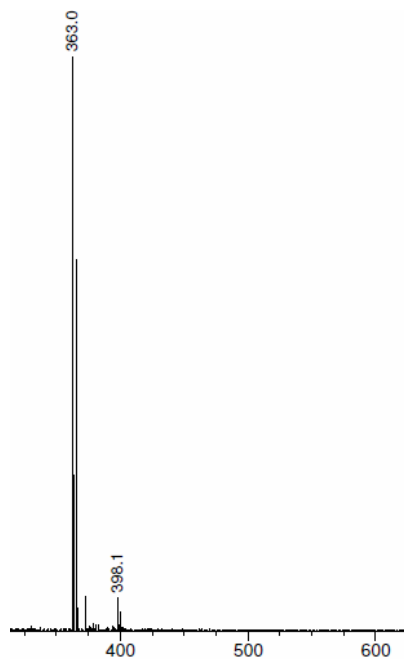


Figure AV.8. ESI-MS spectrum of the compound $[\text{Mn}^{\text{II}}(\text{L}^1\text{SCH}_3)\text{Cl}_2]$ in the methanol. ESI-MS found (calcd) for $[\text{M}-\text{Cl}]^+ m/z$ 363.0 (363.1).

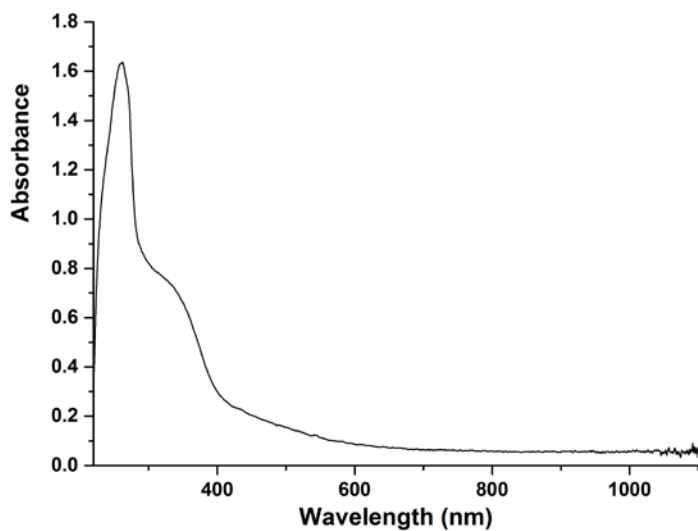


Figure AV.9. UV-vis spectrum of the compound $[\text{Mn}^{\text{II}}(\text{L}^1\text{SCH}_3)\text{Cl}_2]$ in the solid state.

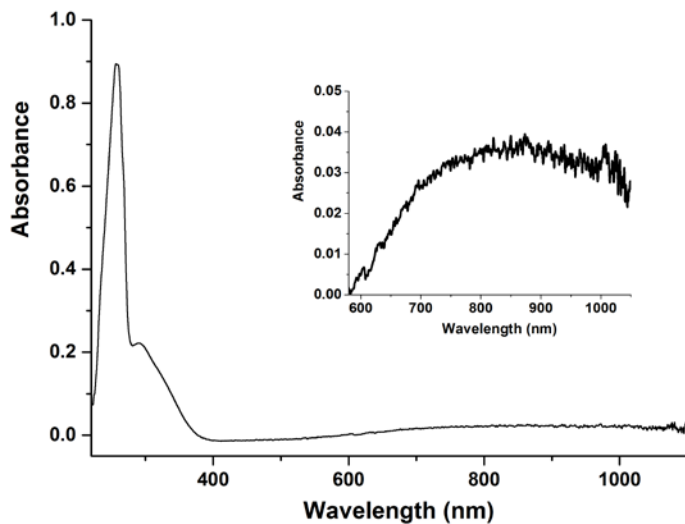


Figure AV.10. UV-vis spectrum of the compound $[\text{Cu}^{\text{II}}(\text{L}^1\text{SCH}_3)\text{Cl}_2]$ dissolved in acetonitrile, recorded using a solution 1 mM in $[\text{Cu}]$ with a transmission dip probe path length of 1.2 mm. The inset shows the UV-vis spectrum of a solution 2 mM in $[\text{Cu}]$.

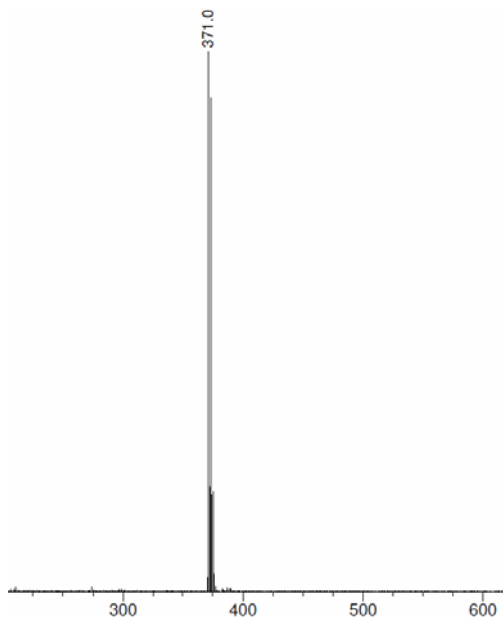


Figure AV.11. ESI-MS spectrum of the compound $[\text{Cu}^{\text{II}}(\text{L}^1\text{SCH}_3)\text{Cl}_2]$ in the methanol. ESI-MS found (calcd) for $[\text{M}-\text{Cl}]^+$ m/z 371.0 (371.0).

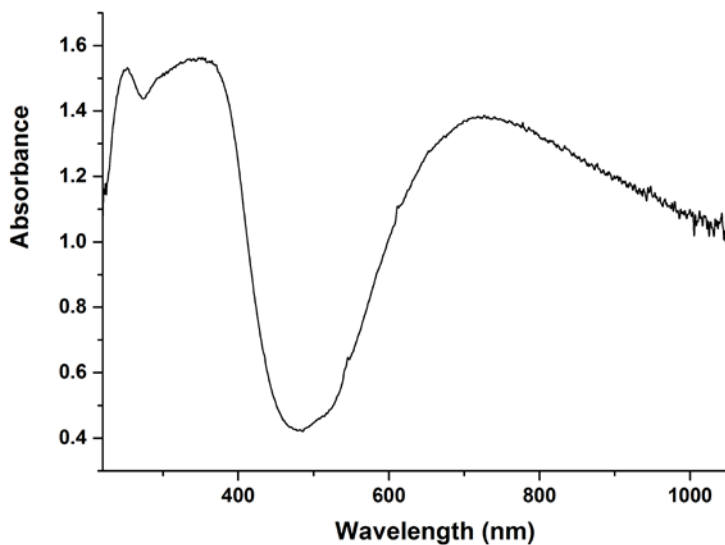


Figure AV.12. UV-vis spectrum of the compound $[\text{Cu}^{\text{II}}(\text{L}^1\text{SCH}_3)\text{Cl}_2]$ in the solid state.

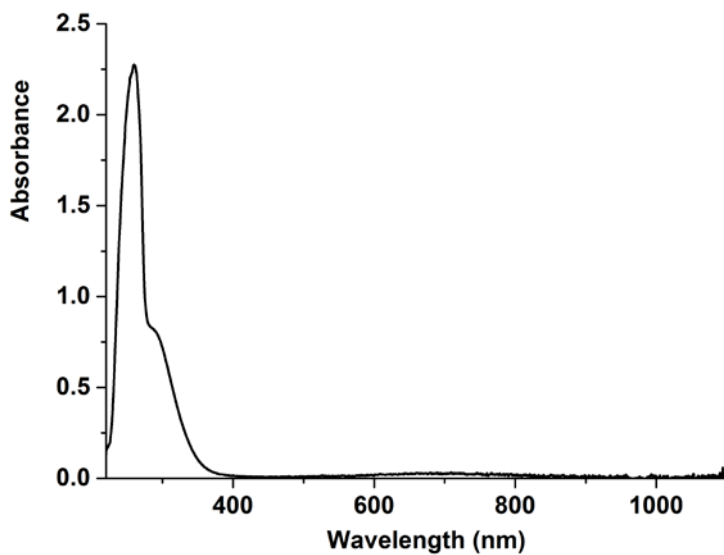


Figure AV.13. UV-vis spectrum of the compound $[\text{Cu}^{\text{II}}_2(\text{L}^1\text{SSL}^1)\text{Cl}_4]$ dissolved in methanol, recorded using a solution 5 mM in $[\text{Cu}]$ with a transmission dip probe path length of 0.9 mm.

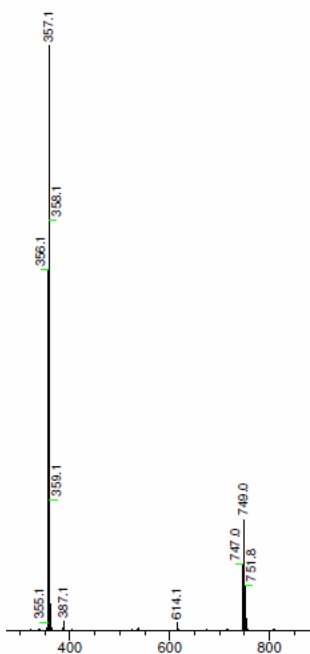


Figure AV.14. ESI-MS spectrum of the compound $[\text{Cu}^{\text{II}}(\text{L}^1\text{SSL}^1)\text{Cl}_4]$ dissolved in methanol. ESI-MS found (calcd) for $\frac{1}{2} [\text{Cu}^{\text{II}}(\text{L}^1\text{SSL}^1)\text{Cl}_4-2\text{Cl}]^+$ m/z 357.1 (357.4), $[\text{Cu}^{\text{II}}(\text{L}^1\text{SSL}^1)\text{Cl}_4-\text{Cl}]^+$; m/z 747.0 (747.0).

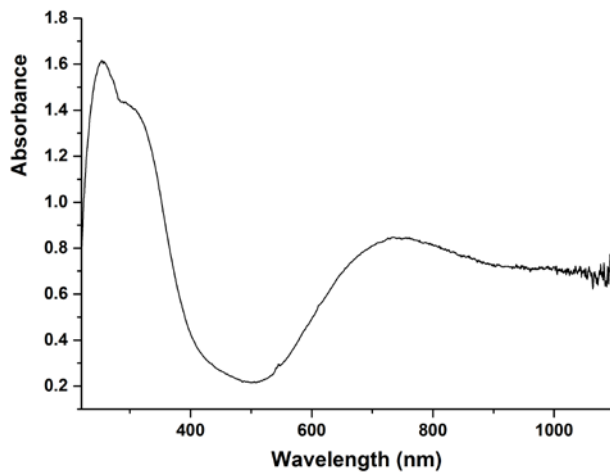


Figure AV.15. UV-vis spectrum of the compound $[\text{Cu}^{\text{II}}(\text{L}^1\text{SSL}^1)\text{Cl}_4]$ in the solid state.

Table AV.1. Crystallographic and structure refinement data of compounds [Co^{II}(L¹SCH₃)Cl₂], [Fe^{II}(L¹SCH₃)Cl₂] and [Mn^{II}(L¹SCH₃)Cl₂].

	[Co ^{II} (L ¹ SCH ₃)Cl ₂]	[Fe ^{II} (L ¹ SCH ₃)Cl ₂]	[Mn ^{II} (L ¹ SCH ₃)Cl ₂]
Chemical formula	C ₁₅ H ₁₉ Cl ₂ CoN ₃ S	C ₁₅ H ₁₉ Cl ₂ FeN ₃ S	C ₁₅ H ₁₉ Cl ₂ MnN ₃ S
M_r	403.22	400.14	399.23
Crystal system, space group	Monoclinic, <i>Cc</i>	Monoclinic, <i>P2₁/c</i>	Monoclinic, <i>P2₁/c</i>
Temperature (K)	110	110	110
a, b, c (Å)	11.2309 (3), 11.5965 (3), 13.6869 (3)	13.9394 (4), 8.3480 (2), 14.9559 (5)	14.0971 (3), 8.41155 (19), 14.9411 (3)
β (°)	101.207 (3)	90.723 (3)	91.435 (2)
V (Å ³)	1748.58 (8)	1740.22 (9)	1771.14 (7)
Z	4	4	4
Radiation type	Mo $K\alpha$	Mo $K\alpha$	Mo $K\alpha$
μ (mm ⁻¹)	1.41	1.29	1.16
Crystal size (mm)	0.35 × 0.18 × 0.15	0.40 × 0.38 × 0.23	0.50 × 0.32 × 0.22
Diffractionmeter	SuperNova, Dual, Cu at zero, Atlas	SuperNova, Dual, Cu at zero, Atlas	SuperNova, Dual, Cu at zero, Atlas
T_{\min}, T_{\max}	0.556, 1.000	0.463, 1.000	0.360, 1.000
No. of measured, independent and observed [$I > 2\sigma(I)$] reflections	13203, 4062, 3977	13654, 3988, 3525	16904, 4064, 3752
R_{int}	0.023	0.030	0.023
$(\sin \theta/\lambda)_{\text{max}}$ (Å ⁻¹)	0.653	0.650	0.650
$R[F^2 > 2\sigma(F^2)], wR(F^2), S$	0.020, 0.044, 1.04	0.029, 0.072, 1.05	0.022, 0.053, 1.03
No. of reflections	4062	3988	4064
No. of parameters	200	200	200
No. of restraints	2	-	-
H-atom treatment	H-atom parameters constrained	H-atom parameters constrained	H-atom parameters constrained
$\Delta\rho_{\text{max}}, \Delta\rho_{\text{min}}$ (e Å ⁻³)	0.23, -0.19	0.56, -0.36	0.30, -0.24
Absolute structure parameter	0.011 (5)	n/a	n/a

Table AV.2. Crystallographic and structure refinement data of compounds $[\text{Cu}^{\text{II}}(\text{L}^1\text{SSL}^1)\text{Cl}_4]$ and $[\text{Cu}^{\text{II}}(\text{L}^1\text{SCH}_3)\text{Cl}_2]$.

	$[\text{Cu}^{\text{II}}(\text{L}^1\text{SSL}^1)\text{Cl}_4]$	$[\text{Cu}^{\text{II}}(\text{L}^1\text{SCH}_3)\text{Cl}_2]$
Chemical formula	$\text{C}_{28}\text{H}_{32}\text{Cl}_4\text{Cu}_2\text{N}_6\text{S}_2$	$\text{C}_{15}\text{H}_{19}\text{Cl}_2\text{CuN}_5\text{S}$
M_r	785.59	407.83
Crystal system, space group	Monoclinic, $P2_1$	Monoclinic, $P2_1/c$
Temperature (K)	110	110
a, b, c (Å)	9.28859 (17), 23.6394 (4), 14.6113 (2)	13.3848 (3), 8.60982 (16), 14.9420 (3)
β (°)	90.0369 (15)	90.3062 (18)
V (Å ³)	3208.30 (9)	1721.90 (6)
Z	4	4
Radiation type	Cu $K\alpha$	Mo $K\alpha$
μ (mm ⁻¹)	6.16	1.70
Crystal size (mm)	$0.29 \times 0.11 \times 0.05$	$0.56 \times 0.37 \times 0.23$
Diffractometer	SuperNova, Dual, Cu at zero, Atlas	SuperNova, Dual, Cu at zero, Atlas
$T_{\text{min}}, T_{\text{max}}$	0.373, 0.776	0.449, 1.000
No. of measured, independent and observed [$I > 2\sigma(I)$] reflections	22043, 10533, 10107	23663, 3959, 3762
R_{int}	0.028	0.024
$(\sin \theta/\lambda)_{\text{max}}$ (Å ⁻¹)	0.616	0.650
$R[F^2 > 2\sigma(F^2)], wR(F^2), S$	0.032, 0.083, 1.02	0.019, 0.049, 1.06
No. of reflections	10533	3959
No. of parameters	804	200
No. of restraints	131	
H-atom treatment	H-atom parameters constrained	H-atom parameters constrained
$\Delta\rho_{\text{max}}, \Delta\rho_{\text{min}}$ (e Å ⁻³)	0.74, -0.58	0.36, -0.27

Samenvatting

Inleiding

Metaalenzymen die assisteren bij elektronenoverdrachtreacties komen overal voor en spelen een fundamentele rol in veel biologische systemen, zoals bij het vervoeren van zuurstof in het lichaam, de reductie van nitrietionen, alsook bij de synthese van neurotransmitters [1-4]. Alhoewel deze reacties alom bekend zijn is het nog steeds een uitdaging om een duidelijk mechanisme op te stellen voor veel van deze elektronenoverdrachtreacties [2]. In het afgelopen decennium is door middel van synthese van modellen van de actieve plaatsen van bepaalde enzymen een beter beeld verkregen van de chemische reacties die er plaatsvinden, gebruik makend van goed ontworpen liganden [5-8]. Een van klasse van modellen waar onderzoek naar is gedaan, omvat koper(II)-thiolaatverbindingen met een ruitvormige $[\text{Cu}_2\text{S}_2]$ -structuur. Deze verbindingen kunnen een redox interconversie ondergaan naar de isomere koper(I)-disulfideverbindingen [9-14]. Dit onderzoek was erop gericht om opheldering te verschaffen omtrent de structuur en spectroscopische eigenschappen van de actieve plaats in Cu_A enzymen, alsmede de processen die een rol spelen in de elektronenoverdracht.

Redox interconversie tussen kobalt thiolaat/kobalt(II) verbindingen

Zoals beschreven in hoofdstuk 1 is de redox interconversie tussen koper(II)-thiolaat en koper(I)-disulfideverbindingen uitgebreid onderzocht. Er is echter nog maar weinig onderzoek gedaan naar andere overgangsmetalen welke soortgelijke verbindingen met disulfide/thiolaatliganden kunnen maken. In hoofdstuk 2 is beschreven hoe met het disulfideligand L^1SSL^1 een kobalt(II)-disulfideverbinding en twee kobalt(III)-thiolaatverbindingen kunnen worden gemaakt, door reacties met verschillende kobalt(II)-zouten. Kobalt(III)-thiolaatverbindingen bleken te worden gevormd wanneer een kobalt(II)-zout met BF_4^- , PF_6^- , of NCS^- anionen werden gebruikt in het oplosmiddel acetonitril, terwijl een kobalt(II)-disulfideverbinding werd verkregen bij gebruik van CoCl_2 . Verder onderzoek toonde aan dat er een kobalt(II)-disulfideverbinding wordt gevormd wanneer chloride-ionen worden toegevoegd aan een oplossing van een kobalt(III)-thiolaatverbinding in acetonitril; deze omzetting werd gevolgd met UV-vis spectroscopie. Na toevoeging van AgBF_4 werd de Co(III)-thiolaatverbinding weer gevormd. Computatieel onderzoek door middel van DFT-berekeningen wijzen erop dat de uitwisseling van een gecoördineerd acetonitril molecuul of thiocynaat anion in kobalt(III)-thiolaatverbindingen

met een chloride anion een kleine verandering veroorzaakt in de hoogst-bezette molecuulorbitaal: een verlaging van de bijdrage van een *p*-orbitaal van zwavel en een verhoging van de bijdrage van de *d*-orbitaal van kobalt.

Een dinucleaire ijzer(II)-disulfideverbinding wordt gevormd uit de reactie tussen ligand L^1SSL^1 en $FeCl_2 \cdot 4H_2O$. De twee ijzer(II)-centra in deze verbinding hebben twee verschillende geometrieën, die ook weer anders zijn dan in de gerelateerde kobalt(II)-disulfideverbinding. Reactie van het ligand L^1SSL^1 met $[Fe(MeCN)_6](BF_4)_2$ resulteerde in een ijzer(II)-fluoridecluster in plaats van de verwachte Fe(III)-thiolaatverbinding. Deze nieuwe tetranucleaire cluster bevat zowel eindstandige alsook bruggende fluoride-ionen, en omvat een unieke en bijna volledig vlakke $[Fe_4F_4]$ -structuur, zoals is beschreven in hoofdstuk 5.

Vier kobalt(II)-disulfideverbindingen met twee verschillende disulfideliganden (L^1SSL^1 , L^2SSL^2) en twee verschillende anionen ($PO_2F_2^-$, NO_3^-) zijn geïsoleerd en gekarakteriseerd door middel van verschillende technieken, zoals staat beschreven in hoofdstuk 3; ligand L^2SSL^2 heeft een extra methylgroep op twee van de pyridineringen. De kobalt(II)-verbindingen met $PO_2F_2^-$ anionen werden onverwachts gevormd doordat een oude batch $AgPF_6$ werd gebruikt, maar zijn succesvol gereproduceerd door gebruik van het zout $LiPO_2F_2$. Röntgenkristallografie toonde aan dat alle kobalt(II)-verbindingen kobalt(II)-ionen in een octaëdrische geometrie bevatten. De kobalt(II)-disulfideverbinding met het ligand L^1SSL^1 en $PO_2F_2^-$ anionen is stabiel in oplosmiddelen als dichloormethaan en methanol, maar in acetonitril vindt er een redox interconversie plaats waarbij de kobalt(III)-thiolaatverbinding $[Co^{III}(L^1S)(MeCN)_2]^{2+}$ wordt gevormd. Deze interconversie is niet waargenomen voor de verbinding met NO_3^- anionen. Verder onderzoek liet zien dat beide kobalt(II)-disulfideverbindingen met het disulfideligand L^2SSL^2 geen redox interconversie ondergaan in de onderzochte oplosmiddelen.

Reactiviteit van Fe^{II}- en Co^{II}-disulfideverbindingen met waterstofperoxide

Onderzoek naar de reactiviteit van metaal-thiolaatverbindingen met zuurstof heeft in de laatste decennia veel aandacht getrokken, vooral om een beter beeld te krijgen van de oxidatiegevoeligheid van metaalenzymen in biologische systemen [15-22]. Er is echter nog niet veel onderzoek gedaan naar de oxidatie van metaal-disulfideverbindingen [19]. Oxidatie van de ijzer(II)-disulfideverbinding die beschreven is in hoofdstuk 2, resulteerde in de vorming van een mononucleaire, hoog-spin ($S = 5/2$) Fe(III)-sulfonaatverbinding, terwijl oxidatie van de overeenkomstige kobalt(II)-disulfideverbinding resulteerde in

een laag-spin ($S = 0$) kobalt(III)-sulfinaatverbinding. Massaspectra van de reactiemengsels, in combinatie met de resultaten van vorige studies, duiden erop dat oxidatie van de kobaltverbinding verloopt via een relatief stabiele kobalt(III)-sulfenaatverbinding [23].

Synthese en karakterisatie van een aantal overgangsmetaalverbindingen met thioether- en disulfideliganden

In hoofdstuk 6 is de synthese en karakterisatie beschreven van een aantal overgangsmetaalverbindingen met algemene formule $[M^II(L^1SCH_3)Cl_2]$ ($M = Co, Cu, Mn, Fe$), waarbij L^1SCH_3 een tetradentaat ligand is met een thioether donor. De structurele en spectroscopische eigenschappen van deze verbindingen zijn vergeleken met die van de gerelateerde disulfide verbindingen $[M^{II}_2(L^1SSL^1)Cl_4]$. De kristalstructuren, samen met de resultaten van magnetische metingen, bevestigen dat de metaalcentra in deze verbindingen zich allemaal in de hoog-spin toestand bevinden. De structuren van deze serie $[M^II(L^1SCH_3)Cl_2]$ verbindingen laten een interessante trend zien: terwijl het ijzer(II)-ion in $[M^II(L^1SCH_3)Cl_2]$ zich in een octaëdrische geometrie bevindt met coördinatie van de thioetherzwavel (op 2.6972(6) Å), bevindt de thioetherzwavel zich op steeds grotere afstand van het metaalion gaande via de mangaan(II) (2.8325(4) Å) en koper(II) (2.9961(4) Å) naar de kobalt(II)-verbinding (5.8887(8) Å). Dit resulteert in een verstoorde vierkante-piramide-geometrie voor de koper(II)- en mangaan(II)-ionen en een trigonale-bipiramidale geometrie voor het kobalt(II)-ion. Deze trend is ook deels zichtbaar in de structuren van de dinucleaire verbindingen $[M^{II}_2(L^1SSL^1)Cl_4]$. In het algemeen zijn de M-S afstanden langer in de dinucleaire disulfideverbindingen dan in de gerelateerde mononucleaire thioetherverbindingen, wat erop duidt dat de disulfide-zwavelatomen een iets zwakker ligand zijn dan de thioether-zwavelatomen.

Referenties

- [1] S. Iwata, C. Ostermeier, B. Ludwig, H. Michel, *Nature*, 376 (1995) 660-669.
- [2] C. Jacob, G.L. Giles, N.M. Giles, H. Sies, *Angew. Chem. Int. Edit.*, 42 (2003) 4742-4758.
- [3] J.A. Kovacs, *Acc. Chem. Res.*, 48 (2015) 2744-2753.
- [4] J.T. Pedersen, C. Hureau, L. Hemmingsen, N.H. Heegaard, J. Østergaard, M. Vašák, P. Faller, *Biochem.*, 51 (2012) 1697-1706.
- [5] K.D. Karlin, *Science*, 261 (1993) 701-708.
- [6] E. Kim, E.E. Chufán, K. Kamaraj, K.D. Karlin, *Chem. Rev.*, 104 (2004) 1077-1134.
- [7] E.Y. Tshuva, S.J. Lippard, *Chem. Rev.*, 104 (2004) 987-1012.
- [8] S. Friedle, E. Reisner, S.J. Lippard, *Chem. Soc. Rev.*, 39 (2010) 2768-2779.

- [9] E.C.M. Ording-Wenker, M. van der Plas, M.A. Siegler, S. Bonnet, F.M. Bickelhaupt, C. Fonseca Guerra, E. Bouwman, *Inorg Chem*, 53 (2014) 8494-8504.
- [10] E.C.M. Ording-Wenker, M. van der Plas, M.A. Siegler, C. Fonseca Guerra, E. Bouwman, *Chem. Eur. J.*, 20 (2014) 16913-16921.
- [11] A.M. Thomas, B.L. Lin, E.C. Wasinger, T.D.P. Stack, *J. Am. Chem. Soc.*, 135 (2013) 18912-18919.
- [12] A. Neuba, R. Haase, W. Meyer-Klaucke, U. Flörke, G. Henkel, *Angew. Chem. Int. Edit.*, 51 (2012) 1714-1718.
- [13] Y. Ueno, Y. Tachi, S. Itoh, *J. Am. Chem. Soc.*, 124 (2002) 12428-12429.
- [14] S. Itoh, M. Nagagawa, S. Fukuzumi, *J. Am. Chem. Soc.*, 123 (2001) 4087-4088.
- [15] E.C.M. Ording-Wenker, M.A. Siegler, M. Lutz, E. Bouwman, *Inorg. Chem.*, 52 (2013) 13113-13122.
- [16] A. Dutta, M. Flores, S. Roy, J.C. Schmitt, G.A. Hamilton, H.E. Hartnett, J.M. Shearer, A.K. Jones, *Inorg. Chem.*, 52 (2013) 5236-5245.
- [17] A.C. McQuilken, Y. Jiang, M.A. Siegler, D.P. Goldberg, *J. Am. Chem. Soc.*, 134 (2012) 8758-8761.
- [18] C.S. Mullins, C.A. Grapperhaus, B.C. Frye, L.H. Wood, A.J. Hay, R.M. Buchanan, M.S. Mashuta, *Inorg. Chem.*, 48 (2009) 9974-9976.
- [19] Y. Lee, D.-H. Lee, A.A.N. Sarjeant, K.D. Karlin, *J. Inorg. Biochem.*, 101 (2007) 1845-1858.
- [20] P. Lugo-Mas, A. Dey, L. Xu, S.D. Davin, J. Benedict, W. Kaminsky, K.O. Hodgson, B. Hedman, E.I. Solomon, J.A. Kovacs, *J. Am. Chem. Soc.*, 128 (2006) 11211-11221.
- [21] R.A. de Sousa, E. Galardon, M. Rat, M. Giorgi, I. Artaud, *J. Inorg. Biochem.*, 99 (2005) 690-697.
- [22] J.A. Kovacs, *Science*, 299 (2003) 1024-1025.
- [23] F. Jiang, M.A. Siegler, X. Sun, L. Jiang, C. Fonseca Guerra, E. Bouwman, *Inorg. Chem.*, 57(2018) 8796-8805.

List of Publications

1. Density functional theory study of the mechanisms of iron-catalyzed cross-coupling reactions of alkyl Grignard reagents

Qinghua Ren, Shuhui Guan, Feng Jiang, Jianhui Fang, *J. Phys. Chem. A*, 117 (2013) 756-764

2. Electrodeposited nitrogen-doped graphene/carbon nanotubes nano-composite as enhancer for simultaneous and sensitive voltammetric determination of caffeine and vanillin

Lin Jiang, Yaping Ding, Feng Jiang, Li Li, Fan Mo, *Anal. Chim. Acta* 833 (2014) 22-28

3. Reaction mechanisms of Ni-catalyzed reductive cross-coupling of aryl halides

Feng Jiang, Qinghua Ren, *Acta Phys.-Chim. Sin.* 30 (2014) 821-828

4. Theoretical investigation of the mechanisms of the biphenyl formation in Ni-catalyzed reductive cross-coupling system

Feng Jiang, Qinghua Ren, *J. Organomet. Chem.* 757 (2014) 72-78

5. DFT study of the single electron transfer mechanisms in Ni-catalyzed reductive cross-coupling of aryl bromide and alkyl bromide

Qinghua Ren, Feng Jiang, Hegui Gong, *J. Organomet. Chem.* 770 (2014) 130-135

6. Facile and novel electrochemical preparation of a graphene-transition metal oxide nanocomposite for ultrasensitive electrochemical sensing of acetaminophen and phenacetin

Lin Jiang, Shuqing Gu, Yaping Ding, Feng Jiang, Zhen Zhang, *Nanoscale*, 6 (2014) 207-214

7. An ultrasensitive ethene detector based on a graphene-copper(I) hybrid material

Wangyang Fu, Thomas F. van Dijkman, Lia M. C. Lima, Feng Jiang, Grégory F. Schneider, Elisabeth Bouwman, *Nano Lett.*, 17 (2017) 7980-7988

8. Redox interconversion between cobalt(III) thiolate and cobalt(II) disulfide compounds

Feng Jiang, Maxime A. Sieglér, Célia Fonseca Guerra, Elisabeth Bouwman., *Inorg. Chem.* 57 (2018) 8796-8805

9. A Tetranuclear Fluorido-bridged Iron Compound: Fluoride Abstraction from the Tetrafluoridoborate Anion

Feng Jiang, Maxime A. Siegler, Elisabeth Bouwman. *Inorg. Chem. Comm.* 94 (2018) 53-56

10. The reactivity of Fe(II) and Co(II) disulfide compounds with dihydrogen peroxide

Feng Jiang, Maxime A. Siegler, Elisabeth Bouwman, *Eur. J. Inorg. Chem.* 2018, in press

11. Synthesis and characterization of a series of transition metal compounds of thioether and disulfide ligands

Feng Jiang, Maxime A. Siegler, Elisabeth Bouwman, *Inorganica Chim. Acta* 2018, in press

12. Solvent-dependent redox interconversion of cobalt(III) thiolate and cobalt(II) disulfide compounds

Feng Jiang, Amaya C. Verschuur, Christian Marvelous, Maxime A. Siegler, José Sánchez Costa, Elisabeth Bouwman, to be submitted

Curriculum Vitae

Feng Jiang was born in Huai'an, Jiangsu Province, China, on July 14th in 1988. In 2005, he graduated from Huaizhou high school in Huai'an. He then moved to Tsingtao and began his BSc study in marine science at Qingdao University of Science and Technology. After 4 years, he obtained his BSc degree on the thesis entitled "Synthesis and characterization of the cationic starch" under the supervision of Prof. Kongcheng Hu. After that, he moved to Shanghai and enrolled the MSc programme in Shanghai University with a major in theoretical chemistry. In 2014, he obtained his MSc degree with the thesis entitled "Mechanism investigation of Ni-catalyzed cross-coupling reactions" under the supervision of associate Prof. Dr. Qinghua Ren and Prof. Dr. Hegui Gong. During this period, he was awarded the "Chen Nianyi" scholarship in 2014.

On the 15th of September 2014, he started his PhD research with a personal grant from the Chinese Scholarship Council (CSC, 201406890016) in the Metals in Catalysis, Biomimetics & Inorganic Materials (MCBIM) group at Leiden University under the supervision of Prof. Dr. Lies. Bouwman and Prof. Dr. Célia Fonseca Guerra. During his PhD studies, he supervised several BSc and MSc students (Joe Macginley, Jodie Denmark, Sjoerd Verbeek, Amaya Verschuur). Furthermore, he followed a number of courses from Leiden University and the Holland Research School of Molecular Chemistry (HRSMC) including "Time management", "Effective Communication", "On being a Scientist", "Communication in Science", "Molecular Modelling", "Physical Methods in Inorganic Chemistry", "Peer Review", and "Scientific Writing".

The results reported in this thesis were presented at several national and international conferences as listed below:

Poster Presentation HRSMC Symposium 2015, Amsterdam, the Netherlands

Poster Presentation CHAINS Conference 2016, Veldhoven, the Netherlands

Poster Presentation Reedijk Symposium 2016, Leiden, the Netherlands

Poster Presentation European Inorganic Chemistry Conference (EICC-4) 2017, Copenhagen, Denmark

Poster Presentation HRSMC Symposium 2018, Leiden, the Netherlands

Poster Presentation Reedijk Symposium 2018, Leiden, the Netherlands

Oral Presentation CHAINS Conference 2017, Veldhoven, the Netherlands

